DISCLAIMER NOTICE

THIS DOCUMENT IS BEST QUALITY AVAILABLE. THE COPY FURNISHED TO DTIC CONTAINED A SIGNIFICANT NUMBER OF PAGES WHICH DO NOT REPRODUCE LEGIBLY.

ARL 154

RESEARCH ON OPTICAL AMPLIFICATION EMPLOYING ELECTRONIC SCANNING TECHNIQUES

JAMES A. HALL
HARRY SHABANOWITZ

WESTINGHOUSE ELECTRIC CORPORATION
ELMIRA, NEW YORK

DECEMBER 1961

AERONAUTICAL RESEARCH LABORATORY
OFFICE OF AEROSPACE RESEARCH
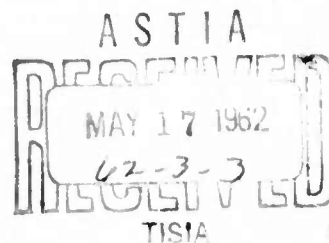UNITED STATES AIR FORCE

RESEARCH ON OPTICAL AMPLIFICATION EMPLOYING ELECTRONIC SCANNING TECHNIQUES

JAMES A. HALL
HARRY SHABANOWITZ

WESTINGHOUSE ELECTRIC CORPORATION
ELMIRA, NEW YORK

DECEMBER 1961

FOREWORD

This final technical report was prepared by the Electronic Tube Division
of the Westinghouse Electric Corporation, **Elmira**, New York, on Contract af 33-
(616)-7254 for the Aeronautical Research Laboratory, Office of Aerospace Research.
The work reported herein was accomplished on Task 70827, "Light Amplification" of
Project 7072, "Research on the Quantum Nature of Light" under the cognizance of
Mr. K. H. Gebel of the Solid State Physics Research of ARL.

The contract efforts formed part of the United States Air Force "Cat-Eye"
research program for achieving an imaging device whose sensitivity would be limit-
ed only by the ineluctable restrictions imposed by the irregular statistical
variations in the rate of emission of photo-electrons and in the dark current of
the first photocathode. Under this program, Mr. Radames K. H. Gebel had con-
ceived a system of realizing an imaging device for extremely low light level
performance, by the use of a television camera tube employing electron image
amplification together with electronic background suppression techniques. As
task scientist, Mr. Gebel was responsible for the technical direction of the
contract efforts towards which he made many valuable contributions.

Acknowledgement is made to Mr. Joseph Lempert of the Westinghouse Research
Laboratories for his contribution to the technical direction of the program
from its initiation until June, 1956. Included among those who cooperated in the
research and the preparation of the report were Messrs. Robert A. Shaffer, John
C. Kylander, Robert H. Clayton, H. Richard Groo, A. L. Korner, Robert Carpentier
of the Electronic Tube Division, Westinghouse Electric Corporation and Eugene
R. Heath, William J. Soule, and Robert A. Floyd.

Acknowledgement is also made to Dr. E. J. Sternglass, Messrs. A. E. Anderson

ii

ABSTRACT

The primary objective of the investigation summarized in this report was to determine, through research, a basis for subsequent development of a highly sensitive optical to electrical transducer or television camera tube for obtaining useful images at extremely low levels of illumination.

An analysis of television camera tube limitations concludes that an advanced scanned optical amplifier of the image orthicon type, embodying suitable means of image intensification, is an effective approach to an ideal imaging tube performance limited only by statistical fluctuations of the input signal. Various means of intensifying the picture signal electronically, before the scanning process, are described.

Image amplification approaches investigated include the use of front surface secondary electron emission from solid members, in order to retain the feature of low voltage operation. The feasibility of applying the principle of transmission secondary electron emission by the use of thin film dynode structures on pre-scanning beam electron multipliers has been successfully demonstrated.

Also investigated was the feasibility of reducing the energy distribution in the electron scanning beam to minimize noise sources in the tube. In addition, a means was invented and shown to be feasible for minimizing spurious signals in pickup tubes when viewing scenes with extremely high contrast.

The research has, therefore, accomplished its objective of supplying the basis for the development of a new type of scanned optical amplifier, having a sensitivity and resolution potentially better than that obtainable from presently known television camera tubes.

TABLE OF CONTENTS

Section		Page

LIST OF ILLUSTRATIONS

LIST OF TABLES

LIST OF SYMBOLS

A	Angstrom
Ag	Silver
Al	Aluminum
Au	Gold
Ba	Barium
Bi	Bismuth
$^{\circ}C$	Degrees Centigrade
Cl	Chlorine (chloride)
Cs	Cesium
F	Fluorine (fluoride)
$^{\circ}K$	Degrees Kelvin
K	Potassium
Mg	Magnesium
Na	Sodium
O	Oxygen
Si	Silicon
μ	Micron

LIST OF ABBREVIATIONS

Const.	Constant
CRT	Cathode Ray Tube
DC	Direct Current
EBIC	Electron Bombardment Induced Conductivity
Eq.	Equation
exp	Base of Natural Logarithm, e
KV	Kilovolt
Max.	Maximum
Proc.	Procedure
RF	Radio Frequency
RMS	Root Mean Square
Sig.	Signal
TSE	Transmission Secondary Emission
TSEM	Transmission Secondary Emission Multiplier
TV	Television

GLOSSARY

anisotropic conductivity - exhibiting different electrical conductivities along lateral and transverse axis of a dielectric target storing electric charges.

back-scattered electrons - electrons emitted in the process of secondary electron emission with energies ranging from maximum energy for "true" secondary electrons to incident energy of primaries.

chromatic aberration - variation in the focal length of an electron lens caused by a variation in electron energy. Analogous to chromatic aberration in geometrical optics arising from the fact that light of different wave lengths, passing through a lens, is refracted to a different degree leading to a variation in focal lengths.

contact potential - small potential difference existing between the surfaces of two dissimilar metals in electrical contact, arising from the difference in work function of the metals.

dark current - electron current associated with a photoelectric surface in the absence of incident radiation and with the application of an electric field. In photoemissive surfaces, the dark current arises from thermionic electron emission of the surface, while in photoconductive surfaces it arises from the semi-conducting nature of the surface.

dynode - electrode structure exhibiting property of secondary electron emission when bombarded by charged particles and thus capable of effecting amplification.

ebicon - television camera tube in which an electron image is produced by a photoemitting cathode and focused on an electron bombardment induced conductivity target which is scanned on its opposite side by a low velocity electron beam.

electrical transducer - device for converting power from one system into another system.

front surface secondary electron emission - condition in which secondary electrons are emitted on the same side of the bombarded solid as the incident primaries.

Gaussian distribution - distribution of current density as a function of the radial distance from the electron beam axis, of the form:

$$\rho = \rho_o \quad \exp - Kr^2$$

where: ρ is the current density
K is the distance from the electron beam axis

halation - phenomenon observed in an image orthicon in which a small bright image area in a darker background is surrounded by a dark ring and an outer bright halo.

image orthicon - television camera tube in which an electron image is pro-
duced by a photoemitting cathode and focused on an insulating storage
target, which is scanned on its opposite side by a low velocity electron
beam. Scanning beam electrons specularly reflected at the surface of the
target return to a secondary emission multiplier structure and thence to
anode of tube.

integration time - time during which signal in form of electric charge is
being accumulated and stored on target plate.

Isocon - television camera tube, similar to image orthicon, with the exception
that scanning beam electrons scattered at the surface of the target are
permitted to return to a secondary emission multiplier structure.

Johnson Noise - the noise produced by thermal agitation of charges in conductor.

Maxwell-Boltzmann Distribution - distribution of velocities among the electrons
emitted by a cathode, of the form:

$$N\ (v)\ =\ 4\,\pi\,N\ \left(\frac{m}{2\,\pi kT}\right)^{3/2}\ v^2\ \exp\ \frac{-mv^2}{2kT}$$

where: $N\ (v)$ is the number of electrons with velocities between v and
$v + dv$; N, the total number of electrons; m, the mass of an
electron; k, Boltzmann's constant, and T the absolute temperature.

paraxial ray - a ray which makes a very small angle with the optical axis of
a system and lies close to the axis throughout its length.

photocathode - an electrode used for obtaining photoelectric emission when
irradiated.

photoconductivity - phenomenon of change in conductivity of certain materials
as a result of incident radiation.

photoelectric emission - phenomenon of emission of electrons by certain materials
as a result of incident radiation.

raster - in television, a predetermined pattern of scanning lines which provides
substantially uniform coverage of an area.

resolution - term used to denote the process of defining certain repetitive
patterns or the degree to which they can be discriminated.

resolution chart - chart used to check the linearity, definition, and contrast
of television systems.

secondary electron emission - emission of secondary electrons from a solid due
to the impact on the solid of charged particles. Each incident particle may
release more than one secondary electron, thereby resulting in a multiplication
process.

sensitivity - the signal current developed per unit incident radiation density (i.e., per watt per unit area).

shot noise - noise resulting from the random nature of the emission and flow of electrons in electron tubes.

spurious signal - signal originating from a source other than scene being imaged.

transmission secondary electron emission - condition in which secondary electrons are emitted on the far side of the bombarded solid opposite to the side first struck by the incident primaries.

target - electrode structure, usually a semi-conducting or insulating material, upon which radiant energy or charged particles are incident to provide a desired effect, e.g. storage of electric charges, secondary electron emission.

Vidicon - television camera tube in which an electric potential image is produced by a photoconductive cathode which is scanned by a low velocity electron beam. Changes in potential at the photoconductor surface gives rise to an electrical signal.

work function - the energy needed to remove an electron from the Fermi level to a point outside the surface, an infinite distance away.

SECTION I

INTRODUCTION

This work was undertaken at the request of the Wright Air Development Center to determine through research a basis for subsequent development of an optical to electrical transducer or television type pickup tube for obtaining useful images with extremely low levels of illumination. Although the initial statement of work was broad, and a general survey was made of the possible approaches to more sensitive optical amplifiers, the detailed course of this research was guided through frequent conferences between the contractor's scientists and the Air Force Task Scientist. In particular, the topics investigated under this contract were chosen so that they did not duplicate work being performed in other laboratories, and the choice of approaches was made after considering the ultimate application of any device which might be developed as a result of this research. Hence, ruggedness, compactness, use of flat input photosurfaces, and in particular use of as low tube operating potentials as possible were considered desirable features and approaches were favored whose principles did not rule out these features.

The approaches investigated included use of large area input photocathodes in conjunction with suitable light optics to collect as large a number of light quanta as possible, and subsequent demagnification of the electron image to concentrate this information for easier detectability. Also investigated was the feasibility of reducing the energy spread in the scanning beam to minimize noise sources within the tube. Imaging pre-amplifier structures were used to intensify the picture signal electronically before the scanning process, in which front surface secondary emission from solid members was used to retain the feature of low voltage operation. A means was invented and shown to be feasible for minimizing spurious signals in pickup tubes when viewing scenes with extremely high contrast. Finally, and most successful, the phenomenon of transmission secondary electron multiplication in thin

1

films, invented and developed at the Westinghouse Research Laboratories, has been used in the design of an imaging preamplifier to complement the structure of the image orthicon, the most sensitive camera tube in general use today. As shown in the body of this report, experimental tubes assembled using this approach have had pre-amplifier gains of 25 with an added tube operating voltage of only 7000 volts, and have reproduced pictures with 500 T.V. lines per inch resolution at the photo-cathode and 5 shades of grey. The research has, therefore, accomplished its objective of supplying the basis for the development of a new type of scanned optical amplifier, having a sensitivity and resolution potentially better than that obtainable from any standard camera tube, and also from those developmental tubes with which we are familiar. Especially important is the fact that this type of pre-amplifier could in a subsequent tube development be combined with a sensitive multi alkali-photocathode, with a special thin film charge storage element or target with high secondary emission gain for improved sensitivity and improved resolution and integration, and with alternate methods of electron beam scanning for improved signal to noise ratio and wider dynamic range. Figure 1 is an outline drawing of a tube which was described in a proposal submitted to the Electronic Technology Laboratory of Wright Air Development Center as an outgrowth of this program.

In the body of this report, the first section is a general description of the operation of present day television camera tubes and their performance limitations. In particular, the principles of operation of the image orthicon, the most sensitive television camera tube in general use today, on which most of the experimental approaches were based, are reviewed.

The second section discusses the limitations to "seeing", or image formation at low light levels imposed by the quantum nature of light and the randomness of photo electron emission. This section is necessary to explain why certain approaches were followed, and to estimate the ultimate limits set by natural laws which will

2

limit our ability to see "in the dark". Included also here is a discussion of the effect of noise sources within the tube. The remaining sections, which form the bulk of this report, describe the experimental approaches taken, the degree of success achieved, the reasons why some approaches were dropped, and mathematical analyses where appropriate. An attempt has been made to be reasonably complete so that other workers may build on the results of this work rather than starting from the beginning, if they decide to investigate further some of the approaches which we have dropped or shelved in favor of more promising avenues.
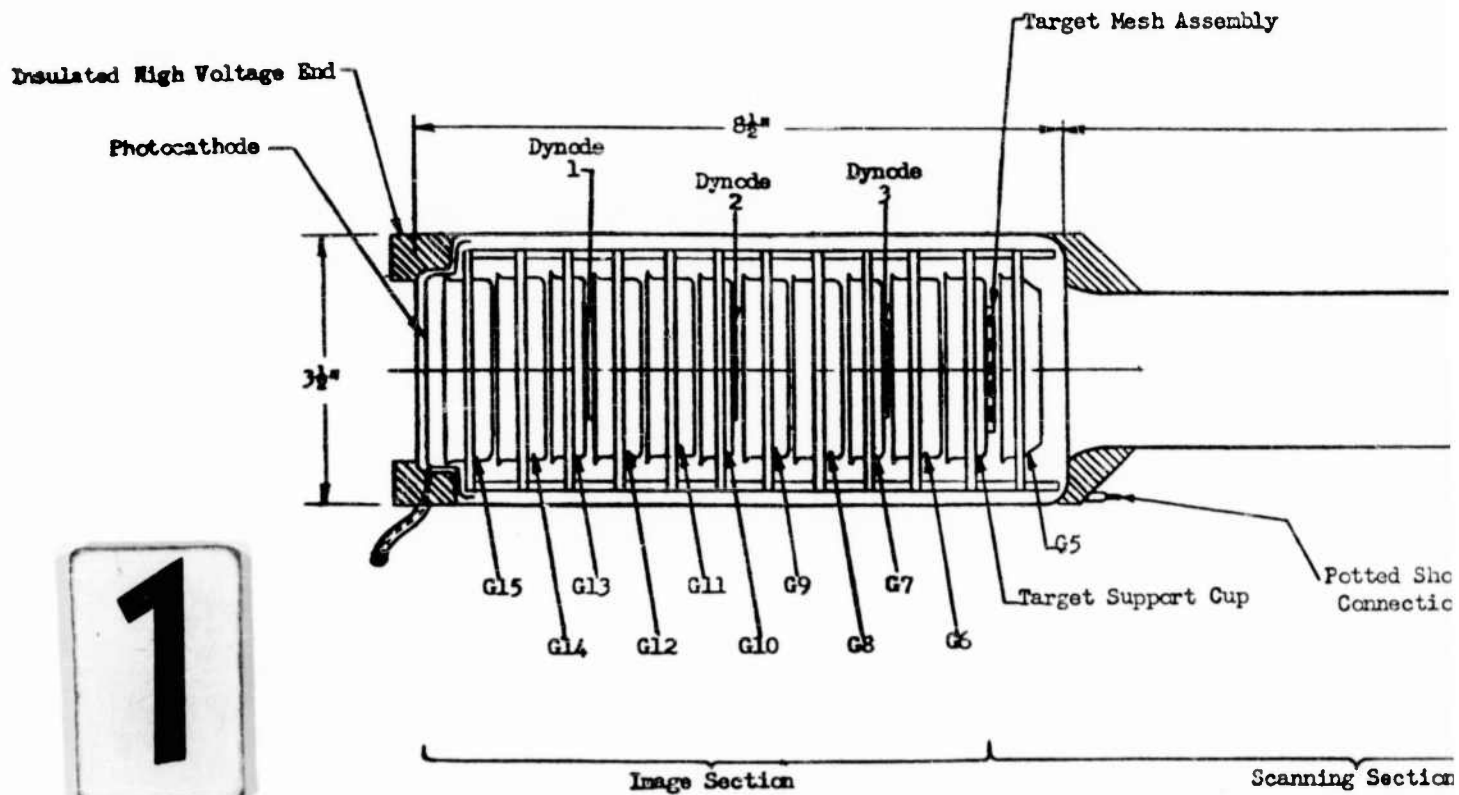
Figure 1 Transmission Secondary Emission Multiplier Camera Tube

4

Target Mesh Assembly

Dynode 1

8½"

11-3/4"

3"/4

Dynode 1

Dynode 2

Dynode 3

Dynode 1

Dynode 6

2"

G4

G3

Anode

Dynode 5

Dynode 4

Dynode 3

Dynode 2

G13 G11 G9 G7

G5

Target Support Cup

Potted Shoulder Connections

G14 G12 G10 G8 G6

Image Section

Scanning Section

Multiplier Section

n Secondary Emission Multiplier Camera Tube

4

2
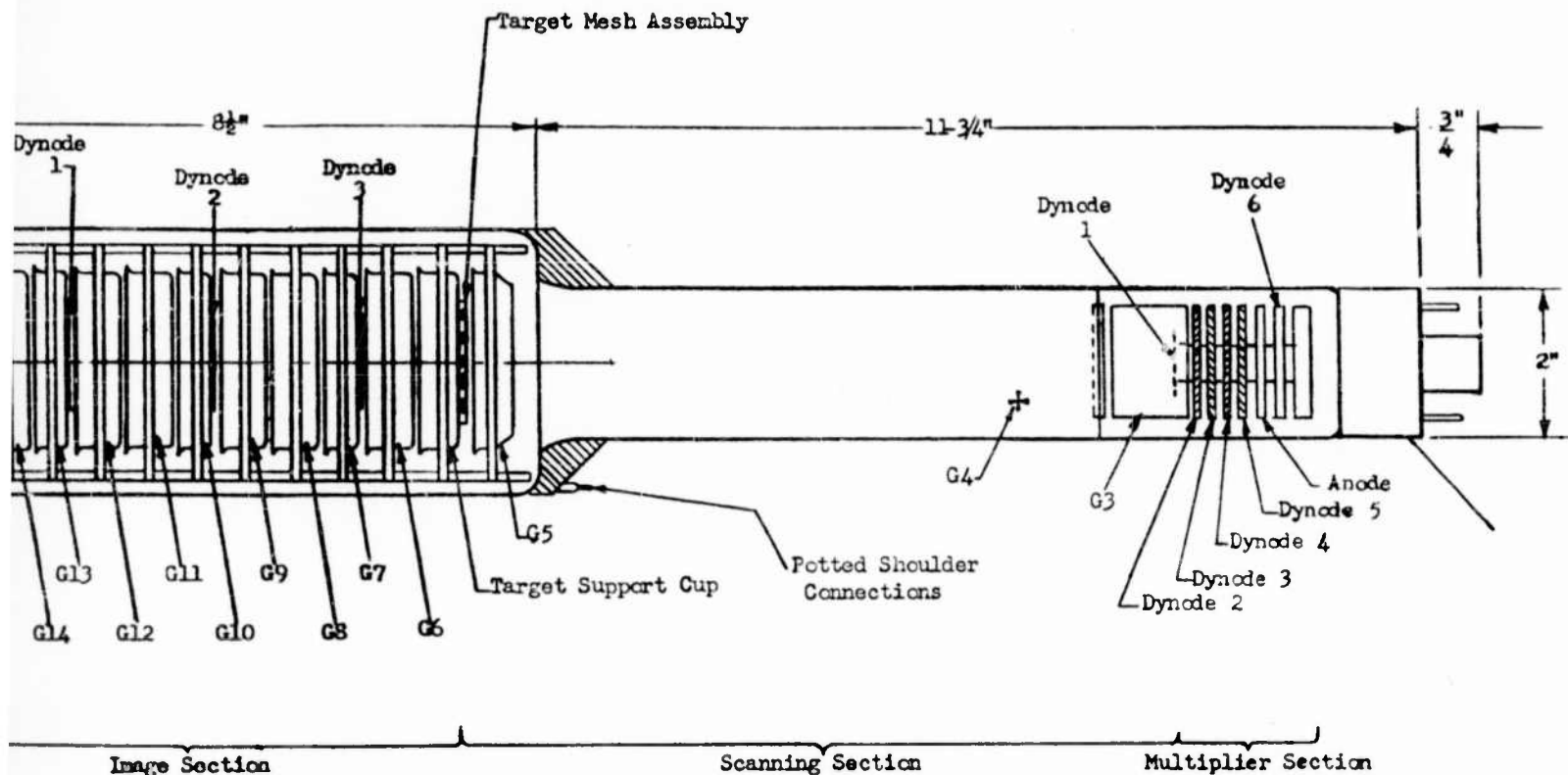
PRINCIPLES OF TELEVISION CAMERA TUBE OPERATION

1. INTRODUCTION

The basic purpose of a television camera tube is to translate the information contained in an optical image into an electrical signal suitable for transmission over a transmission line or radio link. To do this, the tube must perform at least two basic functions. First, a photosensitive member is used to translate the brightness pattern in the optical image to a corresponding electrical pattern. Second, the intensity of each small area of the electrical image is measured in turn to generate an electrical signal whose amplitude varies in time; the type of signal which can be transmitted over a distance. This scanning process may be considered as a type of mathematical trans-formation in which the brightness or intensity as a function of position in the picture is transformed into intensity or amplitude as a function of time. The signal thus generated is normally fed to a vacuum tube or transistor amplifier, then through the appropriate circuits for broadcast of wire transmission. Beside these two essential functions, all modern camera tubes contain at least one and frequently three other functions. These are, respectively, a provision for the accumulation and storage of electrical picture information ahead of the scanning process, always included; a provision for amplification of the electrical image information ahead of the scanning process, often included; and a provision within the tube for electronic amplification of the television signal before it is fed to the vacuum tube or the transistor video amplifier.

Because each of these five functions may be performed in various ways, and because several desirable combinations exist, there were a number of camera tubes in use or under development at the time this research was begun. The most popular tubes were variations of the vidicon, in which the intitial transformation from the optical to electrical image is accomplished with a thin photoconductive layer which

also provides the image storage function, and the image orthicon, in which a photo-emissive surface provides the initial transformation and image storage is accom-plished on a separate charge storage element known as the target. The chief ad-vantages of the vidicon are small size and operating simplicity. The image orthicon, while larger and requiring more complex equipment is far more sensitive, having the ability to generate quality television signals from a scene illuminated by moonlight. Tubes under development in various laboratories during the contract period from March 1956 to August 1959 included the image isocon, the intensifier-image orthicon, the electron multiplier vidicon, the ebicon, the image orthicon with secondary emission image amplifier, image orthicons in which high gain was achieved by improved secondary emission from the target, and modifications of these types for ruggedness, higher output signal, or other special operating features.

To understand the advantages of each of these camera tube variations, their operating limitations, and the directions in which improvement can be made, one must first understand the operation of the two basic modern camera tubes, the vidi-con and the image orthicon.

a. The Vidicon

The vidicon, the simplest of modern camera tubes, is pictured in Figure 2. A cross section view of the tube, which indicates the essential parts and the manner of connection of the electrical output signal to the video amplifier is shown in Figure 3. A camera lens is positioned to form an inverted real optical image of the scene to be televised on the photoconductive coating on the inner surface of the glass face. The photoconductor, often antimony trisulfide or amorphous selenium, is a fairly good insulator unless exposed to light. When light falls on the thin layer, charge carriers are formed within the film at a rate which is a function of the in-tensity of illumination at each point. A potential difference is maintained across the photoconductor layer during tube operation so that these charge carriers give

6

rise to an electric current through the layer which varies from point to point as a function of image brightness. If a fixed potential is applied to the front or glass side of the photoconductor, and a different, say more negative, fixed potential is initially applied to the back or free side of the photoconductor, this flow of current through the layer will soon give rise to a voltage pattern on the free side, in which more positive areas will correspond to brighter areas in the picture. The process may be visualized by considering the photoconductor as if it were divided into a large number of small areas, each as small as the finest detail we intend to reproduce in the picture. Such imaginary small areas are known as picture elements. Each element may, as indicated in Figure 4, be thought of as consisting of a capacitor, having as its plates the front or glass surface and the free surface of the layer respectively, and as its dielectric the material of the layer. This elemental capacitor is shunted by a resistor whose value is very large when the element is unilluminated, but which decreases in resistance as the illumination is increased. At the beginning of each picture taking interval, or frame time, each capacitor is charged to a fixed potential difference. During each picture taking interval, this charge leaks off through the shunting resistor at a rate dependent on the illumination. The front or glass sides of the elemental capacitors are kept at a common essentially fixed potential, since the inner glass surface is coated with a transparent electrically conductive coating, usually tin oxide. This coating, which forms the signal output electrode for the tube, is connected to a power supply through a load resistor, as shown in Figure 4. At the beginning of a picture taking interval, the free side of each elemental capacitor is charged to the same voltage, more negative than the signal electrode supply voltage. At the end of a picture taking interval, each elemental capacitor will be partially discharged and the difference between the voltage found at its free terminal and the initial voltage will be a measure of the intensity of illumination on that element of the optical image.

7

Figure 2.   7325 Vidicon

8
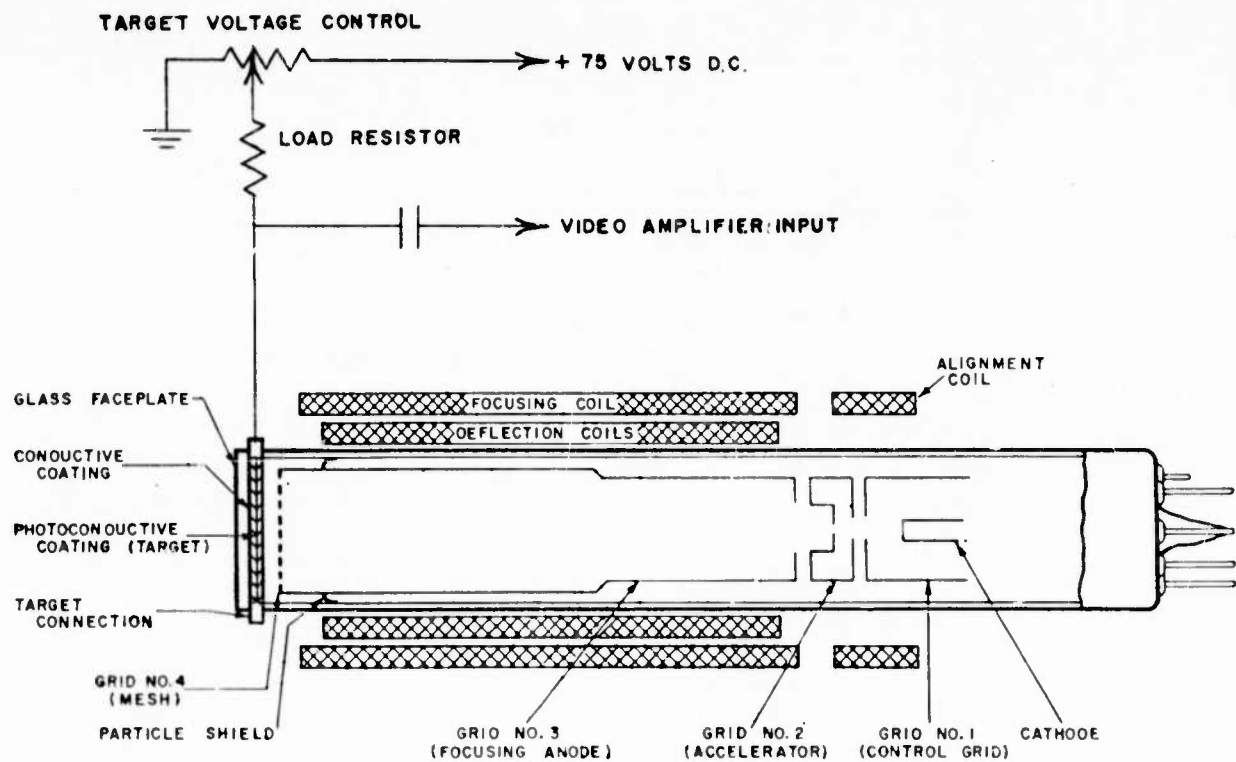
Figure 3.   Cross Section Type 7325 Vidicon

9
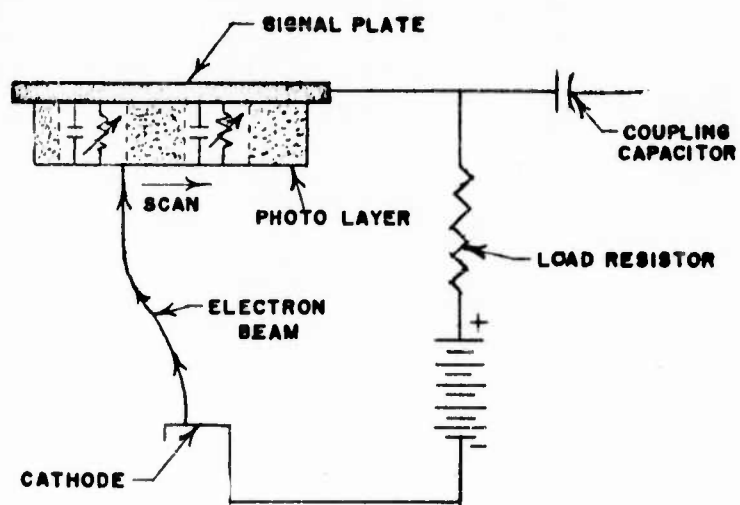
Figure 4. Detailed Cross Section Photoconductive
Vidicon Target

This geometrical pattern of a voltage varying as a function of position on the surface can be converted to a time varying signal suitable for transmission by the scanning process.

In a vidicon, as in most other camera tubes, scanning or reading the signal from the storage layer is accomplished with an electron beam. The electrons originate from a thermionic cathode and are formed into a beam in the electron gun at the right end of the vidicon as shown in Figure 3. The electrons are accelerated to a potential of 300 or more volts as they pass through the electrodes labeled G_2 and G_3, and are focused under the influence of an axial magnetic field supplied by the focus coil to strike the free side of the photoconductor in a small area or spot. The electrons are decelerated in the region beyond the field defining mesh G_4, to strike the photoconductor with an energy of only a few volts. At this energy, the secondary emission ratio is much less than one, that is, most of the beam electrons which strike the surface will remain there, and no or at most very few secondary electrons will be produced. The energy of the beam electrons reaching the surface will depend only on the difference in potential between the free surface of the photoconductor and the thermionic cathode in the electron gun. It is necessary for normal vidicon operation that the beam electrons land and result in a more negative charging of the surface. For most materials, low energy electrons do land, but as the energy of the electrons increases, an increasing number of secondary electrons are liberated from their bonds within the material and leave the surface. To insure that the free surface of the photoconductor never reaches voltages so positive with respect to the cathode that the number of secondaries exceeds the number of beam electrons, the potential of the signal electrode or conductive backing layer is made only a few tens of volts positive with respect to the gun cathode. If the electron beam is now directed at one element of the surface, electrons will land and charge the free surface of that element negatively with respect to the signal

11

electrode supply voltage. Electrons will continue to land until the potential of the free surface is equal to the potential of the thermionic cathode, except for a small correction constant to include the effects of electron emission velocities, of work function and of contact potential differences. At this point. it becomes energetically impossible for more electrons to reach the target surface.

In practice, the electron beam is not directed continuously at one target element, but is deflected to land on all of the target elements, one after antoher, in a geometrically fixed scanning pattern. In normal entertainment television practice, scanning of the entire picture is accomplished once in each 1/30 second. Thus the beam lands on any one element very briefly and only once in 1/30 second. If the beam is made to scan the entire target surface several times while no light is falling on the photoconductor, all of the elemental capacitors will be charged to the voltage difference between the signal electrode voltage and the cathode, and essentially no further beam electrons will reach the target. If light is allowed to fall on a picture element immediately after it has been scanned, the potential difference across that elemental capacitor will drop at a rate depending on the illumination level until the beam returns 1/30 second later. Many beam electrons can now land on the illuminated picture element. The beam current is normally set to a relatively high value, so that in the very brief time that the beam is aimed at the element, enough electrons land to recharge the capacitor to essentially its initial light value. That is, the free surface of the illuminated element is returned essentially to cathode potential, and that element is ready to receive more information. Since the electrons landing on the element arrived in a very short length of time, the current pulse they constitute is coupled to the signal electrode by the capacitance of the element, and appears as a pulse of current in the signal electrode lead, and hence as a voltage pulse across the load resistor which is fed to the video amplifier. We have considered a case in which only one of the elements was illuminated.

12

In practice, the whole photoconductive area will be illuminated with the image of the scene to be televised. Thus some of the beam will land on each of the elements, more on those which have been more brightly illuminated, and this landing current, coupled to the signal lead, constitutes the video signal.

It is important to note that the signal read from each element is a function of the average light intensity falling on that element during the preceding 1/30 second. Thus, to a fair approximation, the tube will respond equally well whether continuously exposed or whether the light is made to arrive at the photoconductor in one short pulse during a frame time by use of a camera shutter or possibly of a pulsed light source to illuminate an otherwise darkened scene.

Since each element of the photoconductor can receive light and store information all the time, the vidicon's sensitivity is high compared to earlier types of camera tubes like the image dissector. Also important is the inability of the vidicon, or any other camera tube, to follow motion which takes place in a time shorter than frame time. Obviously, such motion could only result in a smeared image unless a pulsed light or similar means were used to freeze motion during each exposure.

The vidicon type camera tube whose operation has just been descrived, is very simple and operates in simple equipment. If suffers from limitations which at present restrict its usefulness. These are low sensitivity when compared with other camera tube types, and lag, that is inability to follow rapidly changing scenes because the act of scanning does not completely erase the image information stored on an element during the preceding frame.

To understand the sensitivity limitation, we must consider the input circuit of the video amplifier into which the signal is fed. It can be shown for a well designed low noise video amplifier using an unpeaked camera tube load resistor circuit, but in which the gain versus frequency curve of the entire system is equalized at a

13

later stage, that a spontaneous fluctuating signal will appear at the amplifier terminals which is caused by electronic motion in the camera tube load resistor. Known as "Johnson noise" this fluctuation could only be reduced by operating the resistor in a cryostat at a very low temperature. Calculations based on fundamental thermodynamic considerations show that this fluctuation signal has an equivalent RMS value of about 2×10^{-9} amperes. Since it is always present, this fluctuation or noise signal sets a lower limit to the current signal from the camera tube which will produce an intelligible picture. Although detailed studies described in a later section indicate that the human eye can detect a picture when the video signal to fluctuations ratio is considerably less than unity, it is found experimentally that the vidicon ceases to produce a detectable picture when the light level is reduced so that its output signal current is in the order of 10^{-9} amperes.

Thus any attempt to improve the low light level performance of the vidicon depends on increasing the output signal for a given amount of light falling on the photoconductor. Within the structure of the tube as described there are only two ways of accomplishing this. First, the scanning standards may be changed so that a picture is read out only every tenth of a second, or every second. In this case, more light energy will have fallen on the photoconductor and a larger signal can be produced, although at the expense of a lessened ability to detect motion. Second, and more desirable, the photoconductive layer may be modified to improve its effectiveness at translating energy into an electrical charge pattern. Unfortunately, the physics of the photoconductor are such that increased sensitivity is most easily obtained at the expense of incomplete erasure during the scanning process and hence of decreased ability to follow rapid motion.

The action of the photoconductive layer may be visualized approximately as follows. In the dark, very few charge carriers exist in the layer. When light falls

14

on the layer, the energy of some of those light quanta which are absorbed is transferred to electrons within the layer, raising them to the conduction band and usually permitting both the electrons and the vacancies or holes they left behind to move through the solid. If a potential difference is set up across the layer, the holes will move toward the more negative surface, the electrons toward the more positive signal electrode.

It was expected in accordance with this explanation that if a given number of light photons were absorbed by the surface in a given time, a current equivalent to a somewhat smaller number of electrons would be conducted through the film. Actually, under some circumstances, the charge transferred was equivalent to a number of electrons larger than the number of photons. This apparent inconsistency is explained by reasoning that if a charge carrier leaves one side of the semi-conductor layer, another may be injected to take its place. The general relation characterizing photo-conductivity can be expressed as $n = ft$. The relation between the current flowing through the layer and the number of charge carriers creasted is:

$$i = neuE$$

where:

   f is the number of charge carriers created per second per unit volume by the incident radiation

   n is the steady state increase in the density of charge carriers created by the incident light flux

   t is the life time of the carriers

   e is the electronic charge in coulombs

   u is the mobility of the carriers

   E is the applied electric field

It is important to note that t, the life time, may be several times as long as the time necessary for a given charge carrier to pass through the layer because of the probability that another charge carrier will be injected to take its place. It

15

is customary to operate a vidicon with as high an electric field, E, across the layer as possible in order to maximize the signal current. Under the control of the physicist developing the layer are the quantities f, u, and t. For sensitivity, it is desirable that all of these be increased. Unfortunately, an increase in t may mean the development of an undesirable memory for events that happened in a previous scan. It is generally true that experimental approaches to incrase vidicon sensitity can most easily be made at the expense of increased lag.

Whether because of the injection of additional charge carriers at the electrode surface or because of the transit time of carriers through the photoconductive layer, no modern vidicons can be operated at normal television scanning rates in such a manner that totally new information is presented at each 1/30 second frame time. Normal testing procedure for these tubes call for imaging a stationary scene, and for removing the illumination abruptly after stable operation has been achieved. Using an interlaced system, one would expect to find information in the first two fields scanned after removal of the illumination, even on an ideal tube. In normal testing, the amount of signal remaining on the third field is checked as a measure of persistence, and figures of 20 to 40% remanent signal compared to the initial steady state value are common. On the other hand, certain vidicons operated in slow scan service, in which the tube may be flash illuminated and then scanned after a period of several seconds, show much more complete erasure of information during read out, indicating that the transit time of the charge carriers contributing to lag through the photoconductor may be the most significant factor. The lag or persistence phenomena briefly described here are far more pronounced at low light level. The remanent signal appears to follow a decay curve with a large initial slope which changes to one with a long time constant for low level signals. This can probably be explained in terms of the effects of shallow traps within the photoconductor which fill during exposure, but empty gradually, releasing carriers for some time after the exposure is complete.

16

Despite its small size and technical and operational simplicity, the low sensitivity obtainable from the vidicon and the lag effect just described made it relatively undesireable as a starting point for research on camera tubes intended for high sensitivity applications.

b. The Image Orthicon

The second popular camera tube today is the image orthicon. Invented at the R.C.A. Laboratories during World War II, it was first described in an article, "The Image Orthicon - A Sensitive Television Pickup Tube", by Albert Rose, Paul K. Weimer, and H. B. Law, published in Proceedings of the I.R.E. $\underline{34}$ - 7 - 424, in July, 1946. Its primary advantages are its great sensitivity, its ability to accommodate rather wide variations in illumination level without saturating, and an action which tends to overpeak white to black transitions to make the picture appear crisper than on other types of camera tubes. Its disadvantages are related to the second and third advantages. Although the tube does not saturate at comparatively high light levels in the sense that a photographic film saturates when overexposed, the gray scale rendition is not faithful for brightly lighted scenes. Further, the electron redistribution effect, which accounts for the crispening of white to black transitions, also results in the generation of spurious signals in some types of operation. Also a disadvantage are the large physical size of the tube and of its associated components, the complexity of the associated circuitry, and the numerous adjustments which must be made and maintained to keep tube and camera in top operating condition during a telecast. Further, one major tube element, the storage target, represents a compromise design for normal 30 frame per second entertainment television scanning standards, so that the standard 5820 or 7198 image orthicon is basically unsuited for slow scan applications. To understand the reasons for these limitations, and the directions in which the design of these tubes may be improved, one must consider the operation of the image orthicon in detail.

17

SCHEMATIC ARRANGEMENT OF WL-5820
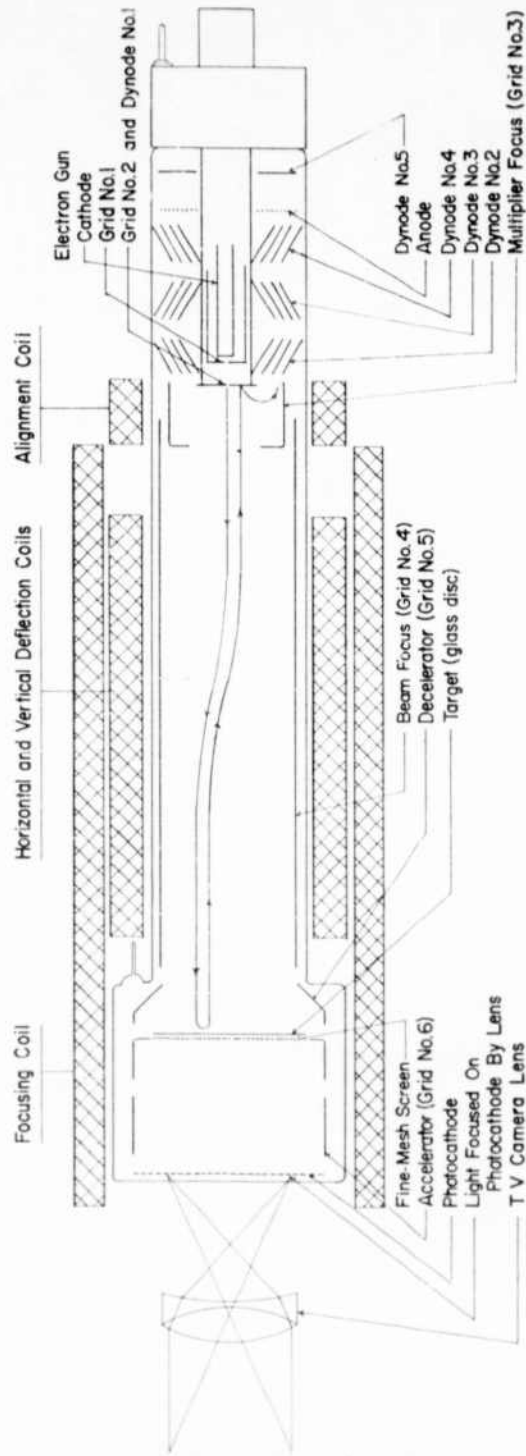
Figure 5. Schematic Arrangement of Wl-5820

As shown in Figure 5, a lens, positioned to the left of the tube is used to form an optical image of the scene being televised on the photo emissive layer which has been deposited on the inner surface of the optical quality faceplate at the left end of the tube. The function of this layer is to transform the optical image into a corresponding electrical image by emitting electrons to the right into the interior of the tube when light falls on it from the left. The number of electrons emitted at each point is, under normal circumstances, directly proportional to the intensity of the illumination in the image at that point.

The electrons are accelerated to the right through the application of a potential difference of several hundred volts between the photocathode and a thin copper mesh located about 1.8" to the right, and an axial magnetic focusing field is supplied by a solenoid which surrounds most of the tube. The distance between the photocathode and the mesh and the voltage difference applied between them are so chosen that electrons which leave the photocathode with a component of velocity perpendicular to the axis of the system describe one loop in the magnetic field before passing through the mesh and striking the glass membrane or target located just beyond it. Thus, to a first approximation all electrons leaving one point on the photocathode can be made to strike one point on the glass target. Those having a larger initial radial velocity component will describe larger loops, but since all electrons will require the same time to describe one loop, whatever the size, all will converge as they approach the target. Electrodes designated as G6 and target support cup in Figure 5 are supplied with proper voltages to set up a reasonably uniform electrostatic accelerating field in the region between the photocathode and the mesh. In practice, both the magnetic and the electrostatic field lines tend to flare slightly toward the photocathode so that both fields are weaker in this region.

The electrons passing through the mesh strike the glass target with sufficient

19

energy so that several secondary electrons are released from the target surface for each incident primary electron. Most of these secondaries are collected by the mesh, which is normally maintained a volt or two positive with respect to the surface of the glass target. Hence, after a short period of time, a positive charge pattern will be set up on the target, in which more positive areas will correspond to brighter areas in the optical image.

The rear or right hand side of the glass target is scanned by a low velocity electron beam in the same manner as has already been described for the vidicon. A beam of electrons originates from a thermionic cathode whose potential is close to that of the surface of the glass target. The electrons are accelerated toward the target by voltage applied to electrodes labeled G_2, G_3, and G_4, and focused by the axial magnetic field from the focusing solenoid. In the region just to the right of the target, the beam passes through a decelerating field caused jointly by the G_4 or wall coating electrode, G_5 or decelerating ring, and the target itself. If the target is negative with respect to the surface of the cathode from which the electrons originated, it is energetically not possible for the electrons to reach the target surface. If it is slightly positive, electrons can land on the target. These statements ignore the effects of electron emission velocities, contact potential differences, and work functions or electron affinities. The beam is caused to scan the target surface by the application of two sets of magnetic deflecting fields in the region between the electron gun and the target.

Those electrons which do not land, or which are reflected as they strike the target surface, are momentarily stopped near the right hand surface of the target in an electrostatic field which acts to urge them back toward the electron gun at the right end of the tube. These electrons will be refocused by the solenoidal magnetic field, but the influence of the second passage through the magnetic deflecting field

20

will be to cancel the first. Thus the returning beam will be focused and will strike the end of the electron gun not far from its point of origin. This returning electron beam will be shown to carry the video output signal information.

To amplify this signal in a relatively noise-free manner before it is fed to the video amplifier, the return beam is fed to an electron multiplier structure. To provide an effective first secondary electron emitting electrode, the end of the gun structure is covered with a metal cap, dynode #1, which has been coated with a secondary emitting material such as beryllium oxide, chronium oxide, or aluminum oxide. A very small hole is provided in the center of this cap to allow passage of the primary electron beam. Each electron in the returning beam strikes the first dynode with sufficient energy to release several secondary electrons. These in turn are accelerated into the pinwheel multiplier structure. Secondary emission gains for a typical five-stage electron multiplier are between 500 and 1500. The output current is closely proportional to the current in the return beam.

To understand the operation of the image orthicon, assume that the electron beam is caused to scan the target in a standard television scanning pattern while no light falls on the photocathode. Electrons will be deposited until the target surface has been uniformly charged to a potential equal to or just less than that of the thermionic cathode and the entire beam is being returned to the electron multiplier. Next assume that an element of the photocathode is illuminated immediately after the beam has scanned the corresponding element of the target. Electrons are emitted from the photocathode element, and accelerated and focused onto the corresponding target element. Secondary electrons leave the target element and are collected by the mesh, which was initially set to be a few volts positive with respect to the dark potential of the target. During the 1/30th second before it is next scanned, therefore, the target element is charged more positively, approaching the potential of the collector mesh at a rate depending on the brightness of the corresponding

21

photocathode illumination. When the electron beam returns to scan the element, charge is deposited on the element to restore the scanned surface again to gun cathode potential. Therefore, during the instant that the beam scans the element, the beam current returning to the multiplier, and hence the multiplier output current, is reduced. If the target element has not reached mesh potential between scans, the reduction in output current is nearly proportional to the intensity of photocathode illumination at the corresponding element.

Normally the entire photocathode is illuminated when a scene is imaged upon it. In this case the charge with respect to its dark potential which each element of the target acquires between scans is, for low light levels, proportional to the brightness of that element of the scene, and the current in the return beam is correspondingly reduced as that element is scanned. This return beam current from the scanning beam therefore carries a signal varying in time corresponding to brightness variations in the picture. Amplified by the electron multiplier structure, it is fed to the video amplifier and to suitable transmission circuits.

To understand the limitations of the tube this first order explanation of image orthicon operation requires some refinement:

1.) The Signal Transfer Characteristic

Curves showing typical output video signals as a function of photocathode illumination levels for three types of image orthicons are shown in Figure 6. In taking data for these curves, the mesh potential was set to be two volts positive with respect to that value which caused the picture to disappear by preventing beam electrons from landing. As indicated above, the output signal is essentially proportional to the input illumination for dimly lighted scenes. At these illumination levels, each target element acquires a small positive charge during a frame time, but its potential immediately before scanning is still appreciably more negative than the collector mesh. As the illumination level is increased, however, the voltage swing

22

INAGE ORTHICON TRANSFER CHARACTERISTICS

Highlight Illumination on Photocathode – Foot Candles
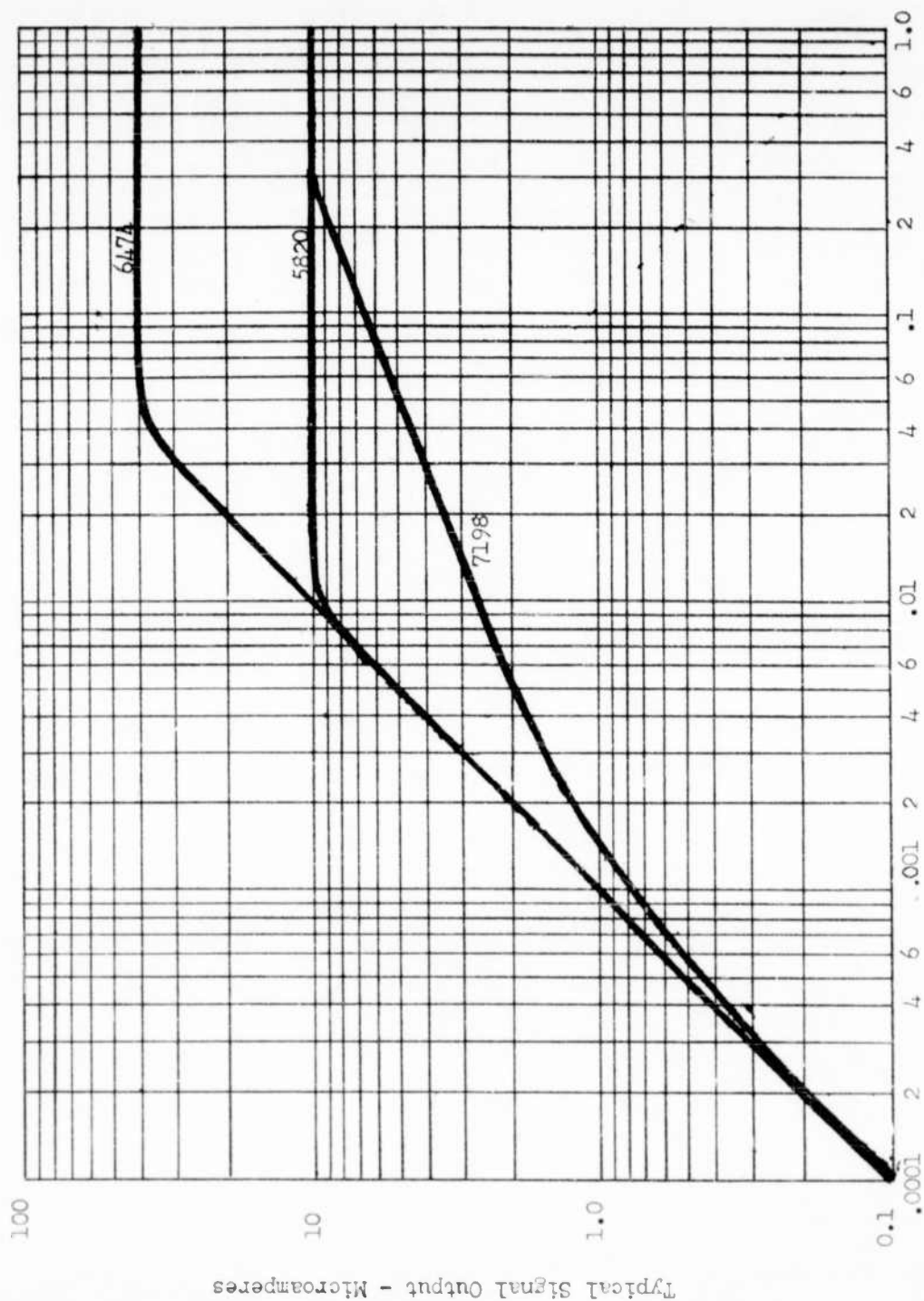
Figure 6. Image Orthicon Transfer Characteristics

of an element between scans approaches the mesh potential more closely, and the effectiveness of the mesh for collecting secondary electrons is reduced. Thus an increased flux of photoelectrons does not produce a corresponding increase in the positive charge pattern stored on the target, and the slope of the transfer curve decreases. For tubes like the 7198 with comparatively wide target to mesh spacing, in the order of .100", the change in slope of the transfer characteristic is gradual. For tubes with small target to mesh spacing, .002" for the 5820, .0005" for the 6474/1854, the slope changes abruptly from a proportional region to one in which the signal from white objects increases almost not at all as the illumination is increased. This point of sharp transition is known as the knee of the transfer characteristic.

Although the transfer characteristic for the 5820 and the 6474 indicates nearly complete saturation, the reproduced picture of a scene containing a number of bright areas all of which are over the knee shows a brightness difference between them. This rather surprising result is caused by the redistribution back onto the target of secondary electrons which are not collected by the mesh. The secondary electrons from the brightest area fall back on that area but also on all other nearby regions of the target. Thus if two adjacent bright areas are both over the knee, the larger current of redistributed secondaries from the brighter reduces the signal current to the less bright area, especially near the line of demarkation between them. Since the eye is very sensitive to changes in brightness across a dividing line, but not to gradual changes in brightness, the observer sees several shades of grey in the reproduced picture even though all grey areas by themselves are over the knee.

The redistribution of secondary electrons from a high signal area on the photocathode side of the target also tends to reduce the signal from adjoining darker areas even though none of them are over the knee. This effect, which becomes stronger

24

if the brighter object is over the knee, produces an artificial crispening of black to white transitions and an impression of improved resolution in the reproduced picture. Since this effect is subjectively desirable, television camera men in broadcasting studios normally operate their cameras so that the brightest objects in the scene will produce a photocathode current density which is two to four times the value for the knee. This mode of operation also improves the signal to noise ratio in the darker parts of the display.

Although these secondary electron redistribution effects give a desirable effect in some circumstances, they are undesirable in many others. For example, a single very bright object in a scene can obscure the information in surrounding dimly lighted areas by charging the corresponding target elements negative to black. This appears as a large black halo around the reproduced image of a bright spot. The secondary electrons from a positively charged bright area on the target can charge surrounding areas relatively negative because the average emission energy of the secondaries is of the order of two electron volts.

A typical charge-discharge cycle for a target element in a 5820 or 6294 is shown in figure 7. As indicated, the charging rate between scans is proportional to the light level, and constant with time until the target element approaches mesh potential. For a large area of constant illumination, the target and mesh can be considered like a planar diode. For normal light levels, the initial diode current immediately after a scan, when the target collector voltage is approximately two volts, is essentially emission limited and hence proportional to the photoelectron current. As the target approaches mesh potential, the collection current decreases, partly because of space charge and partly because of the poor collection efficiency of the mesh for secondary electrons whose emission energies may considerably exceed the target to mesh voltage at this time. Figure 8 shows typical paths for some of these

25
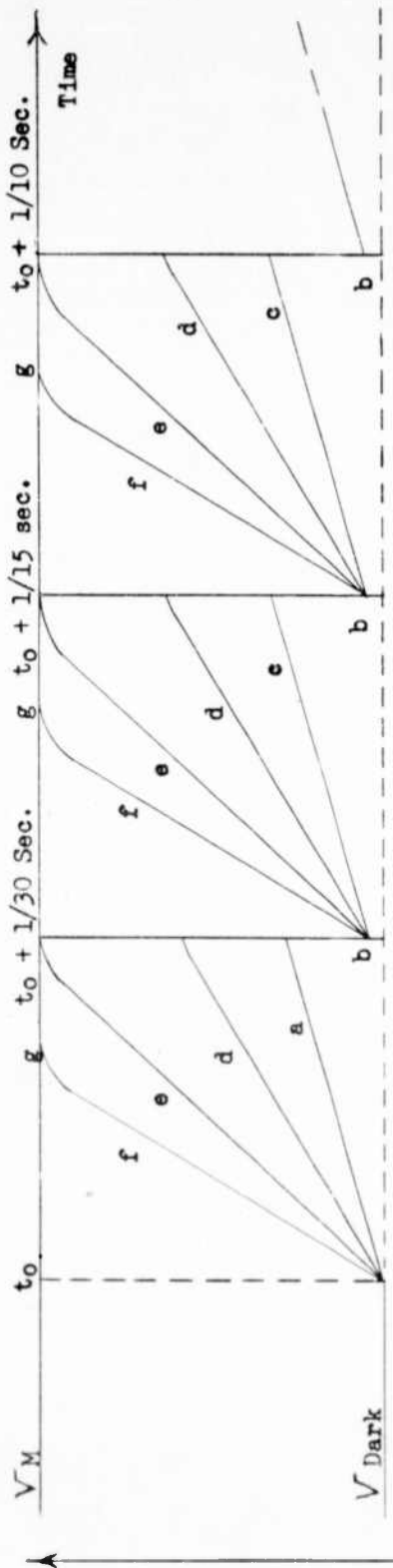
a. At low light levels, target element accumulates charge linearly with time for entire frame time.

b. Scanning reduces target element potential in time very short compared to frame time. Potential after scanning is more positive than when lens was capped because of velocity spread in beam, resistance through target.

c. Target element again charges at some constant rate with time, to slightly more positive potential.

d. At a higher light level, still below the knee, charging rate is higher but constant throughout a frame time.

e. At the knee, charging rate for a target element is constant for most of each frame time, but decreases just before each scan as the element approaches mesh potential.

f. Well above the knee, the target element reaches the mesh potential early in each frame time. Beyond point g the stored signal does not increase and redistribution effects become dominant.

Lens uncapped at t_o, immediately after scanning a given element.

Figure 7. Typical Change - Discharge Cycle for Image Orthicon

26

Some electrons strike mesh
on second transit →

High energy back
scattered electrons
return to target
far from origin

Mesh ⬭

Some electrons strike
mesh on first transit

Some electrons miss mesh
and return to target →

Target

- 0.10
- 0.75   0
- 0.50   -0.25
        -0.30
- 0.35
- 0.30
- 0.25

- 0.15 V

0 VOLTS

2   1.82 1.61 1.46 1.35v 1.26 V

+ 1.17 V
+ 1.08 V

+ 0.92 V

+ 0.56 V
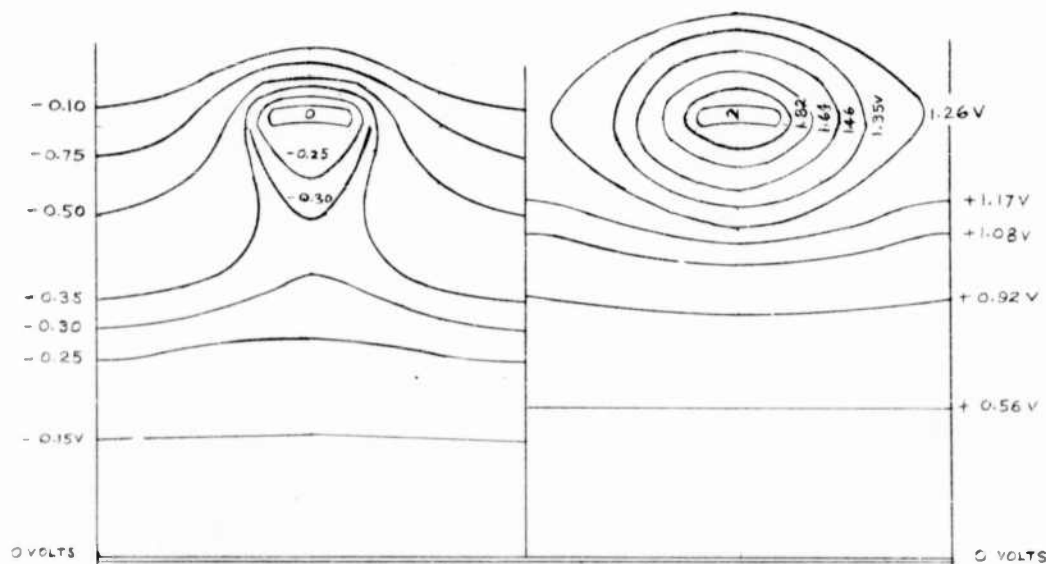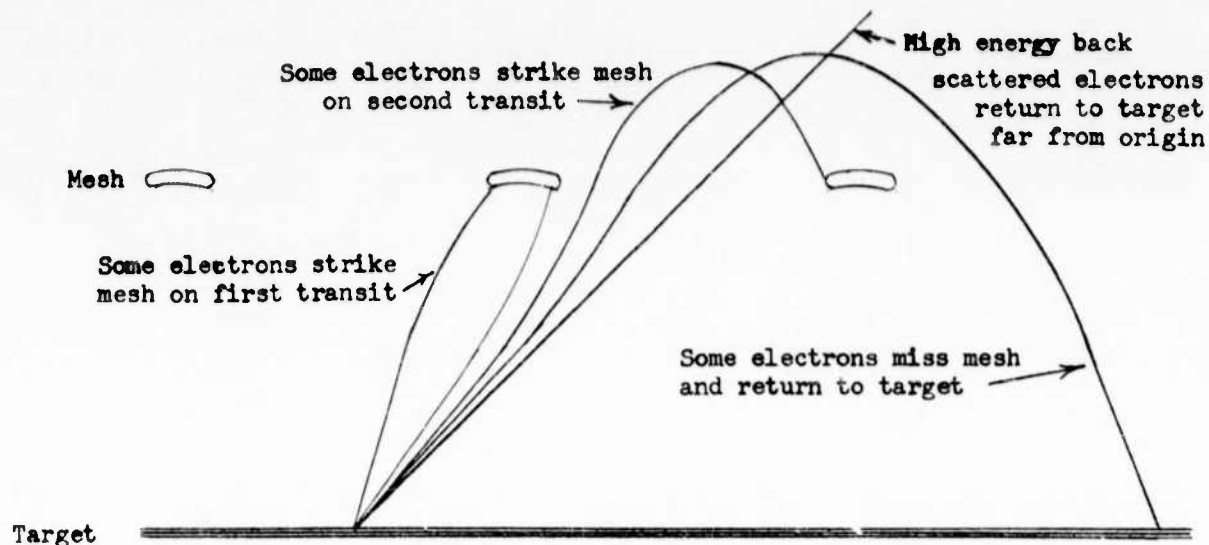
0 VOLTS

Mesh at 0 volts with respect
to target. Very weak field at
mesh results from voltage at
photocathode, has little in-
fluence on secondary electrons

Mesh at 2 volts with respect
to target. Field at mesh bends
secondary electrons toward
mesh bars increasing collection
efficiency.

ELECTRON TRAJECTORIES IN REGION OF IMAGE ORTHICON TARGET

Figure 8.   Typical Paths for Low Energy Electrons

27

low energy electrons. Passing through the mesh, they are reflected back toward the target by the field from the far more negative photocathode. Since the mesh is usually 65-70% open area, 70% of the scondaries pass through initially, and 70% of these return to the same or neighboring target elements. The close spaced tubes show a sharper transition region because of the stronger extraction field at the target produced by even a slightly positive collector mesh, and the reduction in space charge effects.

The value of illumination to reach the knee of the signal transfer curve may be calculated for the 5820 and 6474 by assuming that the capacitance between each target element and the target mesh is large compared to inter-element capacitance. To simplify the mathematics, all elements are considered to becharged as a unit, so that the target and mesh can be regarded as a parallel plate capacitor. For the 5820, the target mesh spacing is .002", the scanned area of the target is 1.12" x .84", and the calculated target mesh capacitance is 106 microfarads. To discharge such a capacitor in 1/30 second at a constant rate from an original 2 volt charge requires a current of 6.4×10^{-9} amperes. For a 5820 with a 60% transmission collector mesh, and assuming a secondary emission ratio for the target of 4, a target mesh assembly gain $G = T (\delta -1) = 1.8$ is realized where T is the optical transmission of the collector mesh and δ is the secondary emission ratio at the target. Hence the calculated charging current corresponds to a photocathode current of 3.6×10^{-9} amperes. Assuming 40 microampere per lumen photocathode, and an illuminated area of 1.28" x .96", this requires a photocathode illumination of 1.06 x 10^{-2} foot candles. The close agreement between this calculated illumination and the experimentally observed value of 1 x 10^{-2} foot candles is good evidence that this simple theory is adequate.

A further corrollary of this analysis is that the amount of information which

28

can be stored on the target mesh assembly in a frame time is limited. In a later section this will be shown to limit the maximum signal to noise ratio. To lengthen the linear part of the transfer characteristic, to increase the information handling capacity, and to improve the optimum signal to noise ratio, the type 6474 image orithicon is made with a nominal .0005" target mesh spacing. By the foregoing analysis, this raises the knee of the transfer characteristic to about 4×10^{-1} foot candles. The closer target to mesh spacing makes these tubes more likely to be microphonic. The 6474 is used primarily for color telecasting in a camera with 3 image orthicons. Since the signals from each of the 3 tubes must be combined to form the color signal, it is desirable in this application that the camera tubes be used only in the linear part of the transfer characteristic.

2.) The Action of the Target

As indicated above, the image orthicon target must perform several functions:

(1) The secondary emission ratio of the front or photocathode side should be as high as possible to produce a large stored signal from a limited photocathode current. As shown in Figure 9, the net charging current at the target is equal to

$$i_{ch} = i_{pr} \ (\delta - 1), \tag{1}$$

where i_{pr} is the photoelectron current reaching the target. This current will be less than the current leaving the photocathode, since some electrons will be intercepted by the collector mesh. Since the photoelectrons have been accelerated through 400 or more volts, they are essentially undeviated by the fields near the mesh, and the fraction which reach the target is essentially equal to the optical transmission of the mesh. Hence $i_{ch} = i_{po} \ t \ (\delta - 1)$

$$\text{or Gain} = \frac{i_{ch}}{i_{po}} = t \ (\delta - 1) \tag{2}$$

Typical type 5820 image orthicons with glass targets have measured gains of about 2. For an assumed mesh transmission of 65%, this corresponds to a secondary emission ratio, δ, of 4.

29

Photocathode   Mesh   Target
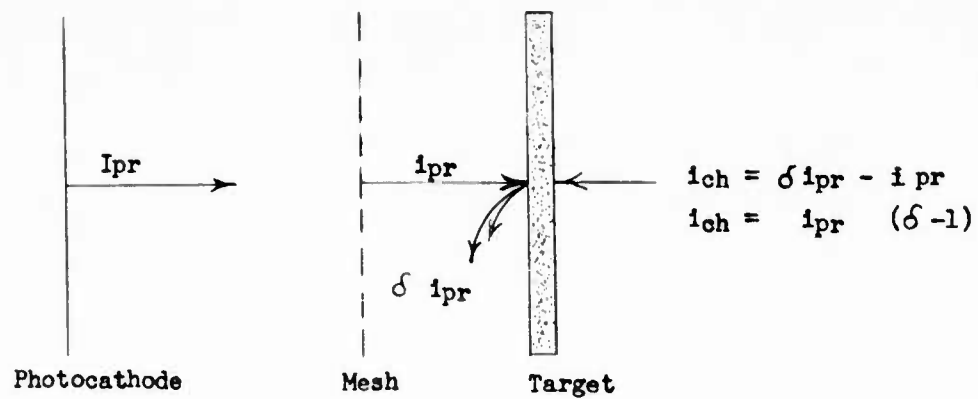
$$i_{ch} = \delta \, i_{pr} - i_{pr}$$

$$i_{ch} = i_{pr} \, (\delta - 1)$$

$$\text{Gain} = \frac{i_{ch}}{I_{pr}} = \frac{i_{pr} \, (\delta - 1)}{I_{pr}} = \frac{t \, I_{pr}}{I_{pr}} \, (\delta - 1)$$

$$= t \, (\delta - 1)$$

Figure 9. Target=Mesh Assembly Gain - Image Orthicon

30

(2) The charging current acts to create a positive charge pattern on the
photocathode side of the target. During the scanning process, the electrons from
the scanning beam are deposited to restore the scanned side of the target to the
potential of the scanning gun cathode, disregarding the effects of emission veloci-
ties and contact potential differences. Although a net charge is left on each sur-
face, the photocathode side of the target is restored nearly to its dark potential
because of the strong capacitative coupling through the target between its two sur-
faces. Immediately after the first scan the voltage across the target between the
surface of a given element will be equal to the signal charge transferred in that
frame time divided by the capacitance through the target. If the target swing was
2 volts, the charge transferred is $C_{tm}\Delta V$, the product of the target mesh capacitance
and the voltage swing corresponding to a highlight at the knee. Hence, the voltage
across the target after scanning will be

$$\frac{C_{tm}}{C_{tt}} \times 2 \text{ volts} \tag{3}$$

where C_{tm} is the capacitance between the active area of the target and the mesh, and
C_{tt} is the capacitance through the target between the corresponding active areas.
Since the active areas are the same, the ratios of the capacitances are

$$\frac{C_{tm}}{C_{tt}} = \epsilon_0 \frac{\frac{A}{d_{tm}}}{K\epsilon_0 \frac{A}{d_{tt}}} = \frac{d_{tt}}{K\, d_{tm}} = \frac{.0002}{5 \times .002} = \frac{1}{50} \tag{4}$$

where ϵ_0 is the permittivity of free space, K is the dielectric constant for the target
material, A is the active area, d_{tm} is the target mesh spacing, and d_{tt} is the thick-
ness of the target. Hence, the voltage across a target element immediately after
the first scan is .04 volts, if the target had been charged to the knee unless some
method is provided for charge conduction through the target, this remanent charge
will be increased in subsequent scans until the tube ceases to reproduce prictures
because the voltage across each target element reaches the potential difference be-
tween the collector mesh and the scanning gun cathode. In the image orthicon as

31

originally developed, this conduction is provided by making the target of glass whose resistivity at operating temperature is in the order of 10^{11} ohm centimeters. A homogeneous membrane of this glass, .0002" thick, is stretched across a supporting rim. The resistance through the 1.12" x .84" useful area of this target is then about 8.4×10^6 ohms. In a steady state condition, the signal or charging current at the target must be conducted through this resistance without an excessive voltage drop. Since for a 5820 the charging current for a white scene at the knee is 6.4×10^{-9} amperes, the maximum average steady state voltage drop across the target is 5.4×10^{-2} or .05 volts. This value is small compared to the normal 2 volt target mesh potential, and in general does not cause any objectionable memory effects.

(3) Although use of a homogeneous target made of a glass with a resistivity of 10^{11} ohm centimeters gives proper charge conduction through the target, there are three disadvantages. First, the resistivity of the glass changes rapidly with temperature, and proper tube operation is obtained in most broadcast studio equipment by thermostatic control of bulb temperature to $40^{\circ} \pm 2^{\circ}$ to $\pm 5^{\circ}$C. This range is inconveniently narrow for some military applications. Secondly, the standard glass target 5820 and similar image orthicon tubes have a rather limited operating life set by target performance. After several hundred hours, the tube tends to retian for some seconds or minutes a negative image of any scene whose electrical image is allowed to remain stationary on the target. This effect, known as "sticking", is thought to be due to a depletion of charge carriers in the glass target. Third and perhaps most important, the target glass not only conducts charge through itself parallel to the tube axis, but also provides lateral charge conductivity between adjacent image elements and acts to limit the amplitude of the reproduced signal from parts of the scene with fine detail. This lateral conductivity could be minimized by making the target substantially thinner, and in this case the bulk resistivity of the target glass could also be increased without causing objectionable voltage drop

32

through the target. However, glass targets are made by cutting a small section from a hand blown bubble and sealing it to a metal ring which has been previously enameled with a glass which melts at a lower temperature. With this technique target thickness could be decreased by at most a factor of 2, an insignificant improvement for most applications.

The effect of lateral charge leakage has been analyzed by H. B. DeVore: "Limiting Resolution in an Image Orthicon Type Pickup Tube", Proc. I.R.E., $\underline{36}$-3-335, March 1948. The results of DeVore's analysis are shown in Figure 10 as applied to a 5820 with parameters as shown in the figure. Although DeVore's assumptions make the results shown too pessimistic for resolution beyond 200 to 300 lines, the curve shows that lateral charge leakage limits tube performance even when the tube is used for standard 30 frames per second broadcast television. The critical assumption made in DeVore's article is that the capacitance between a resolution element on the target and the collector mesh is effective in determining the charge storage capacity for that element. This is true only if the target to mesh spacing is considerably smaller than the width of a resolution element. For a 5820, this condition is not satisfied for resolutions beyond 200 to 300 lines. For finer resolution patterns, the capacitance between each target element and all its surroundings becomes important, leading to a larger charge storage capacity, and therefore to greater resolution capability than are indicated in DeVore's analysis.

Unfortunately, for many military purposes, it is desirable to scan the tube more slowly than 30 frames per second. For example, in operation at very low light levels, there may be insufficient light available to form a useable picture each thirtieth of a second. For a film camera in such cases the operator lengthens the exposure time for each frame and reduces the frame rate. With an ideal camera tube also, acceptable pictures can be obtained at lower light levels by allowing a longer

33

Amplitude Response Relative to Coarse Test Pattern

Test Pattern Resolution in T.V. Lines per Pattern Height
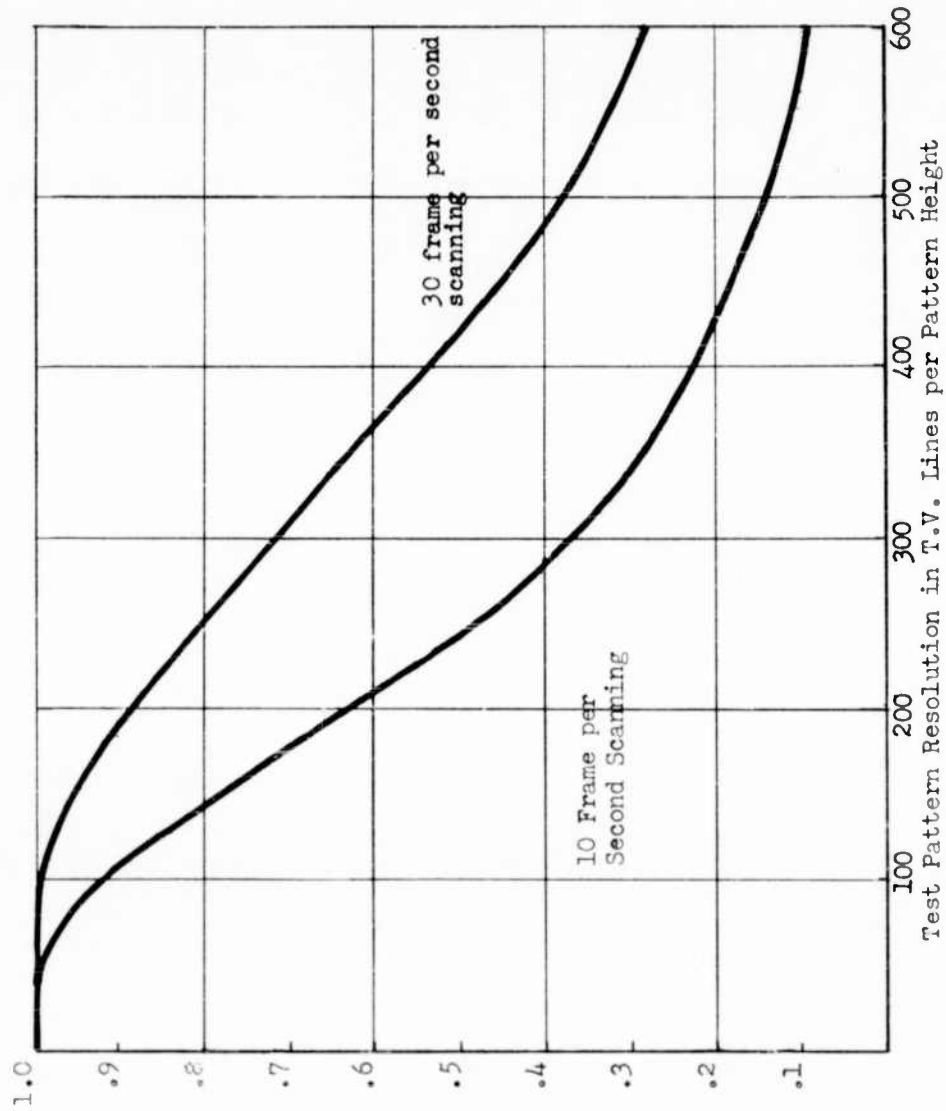
Target Thickness .0002"
Target Mesh Spacing .002"
Target Glass Resistivity 10" ohm cm.

Pattern Size on Target 1.12" x .84"
Square Wave 100% Contrast Test Pattern
Continuous Illumination Below the Knee

FIGURE 10

Amplitude Response at the Target for a 5820

34

exposure time for each frame. This procedure yields scant improvement for the 5820, 6474. or 7198 because lateral target leakage degrades the image severely at longer frame times as shown in Figure 10. Alternatively, for an application like mapping from an aircraft, it may be desireable to expose the camera tube for a relatively short time during each frame time to "stop" scene motion. In such cases, it is often desireable to scan without interlace over a period longer than 1/30 second to transmit the information over a data link of modest bandwidth. In this mode of operation, the degradation of image quality during the scanning period on a tube like a 5820 is definitely objectionable for scanning times longer than about 1/20 second.

Thus, the standard glass target represents a compromise. High performance image orthicons of the future will almost certainly use far thinner targets made by thin film techniques to obtain reduced lateral leakage, possibly in conjunction with creation of an anisotropic conductivity pattern to favor charge conduction through the target.

3.) Resolution Limitations - The Image Section

The photoelectrons in the image section of an image orthicon are focused at the target by use of a nearly uniform magnetic field. In such a field, any electron emitted with a velocity component perpendicular to the axis of the tube describes a helical path. The time to complete one loop of the helix is the same for all electrons, although the diameter of each loop is larger for electrons with larger radial velocity components. If the fields were completely uniform, focusing for this arrangement would be perfect except for the effects of varying photoelectron emission velocities parallel to the axis of the tube which cause variations in transit time to the target. This type of image defect is often compared to chromatic aberration in light optics and could be essentially eliminated if the emission energies of the photoelectrons were restricted to a very low value. According to the Einstein photo

35

electric equation

$$1/2 \, m v_0^2 = h_\nu - h_{\nu_0} = \frac{hc}{\lambda} - \frac{hc}{\lambda_0} \qquad (5)$$

where ν_0 is the frequency and λ_0 the longest wavelength of light which will produce photoemission from the photocathode. That is, the maximum kinetic energy of emission for a photoelectron is the energy of the exciting photon less the photoelectric work function, or minimum energy needed to remove a photoelectron from the surface. Electrons will leave the photocathode with energies up to this maximum, depending on whether the electron when initially excited started moving directly toward the surface or followed an oblique path, and on the energy state from which it was excited. To restrict the emission energy to low values, one may allow only exciting radiation with wavelengths near the long wavelength threshold to fall on the surface.

This type of imaging defect has been analyzed for a typical image orthicon image section by H. B. DeVore, "Limiting Resolution in an Image Orthicon Type Pickup Tube", Proc. I.R.E., 36-3-335, March 1948, and by H. Kanter, "Resolution Limitations in the Secondary Electron Image Amplifier", Westinghouse Research Report 6-94410-2-R14. Figure 11 shows the results of this analysis as applied to the image section of an image orthicon or image isocon when the illumination is monochromatic light of the wavelength indicated. The assumptions made include use of an S-10 photocathode with a long wavelength cutoff of 7000 angstroms, a uniform 75 gauss magnetic focusing field, 450 volts between the photocathode and the target, and use of a 2.8 centimeter pattern width at the target, all typical of standard tubes. A high contrast test pattern is assumed, and the result is expressed as the contrast in the photoelectron current image approaching the target to separate the effect of focusing imperfections from other factors. This data shows that to obtain a resolution of 1250 T.V. lines per pattern height (1650 lines in 2.8 cm) at 50% contrast, light of a wavelength no shorter than 6000 angstroms, or within 1000 angstroms of the long
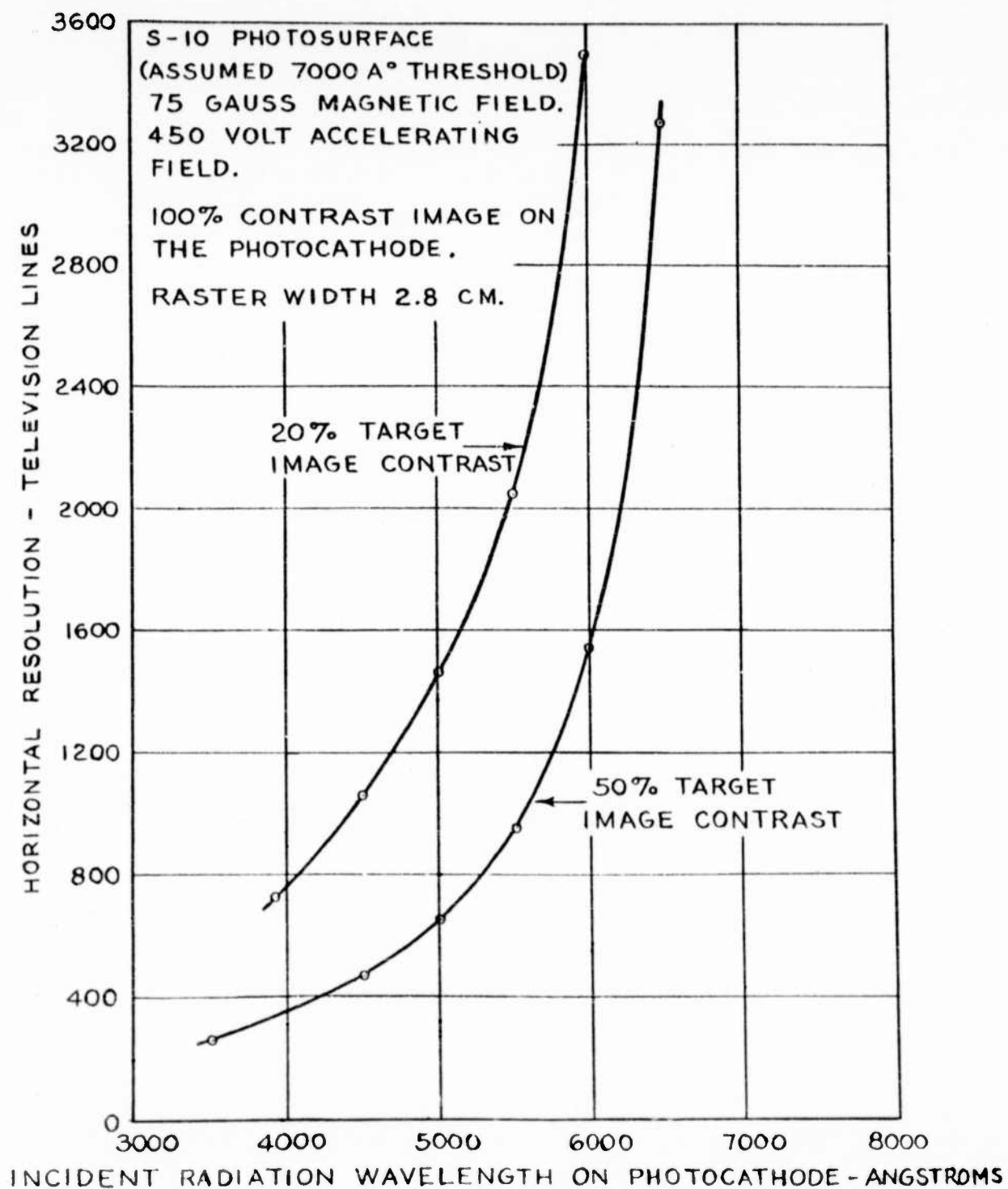
Figure 11. Theoretical Resolution of Photoelectron Current at the Target of an Image Orthicon

wavelength threshold must be used.

Experimental tests of limiting resolution on an image orthicon have been made in this laboratory, in which the scanning amplitude was reduced so that high resolution test pattern information could be reproduced without exceeding the frequency pass band capabilities of the video amplifiers in the available test equipment. Resolution patterns as fine as 3000 TV lines per standard pattern height have been reproduced. Under these conditions, some small difference in resolution could be seen when a 2000 line test pattern was alternately illuminated with red light and blue light. In practice, then, DeVore's analysis appears too pessimistic, as he indicates, since the image section focus adjustment is presumably set for electrons of an average emission energy, rather than for zero emission energy as assumed in the calculations, and because the assumptions on distribution energy and direction for the emitted electrons are very difficult to check and are probably incorrect. Results of the analysis are included, however, since they indicate that image section emission velocities should be considered as a limitation whenever extremely high resolutions are required.

A tube designer may improve the limiting resolution of an image section by increasing the electrostatic field at the surface of the photocathode. The result may be expressed as:

$$R = \frac{2}{\pi} \frac{V}{d} \frac{1}{V_o} \tag{6}$$

where: R is the limiting resolution

V is the image section accelerating voltage

d is the distance between the photocathode and the target or collector mesh

V_o is the emission energy in volts

For a typical magnetically focused image section, an increase in V/d can be accomplished by increasing the overall accelerating voltage V, or decreasing the

image section length d, but in either case the magnetic field must be increased to maintain image focus by shortening the period of revolution for radially moving electrons. The condition for focus with uniform magnetic and electrostatic fields is

$$B = \frac{\pi}{4} \sqrt{\frac{2m}{e}} \sqrt{V} \qquad (7)$$

where m and e are the mass and charge of the electron respectively and B is the magnetic flux density. Inspection of this equation shows that if image section voltage cannot be increased because, for example, of the secondary emission characteristics of the target, the resolution will also increase linearly with the magnetic field. The combined equation is:

$$R = \frac{1}{3} \frac{e}{m} B^2 d \frac{1}{\sqrt{V_0}} \qquad (8)$$

If V is to be kept constant, the product Bd must be kept constant. If however, the magnetic field is doubled and the image section length halved, the resolution will be doubled, as stated above.

4.) Sensitivity Limitations

Basic limitations on the sensitivity of any camera tube or light amplifier device are given in detail in the following sections. For an image orthicon, the principal limitations are those affecting the signal to noise ratio in the reproduced image. First, and most important, the type of scanning used in the image orthicon introduces a fairly large relatively constant noise contribution due to shot noise in the scanning beam. To optimize signal to noise ratio for greatest sensitivity, the signal current at the target should be made as large as possible before introduction of noise in the scanning process. This can be accomplished by use of more sensitive photocathodes, of targets with higher secondary emission gains, or by use of an image pre-amplifier ahead of the target. Further, the beam should be adjusted to be as small as possible while still completely charging the target to its dark potential. The required beam current is, as discussed below, a function of the

39

velocity distribution in the beam, and of the micro-structure of the scanned side of the target.

The second noise contribution limiting sensitivity in the image orthicon is the fluctuation signal generated in the camera tube load circuit and the video preamplifier. Known as Johnson noise, for a good low noise camera amplifier with the image orthicon load resistor operating at room temperature this fluctuation signal has an r.m.s. current value of approximately 2×10^{-9} amperes. One of the advantages of the image orthicon is that for normal scene brightnesses, its essentially noise free output electron multipler can be used to make the output signal large compared to the amplifier input noise. For low light level applications, however, care must be taken to supply sufficient overall tube gain so that the most dimly illuminated scene will produce a signal which is large compared to the Johnson noise.

Thirdly, there is the fundamental limitation on sensitivity set by the randomness of the photo emission process. Since photons are absorbed and photoelectrons are emitted randomly, when a scene is very dimly lighted one cannot be sure that in each frame time that more photoelectrons will leave the area of the photocathode which corresponds to a brighter area of the picture than one which corresponds to a dimmer area. This last effect sets a fundamental limitation for every light amplifying device and is discussed at length later in this report. The first and second limitations apply primarily to the image orthicon and are discussed here to complete the description of this tube.

(a) The Overall Gain Requirement

It was shown that the signal current at the target of a 5820 operating at the knee is about 6.4×10^{-9} amperes for a photocathode illumination of 1×10^{-2} foot candles. At this illumination level, the output signal current for a typical electron multiplier gain of 500 to 1500 is 3 to 9 microampers, far above the 2×10^{-9}

40

microampere amplifier input noise. However, such a camera tube can reproduce useful images with photocathode illuminations as low as 10^{-4} to 10^{-5} foot candles. The lower figure predicts an output signal of only 3 to 9 x 10^{-9} amperes if the multiplier gain is constant, and this output signal is of the order of the amplifier noise. Thus, the image orthicon with a good 5 stage multiplier has just adequate gain to override amplifier noise at its normal sensitivity threshold and if steps are taken to improve effective tube sensitivity by lowering the beam noise contribution, the overall tube gain may have to be increased to maintain the output signal above amplifier noise.

(b) Beam Noise in Image Orthicon Scanning

Of all limitations presently found to limit the sensitivity of this already sensitive camera tube, the shot noise contributed by the necessarily large scanning beam is a problem unique to the image orthicon. As explained in the introductory section describing the tube operation, the charge pattern is read from the storage target by scanning it with a beam of low energy electrons so that some of the electrons will land on the target to neutralize the charge, and the rest will return to an electron multiplier structure. When the beam is scanning a negatively charged target element corresponding to a black spot in the scene, all of the beam returns to the multiplier. When the beam scans a rather more positive element, corresponding to a light grey or white, some of the beam electrons land and the return beam current is momentarily reduced. In general this reduction, which constitutes the video signal, is never larger than about 30% of the beam current, and for dimly lighted scenes is usually much less. The amount of variation in the returning beam is defined as the modulation, M, so that $M\% = \dfrac{I_b - I_{rb}}{I_b}$ x 100. To maximize the modulation, the beam current is always adjusted to the minimum value which will supply the signal current for the brightest elements in the scene which is to be televised.

Experimental and theoretical data agree fairly well that the beam behaves as a

41

random noise generator, whose rms noise current output is

$$I_n = \sqrt{2e \, I_b \Delta f} \tag{9}$$

where e is the electronic charge, 1.6×10^{-19} coulombs, I_b is the beam current in amperes, and Δf is the system bandwidth in cycles per second. In televising low light level scenes, most of the beam is returned to the multiplier, and the signal at the target is divided by this entire noise current to obtain a signal to noise ratio which compares favorably with the experimentally measured value.

To indicate the importance of the beam shot noise, a calculation of the signal to noise ratio for a 5820 operating at the knee follows. As indicated in an earlier section, the signal current at the target is 6.4×10^{-9} amperes. This current must be supplied by the beam, but if 30% beam modulation is assumed, the beam current will be $\frac{1}{.3} \times 6.4 \times 10^{-9}$ or 2.1×10^{-8} amperes. Since the output electron multiplier is assumed to cause no degradation in signal to noise ratio, the ratio of signal at the target, 6.4×10^{-9} amperes, to beam noise,

$\sqrt{2eI\Delta f} = \sqrt{2 \times 1.6 \times 10^{-9} \text{ coul} \times 2.1 \times 10^{-8} \text{ amperes} \times 8 \times 10^{6} \text{ sec}^{-1}}$ is a valid signal to noise ratio, and gives a figure of 27.4:1. Use of an 8 megacycle video bandwidth is assumed. This value compares with a measured value of 35:1, indicating that the beam noise is indeed dominant in limiting signal to noise ratio. This limiting value for well lighted scenes can be raised if the signal handling capability of the target is raised. The 6474, which can store a signal 4 times as large, will require a beam current 4 times as large if modulation is assumed constant. Since the signal to noise ratio varies as $I_{sig.} / \sqrt{I_{beam}}$, the 6474 will achieve essentially twice the optimum signal to noise ratio of the 5820.

At lower light levels, the signal to noise ratio for the 5820 will be poorer. If the photocathode illumination for objects in a given scene extends from the knee, 10^{-2} foot candles in the highlights, to a very low value, the beam current must be

set to discharge the highlights. Grey areas corresponding to a photocathode illumination of 3×10^{-4} foot candles will then give a signal to noise ratio of 1, and less bright detail will be essentially lost. If generally dim scenes are to be televised, the beam current is usually reduced to a value just sufficient to discharge the highlights in that scene. If the beam modulation in the highlights were that which was obtained at the knee, the signal to noise ratio would decrease as the square root of the signal current. Unfortunately, the optimum beam modulation decreases rapidly photocathode illumination decreases, and a 5920 in general gives a barely discernable picture at 10^{-2} foot candles highlight illumination even though the beam current is reduced as much as possible.

The reasons for low beam modulation are these: First, the beam electrons approach the target at very low velocity. While phenomena in this velocity range are difficult to study, we believe that of those electrons which actually strike the target surface, only about half remain. The rest interact with the surface but are scattered back toward the multiplier. On an electronic scale, the glass surface is very rough and the scattering process is the result of interactions between the field of a beam electron and the fields of the particles which make up the glass surface. The process is probably not elastic, and the velocity components after scattering are often far different from those of the incident electrons. This fact is used in the image isocon, another type of camera tube described below. Now, if only 50% of those which reach the target remain, under any circumstances the beam modulation will never exceed 50% of that which would otherwise be calculated. The process by which these very low energy electrons interact with the surface is one on which more knowledge is needed, since an improvement in scanning efficiency would help to obtain higher signal to noise ratios and greater sensitivity.

A second fundamental and more important factor limiting beam modulation is the

43

electron velocity spread in the scanning beam. Since the electron beam is made to approach the surface of the target at nearly zero energy, the number of beam electrons which land on any target element is a function of the instantaneous potential of that element and of the kinetic energy of the beam electrons. Hence, small variations in beam electron energy exert a very significant effect on tube operation. Properly speaking, it is not the kinetic energy of the beam electrons, but rather that portion of the kinetic energy of each electron which is associated with its forward motion, parallel to the tube axis, which determines whether a given electron can land on a target element at a given voltage. If all electrons approached the target normal to its surface and if all had the same energy, all could land on an element which was slightly positive, none could land on an element slightly negative with respect to the zero point for kinetic energy. If a given beam electron started from rest at the cathode were accelerated by the electron gun, and decelerated as it approached the target, it would just reach a target element at cathode potential, provided that none of its energy had been converted to motion in a plane perpendicular to the tube axis. This statement neglects the effects of contact potentials and work functions. Unfortunately, the beam electrons do not all start from rest at the cathode, but are emitted from the surface with energies ranging from zero up to several tenths of a volt. The emission velocities are distributed also in direction. Further, the potential of the surface of an oxide coated cathode from which current is being drawn is, on a microscopic scale, probably not uniform, and the work function probably varies from microscopic point to point. Additionally, the electric and magnetic fields used to form, accelerate, and focus the beam may tend to transfer some energy to a motion perpendicular to the tube axis, and although all electrons may have been accelerated through the same potential drop, the forward component of their motion may vary considerably.

44

All of these effects combine to produce a rather large spread in the paraxial velocity components of the electrons approaching the target, and measurements, although admittedly difficult to perform, have shown a spread of more that a volt under some conditions, although the spread in emission energies alone is only .1 or .2 volts. Hence, the instantaneous current landing on a target element depends on the instantaneous potential of the element, on the total beam current, and on the distribution in paraxial kinetic energy for the beam electrons. Although other factors are important in broadening the distribution, authors such as Dr. Hans Heil, "On Image Defects Arising From the Electron Velocity Distribution in the Reading Beam of Image Orthicons" published in the Proceedings of the Image Intensifier Symposium, October 6-7, 1958 by U.S. Army Engineer Research and Development Laboratory. or R. J. Floyd, whose analysis is Appendix I of this report, have deduced a reasonable explanation of the action of the beam in discharging the target by assuming a Maxwellian distribution and using the relation $I_{target} = \text{const} \times I_{beam} \times \exp \frac{eV}{kT}$ (10)

where V is the instantaneous potential of the target surface, usually negative, with respect to the gun cathode, T the effective temperature of the beam in degrees Kelvin, higher than the actual cathode temperature because of the broadening effects, and e the electronic charge and k the Boltzman constant respectively.

This relation emphasizes that if the target is scanned repeatedly while the lens is capped, its potential will be brought to a value far negative with respect to the value at which an electron starting from rest at the cathode would just land, and the beam current landing on the target will increase very slowly as the target is made more positive from this dark point. If a very dim scene is imaged on the photocathode, a small current of photoelectrons will strike the target, creating a small positive signal current which acts to charge the target mesh capacitance during the first frame time. Although beam electrons will land on each target element

45

.005

0   -1   -2   -2.3   -3   -4

Target Voltage In Units Of $\frac{kT}{e}$
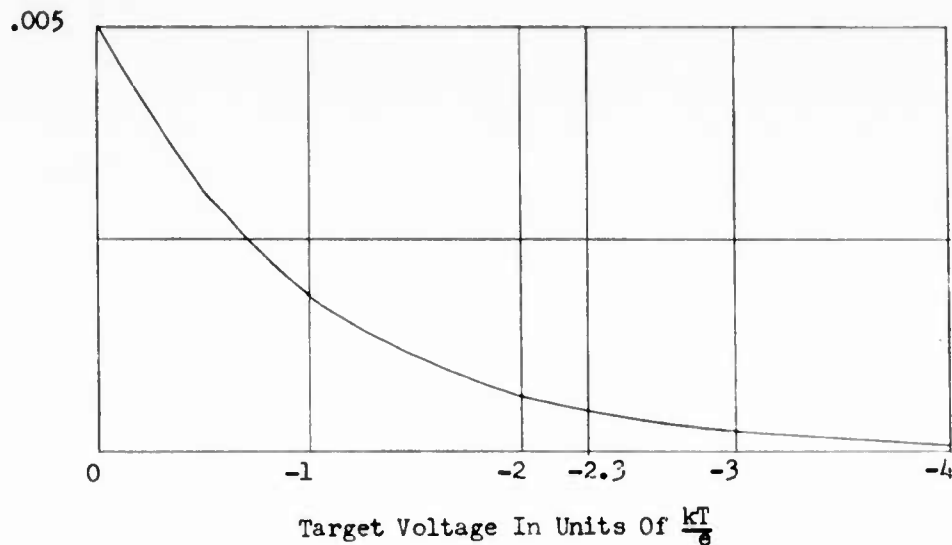
Measured beam spread of 1 volt corresponds to 2.3 $\frac{kT}{e}$. At very low signal levels, target is several volts negative, only very small currents can land, and beam will require several frames to establish equilibrium after change in signal level.

$$I_{Target} = \text{Constant} \times I_{Beam} \times \exp\frac{ev}{kT}$$

ASSUMPTIONS: Constant= 0.5

I_{Beam}= 0.01

e= 1.6×10^{-19} coulomb

v= Instantaneous target voltage below values at which all current lands

k= Boltzmanns Constant = 1.38×10^{-23} Joules/degree K

T= Effective Temperature of Beam

Figure 12. Charging Current as a Function of Target Voltage

46

when scanned, the current is so small that the target is not restored to its previous condition. The same amount of charge is added to the target by removal of secondary electrons in the second frame time, and again the beam lands more electrons but not enough to neutralize the charge created by the signal current. This process is repeated many times until the operating voltage of the target reaches a value at which the beam can deposit sufficient electrons to equal the signal current which is charging the target. The process can be most easily visualized by reference to Figure 12 which shows the instantaneous current which a typical .01 microampere beam can land as a function of target voltage. The current which the beam can deposit on a given target element is the integral of the instantaneous target current between the voltages existing just before and just after the beam scans the element. These in turn are a function of the voltage before scanning, of the target-mesh capacitance, and of the time during which some part of the beam is directed at a given element. When a steady state has been reached, the current deposited will equal the secondary electron current leaving such element in a frame time. The time to reach equilibrium may be many frame times, or even several seconds for a low light level scene.

Conversely, when the image of a low light level scene is removed from the tube, the beam will require several scans to charge the target to its stable dark potential. Although the target current, and therefore the output signal, will be smaller in each successive scan, an image of a near threshold scene can often be seen for many seconds after the lens has been capped, and a time in the order of seconds is required to reach full signal conditions after re-opening the lens. This lag effect limits the ability of the image orthicon to reproduce an image containing motion when very low light levels are used. To minimize stabilization time, image orthicons for low light levels usually use wide spaced, low capacitance target mesh assemblies.

47

Any preamplifying means which increases the charge information stored on the target at a given light level will also act to reduce the lag effect at that light level.

Ideally, the low level lag effect could be greatly reduced and modulation increased if the broad "axial" energy distribution in the beam could be narrowed. Some improvement can be effected by use of gun designs to minimize axial velocity spreads above the emission velocity distribution. However, this emission velocity spread still has a high energy "tail", and a means for narrowing it has been sought by many investigators. Various velocity analyzers were investigated in the course of the research for which this is the final report but our theory and experiment agree that the rather narrow range into which most of the emitted electrons fall can probably not be narrowed in a practical tube. This is fully discussed in a later section of this report.

5.) Summary

The foregoing discussion of the image orthicon emphasizes some of its disadvantages. Not emphasized was the excellent sensitivity of commercial tubes available at the start of this research, nor the fact that phenomena like the lag effect at low light levels have their parallels in the physiological adjustments of the human eye and have advantages, for example, in smoothing out the effects of statistical fluctuations in the incoming information at low light levels. Because of these advantages, the image orthicon was selected as the basis for most of the research conducted under the subject contract. At the conclusion of this research program, it is apparent that the most important and fruitful approaches to greater sensititity were those in which the charge to be stored on the target was amplified before the noise inherent in the scanning process was introduced into the system. These and other approaches are discussed in the body of the report.

c. Image Isocon

As indicated in the preceding section, the principal limitation to obtaining improved sensitivity from a standard image orthicon is the shot noise in the scanning electron beam. In the image orthicon, essentially the entire scanning beam is returned to the multiplier in the darkest parts of the picture, while a somewhat smaller current is returned when scanning parts of the target corresponding to bright objects in the scene. Thus, maximum return beam noise is generated for those areas of the picture in which the picture is weakest. Since the type of scanning in which a signal is derived from electrons returning from the target permits use of an output electron multiplier and hence removes the sensitivity limitation due to video amplifier noise, Dr. P. K. Weimer and associates at the R.C.A. Research Laboratories investigated an alternate method of deriving the video signal. As described in the preceding section, of those electrons which strike the target, approximately half remain and the other half are non-specularly scattered by interaction with the fields of the atomic particles in the target surface. Dr. Weimer reasoned that if a way could be devised to separate these scattered electrons from those which were reflected in the region ahead of the target because they lacked the energy to reach the target surface, a video signal could be derived which would be essentially zero in the darker parts of the picture and would reach a maximum when the beam was scanning a target element corresponding to a brightly illuminated area. This type of tube, called the image isocon, was described by Dr. Weimer in an article entitled "The Image Isocon - An Experimental Television Pickup Tube Based on the Scattering of Low Velocity Electrons" published in the R.C.A. Review for September, 1949.

Dr. Weimer accomplished separation by causing the normal return beam of the image orthicon to strike one small area near the axis of the electron gun. The scattered electrons on the other hand landed in a somewhat larger area because they

49

had received an additional transverse energy component in the scattering process. Some of these electrons he caused to enter an electron multiplier structure through a small off-axis aperture. To direct the scattered electrons into the multiplier, and to make sure that the reflected electrons did not enter the multiplier, Dr. Weimer incorporated certain additional electrodes for the beam alignment and for the prevention of any scanning motion in the return beam.

A principal problem in the development of a practical isocon is the attainment of complete separation between the scattered and reflected return beams. Methods used at the time of this research included the discarding of half of the desired scattered electrons in order to effect this separation. Further, a field defining mesh used on the scanned side of the target to eliminate scanning motion in the returning beam of reflected electrons caused an additional noise contribution. Since the scattered and reflected electrons were being separated on an energy basis, we believed that development work on the isocon could profitably be delayed until means for narrowing the velocity spread in the electron scanning beam has been achieved. For these reasons, and because of added critical adjustments then considered necessary for isocon operation, we elected not to pursue work on this type but instead to concentrate on preamplifier structures for the image orthicon to provide improved signal-to-noise ratio and better sensitivity.

d. The Westinghouse Ebicon

As indicated in the section on the image orthicon. it is most desirable that image signal amplification be incorporated in any camera tube ahead of the scanning process. In the image orthicon, some amplification is achieved through secondary emission gain in the target. As shown in a later section on signal to noise limitations, for image orthicon type return beam scanning a pre-beam gain of at least 100 is needed in order that the scanning beam noise not be a dominant factor limiting

sensitivity. It is also obvious that a camera tube for maximum usefulness to the military should be simple and compact and use straight forward circuitry requiring little or no maintenance and adjustment. The vidicon described in the introductory section is the simplest of modern camera tubes and operates in many low cost cameras over long periods of time without attention. A highly worthwhile goal would be a combination of tube components to achieve high image signal preamplification before the scanning process in a tube having otherwise the operating simplicity of the vidicon. An approach to this tube is the Westinghouse Ebicon shown in Figure 13.

In this tube, the scene to be televised is imaged on a photoemissive cathode on the inner surface of the optical window at the left end of the bulb. The emitted photoelectrons are accelerated and focused by electrostatic, or by a combination of electrostatic and magnetic fields, and caused to strike a thin semi-conductor target. As shown in Figure 14, this target consists of a thin electron permeable aluminum layer and a semi-conductor layer having high resistance in its unexcited state.

Figure 13. Ebicon

51a

Primary Electrons

Al$_2$O$_3$ (1300A$^\circ$)

Support Ring

Al (1300A$^\circ$)

Selenium (3-5u)

Scanning Electrons
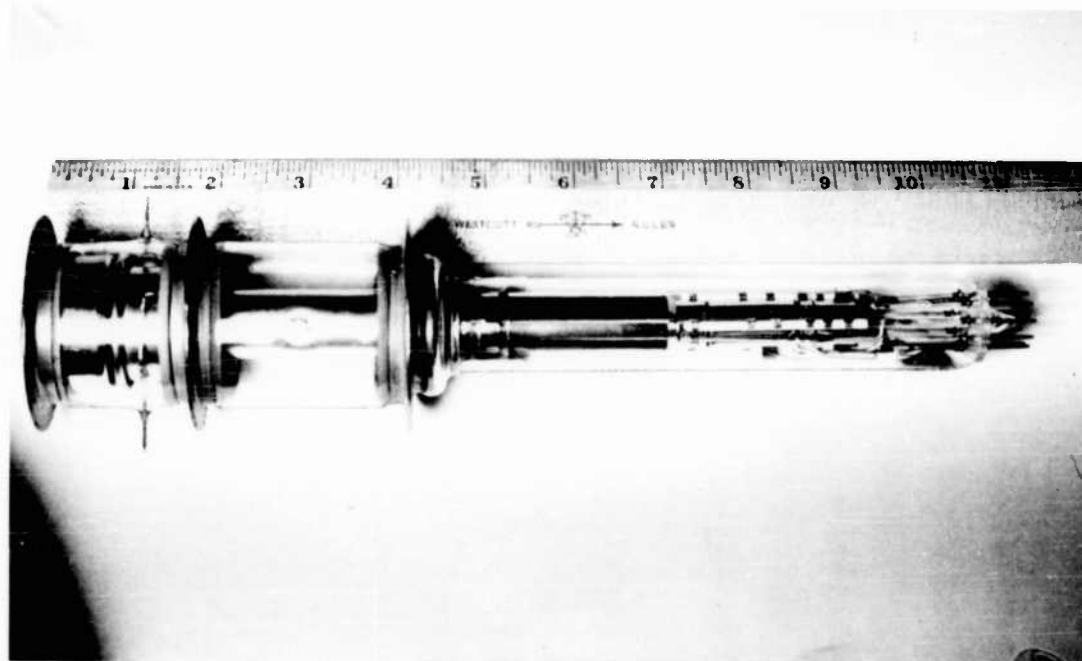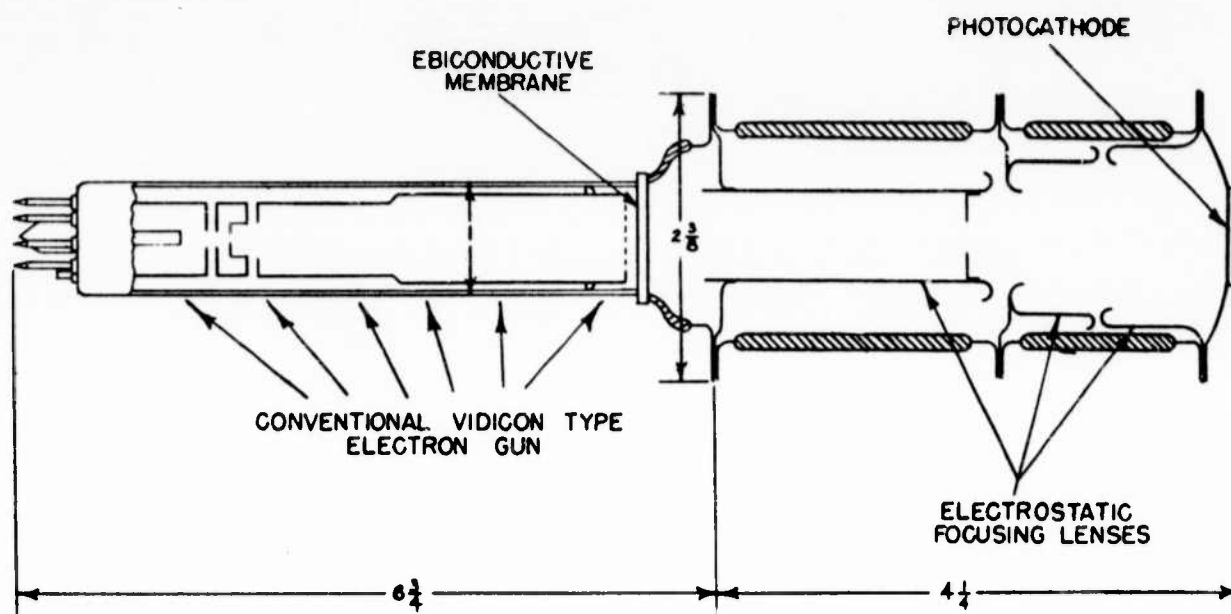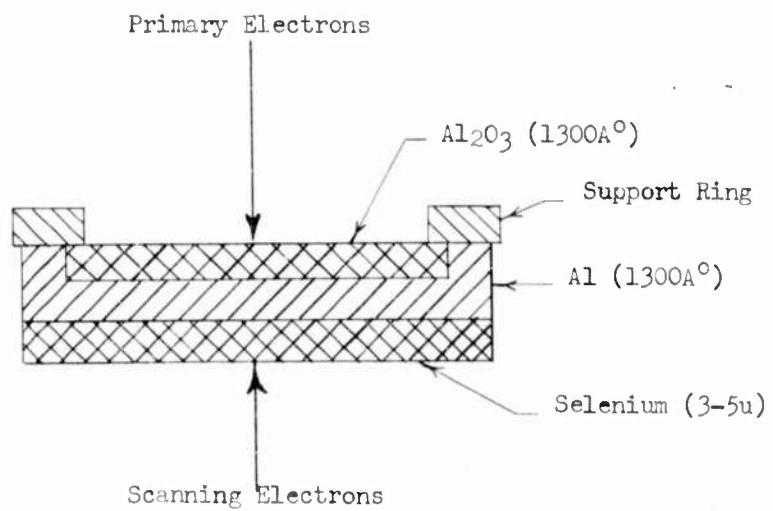
Figure 14. Ebicon Target

The electrons, accelerated through a potential drop of 10 to 20 kilovolts, pass through the aluminum but are absorbed in the semi-conductor with the release of many charge carriers. As in the vidicon, the free side of this layer is scanned with a low energy electron beam so that, if the optical lens is capped and no photoelectrons reach the layer, the free surface is soon charged to scanning gun cathode potential. If now the lens is opened, photoelectrons are emitted from the photocathode and strike the layer. In laboratory tests, it has been shown that from several hundred to 1000 or more charge carriers traverse the semi-conductor layer for each photoelectron which strikes it. As in the photoconductive layer of the vidicon, the electrons travel to the more positive aluminum signal electrode, the holes travel to the free or scanned side of the semi-conductor, and the voltage difference across the layer decreases at a rate which is a function of photocathode illumination. When the electron beam returns to scan a given element, charge is deposited to restore the free surface of that element to gun cathode potential, and a pulse of electrons is capacitively coupled to the signal electrode, which is in turn connected through a load resistor to the positive target voltage power supply, and through a coupling capacitor to the video amplifier. A requirement for any sensitive camera tube is that the output signal be larger than the effective input noise of the video preamplifier at the lowest light levels from which an output image must be obtained. The Ebicon pictured in Figure 13 has an input photocathode area $1/2$"x $3/8$" or 1.3×10^{-3} square feet. Assuming use of a multi-alkali photosurface with a sensitivity of 150 microamperes per lumen and an effective EBIC target gain of 500, a highlight photocathode illumination of 2×10^{-5} ft. candles would be required to obtain a signal equal to the assumed 2×10^{-9} amperes preamplifier input noise current. By analogy with the vidicon, we can assume that this would be close to the threshold for a simple Ebicon, that is for one without an output electron multiplier. Thus, the predicted sensitivity of the simple Ebicon is in the order

53

of that now obtained from a type 5820 image orthicon. Although some work was done on the Ebicon early in ther period covered by this report, it was decided jointly with the Air Force task scientist not to emphasize this approach since, at that time, several low voltage approaches to image preamplification seemed promising. It was subsequently decided under a separate procurement to sponsor research on a version of the Ebicon using a return beam multiplier for optimum sensitivity under Air Force Contract AF33(616)6496 which is now active.

SECTION III

PERFORMANCE LIMITATIONS OF IMAGE ORTHICON

1. INTRODUCTION

The most sensitive basic television camera tube in general use today is the image orthicon. Despite its demonstrated sensitivity, however, the image orthicon has certain significant performance limitations in the conversion of an optical signal into an electrical signal. Its principal limitations, particularly at low light levels, are discussed below.

In camera tubes of the image orthicon type, the optical input is converted into a photoemissive current which is then stored in the form of electrical charges on an insulating membrane or target. This distribution of charge is the integrated input over the time interval between scanning of the target surface by an electron beam. The video signal is generated by modulation of the scanning beam resulting from a neutralization of the accumulated positive charges on the target surface by the removal of electrons from the beam. The electron beam used to scan the stored charge image on the target introduces a substantial spurious signal due to random fluctuations in beam current density. Because of the polarity of signal employed, this shot noise is greater at the lower light levels. Furthermore, with a range of brightness in a given scene, the optimum beam current required to discharge a high light area on the target is in excess of the value required to discharge a low light area. The shot noise of this excess beam current acts to further degrade the low light level performance. In normal operation, this noise contribution is well above the shot noise associated with the photoemissive cathode and establishes the noise level at the output of the tube. When the desired signal falls significantly below this noise level, picture quality becomes too poor to be useful. A measure of the quality of tube performance or resolution capability is the ratio of the useful signal to the spurious signal, referred to as the signal to noise ratio. One can then consider the

55

signal to noise ratio developed at the output of the tube as a limiting factor in the "seeing" ability or limiting image detectability of the tube.

Since the upper limit of signal to noise ratio is determined at the input transducer, it is obviously desirable to use a high sensitivity photocathode to generate a large signal current for a given incident radiant flux. Within the present state of the art, however, there are practical limits to photoemissive cathode sensitivities, so that one must resort to other means for improving the signal to noise ratio developed by the tube. In view of the major noise contribution by the electron beam used to scan the stored charge image on the target, it would then be desirable to amplify the signal subsequent to leaving the input photocathode and prior to arriving at the target. This can be accomplished by various means such as the use of secondary electron emission multiplier or image intensifier stages. It is clear that the requirements for such pre-scanning beam amplifier stages would be high electron gain, low noise contribution, and high resolution capability. Another method of improving the signal to noise ratio is to increase the electron gain at the target by increasing the secondary emission yield of the target surface. This has been accomplished by the use of specially fabricated targets.

Because only a fraction of the broad spectrum of electron beam velocities is able to land on the target and neutralize a charged element, only a small part of the scanning beam is modulated even in the highlight areas. At low light levels, this beam modulation becomes a very small fraction. This contributes to a further degradation of the signal to noise ratio. To improve the scanning beam modulation and, therefore, the signal to noise ratio developed by the tube, one can consider reducing the axial velocity spread of the electron beam by some method of velocity selection.

Another serious limitation in the performance of the image orthicon is the effect of lateral charge leakage in the storage target. This lateral flow of charge effectively reduces the signal to noise ratio at the target by decreasing the signal

amplitude in parts of the scene containing fine detail, thereby degrading resolution. This leakage becomes especially significant in a standard image orthicon if the time required to complete one scan is greater than the normal 1/30 second. A significant improvement in the resolution capability of an image orthicon has been achieved by the use of a thin film insulator storage target. Signal storage and integration without serious resolution degradation, have been demonstrated with such targets over periods up to ten seconds.

The electron multiplier structure of the image orthicon normally assumed to supply essentially noise-free signal amplification does in fact make a substantial noise contribution and may, under certain circumstances, also act to limit the amplitude of the signal, thus degrading the signal to noise ratio.

The only truly fundamental limitation in any camera tube is the random or statistical nature of the process by which the information bearing photocurrent or signal is generated by the photocathode. Because of the quantum nature of light and random nature of photocurrent, in any given sampling time, fewer electrons may actually leave an area of the photocathode corresponding to a bright part of the image than from a neighboring area corresponding to the darker part of the image. This variation in signal at the input transducer imposes an upper limit to the signal to noise ratio that the tube is capable of developing at a given light level, i.e. the tube is said to be photocathode noise limited. This limiting signal to noise ratio is determined by the following factors:

(1) Photocathode illumination - This establishes the rate of arrival of information bearing quanta at the photocathode. Because of the random nature of the process by which quanta is radiated from the scene being imaged, there is a fluctuation in their rate of arrival at the photocathode. For photoemissive cathodes, this noise contribution is well below that due to the shot noise of the photocurrent due to the fact that each incident quanta does not result in the ejection of a photoelectron.

57

(2) **Photocathode sensitivity** - This is usually expressed in terms of microamperes of photocurrent per lumen of incident luminous flux of a given spectral distribution such as a tungsten lamp operating at $2870^\circ K$, in terms of microamperes of photocurrent per microwatt of incident radiant power at each wavelength over a given spectral range, or in terms of quantum efficiency, i.e. the number of photoelectrons generated per incident light quanta at each wavelength over a given spectral range. Peak photoemissive quantum efficiencies are in the order of 20 to 25% for the most sensitive photosurfaces in current use.

(3) **Contrast ratio of the scene being imaged** - This is defined as the ratio of the difference in light quanta per unit time leaving a "white" elemental area of the scene and the light quanta leaving an equivalent elemental area of the scene due to overall background brightness to the light quanta leaving the "white" element, or:

$$C = \frac{F - F_D}{F} \tag{1}$$

Essentially, the ability of a camera tube to image the pattern in a scene being viewed depends upon its ability to discern the variations in brightness over the scene. The signal can be defined as the difference between the total photocurrent leaving a "white" element of the photocathode and the current leaving an element due to background brightness. The signal to noise ratio developed by the tube and therefore the image quality improves with higher contrast ratio.

(4) **Photocathode dark current** - Thermionic electron emission of dark current from the photocathode will act to reduce the contrast ratio in the electron image generated by the photocathode, particularly at low light levels. It is necessary, therefore, to consider the effect of spurious photocathode dark emission on the signal to noise ratio. If the number of spurious electrons per unit time leaving each elemental area of the photocathode is n, the new reduced contrast ratio then becomes:

$$C = \frac{F - F_D}{F + n}$$

58

(5) Scanning time interval - This is defined as the period of the repetitive scanning of the target by the electron beam. Since the distribution of electrical charge on the target is the integrated input over the time interval between scanning of the target by an electron beam, one can increase the signal amplitude by extending this scanning interval. Because the signal increases linearly with storage time, while the noise increases as the square root, there is a resultant improvement in the signal to noise ratio. An implicit assumption is the ability of the target to integrate and store electrical charge without degradation in contrast ratio at the target due to lateral charge leakage.

2. PHOTOCATHODE LIMITATIONS

The random nature of photoemission means that while on the average more electrons leave a photocathode area which is more brightly illuminated than a less illuminated area, in any given sampling time, the actual number of electrons may deviate from the average value. By statistical analysis, the root mean square of the deviations from the average number of electrons leaving a picture element in a sampling or frame time will be the square root of the average number. Thus, if N is the average number, $\sqrt{N}$ is the fluctuation and the average to fluctuation or signal-to-noise ratio is $\frac{N}{\sqrt{N}}$ or $\sqrt{N}$.

Let us now apply this reasoning to the photocathode of an image orthicon. Consider a scene consisting of a resolution pattern with vertical alternate black and white bars of equal width. Selecting elemental square areas of one bar width and assuming a complete absence of electron emission from the black elements, corresponding to a contrast ratio of unity, an idealized signal waveform leaving the photocathode can be represented as follows:

where i = photocurrent leaving white elements of image.

Consider now the effects of scene background brightness and dark current due to thermionic emission. Since these effects tend to degrade the contrast ratio in the electron image, the idealized signal waveform assumes the following shape:
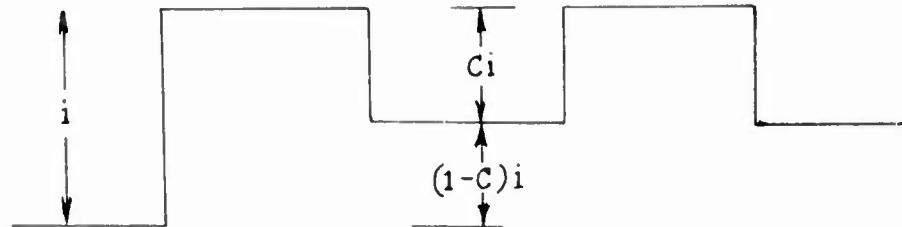
where: i = Total current leaving white element of image. This includes current due to brightness of white elements in scene being imaged, and dark current due to thermionic emission.

$(1 -C)i$ = current leaving black element of image. This includes current due to scene background brightness and dark current due to thermionic emission.

$Ci = 1 - (1 - C)i = Ci$ = signal current

C = Contrast ratio of electron image leaving photocathode

Where no spurious population exists or where the spurious population is small compared to the signal population, the contrast ratio of the electron image, C, is equivalent to the contrst ratio of the scene:

$$C = C_{Scene} = \frac{F - F_D}{F} \tag{3}$$

where: F = population in electrons per second leaving white element of image.
F_D = population in electrons per second leaving black element of image.

60

At low light levels, photocathode dark emission will act to reduce the contrast in the electron image. It is necessary, therefore, to consider the effect of spurious photocathode emission. If the number of spurious electrons per second leaving each resolution element of the photocathode is n, the new reduced contrast is given by the following equation:

$$C = \frac{F - F_D}{F + n} \tag{4}$$

The signal to noise ratio associated with the photocathode can be expressed as follows:

$$\frac{\text{Signal}}{\text{Noise}} = \frac{\text{Number of signal photoelectrons}}{\sqrt{\left(\begin{array}{l}\text{fluctuations in photoelectrons}\\\text{from white element}\end{array}\right)^2 + \left(\begin{array}{l}\text{Fluctuations in}\\\text{photoelectrons}\\\text{from black element}\end{array}\right)^2}}$$

Let us define the following quantities:

L = sensitivity of photocathode in amperes/lumen

A = area of photocathode in square feet

E = photocathode illumination in foot-candles

s = number of resolution elements = $\frac{4}{3} N^2$ assuming the standard 4 X 3 aspect ratio and a resolution N in TV lines.

e = electronic charge = 1.6×10^{-19} coulombs

T = target exposure time or frame time in seconds.

From the above, we can write the signal leaving the photocathode as follows:

$$\sigma = FT - F_D T = \frac{LAET}{se} - \frac{(1-C) \, LAET}{se}$$

or

$$\sigma = \frac{CLAET}{se} \tag{5}$$

61

The fluctuations in photoelectron current or noise for the white and black elements respectively are:

$$\nu_\omega = \sqrt{FT} \quad = \quad \sqrt{\frac{LAET}{se}} \tag{6}$$

$$\nu_b = \sqrt{\frac{F\,T}{D}} \quad = \sqrt{\frac{(1-C)\,LAET}{se}} \tag{7}$$

Combining the noise contributions:

$$\nu = \sqrt{\nu_w^{\,2} + \nu_b^{\,2}} \quad = \sqrt{\frac{LAET}{se}} \,(2-0) \tag{8}$$

The signal to noise ratio associated with the photocathode current can then be written as:

$$\frac{\sigma}{\nu} = \frac{\dfrac{CLAET}{se}}{\sqrt{\dfrac{(2-C)\,LAET}{se}}}$$

$$\frac{\sigma}{\nu} = C\sqrt{\frac{LAET}{se\,(2-C)}} \tag{9}$$

Substituting the relation:

$$S = \frac{4}{3}\,N^2$$

Where N = resolution in TV lines we obtain:

$$\frac{\sigma}{\nu} = C\sqrt{\frac{3\,LAET}{4eN^2\,(2-C)}} \tag{10}$$

The curves shown in Figure 15 thru 18 show the theoretical performance at various values of photocathode sensitivity, target integration time, resolution, and contrast ratio as predicted by Eq. (10). The effects of spurious photocathode emission (n) are shown in the dotted portions of the curves.

The dependence of the theoretical performance limit of an imaging device upon the quantum fluctuation noise of the signal itself has been investigated by J. W.

62

Coltman and A. E. Anderson of the Westinghouse Research Laboratories. (Reference 1) Experiments were conducted on the ability of the eye to recognize a regular bar pattern delineated by randomly fluctuating scintillations and the data used to calculate the resolving power of an ideal image intensifier. The experiments indicate that the eye can just reconstruct a useful image when the signal to noise ratio at each signal element is somewhat less than unity. This apparent paradox is thought to be due to the eye's ability to integrate the available information spatially and in time, combining the output of a number of nearby information elements to recognize a resolution pattern or similar scene.

On the basis of Coltman's experiments, the following general relationship is derived:

$$F \left[\frac{C^2}{2-C} \right] = 1.9N^2 \left[\frac{1}{(T/0.2)^2 + 1} \right] 1/2 \qquad (11)$$

where: F = population in electrons per second of white bars of pattern.

N = limiting resolution in total number of bars.

T = frame time in seconds.

C = contrast ratio of image.

This equation can be rewritten as a function of illumination (E) on the photocathode by relating population to brightness, knowing the photon to electron conversion efficiency of the photocathode and its area. Thus, a photocathode with a sensitivity of 100 ua per lumen, an area of 8.5 sq. cm. will emit 5.7×10^{12} electrons per second with a photocathode illumination of 1 lumen per square foot.

$$F = 5.7 \times 10^{12} \ E$$

Combining the two equations, we have the noise limited resolution:

$$N^2 = \left(\frac{C^2}{2-C} \right) \left[\left(\frac{T}{0.2} \right)^2 + 1 \right]^{1/2} 3 \times 10^{12} \ E \qquad 12)$$

63

Figure 15
Signal/Noise Ratio vs Photocathode Illumination

(Photocathode sensitivity as parameter)

$$\text{Eq. (10)} \quad \frac{\sigma}{\nu} = C \sqrt{\frac{3IAET}{4eN^2(2-C)}}$$

L = photocathode sensitivity in ua per lumen.
C = contrast ratio = 1.0
A = photocathode area = .01 sq. ft.
T = target integration time = 1/30 sec.
N = resolution in TV lines = 400
e = electron charge = 1.6 x 10^{-19} coulombs
n = no. of spurious electrons per second per resolution element.

L=250 ua/lu
L=150 ua/lu
L= 50 ua/lu

n = 10

Signal/Noise Ratio $\left(\frac{\sigma}{\nu}\right)$

E - Photocathode Illumination (Ft. Candles)

64

Figure 16
Signal/Noise Ratio vs Photocathode
Illumination
(Target integration time as parameter)

Eq. (10) $\dfrac{\sigma}{\nu} = C\sqrt{\dfrac{3LAET}{4eN^2(2-C)}}$

T = target integration time in sec.
C = contrast ratio = 1.0
L = photocathode sensitivity = 150 x 10⁻⁶ amp/lumen
A = photocathode area = .01 sq. ft.
N = resolution in TV lines = 400
e = electron charge = 1.6 x 10⁻¹⁹ coulombs
n = no. of spurious electrons per second per
    resolution element.

T = 1 sec.

T = 1/30 sec.

n = 10

n = 10

E - Photocathode Illumination (Ft. Candles)

Signal/Noise Ratio ($\frac{\sigma}{\nu}$)

Figure 17
Signal/Noise Ratio vs Photocathode
Illumination

Eq. (10) $\frac{S}{N} = C \sqrt{\frac{LAET}{4eN^2(2-C)}}$ (Resolution as parameter)

N = resolution in TV lines.
C = contrast ratio = 1.0
L = photocathode sensitivity = 150 x 10⁻⁶ amp/lumen
A = photocathode area = .01 sq. ft.
T = target integration time = 1/30 sec.
e = electron charge = 1.6 x 10⁻¹⁹ coulombs
n = no. of spurious electrons per second per resolution
    element.

200 TV Lines

400 TV Lines

n = 10

n = 10

E - Photocathode Illumination (Ft. Candles)

Signal/Noise Ratio $\left(\frac{S}{N}\right)$

Figure 18
Signal/Noise Ratio vs Photocathode
Illumination

(contrast ratio as parameter)

Eq.(10) $\frac{\sigma}{\gamma} = C \sqrt{\frac{3 LAET}{4eN^2(2-C)}}$

C = contrast ratio
L = photocathode sensitivity = 150×10^{-6} amp/lumen
A = photocathode area = .01 sq. ft.
T = target integration time = 1/30 sec.
N = resolution in TV lines = 400
e = electron charge = 1.6×10^{-19} coulombs
n = no. of spurious electrons per second per
    resolution element.

E - Photocathode Illumination   (Ft. Candles)

Signal/Noise Ratio $\left(\frac{1}{\sigma}\right)$

67

The contrast ratio of the image is determined by:

$$C = \frac{F - F_D}{F + n}$$

where: F_D = population in electrons per second of black bars of pattern

n = spurious population in electrons per second due to dark emission.

The straight line portions of the cruves shown in Figure 19 are plotted from the Eq. (12) where the spurious population n is equal to zero. The curves are terminated at the higher resolution value by approaching the 420 lines set by the system bandwidth. Smoothing between these curves is done by the usual inverse square combining formula for resolution. At low light levels, photocathode dark emission will act to reduce the contrast in the image and thereby reduce the resolving power of the system. The lower end of the 0.2 second frame time, 100% scene contrast curve is drawn for n equal to 10^3 electrons per second and the lower end of the 1/30 second frame time curve for 30% contrast is drawn for n equal to 10^4 electrons per second. These curves clearly show the importance of reducing spurious emission from the photocathode.

Extrapolating the straight line portion of the 1/30 second frame time, 100% contrast curve of Figure 19, it can be seen that a limiting resolution of 400 TV lines is predicted at a photocathode illumination of 5.5×10^{-8} foot-candles, with noise set by signal fluctuations. For the 1 second frame time, 100% contrast curve, a limiting resolution of 400 TV lines is just detected at 10^{-8} foot candles.

3. SCANNING BEAM NOISE LIMITATION

In the previous section, the signal to noise ratio was determined solely by quanta limitations at the photocathode. In the image orthicon, other sources of noise, primarily the noise contribution of the scanning beam, determine the signal to noise ratios developed by the tube. Let us define the following additional quantities:

68
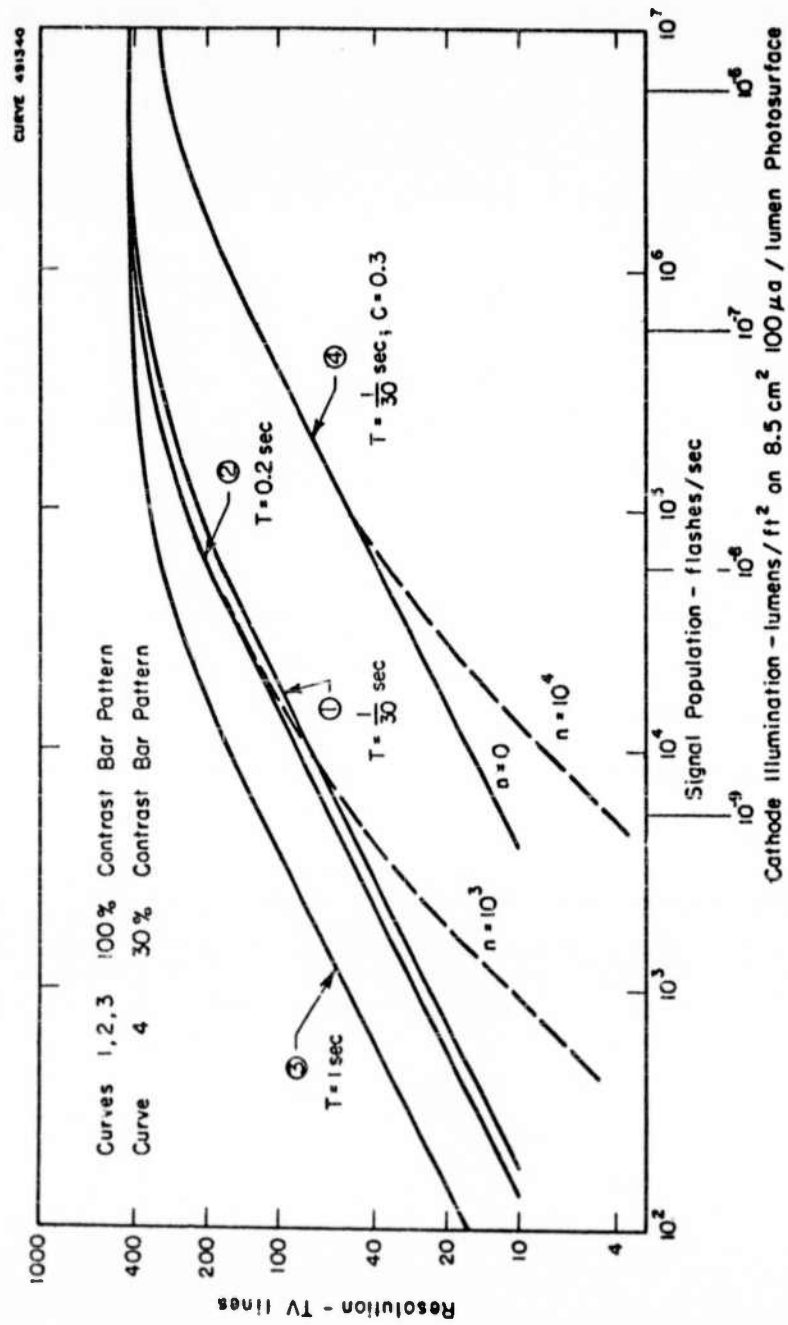
Figure 19. Limiting Resolution for a 4 mc Brandwidth TV system with Noise Set by Signal Fluctuations

69

i_b = total scanning beam current arriving at target of tube.

i_{r_b} = return beam current from a resolution element on target.

$i_b - i_{rb}$ = current necessary to discharge a resolution element on target.

G_t = amplification of signal by secondary emission yield on writing side of target

M = maximum modulation of scanning beam at target.

For the white elements the return beam current is:

$$i_{rbw} = i_b - G_t i = \frac{G_t i}{M} - G_t i = G_t i \left(\frac{1}{M} - 1 \right)$$

where: $G_t i$ = current necessary to discharge white elements of target.

Similarly for the black elements:

$$i_{rbb} = i_b - (1-C)\ G_t i = (i_b - G_t i) + C G_t i$$
$$= \left(\frac{G_t i}{M} - G_t i \right) + C G_t i = G_t i \left(\frac{1}{M} - 1 + C \right)$$

where: $(1-C)\ G_t i$ = current necessary to discharge black elements of target. We can now consider the noise contributions from all sources: Amplification of noise associated with fluctuations in photoelectrons from white element of photocathode =

$G_t \sqrt{\frac{iT}{se}}$ Amplification of noise associated with fluctuations in photoelectrons from black element of photocathode = $G_t \sqrt{\frac{(1-C)\ iT}{s\ e}}$

Noise associated with amplified current from white element at target = $\sqrt{\frac{G_t iT}{s\ e}}$

Noise associated with amplified current from black element at target =

$$\sqrt{\frac{(1-C)\ G_t iT}{s\ e}}$$

Noise associated with return beam current from white element of target =

$$\sqrt{\frac{(\frac{1}{M}-1)\, G_t iT}{s\ e}}$$

Noise associated with return beam current from black element of target =

$$\sqrt{\frac{(\frac{1}{M}-1 \neq C)\, G_t iT}{s\ e}}$$

Combining all the noise contributions:

$$\nu^2 = \frac{G_t^2 iT}{s\ e} + \frac{(1-C)\, G_t^2 iT}{s\ e} + \frac{G_t iT}{s\ e} + \frac{(1-C)G_t iT}{s\ e} + \frac{(\frac{1}{M}-1)G_t iT}{s\ e}$$

$$+ \frac{G_t iT\, (\frac{1}{M}-1+C)}{s\ e}$$

$$\nu = \sqrt{\frac{G_t iT}{s\ e}\left[G_t\ (2-C) + \frac{2}{M}\right]} \tag{13}$$

The signal arriving at the electron multiplier section of the tube can be expressed
as: $\sigma = \frac{G_t iT}{s\ e} - \frac{(1-C)G_t iT}{s\ e}$

$$\sigma = \frac{CG_t iT}{s\ e} \tag{14}$$

Assuming no degradiation in the multiplier section, the signal to noise ratio for

the image orthicon then becomes:

$$\frac{\sigma}{\nu} = \frac{\frac{CG_t iT}{s\ e}}{\sqrt{\frac{G_t iT}{se}\left[G_t\ (2-C) \neq \frac{2}{m}\right]}}$$

$$\frac{\sigma}{\nu} = C\sqrt{\frac{iT}{s_e\left[(2-C)\neq \frac{2}{MG_t}\right]}} \tag{15}$$

Substituting:

$$i = IAE$$

$$\frac{\sigma}{\gamma} = C \sqrt{\frac{IAET}{se\left[(2-C) + \frac{2}{MG_t}\right]}} \tag{16}$$

Substituting the relation:

$$s = \frac{4}{3} N^2$$

$$\frac{\sigma}{\gamma} = C \sqrt{\frac{3IAET}{4eN^2\left[(2-C) \frac{2}{MG_t}\right]}} \tag{17}$$

Plots of Eq. (17) are shown in Figures 20 and 21 together with the curve of the photocathode noise limited equation (10).

4. APPROACHES TOWARD IMPROVED PERFORMANCE

One can approach the theoretical performance limit of a camera tube, imposed by quanta limitations at the photocathode, by the use of pre-scanning beam amplification. The signal to noise ratio determination is similar to the one made in the previous section. Let G_p represent the gain in the preamplifier stage.

Consider the noise contribution from all sources.

The noise associated with the current leaving a white element of the photocathode is $\sqrt{\frac{iT}{se}}$

This is amplified to become $G_t G_p \sqrt{\frac{iT}{se}}$ at the target.

The noise associated with the current leaving a black element of the photocathode is $\sqrt{\frac{(1-C) iT}{se}}$

This is amplified to become $G_t G_p \sqrt{\frac{(1-C) iT}{se}}$ at the target.

The current emitted from a white element of the pre-beam electron multiplier stage is $\frac{G_p iT}{se}$. The noise associated with this current is $\sqrt{\frac{G_p iT}{se}}$ which is amplified at the target to become $G_t \sqrt{\frac{G_p iT}{se}}$.

Similarly, for a black element this noise contribution

becomes $G_t \sqrt{\dfrac{(1-C)\, G_p\, iT}{se}}$

The current arriving at a white element of the target has an

associated noise equal to $\sqrt{\dfrac{G_t G_p iT}{se}}$.

Similarly for a black element this noise contribution

becomes $\sqrt{\dfrac{(1-C)\, G_t G_p iT}{se}}$.

Noise associated with return beam current from white element
of target is $\sqrt{\dfrac{(\frac{1}{M} - 1) G_t G_p iT}{se}}$.

Noise associated with return beam current from black element
of target is $\sqrt{\dfrac{(\frac{1}{M} - 1 + C) G_t G_p iT}{se}}$.

Combining all the noise contributions:

$$\gamma^2 = \frac{G_t{}^2 G_p{}^2 iT}{se} + \frac{G_t{}^2 G_p{}^2 (1-C) iT}{se} + \frac{G_t{}^2 G_p iT}{se} + \frac{G_t{}^2 G_p (1-C) iT}{se}$$

$$+ \frac{G_t G_p iT}{se} + \frac{G_t G_p iT (1-C)}{se} + \frac{G_t G_p iT(\frac{1}{M} - 1)}{se} + \frac{G_t G_p iT(\frac{1}{M} - 1 + C)}{se}$$

$$\gamma = \sqrt{\frac{G_t G_p iT}{se} \left[G_t(G_p + 1)\ (2-C) + \frac{2}{M} \right]} \tag{18}$$

The signal arriving at the electron multiplier section of the tube can be
expressed as:

$$\sigma = \frac{G_t G_p iT}{se} - \frac{G_t G_p (1-C)\ iT}{se} \tag{19}$$

$$\sigma = \frac{C G_t G_p iT}{se}$$

Assuming no degradation in the multiplier section, the signal to
noise ratio then becomes:

$$\frac{\sigma}{\gamma} = \frac{\dfrac{C G_t G_p iT}{se}}{\sqrt{\dfrac{G_t G_p iT}{se} \left[(2-C)\ (G_t G_p + G_t)\ \frac{2}{M} \right]}}$$

$$\frac{\sigma}{\nu} = C\sqrt{se\left[(2-C)\left(1+\frac{1}{G_p}\right)+\frac{2}{MG_tG_p}\right]iT} \qquad (20)$$

Substituting:

$$i = LAE$$

$$\frac{\sigma}{\nu} = C\sqrt{se\left[(2-C)\left(1+\frac{1}{G_p}\right)+\frac{2}{MG_tG_p}\right]LAET} \qquad (21)$$

Substituting:

$$s = \frac{4}{3}N^2$$

we obtain:

$$\frac{\sigma}{\nu} = C\sqrt{4eN^2\left[(2-C)\left(1+\frac{1}{G_p}\right)+\frac{2}{MG_tG_p}\right]3LAET} \qquad (22)$$

As developed, Eq. (22) represents the signal to noise ratio limitations of an image orthicon with pre-scanning beam amplification. A basic assumption implicit in the result is that the target has perfect storage capability so that there is no lateral diffusion of charge during the scanning interval. The effect of the secondary emission multiplier section in the output of the tube on the overall signal to noise ratio has not been considered. From Eq. (22) it can be seen that there are several ways in which the overall signal to noise ratio of the image orthicon can be permitted to approach the basic signal to noise limitation imposed by the photocathode.

Figure 22 is a plot of Eq. (22) showing the effect of varying the pre-scanning beam amplification G_p, together with a comparative plot of Eq. (10) showing the theoretical limit imposed by the photocathode. Figure 23 is a similar plot of Eq. (22) in which a long storage, high gain target is used. Figure 24 is a plot of Equ. (22) showing the effect of varying the pre-scanning beam gain G_p at various illumination levels.

5. EFFECT OF VIDEO RESPONSE AS A FUNCTION OF LINE NUMBER

The foregoing calculations take no account of the factors tending to limit the resolution of a camera tube through the creation of unsherpness in the image. As discussed elsewhere in this report, these factors will include imperfect focus in the image section due to variations in initial velocity of emitted electrons and to imperfections in the focusing fields, lateral leakage of charge in the image orthicon storage target, and the finite spot size of the scanning beam. As indicated in Figure 25, even on an experimental image orthicon, the video amplitude response as a function of line number has fallen to 40% at 600 TV lines. It is this reduced video amplitude which should be used as the signal when the signal to noise ratio as a function of line number is calculated. Note that noise due to the scanning beam will not be reduced for this reduced signal, since beam current will be that necessary to discharge large area white signals on the target.

In a practical experimental setup, the bandwidth of the video amplifier is not varied when observing the resolution limitations of a camera tube. Hence, although the calculations were made on a different basis, the noise contribution from the scanning beam will not vary as a function of the fineness of the test pattern being observed but only as a function of the beam current necessary to discharge the target of the image orthicon and therefore as a function of the light level.

Figure 20
Signal/Noise Ratio vs Photocathode
Illumination

(Target gain as parameter)

Eq. (17) $\dfrac{\sigma}{\nu} = C \sqrt{\dfrac{2 L A E T}{4 e N^2 \left[(2-C) + \dfrac{2}{M G_t} \right]}}$

G_t = target gain
C = contrast ratio = 1.0
L = photocathode sensitivity = 150 x 10^{-6} amp/lumen
A = photocathode area = .01 sq. ft.
T = target integration time = 1/30 sec.
N = resolution in TV lines = 400
M = maximum beam modulation = 0.1
e = electron charge = 1.6 x 10^{-19} coulombs
n = number of spurious electrons per second per
     resolution element.

Limit set by photocathode

$G_t = 10$

$G_t = 2$

$n = 10$

Signal/Noise Ratio $\left(\dfrac{\sigma}{\nu} \right)$

E – Photocathode Illumination (Ft. Candles)

76

Figure 21
Signal/Noise Ratio vs Photocathode Illumination

Eq. (17) $\dfrac{\sigma}{v} = C \cdot \sqrt{\dfrac{2LAET}{4eN^2}\left[\frac{E}{t}(2-C) + \dfrac{2}{MGt}\right]}$ (Beam modulation as parameter)

M = maximum beam modulation
C = contrast ratio = 1.0
L = photocathode sensitivity = 150×10^{-6} amp/lumen
A = photocathode area = .01 sq. ft.
T = target integration time = 1/30 sec.
N = resolution in TV lines = 400
Gt = target gain = 2
e = electron charge = 1.6×10^{-19} coulombs
n = number of spurious electrons per second per resolution element.

Limit set by Photocathode

M = 1
M = 1
M = .01

n = 10

E − Photocathode Illumination (Ft. Candles)

Signal/Noise Ratio ($\frac{\sigma}{v}$)

10^{-8} 10^{-7} 10^{-6} 10^{-5} 10^{-4} 10^{-3}

0.1   1   10   100

Figure 22
Signal/Noise Ratio vs. Photocathode
Illumination

Eq. (22) $\dfrac{\sigma}{\nu} = C \dfrac{\text{(Pre-scanning beam gain as parameter)}}{\sqrt{\dfrac{2LAET}{48N^2}\left[(2-C)(1+\dfrac{1}{Gp}) + \dfrac{2}{MG_tG_p}\right]}}$

G_p = pre-scanning beam gain
C = contrast ratio = 1.0
L = photocathode sensitivity = 150 × 10^{-6} amp/lumen
A = photocathode area = .01 sq. ft.
T = target integration time = 1/30 sec.
N = resolution in TV lines = 400
M = maximum beam modulation = 0.1
G_t = target gain = 2
e = electron charge = 1.6 × 10^{-19} coulombs
n = number of spurious electrons per second per
      resolution element.

E – Photocathode Illumination (Ft. Candles)

Signal/Noise Ratio ($\dfrac{\sigma}{\nu}$)

79

Figure 23
Signal/Noise Ratio vs Photocathode Illumination
(Pre-scanning beam gain as parameter)

Eq. (21) $\quad \dfrac{\sigma}{\gamma} = C \sqrt{\dfrac{2LAET}{4eN^2}\left[(2-C)(1+\dfrac{1}{G_p})+\dfrac{2}{MG_tG_p}\right]}$

G_p = pre-scanning beam gain
C = contrast ratio = 1.0
L = photocathode sensitivity = 150×10^{-6} amp/lumen
A = photocathode area = .01 sq. ft.
T = target integration time = 1 sec.
N = resolution in TV lines = 400
M = maximum beam modulation = 0.1
G_t = target gain = 10
e = electron charge = 1.6×10^{-19} coulombs
n = number of spurious electrons per second per resolution element.

Limit set by Photocathode

$G_p = 400$

$G_p = 1$

Signal/Noise Ratio $\left(\dfrac{\sigma}{\gamma}\right)$

100

10

1

0.1

10^{-8} 10^{-7} 10^{-6} 10^{-5} 10^{-4} 10^{-3}

E – Photocathode Illumination (Ft. Candles)

79

Figure 24
Signal/Noise Ratio vs Pre-Scanning Beam
Gain

(Photocathode Illumination as parameter)

Eq. (22) $\dfrac{s}{\nu} = C \sqrt{\dfrac{3LAET}{4eN^2 \left[(2-C)(1 + \frac{1}{Gp}) + \frac{2}{MG_tGp} \right]}}$

E = photocathode illumination in foot candles
C = contrast ratio = 1.0
L = photocathode sensitivity = 150 x 10⁻⁶ amp/lumen
A = photocathode area = .01 sq. ft.
T = target integration time = 1/30 sec.
N = resolution in TV lines = 400
M = maximum beam modulation = 0.1
G_t = target gain = 2
e = electron charge = 1.6 x 10⁻¹⁹ coulombs

E = 10⁻⁶ f-c.

E = 10⁻⁷ f-c.

Signal/Noise Ratio ($\frac{s}{\nu}$)

G_p – Pre-Scanning Beam Amplification

Figure 25. Relative Amplitude Response as Function of
Resolution for Standard 5820 and Experimental
High Resolution Orthicon

81

TRANSMISSION SECONDARY EMISSION AMPLIFIER

1. INTRODUCTION

The transmission secondary electron emission amplifier approach to the problem of increasing the sensitivity of the image orthicon is based on the extensive and original research and development program instituted by the Westinghouse Electric Corporation. Basic work leading to an improved understanding of the secondary emission process has been conducted on a continuing basis in the Westinghouse Research Laboratories since 1951. From these studies has come fundamental information relative to the formation process of secondary electrons in metals and insulators (References 2, 3, 4, 5, 6); the mean free path and escape process of secondary electrons in these materials (Reference 7); and the penetration, energy loss, and scattering mechanism of kilo-volt electrons in solids (References 8, 9) and through thin film (References 9, 10, 11). This background led to the suggestion of a new principle for transmission electron multiplication employing thin films of insultating materials by E. J. Sternglass of the Westinghouse Research Laboratories in 1953. The principle of electron multiplication transmission through a series of plane-parallel foils has long been recognized as offering important advantages over the conventional front surface 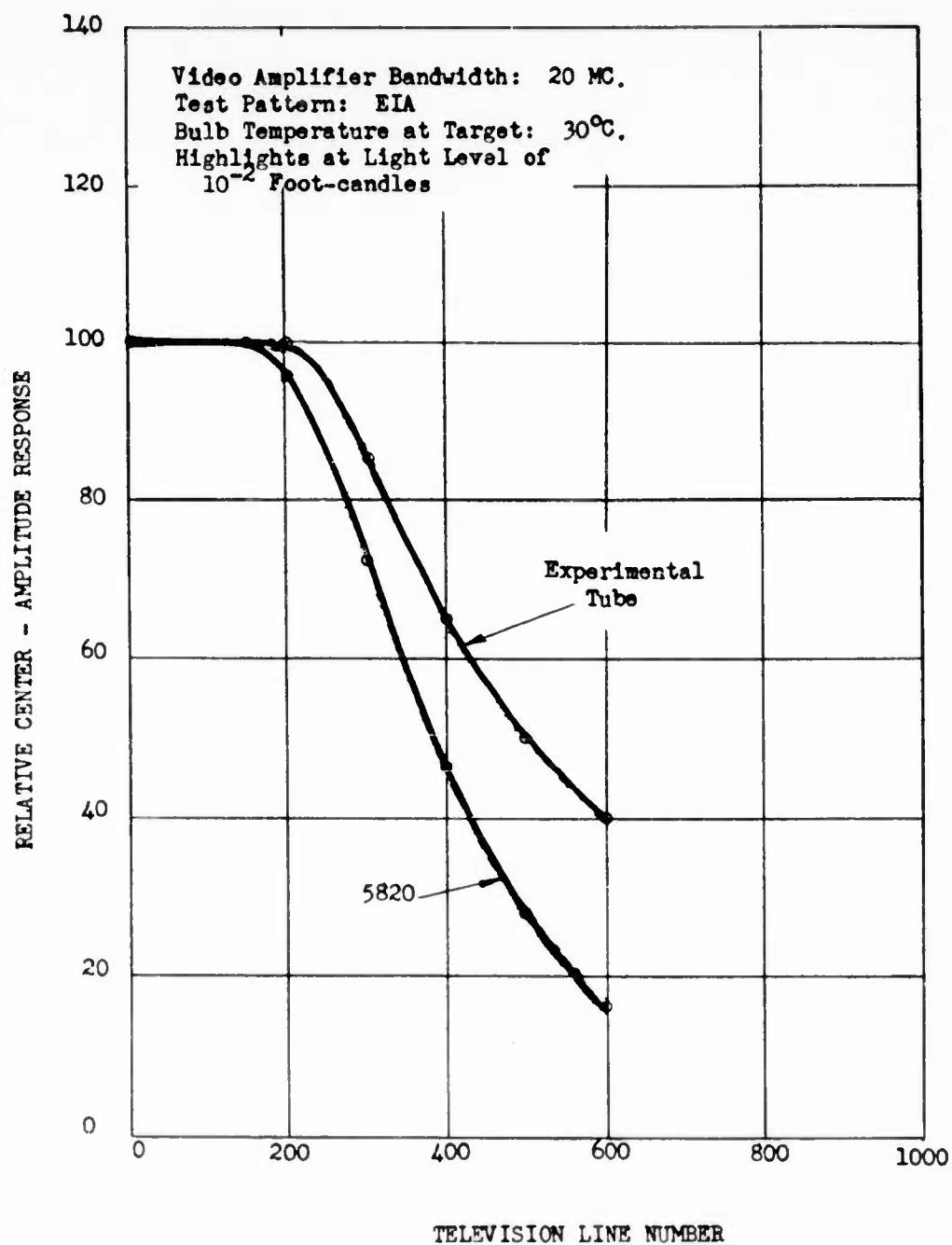type of electron multiplier. Previous efforts to incorporate this principle in a useful device employing thin metallic foils met with the practical difficulties of low yield, large penetration of fast electrons, and relatively high voltages required to penetrate foils of reasonable mechanical strength. These problems were overcome by using thin films of insulating materials as secondary emitters.

Secondary electron yields from insulators such as the alkaline earth oxides and alkali halides are known to be many times larger than those of pure metals (Reference 12). This increased yield may be explained by the much larger distances over which secondaries can diffuse in insulators as compared to metals. Thus, direct
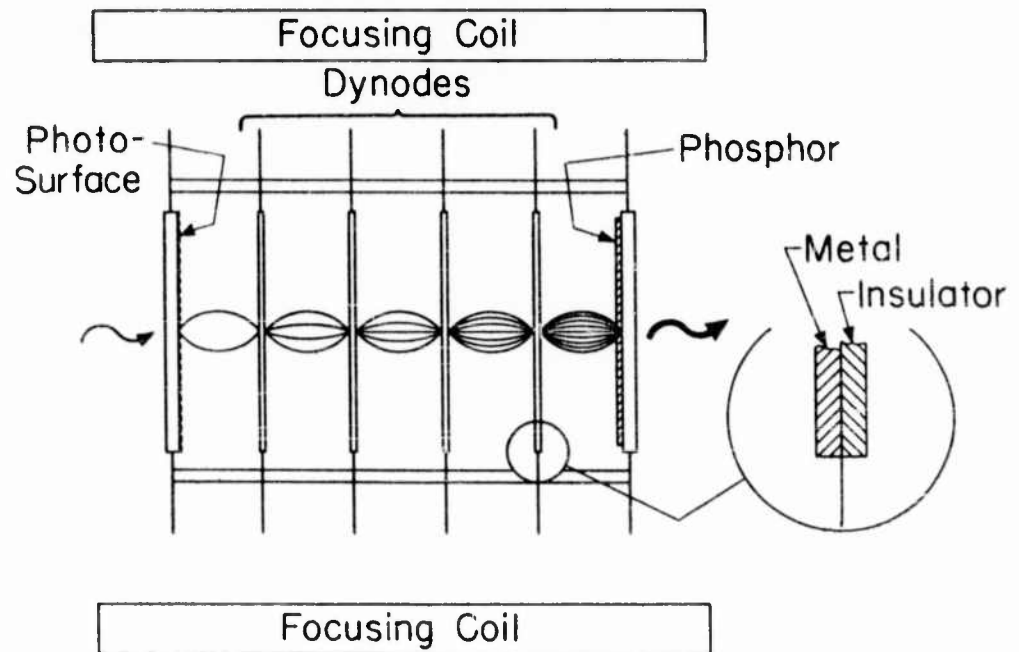
82

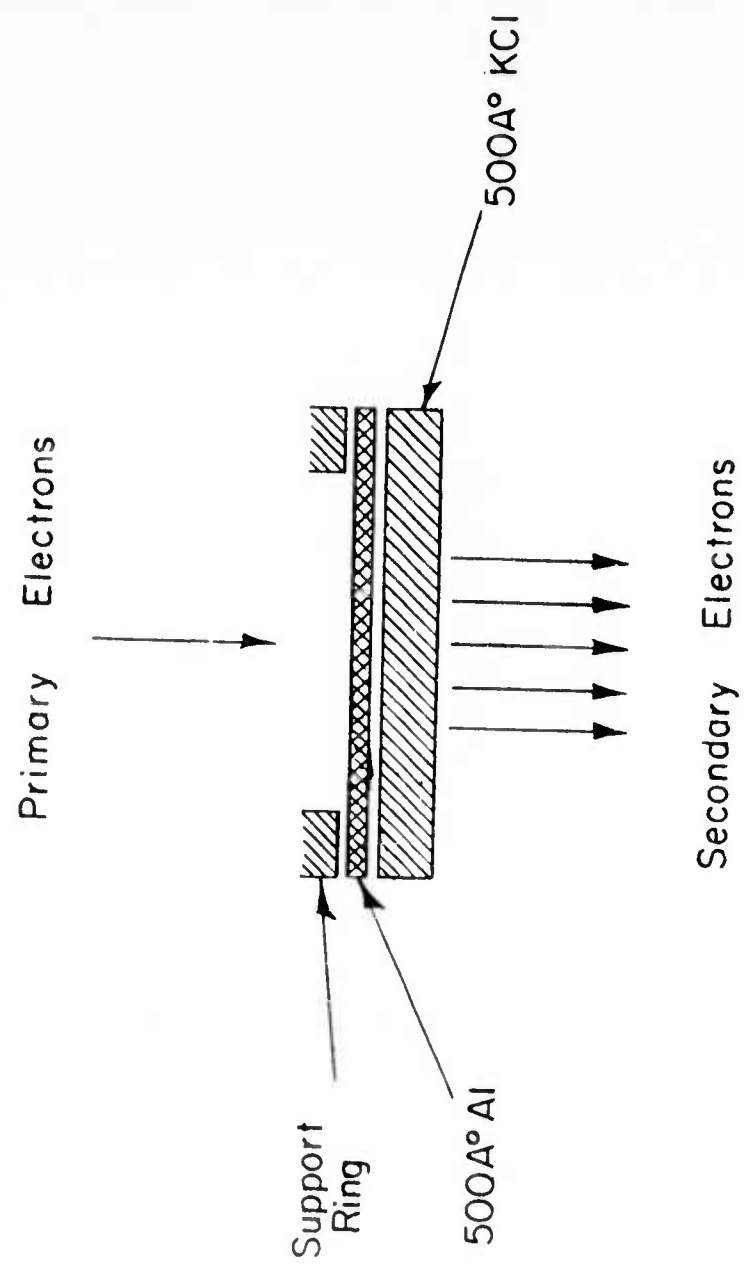Figure 26. Schematic of Transmission Secondary Emission Intensifier

Figure 27. Cross Section of Typical TSE Dynode

experimental evidence is available that the diffusion mean free path of secondary electrons in KCl is about 2400 $\overset{o}{A}$, as compared to approximately 18 $\overset{o}{A}$ in a typical metal such as gold. This increased path length in insulators arises from the fact that secondary electrons whose kinetic energy is less than the magnitude of the gap between the valence and conduction levels cannot lose their energy in inelastic processes with the valence band electrons. Instead, these electrons can only make elastic collisions with the lattice vibrations giving up very small amounts of energy of the order of kT per collision. This enables electrons in insulators with wide energy gaps to diffuse over very large distances before their energy is diminished to such an extent that they are unable to escape into the vacuum. By contrast in the case of metals, where there is no gap across which valence electrons must be lifted, low energy secondary electrons may lose their entire energy in one or two collisions. The long diffusion length in insulators results in high yields by allowing secondaries to escape from great depths. At the same time, the relatively thick layers that are optimum for transmission multiplication in insulators stop a large fraction of the incident fast electrons.

The principle of transmission electron multiplication was developed to the point where the practical feasibility of utilizing thin insulating films in a plane-parallel arrangement for high-speed counting and imaging was demonstrated in 1955-6 (References 13, 14, 15, 16, 17). More recently, new techniques of preparing the thin film dynodes were successfully developed, leading to the practical realization of high gain and high resolution devices suitable for image intensification applications (References 18, 19). The principle involved is shown in Figure 26. Electrons emitted by a photocathode are accelerated and focused on the first secondary electron multiplying dynode by axial electric and magnetic fields. Secondary electrons emitted by the insulator layer of the dynode are in turn accelerated and focused on the following dynode with sufficient energy to eject additional secondary electrons from

its opposite side. This process is continued through several stages of electron multiplication. Electrons from the final dynode are then similarly focused on an output phosphor where the input image appears amplified in brightness.

2. Transmission Secondary Emission Dynode Development

This section describes the work done on transmission secondary emission (TSE) dynodes, both in our laboratory and in related projects at the Westinghouse Research Laboratories (References 20, 21).

a. Characteristics of TSE Dynodes

A number of different types of transmission secondary emission dynode structures have been investigated. All of them basically consist of a support ring, a thin film of metal and finally an insulator layer with good secondary emitting properties. Shown in Figure 27 is an example of a TSE film. The thin metal film used in this dynode structure is aluminum, whose primary function is to provide electrical conductivity while the secondary emitting insulator is KCl. The thicknesses used are not necessarily the optimum as far as yield is concerned. They represent a combination that gives a significant yield at a reasonable voltage. It has been found that the film support ring is an important consideration in this work. The material is chosen on the basis of its non-magnetic nature, working qualities, and thermal coefficient of expansion. Selfsupporting films have been developed, allowing the omission of the supporting mesh structure used in earlier TSE dynodes. The self-supporting films, however, introduce a restriction on size arising from the fact that the greater the diameter, the easier it is to rupture the film, since unbalanced forces may develope due to differences in the electric field on both sides of the film. The size of present dynodes is 3/4" in diameter, although films up to 1" in diameter have been fabricated. The upper limit to size, however, is not yet known for self-supported films.

The Al-KCl films are prepared according to the following schedule (Reference 20, 21):

1.) Nitrocellulose film is stretched over a metallic ring which has a central opening. The film supporting ring is an important consideration in this work. The structure of the ring must be such that the nitrocellulose sattles down on it without wrinkling or tearing. After fabrication, the ring is polished mechanically to remove the gross roughness and then electropolished. It is then annealed in a hydrogen furnace to remove strains. Qualitatively, it was considered necessary that the ring have a smaller coefficient of expansion than the aluminum film in order to keep the Al film under tension and thus flat. Initially, the ring was made of Inconal with an insida diameter of $3/4"$.

The original filming lacquer was made by mixing a number of solvents with nitrocallulose. In forming the organic film, deionized water is let into a large diameter crystallizing dish and a drop of the nitrocellulose solution is gently let fall onto the water. The nitrocellulose film spraads over the surface of the water and as the solvents evaporate, color changes take place showing that the thickness is changing. When the color is constant, tha ring, which is spring-mounted on a large diameter metal disk with a central opening, is carefully dipped into the surface film with a scooping action and then lifted out of the disk with a sideways motion. Care is exercised to prevent submerging the ring below the surface of the liquid in order to produce a smooth, taut film over the ring. The film is then permitted to air dry for approximately 5 minutes. A pair of tweezers is used to cut away the film which extends beyond the ring. The films are about 7000 $\overset{\circ}{A}$ in thickness. The nitrocellulosa films are now baked in an air oven at $110\text{-}120^{\circ}C$ for one-half hour as a film annealing measure.

2.) The filmed rings are mounted on a support in a vacuum evaporator. Seventy milligrams of aluminum are evaporated quickly from a tungsten filament which is at the center of a sphere with a radius of $8"$, of which the support stand is a section. Such a geometry results in an equal thickness of Al on all the films.

87

A deposit of 13.5 ug per sq. cm. results. This is equivalent to a thickness of 500 $\overset{o}{A}$ based on the bulk density of Al.

The films are now placed in an air oven and heated for two hours at $250^{o}C$, causing the nitrocellulose to be pyrolized and go off as gaseous decomposition products. A mirror-like film results. An alternative method is to arrange the film in a firing can and place in a vacuum bell jar. After exhausting the bell jar, oxygen is introduced into the system to a pressure of 3 to 6 mm Hg. The firing can is then uniformly heated with an RF coil at a temperature of 350° - $400^{o}C$ for approximately 10 minutes.

3.) Potassium chloride is vacuum evaporated onto the aluminum to a thickness of 500 $\overset{o}{A}$.

Figure 28 shows characteristic curves of an Al-KCl film as a function of incident energy of primary bombarding electrons. Total secondary electron emission yields have varied in the approximate range of 3 to 7. Also shown in Figure 28 is the fraction of transmitted primaries and the secondary to primary electron ratio as functions of primary energy. This is important because primary electrons, which are here arbitrarily defined as electrons with energies greater than 50 volts, are not focused as well as the secondary emission electrons whose energy is defined as being less than 50 volts. The greater the percentage of poorly focused electrons, the greater will be the be the background. The effect of these transmitted primary electrons on image contrast is discussed later.

Referring to Figure 28, it appears obvious that there is much to be gained in operating the tube somewhat below the peak voltage. There is only a relatively small loss in yield while the secondary to primary ratio is appreciably increased. It should be pointed out that the "primaries" are very likely made up of two components, true incident electrons that pass through the film with more than 50 volts residual energy and high energy secondaries.
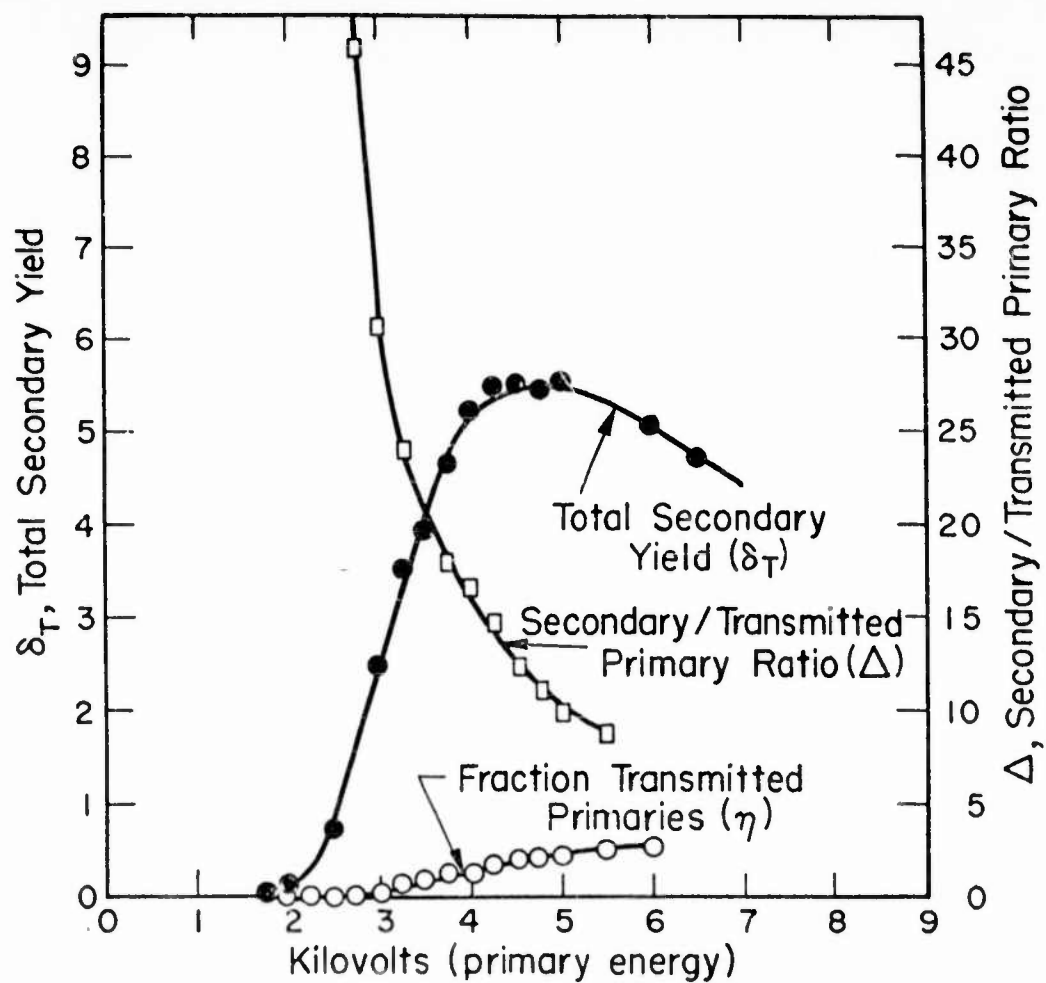
Figure 28. Transmission Secondary Emission Yield of
Self-Supported A1-KCl Film (500 Å Each)

b. Improved TSE Dynodes

During the early course of work on Al-KCl films, two serious problems arose
which made it necessary to seek improved types of TSE films. It was found that the
Al-KCl films tend to tighten as a result of normal tube processing, resulting in
frequent film ruptures. This tightening phenomenon appeared to be due to a combi-
nation of vacuum tightening of the aluminum layer and to a crystal growth and re-
orientation of the KCl. Thermal coefficients between the two materials, as well as
that of the support ring, may also have played a contributing role. To reduce the
probability of film rupture, it was found necessary to use "slack" or "wrinkled"
films and reduced exhaust bake temperatures. This introduced other problems, how-
ever, since film wrinkles could be observed in the image produced by sealed-off tubes
containing such films and lower exhaust bake temperatures did not permit a more
thorough outgassing of tubes.

It was also discovered early in the work that the useful lifetime, based on
secondary emission decay, of KCl is short under high density bombardment by electrons.
The mechanism of decay of scondary yield is not yet well understood. There is no
theory to help in the pre-selection of materials which would have incrased lifetimes.
What is known is strictly empirical, the mechanism of decay being a complex solid
state phenomenon.

As a result of the limitations of the early Al-KCl dynodes, the substitution of
more stable, rupture free, high gain secondary emitting materials was made necessary.

In the course of our work with the use of TSE dynodes as pre-scanning beam amp-
lifiers in an image orthicon camera tube, we encountered the interesting effect of
MgO smoke deposits as the secondary emitting surface of the dynode. Maximum yields
as high as 25 were observed in sealed off tubes. This combined with the ability to
exhaust bake tubes at higher temperatures without resulting in film rupture, led to
a continued investigation of smoke deposits of insulators. Such deposits are

90

composed of very small particles situated one on the other. They are of two types, those that are formed by evaporating a substance, such as BaF_2, in a partial pressure of a non-reacting gas such as argon and those produced by burning a metal, such as magnesium in the presence of air to form MgO. The density of such smoke deposits is very low, of the order of 1% of the bulk material. The smoke particles may contain hundreds or even thousands of molecules. The size of the particles deposited on the substrate is dependent on the gas pressure, the rate of evaporation, the distance of the substrate from the filament, and the temperature of the substrate. A vital consideration is that convection currents influence the height to which the smoke particles are carried and their distribution in space. While quantitative expressions for the physical properties of smoke have not been established, certain important parameters have been found empirically.

The MgO smoke deposits were prepared by burning magnesium metal in air according to the following schedule:

1.) Nitrocellulose film stretched over a metallic ring in the manner described previously with the Al-KCl film.

2.) Aluminum vacuum deposited onto the nitrocellulose film to a thickness of 500 $\overset{o}{A}$ as described previously.

3.) Nitrocellulose film pyrolyzed in an air or oxygen atmosphere as described previously.

4.) Magnesium ribbon placed about one-half inch below the bottom of a foot long, 1-1/2 inch diameter glass tube. Dynode supported on the upper end of the glass tube. Magnesium ribbon ignited and the particles of smoke carried up by convection currents and deposited on the aluminum film. It has been found that 14 inches of ribbon (1/8 inch x .006 inch) will deposit about 20 microns of MgO if the dynode is removed at the instant that the burning begins to die off.
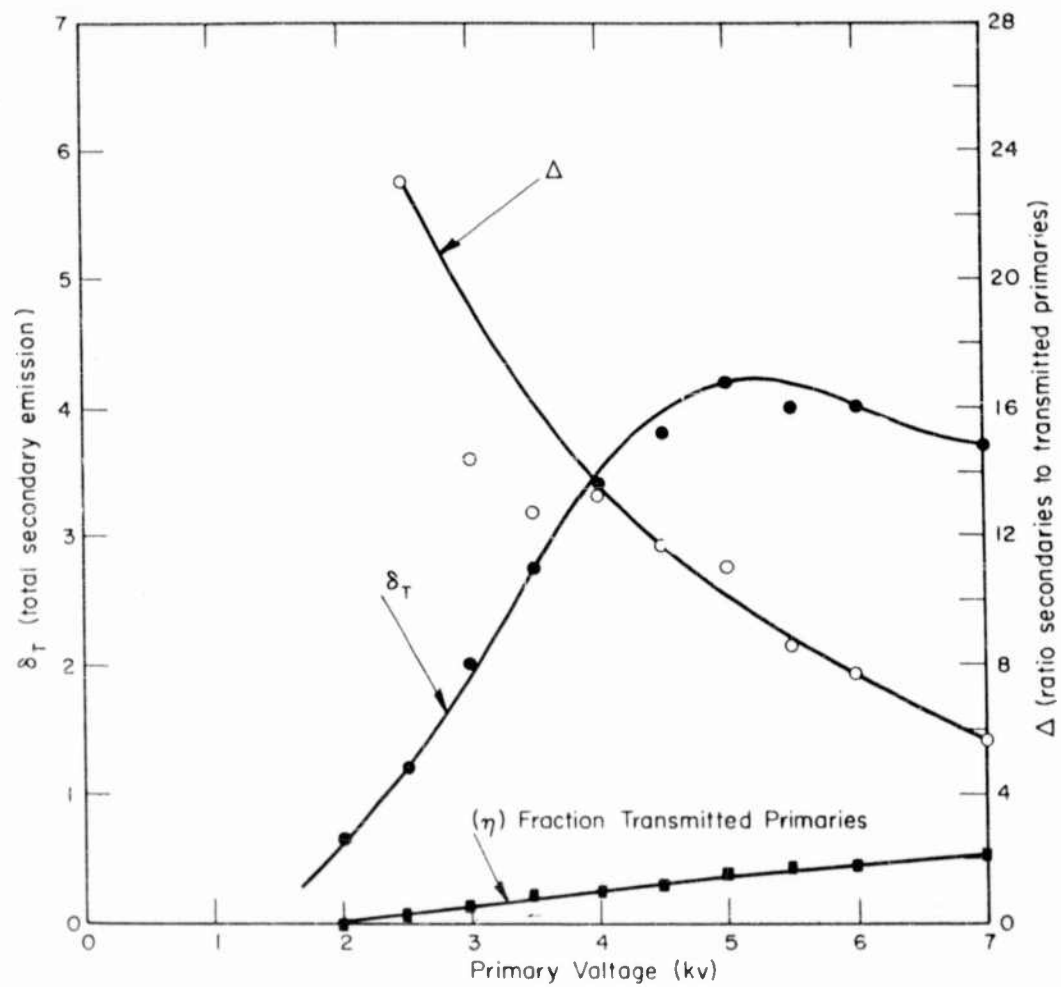
91

Figure 29. Yield Characteristics of Self-Supported Al MgO
Film (AI=500Å, MgO≅20μ)

Various amounts of magnesium have been tried together with modifications of the smoke deposition technique in order to improve the uniformity, reproducibility, and secondary emission yield of the dynodes. Since desirable thicknesses and particle size cannot be predicted from theory, optimum conditions must be determined empirically.

Measurements of yield characteristics made in a demountable tube on a typical MgO dynode prepared with a smoke deposit are shown in Figure 29. When cesium vapor was deliberately introduced into this structure, radical increases in secondary emission yield resulted. Maximum yields as high as 25 have been measured after exposing Al-MgO films to cesium. This increase could not be attributed to cesium enhanced field emission since the wide-spaced collector was only 100 volts positive with respect to the dynode. It was found that sealed-off tubes containing self-supporting Al-MgO dynodes could be subjected to an exhaust bake of at least $300^{\circ}C$ without rupturing. It was also discovered, however, that these sealed-off tubes developed "bright spots" in the output image during operation in the camera. This was attributed to spurious emission points on the film. The residual current due to continuous emission from these points was found to be too small to appreciably affect the electron gain measurements. The cause of this "bright spot" phenomenon was not determined. As a result of this phenomenon, the efforts were shifted to other types of self-supported film which did not exhibit this behavior.

The promising results with the MgO smoke deposit led to the investigation of BaF_2 smoke deposits by our Research Laboratories (Reference 21). The Al-BaF_2 (smoke) films are prepared in the following manner. After fabrication of the aluminum film in the usual manner, barium fluoride is deposited by placing a piece of BaF_2 crystal in a 3/16 inch diameter dimple made in a 1/4 inch wide thin strip of tantalum. The dynodes are placed about 3 to 3.5 inches above the dimple. After evacuation of the bell jar to approximately 10^{-5} mm Hg, argon is admitted to a pressure of a few
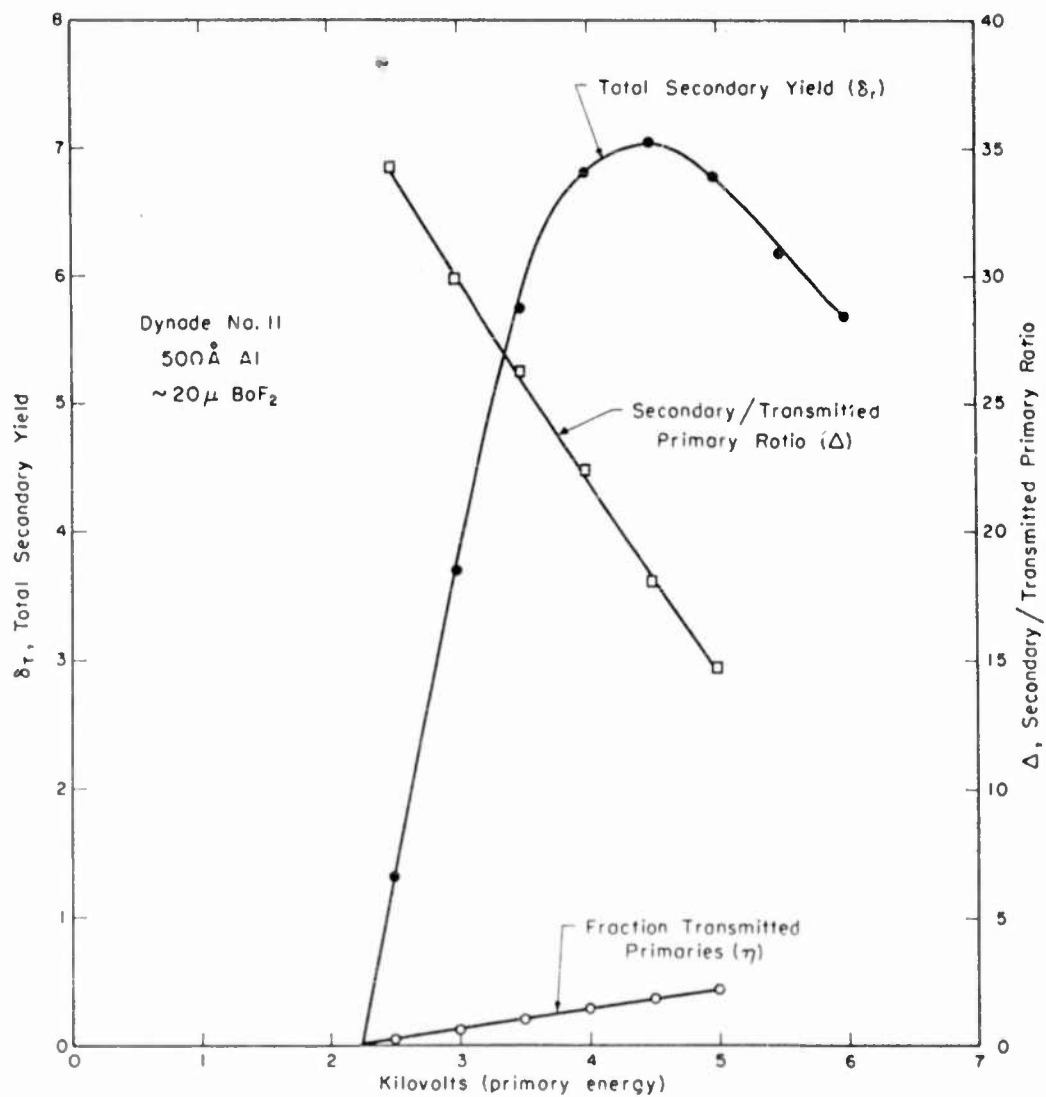
93

Figure 30. Yield Characteristics of Self-Supported AlBaF$_2$ Film

94

millimeters and the tantalum strip is slowly brought up to temperature. Because BaF_2 is colorless, it is not practical to monitor the amount deposited by light ab-sorbing optical methods. For this reason, it has been necessary to establish a reasonable thickness and structure by empirical methods. High gain and low fractions of penetrating primaries serve as a criteria. In an improved method, the dynodes are mounted on a table which turns in vacuum by means of roteting magnets. This has three primary advantages: a relatively large number of films can be made at once, the films are more homogeneous within themselves, and the gain from film to film is more uniform. Typical secondary emission yield characteristics of an Al-BaF_2 film are shown in Figure 30. Electron gains as high as 8 have been achieved in sealed-off tubes. Smooth, self-supporting Al-BaF_2 films have been fabricated capable of with-standing an exhaust bake of at least $300^\circ C$ without rupturing or wrinkling. Success-ful use of Al-BaF_2 (smoke) dynodes is now being made in image intensifier tubes (Reference 21).

During the course of our work with smoke deposit films, an Al-NA_3Al F_6 (cryolite) film was developed to eliminete the limitations of the early Al-KCl dynodes. The films were prepared in the following manner. After fabrication of the aluminum film in the usual manner, cryolite is deposited by placing a known weight of the material, usually 18 mg, in a 1/4 inch diameter dimple in a thin strip of molybdenum. The dynodes are placed in a support 8 inches above the dimple. After evacuation of the bell jar to approximately 10^{-5} mm Hg, argon is edmitted to a pressure of 175 microns and the molybdenum strip is brought up to temperature until the cryolite has been completely evaporated. In an effort to establish optimum yield characteristics, variations in argon pressure as well es vacuum evaportation were tried in addition to changes in the amount of cryolite. Smooth, self-supporting Al-Cryolite films, 3/4" in diameter, have been fabricated capable of withstanding an exheust bake of at least $300^\circ C$ without rupturing or wrinkling. The secondary emission characteristics

95
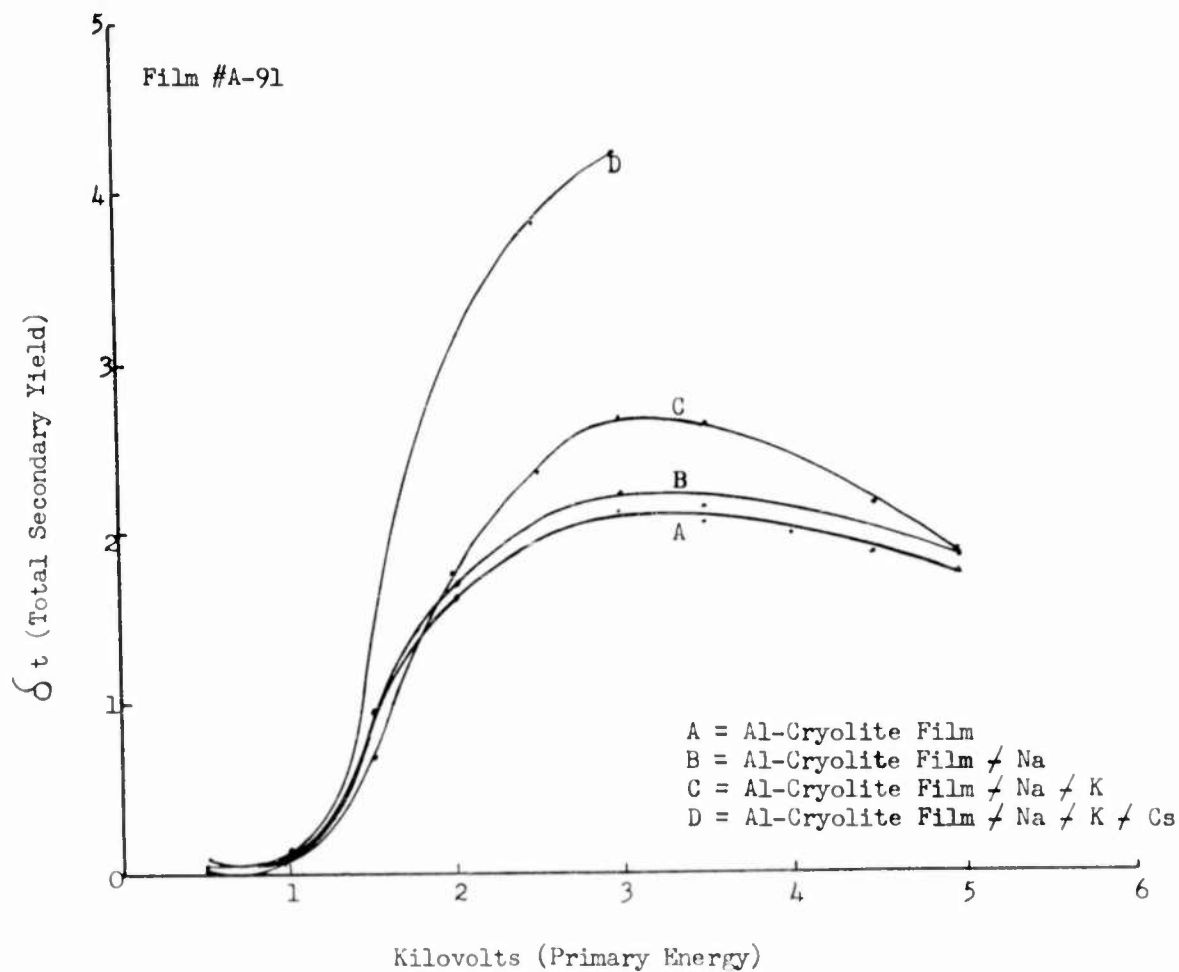
Figure 31. Effects of Tri0Alkali Vapors on Transmission Secondary
Emission Field of Al-Cryolite TSE Film

96

Figure 32. Decay of δ with Time

	δ_{max}	Beam Voltage	Current Density
BaF_2	7.4	4.5 kv	4×10^{-9} A/cm^2
MgO	4.0	5.0 kv	4.5×10^{-9}
KCl	5.55	3.5 kv	4×10^{-9}

(Rest = 16 hours)
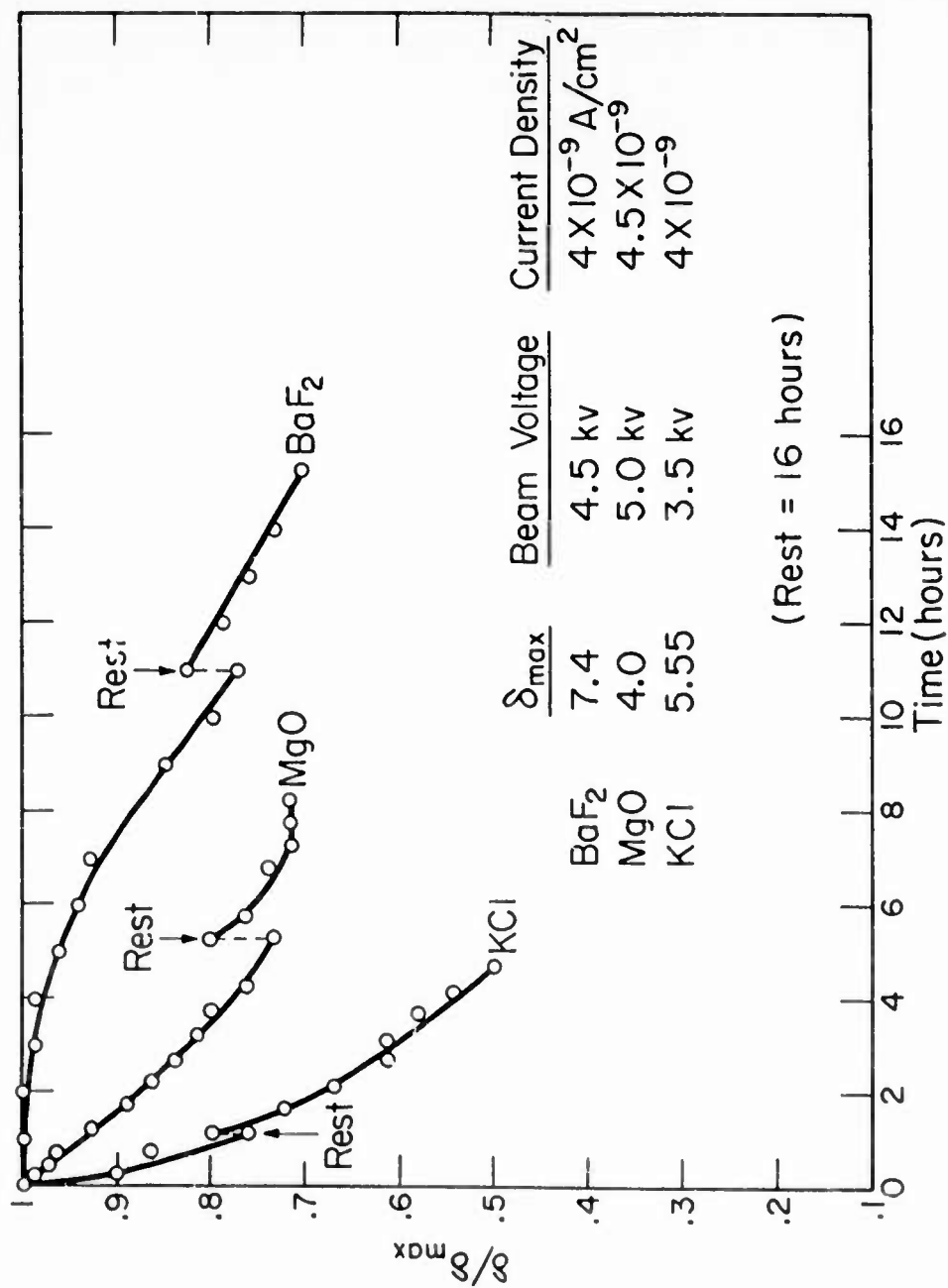
Figure 33. Decay of Secondary Emission Yield with Time (MgO)

of an Al-Cryolite dynode with a smoke deposit of cryolite are shown in Figure 31. The measurements were taken in a demountable tube into which various alkali metal vapors were subsequently introduced to determine the effect on secondary yield. Prior to exposing the film to the alkali metal vapors, the maximum yields were usually in the order of 2 as shown in the curve A of Figure 31. The effects of exposing the same film to various alkali-metal vapors are shown in cruves B, C, and D of Figure 31. Measurements in sealed-off tubes using Al-Cryolite dynodes showed peak yields up to 6.

With the establishment that both $Al-BaF_2$ and Al-MgO films have favorable yields and an improved ability to withstand tube processing, the next step was to check their lifetimes under electron bombardment. Figure 32 shows comparative lifetime curves for these materials and for Al-KCl. The curves have been normalized. The curves clearly show that both MgO and BaF_2 have longer lifetimes than KCl. Note that the secondary yield of Al-KCl films decreases by 50% after 5 hours operation with an input current density of 4×10^{-9} amp/cm^2. Recent $Al-BaF_2$ dynodes have demonstrated a half life of more than 25 hours under the same conditions. In an image orthicon, using three TSE dynode stages with an approximate overall electron gain of 100, this input current density could be reduced to the order of 10^{-11} amp/cm^2, resulting in an increase in dynode life. This increase arises because of the inverse dependence of lifetime on current density as indicated in Figure 33.

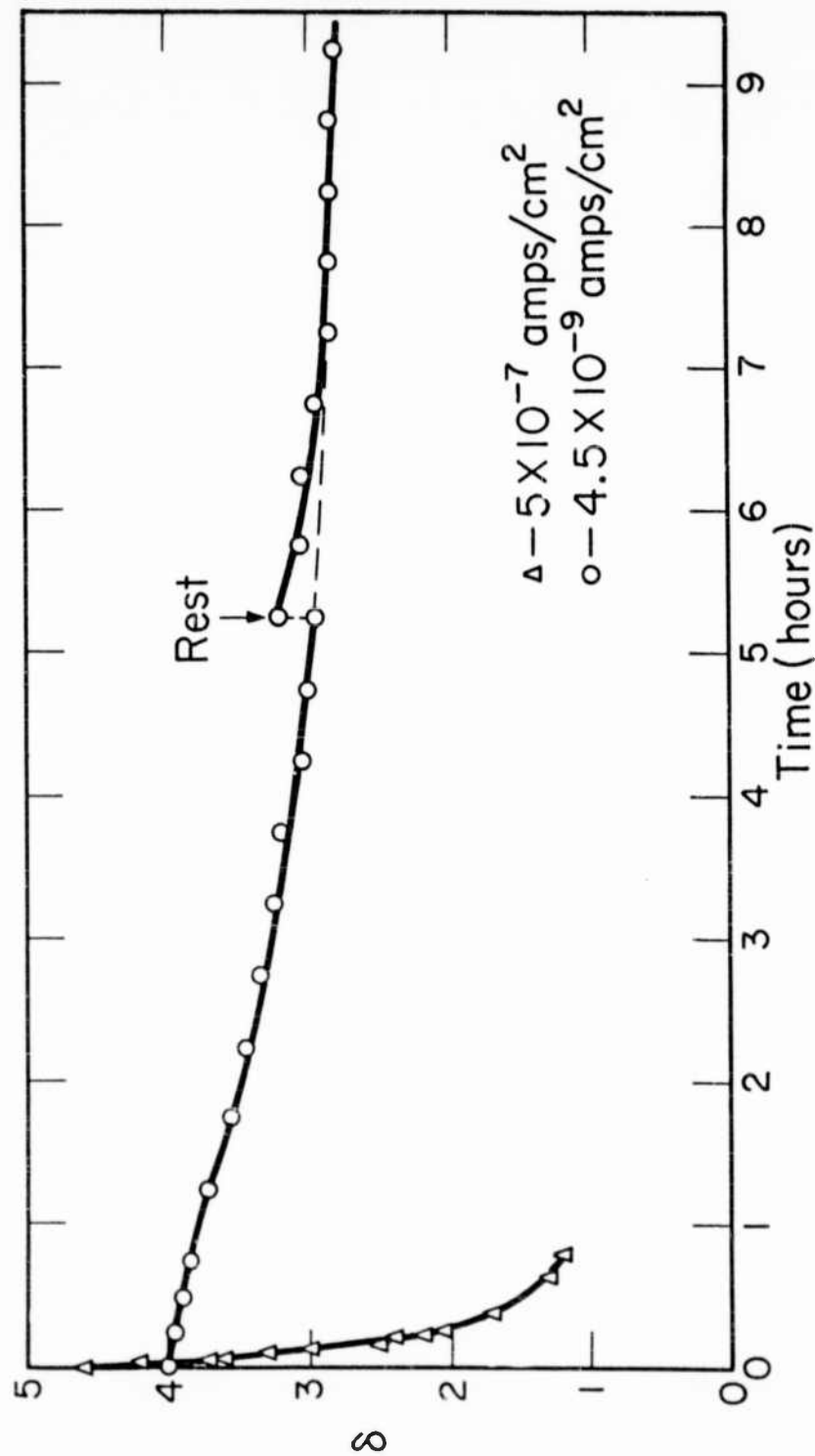While substantial advances have been made in the development of TSE dynodes, some problems remain to be solved. Although film rupture during tube processing has been reduced appreciably, occasional breakage is still encountered with self-supporting films during operation of the tube. While the reason for this breakage has not been definitely determined, a number of factors are distinct possibilities. Statistically, the probability of a film rupture occuring increases as the number of dynode stages is increased. To circumvent the problem of film rupture, our Research

99

Laboratories have been fabricating dynodes using high transmission (99% open area), fine wire (.0005" in diameter) support mesh. The mesh is visible but in an unobjectionable manner.

c. Energy Distribution of TSE Dynodes

As shown in the section of theoretical limitations of resolution of a secondary electron emission amplifier, the effects of spread in emission velocities of secondary electrons ejected from the dynodes is one of the most serious limiting factors in the resolution capabilities of TSE tubes. The fact that both secondaries and penetrating primaries are emitted with a spread in energies and with some angular distribution results in a circle of confusion at the target of the tube corresponding to a point of emission on the photocathode. Consequently, an important phase of the work has concerned itself with the determination of these energy distributions. A knowledge of these energies would make it possible to determine whether a given material is feasible as an emitter.

The original work on the SiO-Au-KCl combination revealed that the energy distribution of secondaries from such films showed a mean energy of about 2 volts. When these measurements were attempted on the Al-MgO and Al-BaF$_2$ films, a difficulty was encountered (Reference 21). It was found that the yield is a function of the electric field across the film. This leads to the conclusion that the surface is charging which does not permit any conclusions as to velocity distribution. This effect is demonstrated in Figure 34 which shows the energy distribution of two dynodes, one consisting of SiO-Au-KCl and the other Al-MgO. In both cases, the normalized values are the currents reaching the collector with a retarding grid between the collector and the emitting film. In addition, these values are also normalized in that the collector current at -50 volts has been subtracted out. Measurements on Al-BaF$_2$ have given results similar to that of Al-MgO.
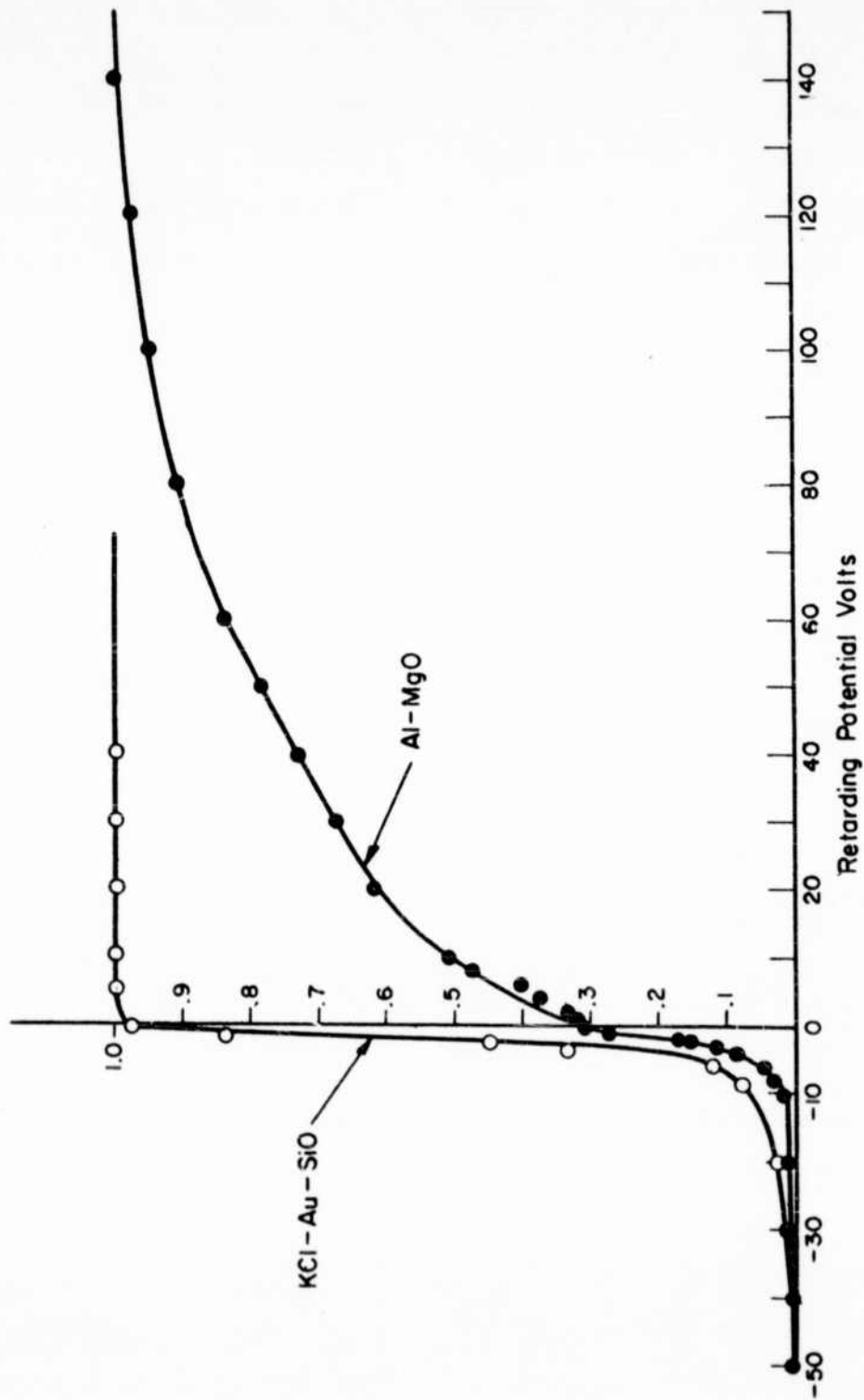
Figure 34. Normalized Integral Energy Distribution Curves of Two
Systems Noted

d. Further Investigation of TSE Dynodes

Whereas the early TSE dynodes employed vacuum evaporated solid films of alkali-halides backed by a conductive coating of aluminum, the new type dynodes consist of low density smoke deposits of insulators on a conductive substrate. The properties of this type of structure are of considerable fundamental as well as practical interest, but they are as yet not too well understood. Thus, it has been observed that the energy distribution of the secondary electrons and the total number emitted from the surface can be influenced by the applied electric field. This leads to the conclusion that the surface is charging thus causing high internal fields. The influence of such internal fields on the escape mechanism is not yet understood. It has also been found that alkali vapors tend to further enhance the secondary emission yield, often increasing the yield to many times that observed for the solid insulator deposits. Generally, secondary emitters show a decrease of initial yield during continuous electron bombardment. The "half life" has been found to be quite different for various emitters. The mechanism of dynode deterioration is not well known.

Further improvement of transmission type dynode performance, particularly as they affect secondary emission yield and stability as well as ultimate resolution obtainable in devices employing such dynodes depends upon a further understanding of these phenomena. An understanding can only be developed by further investigation of TSE dynodes.

3. Experimental Tubes with TSE Amplifiers

a. Experimental Image Orthicon Tubes with Pre-Scanning Beam TSE Amplifiers.
Operable image orthicon tubes with two stages of self-supporting dynodes have been constructed, with resolutions of 400 - 500 TV lines per inch being achieved. Dark current has been reduced to permit quiet operation of tubes at the higher voltages required for increased dynode yields. At the end of the contract period, a two stage tube had been produced in which the threshold performance, with photocathode

102
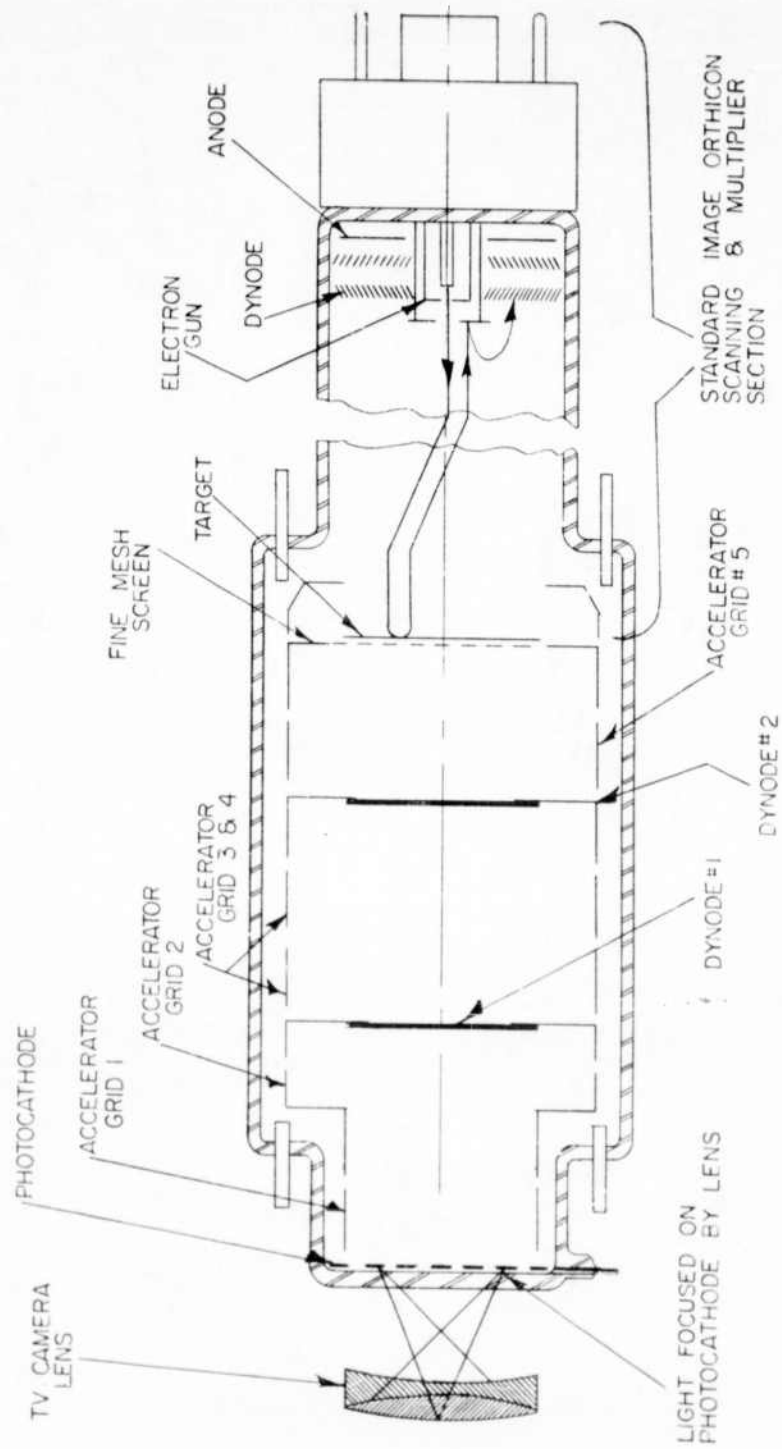
Figure 35. Transmission Secondary Emission Multiplier
Camera Tube

ANODE

DYNODE

ELECTRON
GUN

STANDARD IMAGE ORTHICON
SCANNING & MULTIPLIER
SECTION

TARGET

FINE MESH
SCREEN

ACCELERATOR
GRID # 5

ACCELERATOR
GRID 3 & 4

ACCELERATOR
GRID 2

DYNODE # 2

ACCELERATOR
GRID 1

PHOTOCATHODE

DYNODE # I

DYNODE

TV CAMERA
LENS

LIGHT FOCUSED ON
PHOTOCATHODE BY LENS

103

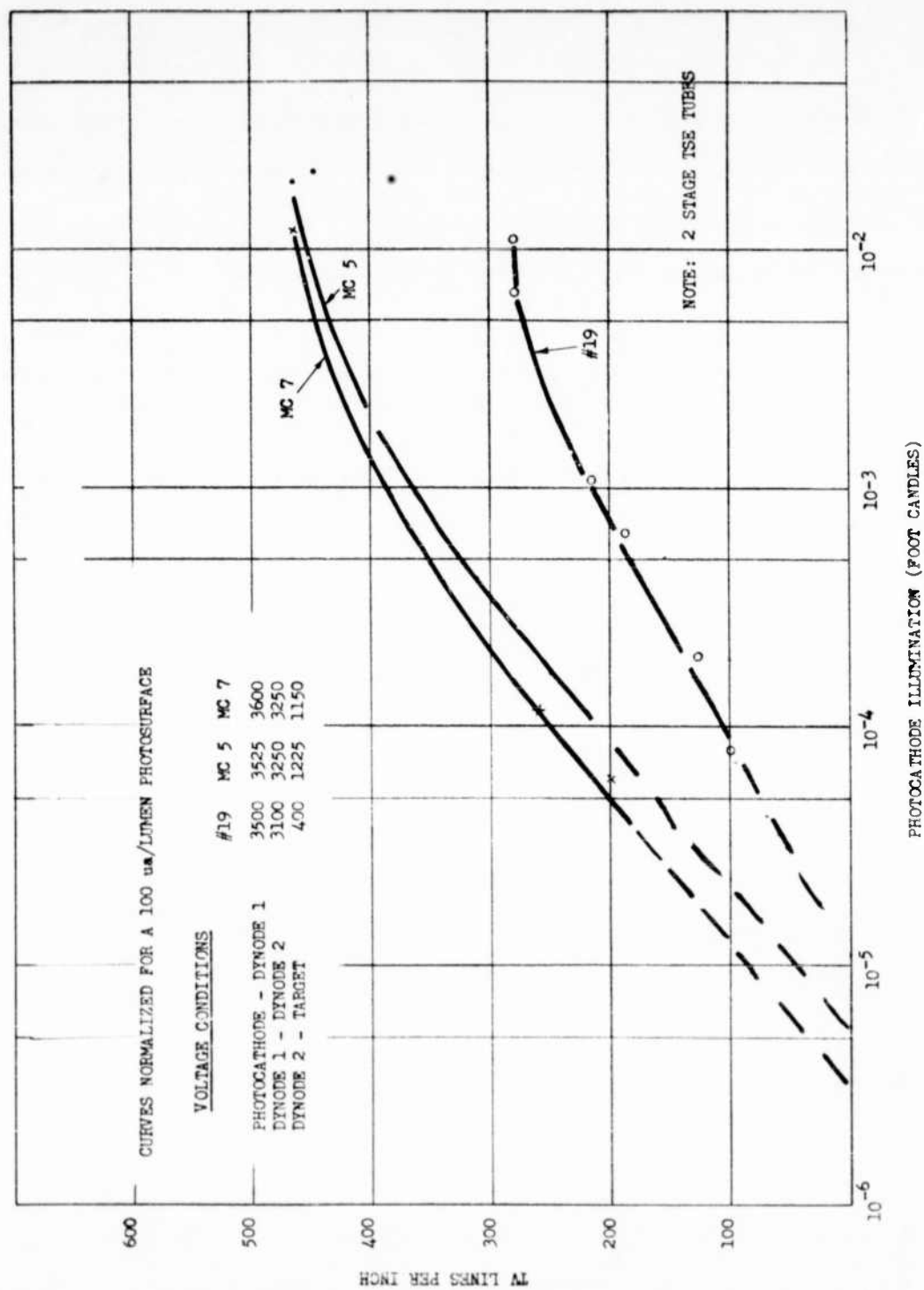Figure 36.   Image Orthicon with two TSEM Stages

Figure 37. Resolution vs Light Level for TSE Tubes Noted

sensitivity adjusted to 100 ua per lumen, exceeded somewhat that of the Westinghouse WL-7198.

Many problems remain to be solved in achieving a tube significantly more sensitive than the standard image orthicon, using the TSE amplifier approach, but there appear to be no fundamental limitations to such a goal.

As shown in Figure 35 and 36, the present tube design consists of an extended image orthicon image section containing a flat photocathode and a series of cylindrical, non-magnetic metal electrodes to establish the accelerating electric field. The TSE dynodes are mounted at the base of various cylindrical electrodes with an approximate inter-dynode spacing of 2 inches. The final dynode to target spacing is closer spaced as a result of the lower target bombarding voltage. Connections to all the additional electrodes in the image section are brought out to a 14 pin stem sealed at the front end of the tube. A low leakage socket is used to connect this front end stem to the terminals of the high voltage power supply. The photocathode is connected to a pin sealed into the front end stem at the base of the faceplate. Cesium-antimony photocathodes were used in most cases. The remaining image section electrodes, including the final dynode, are connected to the normal shoulder pins. A standard image orthicon scanning and multiplier section is employed. The tube is located in a long uniform magnetic focusing coil which is operated at magnetic field intensities in the range of 120 - 160 gauss.

Comparative resolution vs photocathode illumination curves for three tubes constructed with two TSE dynode stages are shown in Figure 37. Tube #19 represents an earlier design, utilizing glass spacers between dynodes, indicating the significant improvement in resolution capability of the more recent TSE tubes MC 5 and MC 7, using a metal cylinder electrode system. It will be noted that the curves are normalized for a 100 ua per lumen photosurface. The method of comparison of performance is based on the fact that photocathode current is directly proportional to the

106

illumination level over the range of interest. Thus, for an image orthicon tube having a photocathode sensitivity of S microamperes per lumen to have the same resolution as a measured tube having a photocathode sensitivity of 10 ua per lumen, the light level for the former would have to be $\underline{\frac{10}{S}}$ times the light level for the measured tube. The actual performance data for tube MC 5, for example, was 465 TV lines per inch at a photocathode illumination of 1×10^{-1} ft. candles and 200 TV lines per inch at 6.5×10^{-4} ft. candles with a measured photocathode sensitivity of 19 ua per lumen.

Figure 38 shows an image of a standard resolution pattern produced by a tube with two TSE dynode stages. Approximately 5 shades of grey and 350 TV lines were observed on the CRT monitor. Referring this to the 3/4" diameter of the dynode gives a resolution limitation of 465 lines per inch.

As has been shown, the resolution capability of image orthicon tubes with TSE dynode stages have been reasonable at the higher light levels where quantum population at the photocathode is not a limitation. This observed maximum resolution is then a measure of the focusing ability of the tube. As the photocathode illumination is reduced, however, so that quantum population becomes a limiting factor in the "seeing" ability of the tube, the resolution begins to degrade. This is shown in the section on theoretical signal to noise ratio limitations of camera tubes. The value of pre-scanning beam amplification lies in its ability to increase the overall signal to noise ratio at the output of the tube.

Measurements taken in the image section of sealed-off TSE tubes have shown that gains of 25 or higher have been attained with two dynode stages. In spite of this pre-scanning beam amplification, however, the expected improvement in threshold light level performance has not been observed. This can be attributed to the following possible causes:

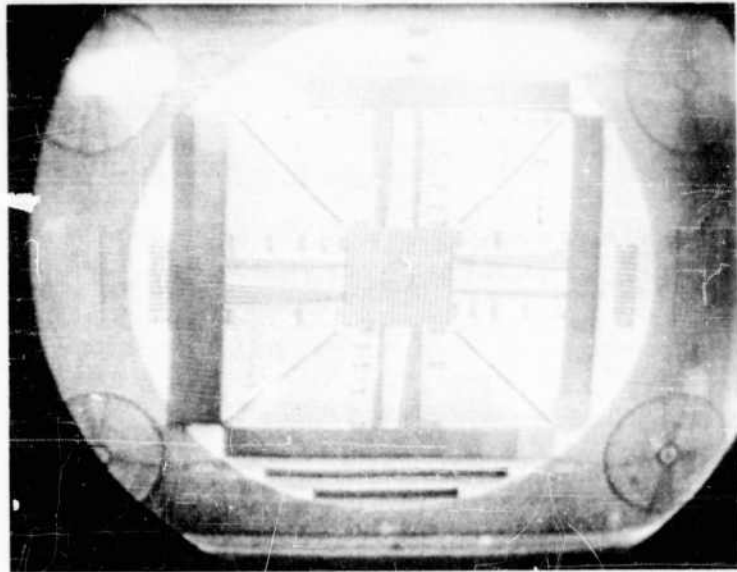1) Spurious electrons reaching the target arising from field emission,

107

Figure 38. Image of Resolution Pattern of 2-Stage
TSEM Image Orthicon

thermionic emission, and stray light photo-emission from the photocathode and other electrodes in the image section. As shown in the section dealing with the theoretical signal to noise ratio limitations, dark emission results in a reduction of the electron image contrast ratio thereby decreasing the signal to noise ratio developed by the tube, particularly at low photocathode illumination levels. By means of suitable electrode geometry, careful cleaning, polishing and surface treatment of image section components, as well as the use of special tube processing techniques, it has been found possible to reduce appreciably the dark current due to spurious emission.

2) Decrease in secondary emission yield of image orthicon target due to the increased primary electron energy used in the final dynode to target stage of the tube or to surface contaminationa resulting from TSE film bombardment and decomposition. Measurements on recent TSE tubes have shown that target gains appear to be as much as a factor of ten below that found in standard image orthicons. This markedly reduced target gain is only partly due to the higher target bombarding voltage usually used. Measurements of target gain vs. primary voltage in standard image orthicon tubes have shown a decrease in gain amounting to somewhat less than a factor of two at voltages up to 1200 volts. We can conclude then that additional factors are contributing to the apparent loss in target gain. This problem remains to be investigated.

A possible solution to the problem of achieving the increased voltages required in the target stage for obtaining higher resolution without undergoing a loss in target gain would be the use of the high gain, thin film target developed under our Contract AF33 (616) 6422. Another approach to the problem would be to coat the writing surface of the standard image orthicon target with a material such as MgO which exhibits maximum secondary emission yields at higher primary energies than the normal glass surface. The problem of possible interaction between the bombarded TSE dynodes and the target surface would remain to be investigated.

Another possible solution to the problem of maintaining the increased voltages required in the final stage for obtaining higher resolution and also for achieving the lower bombarding energy necessary for higher gain at the target would be to insert another mesh parallel to and close spaced with the present collector mesh. The additional mesh on the dynode side of the final stage would be operated at a sufficiently high positive voltage with respect to the final dynode and collector mesh to permit the acceleration of secondary electrons across the final stage and then a deceleration to the target. For example, the following voltages may be used:

Final dynode:	-500 volts
Interposed mesh:	+500 volts
Collector mesh:	+ 2 volts
Target:	0

3) Interaction between the photocathode and the TSE dynodes. It is known that continuous electron bombardment of TSE films results in a decay in yield which is a function of current density and time. This may be due to a gradual decomposition of the secondary emitting insulator layer of the film. The products of decomposition may have an adverse effect on photocathode sensitivity. Although no serious photocathode effects have been observed in our TSEM tubes, further data would be necessary to determine the effects of interaction. As indicated earlier, the effects of the alkali vapors, used in the processing of multi-alkali photocathodes, on TSE dynode yield as well as target gain would also constitute an area of investigation.

4) Decrease in overall gain of multiplier section in output of tube. Recent tests have shown that the gain of the multiplier section of TSE tubes is appreciably below that of standard image orthicons. This appears to be related to the higher magnetic focusing field intensities used in TSE tubes. It has been found possible to increase this gain by the use of a lower magnetic field intensity in the scanning section of the tube, together with a redesign of the final stage of the image section.
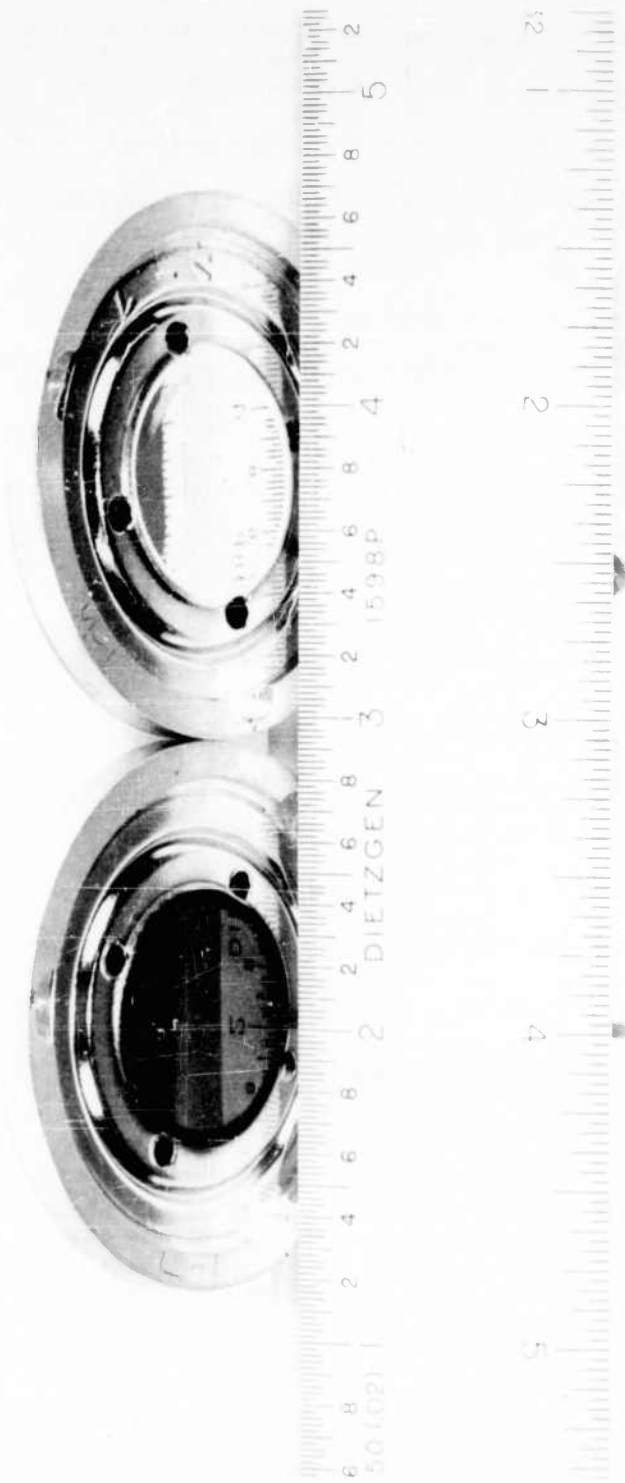
110

Figure 39. Comparison of Blackened and Unblackened Self-Supported Al Films

5) Effect of penetrating primary electrons. Examination of a resolution pattern image produced by a typical TSE tube, shown in Figure 38, indicates approximately 4-5 shades of gray. The effect of primary electrons that have penetrated dynode films is discussed in detail in another section. This analysis does not show any serious degradation in image contrast due to penetrating primaries. In practice, light reflection from the first dynode and high energy backscattered electrons from the dynodes and target will act to further reduce the contrast of the reproduced image. It is known that appreciable amounts of light are transmitted by the photocathode. In the TSE tube such light strikes the shiny aluminum surface of the first dynode and is reflected back to the cathode where it liberates electrons. If the light is reflected back precisely along its incoming path, it would simply add additional electrons to the signal. If, however, the incoming light makes a small angle with the normal, each element of the reflected image will reach the photosurface displaced from its original position. The electrons released as a result of this process have a serious degrading effect on the image. It is obvious that this reflecting surface must be covered with some non-reflecting substance such as aluminum black. Some work has been done along these lines. Figure 30 visually shows the beneficial effect of blackening.

b. Transmission Secondary Emission Image Intensifier

Investigation of transmission secondary emission dynodes had led to the development of a multi-stage image intensifier by our Research Laboratories (Reference 22, 23). As shown in Figure 26, electrons emitted by a photocathode are accelerated and focused on the first dynode by axial electric and magnetic fields. Secondary electrons emitted by the insulater layer of the dynode are in turn accelerated and focused on the following dynode with sufficient energy to eject additional secondary electrons. This process is continued through several stages of electron multiplication. Electrons from the final dynode are then similarly focused on an output phosphor
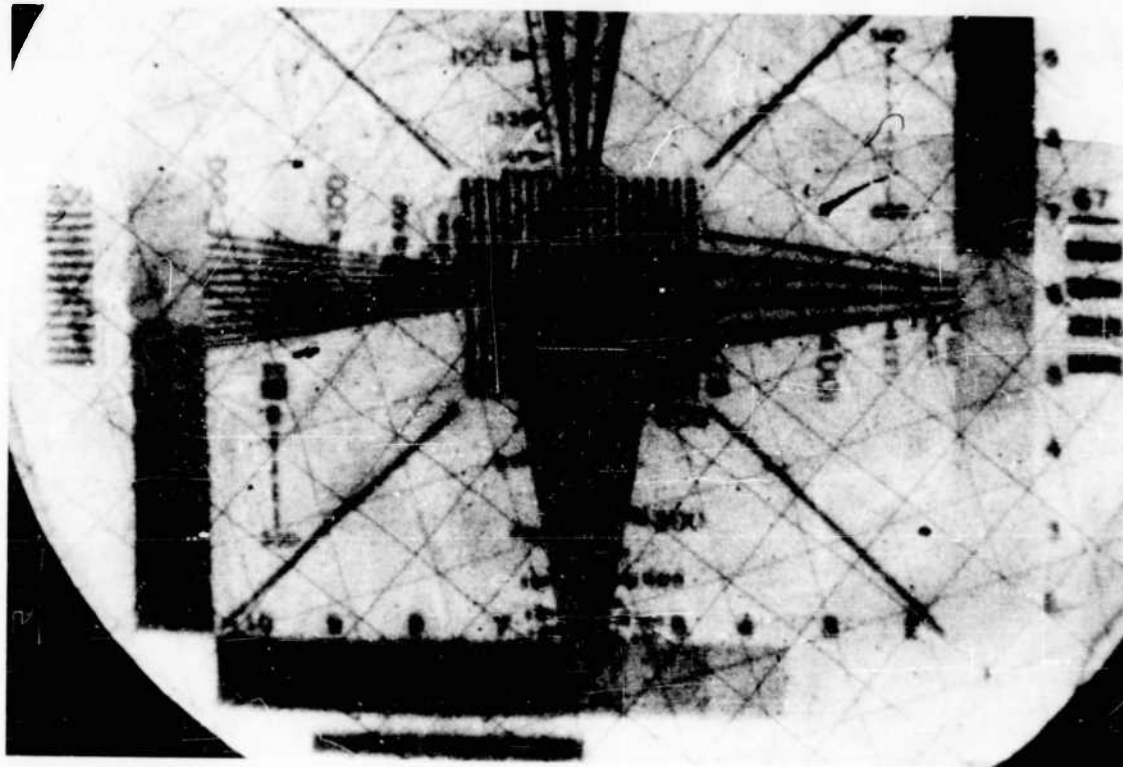
112

Figure 40.   Image of Resolution Pattern 2-Stage
TSEM Image Converter Tube

where the input image appears amplified in brightness. Experimental multi-stage tubes have been constructed using various types of TSE dynodes. Figure 40 shows an image of a resolution pattern produced by a two stage image converter tube using mesh supported dynodes. Four stage tubes have been built using one inch diameter Al-BaF$_2$ dynodes supported on electroformed mesh with about 99% open area. These tubes have electron gains of 1200-2400 when operated with interdynode voltages of 4 KV. The photon gain with 15 KV acceleration from the last dynode to the output phosphor is about 10,000. The limiting resolution is 13 line pairs per mm across 25 mm. With no input and full voltage applied, the visible output from the tubes is essentially due to the amplified room temperature emission from the photocathode.

It is concluded that transmission secondary emission in this metal-insulator film offers a relatively simple and reliable method of constructing image intensifiers which closely approach photoelectron noise limited performance. Therefore, a lens coupled TSE image intensifier and image orthicon introduces another approach to increasing the sensitivity of a television camera tube. Even taking into consideration the light losses due to optical coupling, the photon gain is sufficiently high to approach photocathode noise limited performance.

4. THEORETICAL RESOLUTION LIMITATIONS OF A TRANSMISSION SECONDARY ELECTRON EMISSION AMPLIFIER

The theoretical limitations of resolution of a transmission secondary emission amplifier, using combined electrostatic and magnetic focussing in a plane-parallel electron optical geometry, are treated in a report by H. Kanter of the Westinghouse Research Laboratories and shown in Appendix II. In this analysis, the resolution is calculated as a function of emission velocity, variations in magnetic flux density, electric field strength, and interstage spacings.

In general, the resolution capability is inversely proportional to the diameter of the circle of confusion established at the plane of focus as a result of these electron optical parameters. The resolution per amplifying stage in the

image section can be expressed by the following relationships.

Due to spread in initial emission velocity, ΔV_0, of secondary electrons:

$$R_{\Delta V_0} = \frac{1}{2d} \frac{\phi e}{\phi_o} \tag{1}$$

Due to variation in magnetic flux density, ΔB, of axial magnetic focusing field:

$$R_{\Delta B} = \frac{B}{2\pi n} \sqrt{\frac{e}{2m \phi_o}} \frac{B}{\Delta B} \tag{2}$$

Due to variation in electric field strength, ΔE, of applied electric field:

$$R_{\Delta E} = \frac{1}{d} \sqrt{\frac{\phi e}{\phi_o}} \frac{E}{\Delta E} \tag{3}$$

Due to variation in distance, Δd, between parallel planar electrode:

$$R_{\Delta d} = \frac{1}{2\Delta d} \sqrt{\frac{\phi e}{\phi_o}} \tag{4}$$

Where: d = distance between planar electrodes of amplifying stage

ϕ_o = voltage corresponding to the average initial emission velocity

$\phi_\bullet$ = voltage across amplifying stage

B = magnetic flux density of axial magnetic focusing field

m = electron mass

e = electron charge

n = number of loops per stage described by electron in spiral path perpendicular to the magnetic field.

Assuming a gaussian distribution in electron current density across the circle of confusion and using the independence of all the above factors, one can calculate the total resolving power of one stage by the following equation.

$$\frac{1}{R \text{ stage}} = \sqrt{\frac{1}{R_{\Delta V_0}^2} + \frac{1}{R_{\Delta B}^2} + \frac{1}{R_{\Delta E}^2} + \frac{1}{R_{\Delta d}^2}} \tag{5}$$

The following tables give some examples of quantitative values of resolution

limitations imposed by the various parameters.

Table I shows the resolution limitations for typical TSE multiplier stages.

TABLE I ($\phi_e = 3500$ volts, $\phi_0 = 2$ volts)				
d	1.5	2.0	3.0	inches
$R_{\Delta V_0} = \dfrac{1}{2\,d}\ \dfrac{\phi_e}{\phi_0}$	1165	874	584	lines/inch
$R_{\Delta E} = \dfrac{1}{d}\ \sqrt{\dfrac{\phi_e}{\phi_0}}\ \dfrac{E}{\Delta E}$ for $\dfrac{\Delta E}{E} = .01$	5580	4180	2790	lines/inch
$R_{\Delta d} = \dfrac{1}{2\Delta d}\sqrt{\dfrac{\phi_e}{\phi_0}}$ for $\Delta d\ .015$ in.	2786	2786	2786	lines/inch

Table II shows the resolution limitations for typical photocathode multiplier stages.

TABLE II ($\phi_e = 3500$ volts, $\phi_0 = .5$ volts)				
d	1.5	2.0	3.0	inches
$R_{\Delta V_0}$	4660	3500	2335	lines/inch
$R_{\Delta E}$ for $\dfrac{\Delta E}{E} = .01$	11,160	8360	5580	lines/inch
$R_{\Delta d}$ for $\Delta d = .015$ in.	5572	5572	5572	lines/inch

Table III shows the resolution limitations for typical TSE multiplier target stages.

$$B' = \frac{B}{n} = \frac{4.17\sqrt{V}}{d}$$

d IS DISTANCE BETWEEN PHOTOCATHODE & SCREEN

B',B IS MAGNETIC FIELD INTENSITY

n IS THE NUMBER OF LOOPS OF FOCUS

V IS THE VOLTAGE BETWEEN PHOTOCATHODE & SCREEN
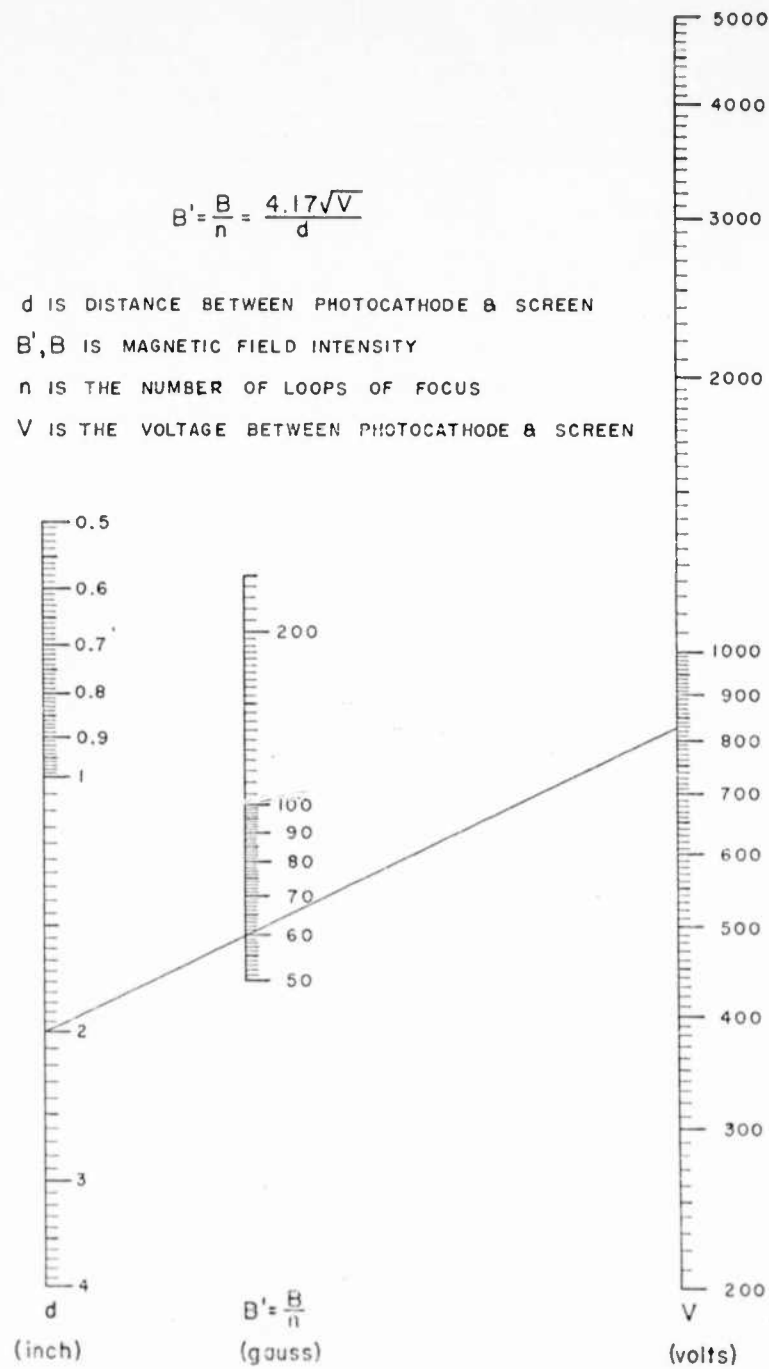
Figure 41. Nomograph for Determining Magnetic Field Intensity
in Image Tubes

TABLE III				
($\phi_e = 500$ volts, $\phi_o = 2.0$ volts)				
d	0.57	0.76	1.15	inches
$R_{\Delta Vo}$	440	330	220	lines/inch
for $R_{\Delta E}$ $\frac{\Delta E}{E} = .01$	5580	4180	2790	lines/inch
for $R_{\Delta d}$ $\Delta d = .015$ in.	1056	1056	1056	lines/inch

Table IV shows the resolution limitations for typical TSE multipliertarget stages.

TABLE IV				
($\phi_e = 1,000$ volts. $\phi_o = 2.0$ volts)				
d	0.8	1.07	1.6	inches
$R_{\Delta V_o}$	625	467	312	lines/inch
$R_{\Delta E}$ for $\frac{\Delta E}{E} = .01$	5580	4180	2790	lines/inch
$R_{\Delta d}$ for $\Delta d = .015$ in.	1490	1490	1490	lines/inch

Figure 41 is a nomograph showing the magnetic flux density as a function of electrode separation and the number of nodes in the electron path for a range of stage voltages. It is useful in readily establishing a consistent set of electron optical conditions assumed in the resolution limitation calculations.

Table V shows the resolution limitations as a function of magnetic field density where $R_{\Delta B} = \frac{3.34 \times 10^{-3} B}{n} \cdot \frac{B}{\Delta B}$

118

TABLE V					
B		165	124	82	gauss
$n = 1$ $\left\{\begin{array}{l}\end{array}\right.$ $\frac{\Delta B}{B} = .02$		1400	1052	685	lines/inch
$\frac{\Delta B}{B} = .01$		2800	2104	1391	lines/inch
$\frac{\Delta B}{B} = .005$		5600	4208	2782	lines/inch
$\frac{\Delta B}{B} = .01$ $n = 2$		1400	1052	695	lines/inch
$n = 3$		933	701	464	lines/inch
$n = 4$		700	526	348	lines/inch

Table VI shows the total resolution per stage as determined by the combining formula for resolution given in Eq. 5.

TABLE VI – TOTAL RESOLUTION PER STAGE									
	$\frac{d}{\text{in.}}$	Δd inches	$\frac{\text{Vend}}{\text{Kv}}$	ϕ_0 Volts	$\frac{\Delta E}{E}$	$\frac{B}{\text{Gauss}}$	$\frac{\Delta B}{B}$	n	Resolution lines/in.
Typical	1.5	0.015	3.5	2.0	0.01	165	.01	1	985
Multiplier	2.0	.015	3.5	2.0	.01	124	.01	1	760
Stage	3.0	.015	3.5	2.0	.01	82	.01	1	518
Cathode	1.5	.015	3.5	0.5	0.01	165	.01	1	2160
Stage	2.0	.015	3.5	0.5	.01	124	.01	1	1680
	3.0	.015	3.5	0.5	.01	82	.01	1	1142
Target	.57	.015	.5	2.0	.01	165	.01	1	400
Stage	.76	.015	.5	2.0	.01	124	.01	1	310
	1.15	.015	.5	2.0	.01	82	.01	1	212
	.8	.015	1.0	2.0	.01	165	.01	1	561
	1.07	.015	1.0	2.0	.01	124	.01	1	433
	1.6	.015	1.0	2.0	.01	82	.01	1	296

Table VII shows the overall system resolution for multi-stage tubes as computed by a combining formula of the type given by Eq. 5.

119

Table VII shows the overall system resolution for multi-stage tubes as computed by a combining formula of the type given by Eq. 5.

				Overall Resolution	
B Gauss	Cathode Stage Lines/in	Multiplier Stage Lines/in.	Target Stage Lines/in.	3 Stage Lines/in.	4 Stage Lines/in.
82	1142	518	296	226	207
124	1680	760	433	330	302
165	2160	985	561	428	393

TABLE VII

OVERALL SYSTEM RESOLUTION

It is clear that the calculations of resolution based on the foregoing analysis are a measure of the electron focusing ability of the image section. One basic assumption is that there is no lateral diffusion of charge along the target of the tube during the scanning interval. Other factors, such as quanta limitations at the photocathode, are not considered. The other donditions assumed in the calculations, such as variation in magnetic focusing field intensity, variation in electric field strength, and variation in stage spacings are only estimated values representing more or less practical design limits. The contribution due to these uncertainties may be kept fairly low. However, radial variations in field strength as well as non-parallel placement of the dynodes give use to image distortions which are not considered in the analysis. The main factor influencing resolution capability appears to be the spread in initial emission velocity particularly for large electrode spacings. Nevertheless, the calculations give a rough approximation of the limits in resolution which could be achieved with transmission secondary emission amplifiers.

As an example, derived in Table VII, the theoretical analysis predicts an image section resolution capability of 428 TV lines per inch for a three dynode stage tube, under the following assumed conditions;

Cathode-dynode stage and interdynode stage voltage: 3500 volts

Dynode-target stage voltage: 1000 volts

Cathode-dynode stage and interdynode stage spacing: 1.5 inches

Dynode-target stage spacing: 0.8 inches

Magnetic focusing field intensity: 165 gauss

Variation in electric field strength: 1%

Variation in stage spacing: .015 inches

Mean energy of electrons emitted from dynode: 2 volts

Variation in magnetic focusing field intensity: 1%

A major limiting factor in resolution capability, particularly in the final dynode-target stage, is the mean energy of electrons emitted from the dynode which has been assumed in the calculations as 2 volts. This value is based on the earlier Al-KCl film. As pointed out in a previous section, the average energy of secondary electrons emitted by the more recent "smoke" type TSE films has not yet been determined due to the observed charging effect. The limiting effect of average energy of electron emission can be seen from the aforementioned relationship:

$$R_{V_0} = \frac{1}{2d} \sqrt{\frac{\phi_e}{\phi_e}}$$

Where:

R_{V_0} = limiting resolution

d = stage spacing as determined by given stage voltage and magnetic focus field intensity.

ϕ_e = stage voltage

ϕ_o = voltage corresponding to mean energy of emission

Applying this to the final dynode-target stage:

d = 0.57 inches

ϕ_e = 500 volts

ϕ_o = 2 volts

R_{V_0} = 220 line pairs/in. = 440 lines/in.

121

Increasing the target stage voltage to 1,000 volts and increasing the spacing to 0.8 inches, corresponding to the same value of magnetic focus field intensity of 165 gauss assumed in the previous calculation, results in an increase of R_{V_O} to 625 lines per inch. This value is still appreciably lower than that obtained for the cathode-dynode stage and the interdynode stages. It can be seen then that higher voltages in the target stage would result in an increase in the resolution capability of the image section. The effect of higher voltages in the target stage on target gain is discussed in another section.

As shown by the calculations, the main factor influencing the resolution limitation is the spread in initial emission velocity particularly for large electrode spacings. The interdynode spacings used in the experimental tubes were determined primarily by a desire to operate the tube in a uniform magnetic focusing field both for the image section and the scanning section. This was based on experimental data which indicated severe resolution degradation in the scanning section of the image orthicon at magnetic focus field flux densities exceeding 160 gauss. To avoid re-design of the scanning section to permit operation at higher magnetic focus field intensities and to further avoid the problem of operating the image and scanning sections at different focus field intensities, it was decided to design the structure to perform in a uniform, relatively low intensity magnetic focusing field.

It is interesting to note that applying the foregoing resolution limitation analysis to the image section of a standard image orthicon, assuming planeparallel electron optics, results in a resolution capability well below that actually observed. This indicates that the predicted resolution performance may be on the conservative side.

5. THEORETICAL LIMITATIONS IN CONTRAST OF A TRANSMISSION SECONDARY ELECTRON EMISSION AMPLIFIER

122

In the transmission secondary emission multiplier, it is known that there is a fraction of primary electrons which penetrate the films, emerging on the exit side with relatively high energies. These electrons have been arbitrarily defined as having energies greater than 50 volts. Such electrons cause a decrease in contrast due to the difficulty of focusing them. Unfocused electrons cause a "halo" around every signal element. The effect of these penetrating primaries is analyzed in a report by H. Kanter of the Westinghouse Research Laboratories and shown in Appendix III. The analysis is carried out assuming that all primaries are stopped after one penetration and converted into secondaries with the same efficiency as are focused secondaries. This assumption should result in the maximum possible degradation of contrast due to penetrating primaries. The results for a three stage TSEM structure using 2 inch spacings between dynodes are computed in the following paragraphs.

The number of electrons in the halo produced by the penetrating electrons relative to the number of electrons in the signal spot is:

$$\frac{N_{halo}}{N_S} = (n-1)\ \frac{\eta_1 \delta_2}{\delta_1^2} + \frac{\eta_1}{\delta_1}$$

where: n = number of stages $= 3$

η_1 = number of penetrating electrons per incoming electron $= 0.2$

δ_1 = secondary emission ratio for secondary electrons $= 5$

δ_2 = secondary emission ratio for electrons which have penetrated the preceding dynode film and arrive with an energy larger than that of the signal electrons $= 5$

therefore:

$$\frac{N_{halo}}{N_S}\ = 0.12$$

The ratio of signal spot area to area of the halo is given by:

123

$$\frac{f}{F} = \frac{4k^2}{R^2 d^2 \, \alpha \, \text{Sin } 2 \, \phi}$$

where: k = number of revolutions per stage of secondaries = 1

R = resolution in line pairs per mm = 8

d = interdynode spacing in mm = 50

α = average energy of the penetrating electrons relative to the primary energy = 0.6

ϕ = scattering angle of penetrating electrons = 20° - 30°

therefore: $\frac{f}{F} = 2.1 \times 10^{-4}$

The ratio of the brightness in the signal spot to the brightness in the surrounding halo for a single point becomes:

$$\left(\frac{B_H}{B_S} \right)_{\text{point}} = \frac{N_{halo}}{N_S} \cdot \frac{f}{F} = (0.12) \quad (2.1 \times 10^{-4})$$

$$\frac{B_H}{B_S} = 2.5 \times 10^{-5}$$

or the contrast ratio is practically one for a reproduced single spot.

Estimating the contrast in the neighborhood of a single line, one must consider the fact that the brightness of the overlapping halos of neighboring points add up and thus the contrast decreases. Taking this effect into account, the brightness ratio for a line becomes approximately one.

Quoting from the conclusions of the research report:

"It should be mentioned, however, that these results are only estimates, since we considered only the most important group of penetrating electrons, namely, those which have penetrated a film once. Those electrons which penetrated more dynodes will give rise to a decrease in the above contrast figures. Also, electrons back scattered from a film will introduce additional background brightness. Because of this complexity, it is difficult to account for the effects of all these "background" electrons in a reliable way. An experiment must give the answer.

124

Nevertheless, the equations developed here show the important factors involved in the contrast of an image.

1. The penetration ratio η , should be as small as possible.

2. The yield for penetrating electrons δ_2 should be as small as possible compared with the yield δ_1.

3. The resolution of the system should be as high as possible.

4. The ($\propto \sin \phi$) of the penetrating electrons should be maximized."

FRONT SURFACE SECONDARY ELECTRON EMISSION AMPLIFIER

1. INTRODUCTION

As explained in a previous section of this report, theoretical calculations and experimental measurements agree that noise introduced in the scanning process is a principal limit in seeing at lower light levels with an image orthicon type camera tube. A practical solution to this problem is to increase the signal stored on the target for a given light level by use of a more sensitive photocathode, by use of a low noise image amplifier between the photocathode and the target, or by use of a target with a higher secondary emission ratio for increased target gain. Early in the term of this research, we decided jointly with the Air Force task scientist to devote our major effort to the second course of action, and to concentrate on image amplifiers using front surface secondary emission from fine venetian blind or mesh structures. This choice was made to obtain the advantage of extremely low operating voltage to lessen insulation and power supply problems in future airborne applications, and to choose an area of effort which was not at that time, as far as we know, being explored in any other laboratory. It was realized that the resolution of the resulting electronic image would be poor, but the prospect of obtaining a gain of 5 or more per stage with a stage voltage of only 300 to 500 volts appeared attractive enough to justify the effort. This decision was also based on the fact that the resolution obtainable in a picture televised at very low light levels is limited by statistical fluctuations in the photo electron emission current. We hoped, of course, to find ways to improve the resolution by design refinement after an amplifier had been developed.

The phenomenon of image intensification which depends upon front surface secondary electron emission is not new. Early work in this field, however, resulted in image intensifiers with rather limited resolution and gain. Two main problems

126

arise in applying the principle of front surface secondary emission amplification to image intensification.

a. Secondary electrons emitted from solid surfaces bombarded by relatively high energy primary electrons have a broad range of initial velocities. A typical emission energy distribution is characterized by two main groups of electrons, one having energies up to several volts and the other with energies near that of the incident primaries. The first group, comprising the true secondaries, contains 80-90% of the total emitted electrons while the second group, comprising the reflected or back scattered primaries, contains most of the remaining electrons with the exception of a small percentage with intermediate energies. Electron optical systems are normally incapable of focusing electrons with a wide energy spectrum, and an attempt to focus electrons emitted from a point source results in a circle of confusion at the plane of focus. This effect is analogous to the phenomenon of chromatic aberration in light optics terminology. Since it is not possible to focus all secondary electrons, even in the low energy group, one usually compromises by designing the electron optical system to focus the most probable emission energy, normally about 2 volts. Electrons with different initial energies will then be defocused and will establish an upper limit to the resolution capability of the device.

b. Another problem associated especially with image amplification employing secondary emission from vanes or mesh is the fact that a significant fraction of high energy incident primaries may be transmitted through the dynode structure resulting in image defocusing and thereby degradation in resolution and contrast.

The general approach taken in all of these tubes is shown in Figure 42. The device consists essentially of an image orthicon containing a series of parallel, close spaced secondary emission multiplier dynodes in the image section between the photocathode and the target. In the most successful version, these dynodes were placed close to the target collector mesh so that the photosurface could be formed
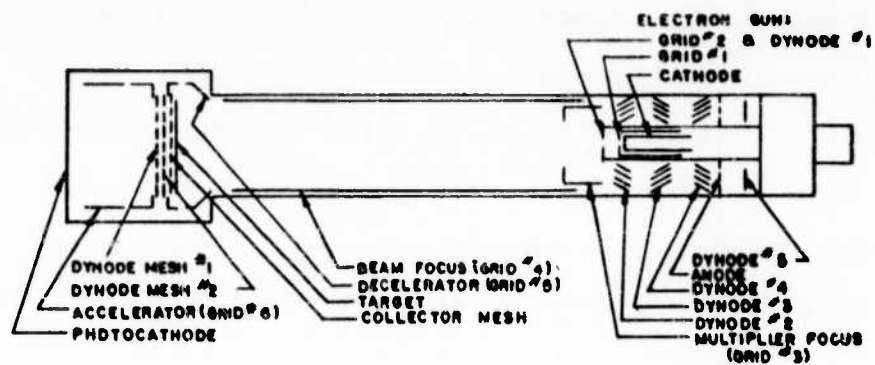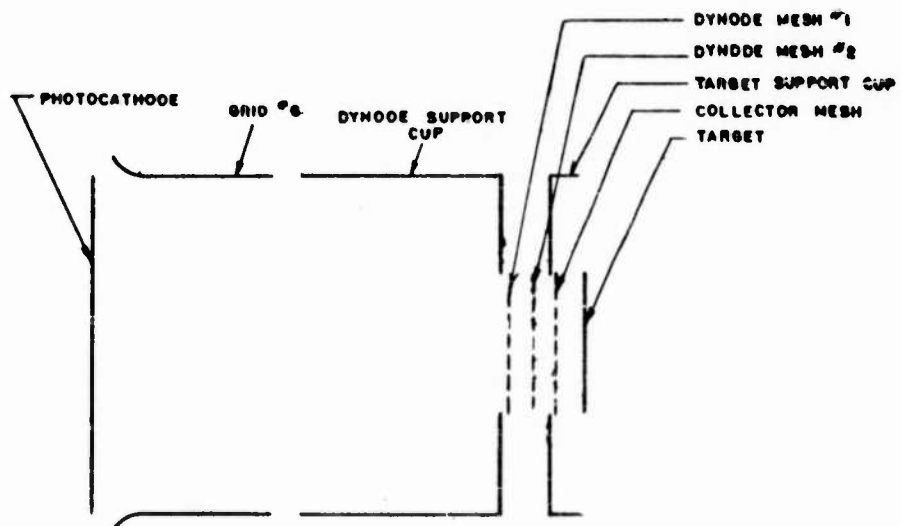
127

Image Section

Figure 42.   Image Orthicon with a Pre-Scanning Beam Front
Surface Secondary Emission Amplifier

128

in the normal manner by evaporation from sources located on the target support cup. The photoelectrons were focused on the first dynode by use of the solenoidal magnetic field. The succeeding dynodes were to be spaced as closely as possible so that secondary electrons would be strongly accelerated by the paraxial electric field with only slight lateral spreading due to emission velocities. Two basic secondary structures were employed in our investigation, the "venetian blind" type of multiplier structure with its array of inclined metal vanes and the fine mesh metal screen. In both cases, the electron bombarded surfaces of these dynode structures were processed so as to possess a high secondary emission yield. In the course of our work, the fine-mesh screen dynode was exclusively selected because its finer structure permitted a higher resolution capability than the coarser "venetian blind" dynode structure.

In the following sections, our experimental work with front surface secondary electron emission amplifiers will be described more or less in chronological order as a means of covering and evaluating all the various avenues of approach that were investigated.

2. VENETIAN BLIND MULTIPLIERS

Although very few experiments were made with the inclined slat venetian blind type structure, certain techniques were devised which are recorded here for reference. In general, the vane structure was made from .005" or thinner silver-magnesium alloy sheet by use of piercing and forming dies. In the interest of minimizing expenditures for experimental tooling, we attempted to form a fine vane structure with a guillotine type die which sheared and formed a vane at a time from the raw stock. Unfortunately, this method did not work well, since stock from the vane was usually drawn into the sheared region, and this resulted in badly distorted vanes when an attempt was made to achieve a fine structure of 50 to 100 vanes per inch. Our initial experimental tubes had only 10 or 20 vanes per inch, showed a measured electron gain of more than 5 per stage, but gave extremely poor resolution and contrast, which so degraded the

image that the threshold sensitivity was worsened rather than improved.

A method was devised but never fully evaluated for forming a fine vane structure from thin silver magnesium alloy foil, in which the stock was formed but not pierced using a rubber die technique. In this method, the surface of a single flat metal die was cut with a shaper or milling machine to have a series of parallel ridges whose cross section was like the shape of sawteeth. The thin metal sheet was laid over the surface of this die and pressed into the grooves with a rubber platen. By suitable design, the unformed metal sheet outside the vane area could be held in place by the pressure between the platen and the die. We then intended to coat the formed sheet with photoresist, and to expose the resist from a single light source placed at an angle so that each vane would shadow the area behind it which was to become a slot in the final dynode assembly. The unexposed resist would then be washed away from the slot area, and the slots opened by acid etching.

After formation of the venetian blind structure, the secondary emission surfaces were prepared by oxidation prior to insertion into the tube, using a schedule similar to that employed in the processing of image orthicon dynodes. In general, this processing schedule consisted of the following:

(1) Dynodes inspected for freedom from excessive burr, holes, tears, or broken vanes.

(2) Arranged dynodes in firing can and placed in vacuum bell jar.

(3) Exhausted bell jar down to approximately 10 mm Hg pressure.

(4) Introduced water vapor to pressure of 300-600 microns Hg.

(5) Uniformly heated firing can with RF coil until dull red color (approximately $650^\circ - 700^\circ C$) is reached.

(6) Reduced RF power and continue heating firing can for four minutes.

(7) Turned off RF power while continually adding water vapor to maintain pressure of 300-600 microns Hg.

130

(8) Allowed firing can to cool and exhausted system to a pressure of approximately 5 microns Hg.

(9) Introduced air into system until pressure reached 300-600 microns Hg.

(10) Uniformly heated firing can with RF coil until dull red color (approximately 650° - 700°C) was reached.

(11) Reduced RF power and continued heating firing can for four minutes.

(12) Turned off RF power while continually adding air to maintain pressure of 300-600 microns Hg.

(13) Allowed firing can to cool and removed from system.

(14) Dynodes should have a shiny straw colored appearance. Rejected for over-oxidation (dark color), under oxidation (metallic silver color), and signs of contamination.

At this time, however, the work with the transmission mesh multiplier structure began to show more promising results, and we chose to shelve the venetian blind approach. This decision was based on our belief that the resolution obtainable from such a structure could not be finer than the dimensions of the vanes. Since our initial mesh multiplier experiments had been performed with 500 line per inch mesh, and we were encountering difficulty in making venetian blind dynodes with more than 30 vanes per inch, the reasons for the change seemed rather compelling.

3. TRANSMISSION MESH MULTIPLIERS

a. Theory

One method for obtaining planar secondary emission dynodes from which the secondary electrons may be readily accelerated and focused is by the use of a transmission mesh multiplier. In this structure, a schematic diagram of which is shown in Figure 43, a metal mesh is coated with a good secondary emitting material, snd bombarded by the electromagnetically focused electrons from the photocathode. Those primary electrons which strike the mesh bars cause liberation of secondaries which
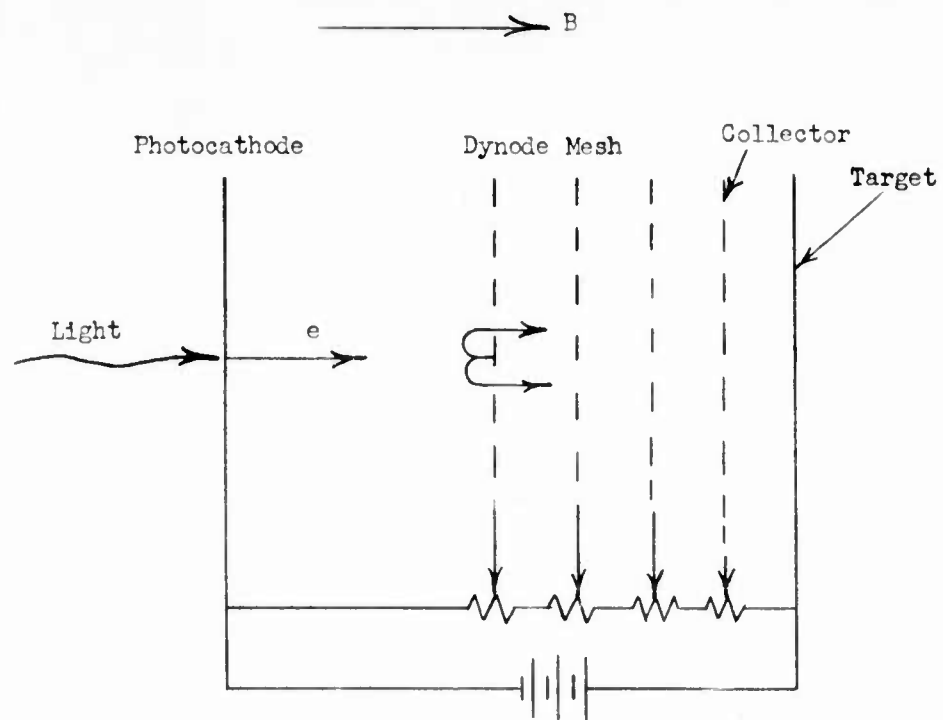
131

Figure 43.   Front Surface Secondary Emission Amplifier

132

are urged through the mesh holes by the electric fields on either side of the mesh. The gain of such a structure may be calculated as follows. Since the primary electrons will have been accelerated through a potential difference of 300 to 800 volts before they approach the mesh, their paths will be essentially straight and undeviated by the small field perturbations around the mesh holes. Therefore, the fraction of the incident primary electron current which passes through the holes without striking the mesh bars will be very closely equal to the optical transmission of the mesh. These electrons will not, of course, result in secondary emission gain, and since they emerge from the mesh with a high initial velocity, may not be focused by a magnetic field appropriate to focus the secondary electrons. Jay Burns of the Chicago Midway Laboratories has proposed a method of bringing electrons with two widely different initial velocities to a focus in the same plane by a combination of proper spacing and voltages between screens. (Reference 24)

The electron gain of a mesh dynode is best expressed as the quotient of the total current leaving the dynode to the right divided by the incident current from the preceding dynode or photosurface. To a first approximation

$$G = \frac{i_2}{i_1} = \frac{T i_1 + \delta (1-T) \quad i_1 T}{i_1}$$

Where G = electron gain of dynode

$\quad i_2$ = current leaving at dynode

$\quad i_1$ = current arriving at dynode

$\quad T$ = optical transmission of mesh

$\quad \delta$ = secondary emission ratio of dynode surface

$\quad G = T + \delta T (1-T)$

In this case, we assume that the secondary electrons are all emitted back toward the photocathode, that they are turned around and rain down on the mesh, and that they are also not influenced by the field perturbations around the mesh holes so that

133

the fraction of secondaries passing through the holes is equal to the optical transmission of the mesh. We have shown experimentally that this is not so. Under conditions in which a weak field is set up immediately in front of the mesh and a strong field employed behind the mesh, there is a substantial field penetration through the mesh holes which may cause nearly all of the secondary electrons to pass through the mesh holes. This factor is added to the equation:

$$G = T + g\delta T \ (1-T)$$

where g usually has a value between 1 and $1/T$.

The importance of achieving a high secondary emission yield from the surface of the mesh bars, as well as high g or a secondary electron extraction factor, is apparent from this analysis. For a typical mesh with a 50% optical transmission, a g factor of 1.2, and a secondary emission ratio, δ, of 6, the electron gain per stage will be only $.5 + 1.2x6x.25 = 2.3$, which compares poorly with a gain of 5 per stage which may be realized in a venetian blind type structure. As described below, during the course of this research we devised dynode processing means, tube structures, and modes of operation to obtain both a very high secondary emission ratio and a high extraction factor. A description of this experimental work follows, and is divided into three stages which occurred in more or less chronological order.

b. Use of Fine Electroformed Mesh

As indicated above, our object was to obtain a very fine mesh structure to permit realizing high resolution in the amplified pattern. Initially, our multiplier dynodes consisted of standard electroformed copper mesh with 500 mesh bars per inch and 65% optical transmission, normally used as camera tube collector mesh. These mesh were placed about .050" in front of the normal image orthicon collector mesh and were pre-coated with a secondary emission material on the photocathode side. In our preliminary work, we selected Ag-O-Cs and KCL as the secondary emitting surface for the dynode structures, both of which had been reported in the literature as having

134

reasonably high secondary electron yield at comparitively low primary voltages.

Initially, the Ag-O-Cs secondary emitting surface was prepared according to the following processing schedule:

(1) Mesh structures located in vacuum bell jar and system exhausted to pressure of approximately 10^{-5} mm Hg.

(2) Evaporated approximately 100 Å of silver on surface of mesh.

(3) Mounted mesh dynodes in tube with silvered photocathode.

(4) Tube sealed to exhaust system and baked.

(5) Silver surfaces of mesh dynodes oxidized by introducing oxygen into tube to pressure of several millimeters Hg, with pumping system cut off.

(6) Applied RF glow discharge to mesh dynodes. Resulting color changes on dynodes surfaces observed until they had passed through the yellow and red stages and reached blue, when the discharge was discontinued.

(7) Cesium added to dynode surfaces during normal sensitization of the photocathode.

Measurements of electron gain as a function of primary voltage were made on tubes containing a single Ag-O-Cs mesh multiplier stage in the image section. In these measurements, the image orthicon collector mesh was held 600 volts positive with respect to the dynode mesh. The dynode electron gain was found to have a maximum of slightly over 2.2 at a primary voltage of 500 volts. Note that this dynode gain implies a considerably larger secondary emission ratio, which as indicated previously, may be about 6.

Imaging tests on these tubes showed no improvement in sensitivity, which was attributed to the effects of other variations in the tubes which were likely to override the small measured gain. The next experiments, therefore, were made with three secondary emission stages from which we hoped to obtain an order of magnitude increased in sensitivity. The choice of structure was at first strongly influenced
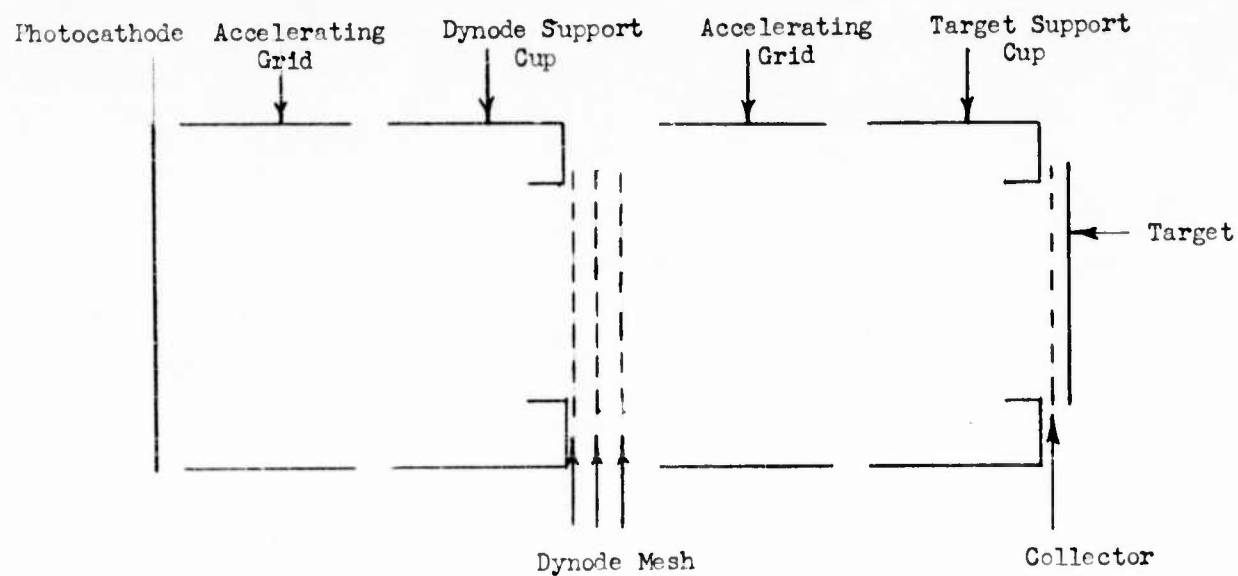
135

Figure 44. Dual Image Section with Front Surface
Secondary Emission Amplifier

136

by mechanical design and tube assembly problems.

To provide the additional leads required for a multi-stage pre-scanning beam amplifier tube, a 14 pin image stem was designed and fabricated by spacing seven additional pins on the same circle diameter, mid-way between the pins of the standard stem. Clearance holes were drilled in the standard image orthicon shoulder socket for these added leads while maintaining the standard image orthicon connections. Thus, experimental image orthicons with multi-stage pre-scanning beam amplifiers could be field tested in standard image orthicon cameras.

As the first approach to obtaining a 3-stage mesh amplifier, a design was adopted employing a dual image section. In this structure, electrons from the photocathode spiral through one magnetic loop of focus onto the first mesh multiplier dynode. Secondary electrons from this multiplier are then accelerated onto a close-spaced second dynode to minimize the lateral spread. Similary, secondaries from the second dynode are then accelerated onto a close-spaced third dynode and finally secondary electrons from this dynode spiral through another loop of magnetic focus onto the target. In this type of structure, the multiplier section could be built into the electrode structure prior to the image bulb to stem glass seal since it was far enough away from the sealing zone to avoid damage from the sealing fires. The target-mesh assembly was mounted on the target support cup after the image seal, by the standard means of passing it through the 2" diameter neck and installing it by use of a long manipulator. A schematic diagram of the tube structure is shown in Figure 44. To use this tandem image section, it was necessary to increase the image bulb length to approximately twice that of a standard image orthicon and a special long magnetic focus coil was designed and constructed to test these tubes. Four tubes of this type were constructed each having three Ag-O-Cs mesh multiplier stages in the image section. Close spacing of the multiplier screens was assumed essential in order to keep transverse spread of secondary electrons at a minimum.

137

However, the tubes that had dynode spacings of .010" and .015" were made inoperable by the fact that the fine mesh screens collapsed toward one another due to the unequal electric fields on either side of the screens. This difficulty was eliminated in later tubes by increasing the multiplier spacing to .050". Test data on these tubes indicated that a maximum resolution of 250 TV lines and fair contrast was obtained. However, overall maximum electron gain measurements for the three stage structure were only about 2, compared to 2.2 for a single stage structure, and compared to an expected gain of up to 40 calculated from an assumed secondary emission ratio of 10 and an electron extraction factor, g, of 1.2.

An effort was made to improve the processing of the Ag-O-Cs secondary emitting surface by forming the silver oxide layer before mounting the dynodes into the tube. This produced surfaces with excellent uniformity but difficulty was encountered in devising a tube exhaust schedule that would permit effective outgassing without decomposing the silver oxide. A change to oxidizing the silvered surface of the mesh by using a d.c. glow discharge between adjacent dynodes, during tube exhaust, resulted in somewhat better control of surface color, but no increase in electron gain. Continued unsuccessful attempts at producing Ag-O-Cs surfaces with high secondary emission yields led to a discontinuation of work on these surfaces. As the time we attributed the poor results to the following factors:

1. A critical step in dynode processing consisted of adding cesium to the silver oxide surface during the normal formation of the Bi-Ag-O-Cs photocathode. With this technique, it appeared that the proper conditions for producing high yield Ag-O-Cs surfaces were incompatible with the formation of efficient cesium-bearing photocathodes.

2. Poor preparation of the Ag-O-Cs surfaces on dynode stages subsequent to the first, due to the apparent shielding effect by the first fine mesh dynode on the oxidizing atmosphere and the cesium vapor.

138

On the basis of our previous experience with the venetian blind dynode structures, we then attempted to form the more stable magnesium oxide secondary emitting surface on our fine electro-formed copper mesh. A first attempt to coat the mesh by evaporation with metallic magnesium and to form a magnesium oxide surface by introducing oxygen during the $400^{O}C$ exhaust bake was unsuccessful. Maximum electron gain per stage was only about 2, and photosurfaces were very poor. We thought this might be caused by evaporation of the magnesium from the mesh before and during the oxidation step. An attempt was made to evaporatively coat the mesh with silver and magnesium to simulate the conditons found in forming a magnesium oxide film on a silver magnesium alloy electrode. The photocathode sensitivity was then satisfactory, but the dynode gain was still poor.

In subsequent experiments, magnesium was vacuum evaporated on one side of a 720 wire per inch electroformed copper mesh with an optical transmission of 55%. The magnesium was then oxidized prior to insertion into the tube structure. With this technique, a maximum electron gain of 4 was obtained.

During the time that these measures were being taken to improve the secondary emission yield of the surfaces, the tube structure was revised to place the transmission mesh multipliers immediately adjacent to the image orthicon collector mesh, so that only one magnetically focused image section was used between the photocathode and the first mesh dynode. Lateral dispersion of the secondaries was again to be limited by use of close inter-dynode spacing and high paraxial accelerating fields. This design change avoided the problem of our inability to focus magnetically both the secondary and penetrating primary electrons. It was accomplished by devising a bulb sealing process which would permit installing the multiplier mesh before the seal without heat damage. The revised tube structure had essentially a standard length image section and hence could be operated or field tested in a standard image orthicon camera with only the addition of a special shoulder socket and a high voltage power supply.

Despite the changes outlined above, resolution and contrast were poor on these tubes whenever the tube wes opereted in the amplifying condition and electron gain continued to be lower than expected. A check was made to determine whether photo-emission from the mesh dynodes was contributing to the poor image quality. While photoemission was found, the resulting photocurrent was less than 1% of thet meesured from the photocathode, and we discarded this factor as e ceuse of poor imaging. Sev-eral single stage multiplier structures were made in which the photocathode side of the copper mesh was ocated with silver end magnesium, but in which the reverse side of the mesh was coated with gold, which wes expected to act as a getter for cesium. Some of these structures showed gains as high as 3.5 at 400 volts compared to 2.5 for structures without gold. Inconsistency in these results, however, discouraged us from pursuing this technique.

c. Use of A Shaped Mesh Structure

A second ssries of experiments was conducted in an attempt to form the dynode mesh bars to increase the effective secondary emission yield, to improve the extrac-tion factor for secondary electrons, and to channel the secondary electrons perferen-tially through the nearest mesh hole to improve resolution. Basically, this consisted of attempts to make mesh bers with ridge shaped faces, the peak of the ridge being aimed toward the preceding stage. This work overlapped both the fine mesh experi-ments described in the preceding section and the etched silver magnesium foil dynode experiments described in the preceding section. The reasoning governing this approach is es follows:

1) For most materials, the secondary emission ratio veries es a function of the angle of incidence of the primary electrons, having a minimum for normal incidence and frequently e significantly higher value for angles approaching grazing incidence. By use of the triangular cross section or similary shaped mesh bars most of the nearly paraxial primaries could be made to strike the surface at an angle to the

140

normal, which should increase the secondary emission yield.

2) Work on secondary emission which had been performed by Dr. Helmut Kanter of the Westinghouse Research Laboratories indicated that the distribution in emission angle for secondary electrons did not follow the usually assumed cosine function about the normal to the surface if the primary electrons approached the surface at an oblique angle. Instead, his results at that time indicated maximum secondary emission along the direction of a specularly reflected ray. Thus there was hope that the use of triangular shaped mesh bars would result in secondary electrons which would be directed down into the nearest mesh hole, resulting both in improved electron gain and resolution. Although other workers in the secondary emission field disagreed with Kanter's results, and found the usually assumed cosine distribution, we reasoned that the shift of the normal to each element of the surface toward its nearest mesh hole was beneficial and hoped through use of sufficiently strong fields to urge the secondaries through these holes, thereby limiting the lateral trajectories of the secondary electrons without decreasing the yield.

3) We also hoped to obtain two further advantages. First, since most of the secondary electrons would originate on the inner tapered walls of the triangular shaped mesh bars within the entrance to a mesh hole, there would be a physical barrier to prevent many of them from drifting to other holes. Secondly, the surface of the mesh would suppress optical reflections of light transmitted through the photocathode which might otherwise generally re-excite the photocathode and cause loss of contrast and resolution.

To confirm this reasoning and to obtain data on an optimum combination of mesh bar shape, mesh thickness, hole size, and inter-dynode spacing, a series of two di-mensional structures were set up on a rubber membrane electron trajectory plotter. Three general shapes of mesh bars were studied, the "kidney bean" or "cupcake" cross section found for the electroformed mesh we had been using, an isosceles triangle

cross section mesh bars, and a variation of the inclined slat or venetian blind shape
which we though possible to reproduce in electroformed mesh. In this study, the
initially horizontal stretched rubber membrane was distorted vertically by small
wooden or plastic blocks whose cross section represented models of mesh bars. The
horizontal surface of contact of each block with the membrane was set at a height to
represent the potential applied to each in the actual tube structure, with the cath-
ode highest and the following collector mesh lowest. Steel ball bearings were started
from rest at the 'cathode surface', and allowed to roll toward the dynodes. Secondary
emission velocity effects could be simulated by starting balls from rest at various
points on the dynode mesh bar surfaces and comparing their trajectories with those
found when controlled initial velocities were used.

Although the work done was of a qualitative nature, several conclusions were
reached:

1) The "kidney bean" shaped mesh bars of normal fine electroformed collector
mesh is not very effective despite orientation to face the convex surfaces toward
the incident electrons. For any typical voltage ratios and spacings there is a
large dead area in the center of each mesh bar. Here, emitted electrons see a strong
retarding field and are repelled back into the surface from which they have been
emitted, hence they do not reach the succeeding multiplier stages. Only a relatively
small percentage of the area of each electrode, therefore, is effective in producing
secondary electrons.

2) Mesh bars with the cross section of an isosceles triangle are far more ef-
ficient, and have for some voltage ratios and spacings practically no dead areas.

3) The venetian blind type structure is still more efficient since it may be
made nearly impervious to primary electrons, so that all primaries will strike a vane
and result in secondaries.

The efficiency of a mesh multiplier, which is defined as the fraction of

142

secondary electrons emitted from a dynode which arrive at the active area of the succeeding one, is not only dependent on mesh bar shape, space, and the optical transmission of the mesh, but also on the relative registration of holes and mesh bars in succeeding stages. Unfortunately, the obvious means to obtain high multiplier efficiency by placing the bars in one stage behind the holes in the previous stage would result in rapid loss of resolution as the number of stages is increased. This results since the electrons which emerge from a single hole are divided among 2 or 4 holes in the succeeding stage and so on, even under ideal conditions. Conversely, for most arrangements, registering the holes in successive meshes gives very poor efficiency since secondaries tend to be focussed down the center of the resultant channel and do not strike the bars of subsequent dynodes, hence result in no further electron gain. Resolution limitations are also imposed by the lateral excursion from hole to hole of secondary electrons due to their emission velocities.

Late in the course of our research on mesh multipliers we became acquainted with the work in this field of Burns and his associates at the Midway Laboratories of the University of Chicago. His work and that of McGee in England on channeled electron multipliers was described at the Conference on Light Amplification held at the U.S. Army Engineer Research and Development Laboratories on October 6-7, 1958. Both workers are attempting to use specially shaped mesh bars, registered holes, and extremely close spacing to form a continuous channel which will prevent leteral transfer of electrons from one channel to another. Unfortunately, the spacing is so close as to require use of a physical dielectric between mesh bars for insulation. Burns relies on the formation of a strong electron lens between dynodes in each channel which causes all electrons from the active area on one dynode to strike the active area on the next, though we did not choose to attempt to follow this approach, partly because of the formidable technological problems, some of which still exist, and partly because we preferred to avoid duplication of Research approaches as a matter of
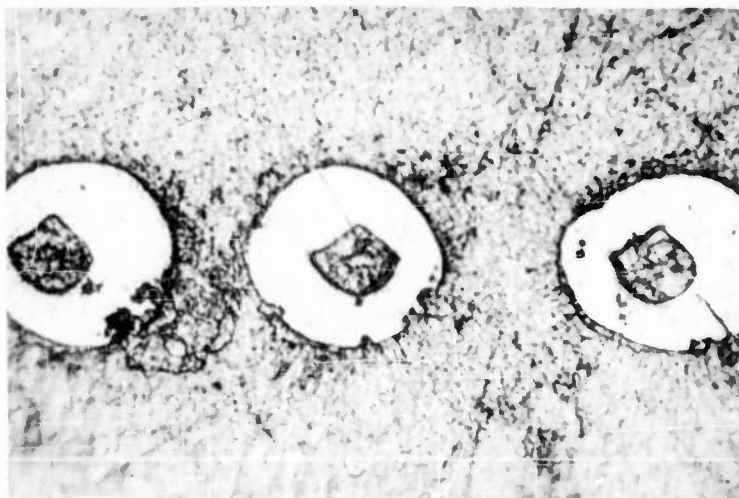
143

Figure 45.   Photomicrograph of 720 Lines/Inch Shaped
Electroformed Mesh 1200 x Magnification

policy.

Our experimental work to produce useable mesh with specially shaped cross sections followed these approaches:

1) Starting with an existing high transmission fine electroformed copper mesh, we plated additional material onto the mesh bars while forcing the plating solution through the mesh holes. The moving electrolyte caused selective plating which resulted in triangular cross section mesh bars. A cross section of some sample mesh is shown in Figure 45. A tube using a single stage mesh dynode of this type with an MgO secondary emitting surface showed somewhat better results than tubes using standard mesh.

2) We coated an existing electroformed mesh with a photo resist, then exposed it to ultraviolet light from one side with a point light source placed at a distance. We then washed away the unexposed resist behind each mesh bar and plated additional copper onto each bar. By exposing at an angle, this method could be used to make fine mesh structure with inclined bars like a venetian blind dynode.

3) Electroformed mesh is normally made through use of a glass "master", a flat glass plate into which a pattern of shallow groovers have been etched. We metallize the surface of the mesh with palladium by sputtering, then wipe the palladium from the flats on the master surface, leaving a conductive network in the bottom of the grooves. The master is then placed in a carefully controlled copper plating bath and the grooves plated full of copper. Very little control of mesh bar shape is obtainable, since the etched grooves are inherently shallow and nearly cylindrical. To obtain electroformed triangular shaped mesh bars with a small included vertex angle, we needed a master with triangular grooves. During this research program we worked briefly with scientists of the Corning Glass Works in an attempt to make such a master from Corning Fotoform glass. The solubility of this glass to an acid etchant can be altered by a factor of 7 to 1 by exposure to ultraviolet light and subsequent
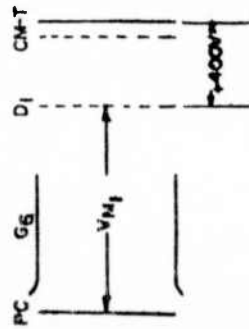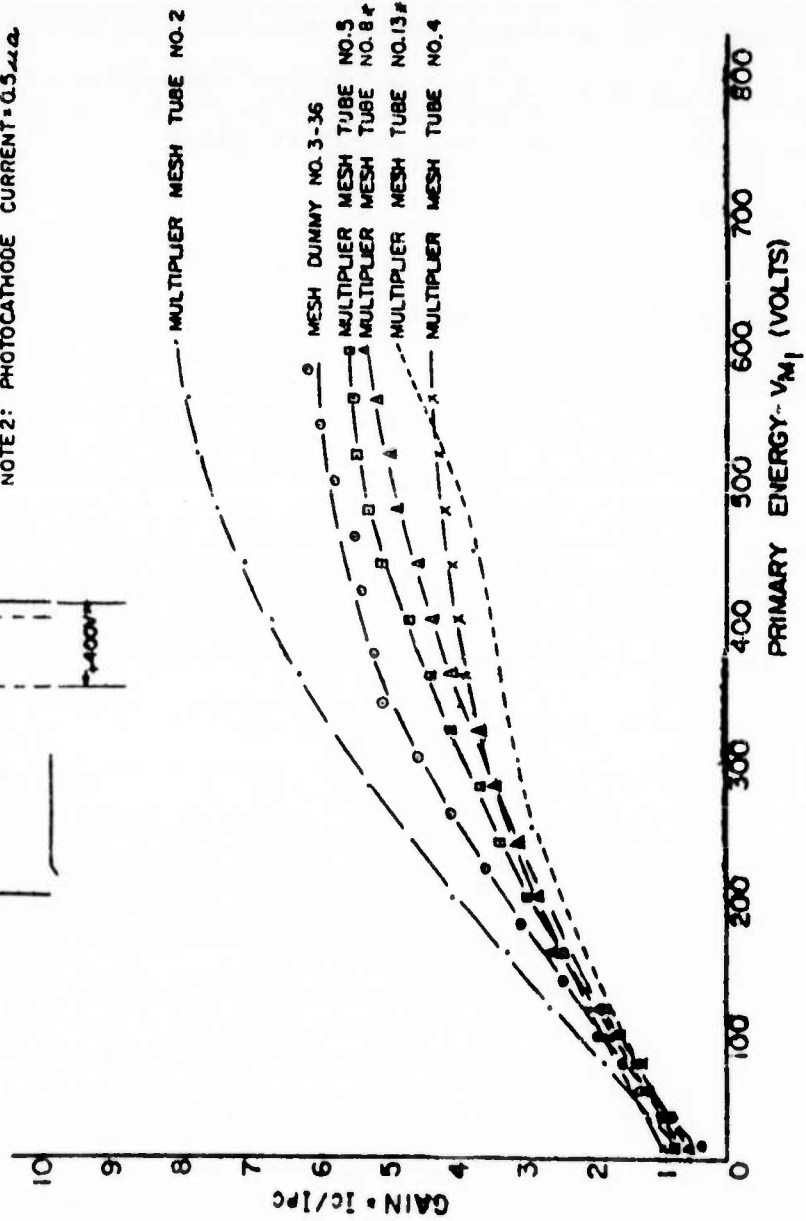
145

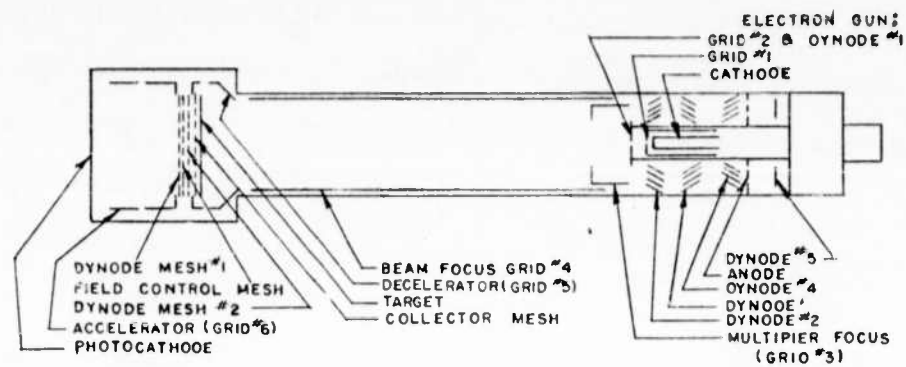Figure 46. Gain Versus Primary Energy (Single-Stage)

146

development. By appropriate exposure, development, and etching from one side. Corning Glass produced a Fotoform plating master with generally wedge shaped grooves. However, the contours were very irregular, which made it unuseable. The experiment was not carried beyond this point because of concentration on other problems.

4) In earlier camera tube work we had obtained thin fine glass mesh of Corning Fotoform for use as experimental image orthicon collection mesh. The glass was metallized by evaporation to make its furface conductive. We also worked with Corning to obtain mesh with triangular shaped mesh bars by this means, but did not build tubes because of concentration on other problems.
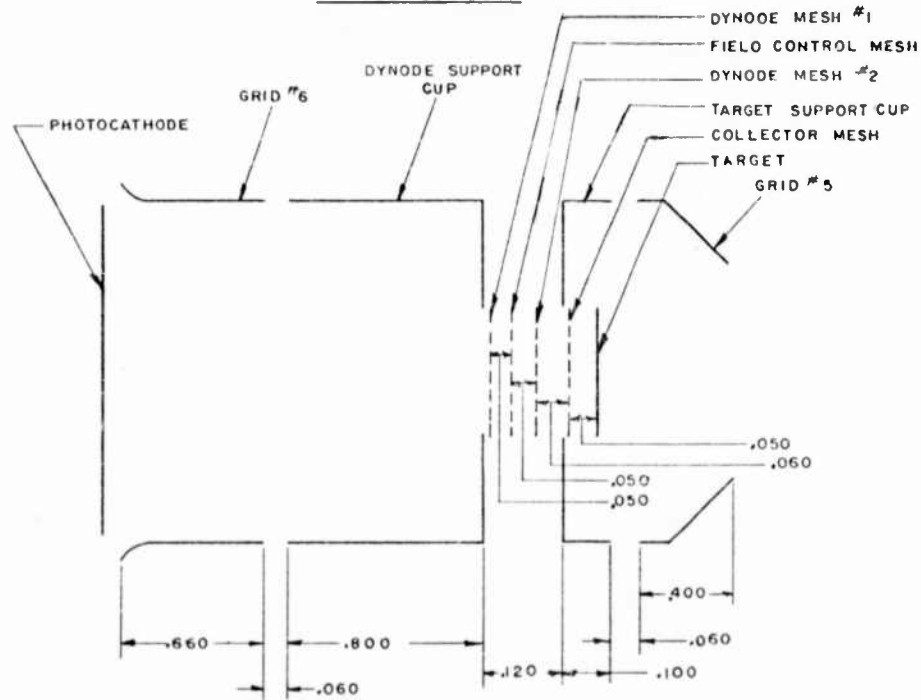
d. Use of Etched Silver Magnesium Foil Dynodes

As described previously, all attempts to form a secondary emitting surface on electroformed copper mesh had yielded maximum electron gains for a single dynode stage tube of at most 4, and multistage structures showed no better gain than single stage structures. At the time, we blamed this disappointing result on the difficulty of forming a good secondary emitting surface, especially on the second and third mesh of our three stage dynode structures. Realizing that we had long achieved good control of the process for making dynodes of a silver magnesium alloy in our standard image orthicon tubes and these dynodes were very stable, we turned our attention to making fine mesh dynodes from this material. As a first step we obtained .001" thick silver magnesium alloy foil, and arranged with Buckbee-Mears to have it selectively etched to form a mesh having 100 holes per linear inch in a square array with 50% open area.

1) These screens were pre-oxidized by the previously described technique employed by Westinghouse for the pinwheel multiplier of the image orthicon and assembled in the image section prior to the image bulb seal. Performance data of several such structures is shown in Figure 46. As can be seen, a current gain of 4 to 6 could be obtained reproducibly when 600 volts was applied between the photocathode

147

ELECTRON GUN:
GRID #2 & DYNODE #1
GRID #1
CATHODE

DYNODE MESH #1
FIELD CONTROL MESH
DYNODE MESH #2
ACCELERATOR (GRID #6)
PHOTOCATHODE

BEAM FOCUS GRID #4
DECELERATOR(GRID #5)
TARGET
COLLECTOR MESH

DYNODE #5
ANODE
DYNODE #4
DYNODE #3
DYNODE #2
MULTIPIER FOCUS
(GRID #3)

DIMENSIONAL DIAGRAM OF WX-3714
WITH FIELD CONTROL MESH
(IMAGE SECTION)

PHOTOCATHODE
GRID #6
DYNODE SUPPORT CUP

DYNODE MESH #1
FIELD CONTROL MESH
DYNODE MESH #2
TARGET SUPPORT CUP
COLLECTOR MESH
TARGET
GRID #5

.050
.060
.050
.050

.400

.660
.800
.060
.120
.400
.060
.100

NOTE: DIMENSIONS IN INCHES

Figure 47. Schematic Arrangement of WX-3714 (Two Stage with
Field Control Mesh)

148

and the dynode of a single stage multiplier structure. One tube showed a multiplier current gain of more than 8. From the formula given earlier, even if one assumes 100% use of the secondary electrons $(\delta = \frac{1}{T})$, this data indicates secondary emission ratios in the range of 7 to 15.

2) Now that satisfactory gain had been obtained from a single dynode structure, we were free to turn our attention to multistage structures and imaging problems. Early two stage versions of this structure, however, gave a gain almost exactly the same as that for a single stage multiplier. Measurements showed that essentially all of this gain occurred in the first stage.

3) The baffling lack of gain in the second stage was investigated and, in this case at least, found not to be a case of a poor secondary emitting surface. The difference in performance between the first and the second dynode mesh was found to be entirely related to the higher electric field strength found on the secondary electron emitting side of the second mesh, which was apparently repelling most of the secondaries back into the dynode surface without permitting them to migrate over to a mesh hole. Conversely, the electric field on the photocathode side of the first mesh was comparitively low, while the field on the opposite side was high, causing excellent extraction of the secondaries. The problem was solved by including an extra mesh between the two dynodes to reduce the electric field in front of the second dynode and allow the secondaries to leave the surface and proceed through the open areas of the screen to the succeeding dynode. In the structure as finally designed, as shown in Figure 47, the intermediate mesh consists of a fine knit 100 wire per inch screen with an optical transmission of more than 80%. The spacings between all mesh in this structure were about .050". The intermediate field control mesh operated at various voltages and the resulting gains are shown plotted in Figure 48. This data demonstrates the need for a low field strength ahead of each dynode. For the spacings and mesh which we used, each field control mesh could be electrically

149

connected to the following dynode with satisfactory results. As shown in Figure 48 this arrangement gave current gains for two stages as high as 25 with only 400 volts per stage. A curve of gain vs. collector voltage for a two stage tube is shown in Figure 49.

In spite of these demonstrated current gains, no improvement in threshold light performance was found. Image quality in terms of resolution and contrast was poor. This was only partially attributable to the lower than normal photocathode sensitivities obtained in these early experimental tubes.

To isolate the reason for poor imaging, a white to black transition in the image of a half black - half white test pattern was used. Careful study of the image reproduced by the two stage tubes showed that a sharp white to black transition, which was reproduced faithfully when the tube was not operated in the amplifying condition, was diffused in the amplifying condition over a distance corresponding to several mesh holes. The video wave form on the oscilloscope when observing the signal along one scanning line showed a corresponding gradual transition from white to black, with the tube operating in the amplifying condition. The cause for poor resolution in the amplified image was attributed primarily to the lateral motion of secondary electrons, particularly at the surface of the first multiplier. The image section structure is such that the secondary electrons are emitted from the surface of the first multiplier screen into the rather weak electric field between the photocathode and dynode and trajectory calculations were made to show that secondary electrons emitted at the first multiplier with an energy of 1.5 electron volts may pass through openings in the screen .15' from their point of origin, thereby forming a circle of confusion

.030" in diameter. This alone would establish a limiting resolution of about 30 TV lines, which agreed reasonably well with the observed diffusions in the image of the white to black transition. Secondary contributing causes of poor resolution were also considered. These included the effect of reflected light from the shiny multiplier surface which resulted in spurious emission at the photocathode and the generation of spurious secondary electrons by back-scattered electron bombardment at the dynode surface.

In order that a complete and meaningful appraisal could be made, the majority of the experimental tubes constructed were confined to a single stage of amplification. Any undesirable conditions that were isolated in these single stage models would also be applicable to a multistage structure. Since our calculations showed that lateral excursions of secondary electrons ahead of the first multiplier screen was one of the important causes of resolution degradation, it was clearly necessary to provide a means of independent control of the electric field gradient preceding the first secondary emitting surface. By proper adjustment of this electric field it should be possible to limit the lateral travel of the secondary electrons ideally from the mesh bar of origin to the adjacent screen opening. This control was accomplished by inserting a high transmission 100 wire per inch tungsten mesh .050" in front of the multiplier screen and electrically insulated from it. The effect of this field control mesh on the secondary emission yield of the first multiplier screen was then considered. Figure 50 shows the single stage current again as a function of the voltage applied to the field control mesh. It was hoped that a significant improvement in image resolution and contrast would result without complete loss of electron gain, but unfortunately this was not found in the experimental tubes utilizing this feature. Apparently other factors were playing an equally important role in establishing the resolution limitations of the tube. Serious limitations in image quality undoubtedly resulted from the use of the relatively coarse

100 hole per inch multiplier mesh structure. In addition, lateral movement of secondary electrons in the inter-stage multiplier regions as well as in the final screen to target spacing certainly tended to degrade resolution.

A mathematical analysis was made of the problem of lateral drift of secondary electrons and the predicted resolution capabilities of multipliers of the type we were then using. The calculations are shown in Appendix IV. Our conclusion was that although we had succeeded in making a transmission mesh multiplier structure with high stable current gain, application of the structure to amplifying an image with even modest resolution would require a series of substantial changes in design, each of which would require development, and which might not be completed within the final year of the contract. In particular, the silver magnesium alloy dynode would have to be somehow fabricated in the form of triangular shaped mesh bars and registered so as to provide independent channeled paths for the secondary electrons in order to prevent lateral electron excursions. A further requirement would be very close dynode spacing and therefore high dielectric strength insulation between stages.

Perhaps most important, the major problem of fabricating such an amplifier with a structure finer than 50 to 100 lines per inch strongly indicated that this device should be applied first to a tube in which the image size was larger than the 0.9" x 1.2". After careful consideration, and in light of the newly acquired knowledge that work on the channeled structure was being conducted in other laboratories, we decided in June of 1958 to recommend a major shift of emphasis to concentrate on application of the Westinghouse TSEM as a preamplifier in an image orthicon. The work on this approach has already been described in Section IV.
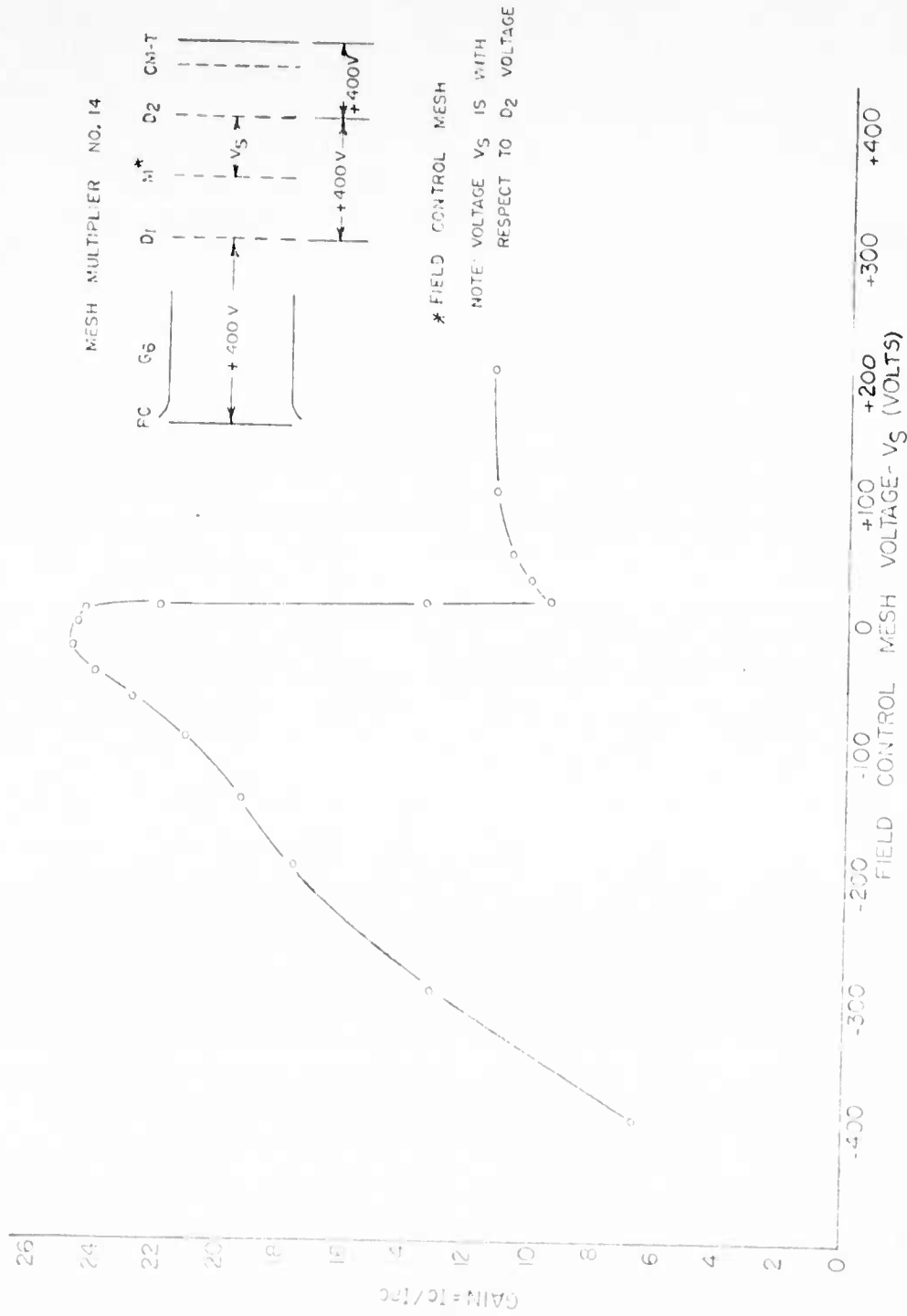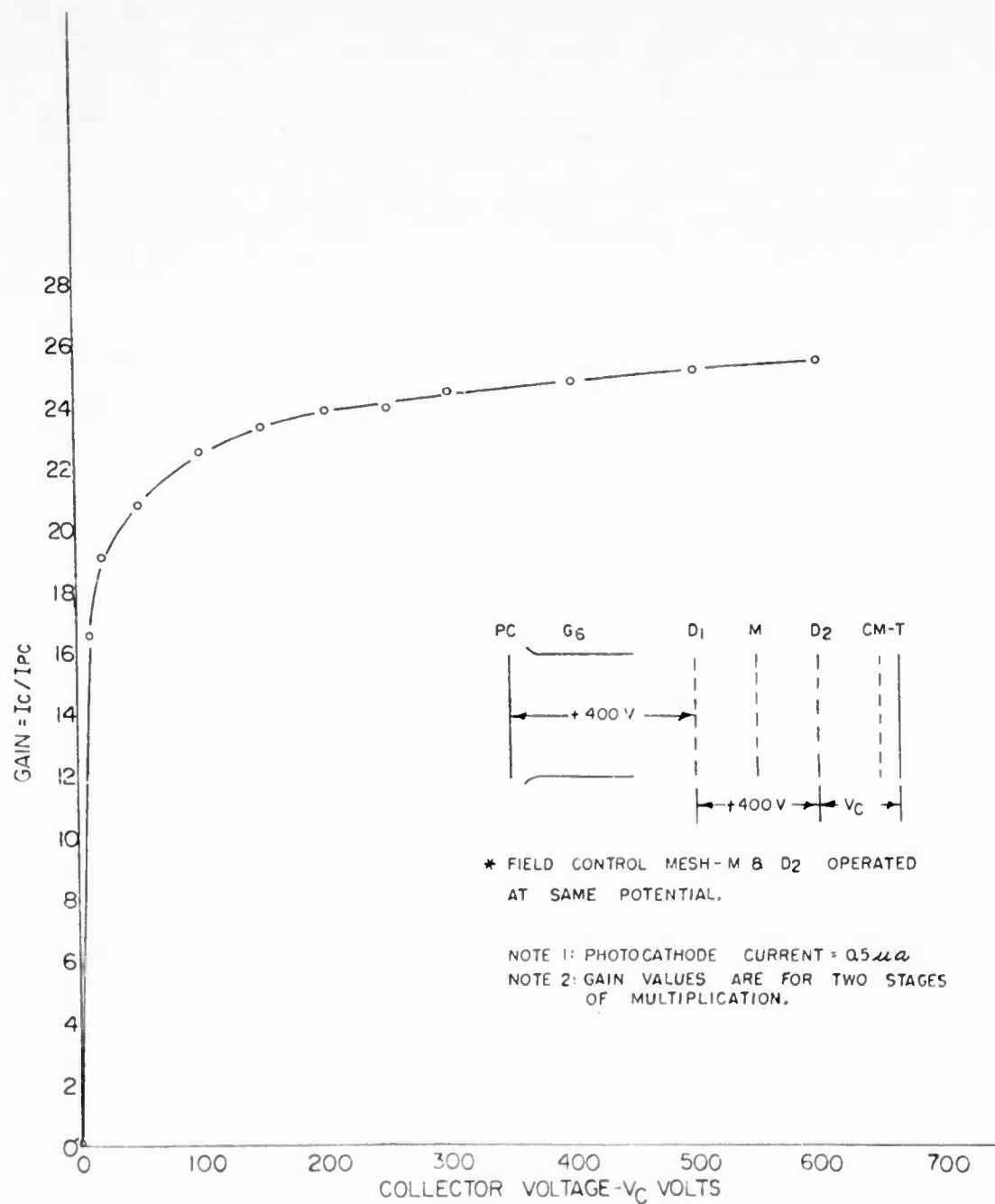
Figure 48. Gain Versus Field Control Mesh Voltage

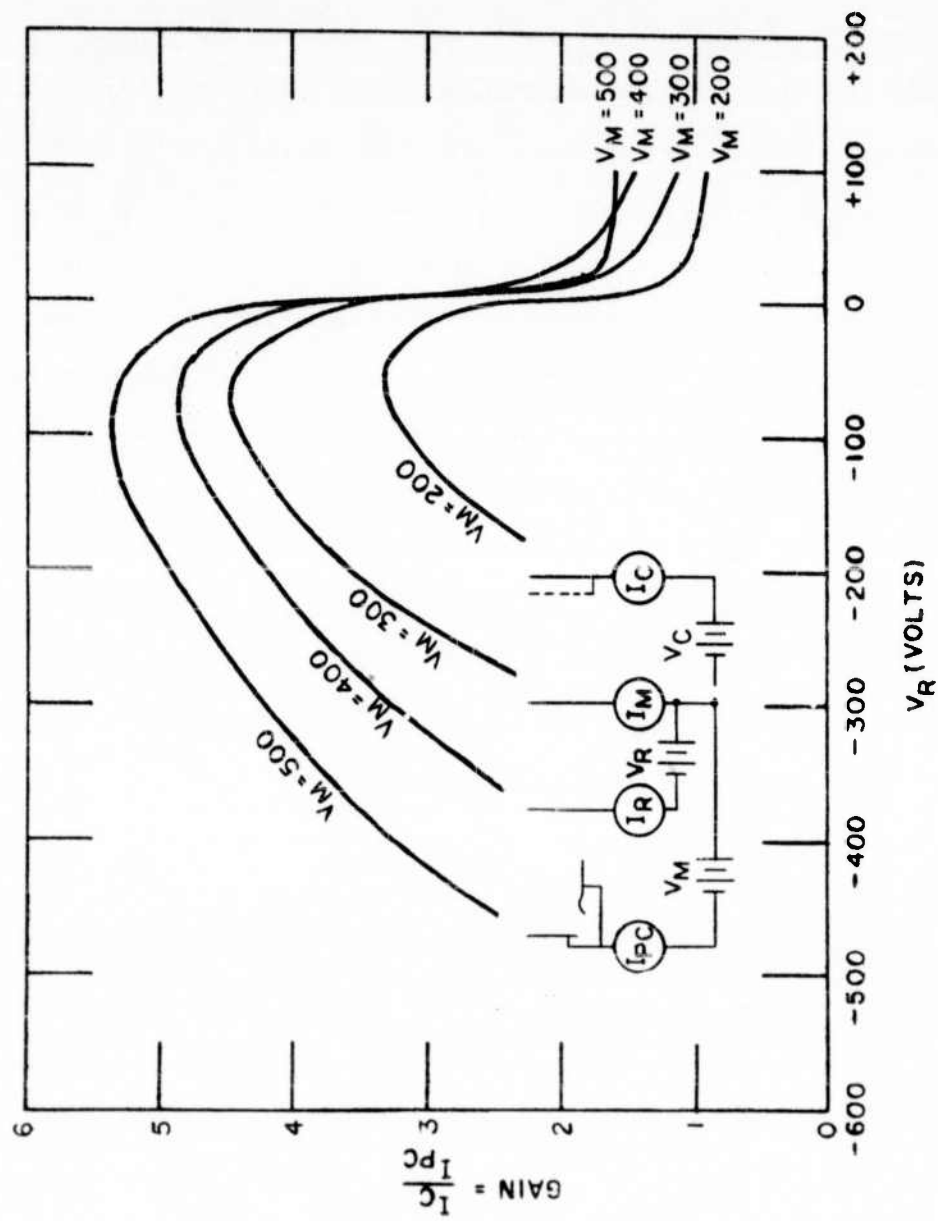Figure 49. Gain Versus Collector Voltage (Mesh Multiplier No. 14)

154

Figure 50. Gain Versus Field Shaping Mesh Voltage

155

ELECTRON VELOCITY SELECTION

1. INTRODUCTION

One of the chief limitations to obtaining improved sensitivity from an image orthicon type camera tube is the shot noise introduced by the scanning beam. As explained in section III, the pattern of positive charge corresponding to the picture is read from the image orthicon target by a low velocity scanning beam. All beam electrons return to the output electron multiplier when scanning an uncharged "black" area, while an increasing number of electrons land on the target when scanning more positively charged "lighter" areas, and fewer electrons return to the multiplier. This reduction in current in the returning beam, depending on picture element brightness, constitutes the video signal. Since the beam must always be large enough to supply signal current for the brightest highlights, and since no more than 50% of the electrons land on even the most positively charged element, the beam current is usually much larger than the signal current. Fluctuations in the beam current caused by the random nature of the thermionic emission process appear as noise in the output signal. As discussed in section III, this beam noise limits the maximum peak to peak signal to RMS noise ratio for the 5820 type image orthicon to about 35:1, and is far more significant for low light level scenes.

To improve tube performance, particularly at low light levels, a method is needed to cause a larger percentage of beam electrons to land on the target during the scanning process. A major part of the problem is caused by the rather wide spread in axial velocity components of the beam electrons approaching the target. Variations in energy of the scanning beam electrons in the image orthicon can be attributed to the following general causes.

(1) Energy distribution predicted by Maxwell-Boltzmann statistics which sets a theoretical lower limit to the total spread in energy of thermally emitted electrons.

(2) Time or position varied cathode coating potential drops.

(3) Radially directed components of initial accelerating field.

(4) Inter-electron coulomb forces.

(5) Stray electrostatic or electromagnetic fields.

(6) Electron gun misalignment.

(7) Electron gun aberrations.

Investigators such as Hans Heil (Reference 25) and R. W. Floyd (Appendix I) have analyzed the performance of the image orthicon by assuming that the electron beam axial velocity distribution can be expressed by:

$$i_T = \text{const} \times i_b \times \exp \frac{-eV}{kT}$$

where: i_T = current landing from the electron beam onto a target element at a voltage V.

  i_b = total current in the primary scanning beam

  V = instantaneous voltage of the surface of the target element being scanned by the electron beam with respect to that voltage at which all electrons are permitted to land.

  k = Boltzmann constant

  e = electron charge

  T = effective absolute temperature of the electron beam, usually greater than the cathode temperature because of the broadening of the velocity distribution in the electron gun and focusing system.

Primarily suspected in the search for sources of broadening of the electron beam velocity spread are the aberrations intrinsic in the geometry of conventional triode electron guns. A triode emission system obtains favorable current density by converging electrons from a larger cathode area to a small focal point called the "crossover". This convergence is carried out by portions of the electrostatic accelerating field with components directed radially inward toward the axis of the tube.

157

After the electrons pass through the "crossover", they emerge as a divergent bundle of electron rays. Ignoring, for the moment, initial emission velocities and inter-electron coulomb forces, all electrons in this bundle will have equal total energies having obtained their kinetic energy from acceleration through identical potential drops. The velocity component of each of these electrons normal to the target and parallel to the tube axis, however, will be the product of its total velocity and the cosine of its angle of divergence from the beam axis. The stopping potential, V_3, at the target can be expressed as:

$$V_3 = V_2 - (V_2 - V_1) \cos^2 \theta$$

where $V_2 - V_1$ = accelerating potential drop

V_2 = anode potential

θ = divergence angle

At potentials more positive than the stopping potential, electrons with a given axial velocity will land and conversely at more negative potentials, such electrons will be reflected. Since the angle of divergence is not constant for all electrons in the beam, it is clear that there will be a variation in stopping potentials at the target, i.e. not all electrons will land for a given voltage established at the target element. For very small target signal voltages, only the scanning beam electrons of highest axial velocity land on the target. The lower energy electrons, which are reflected at the target surface, contribute to noise without adding to the signal. It is evident, therefore, that an approach to reducing velocity variations in the electron scanning beam is to reduce the beam convergence angle in the electron gun. This problem is complicated by the effect of the axial magnetic focusing field which is not constant strength or direction in the region near the cathode. Because of this field, any force tending to make an electron move radially will result in imparting a spiral motion to the electron.
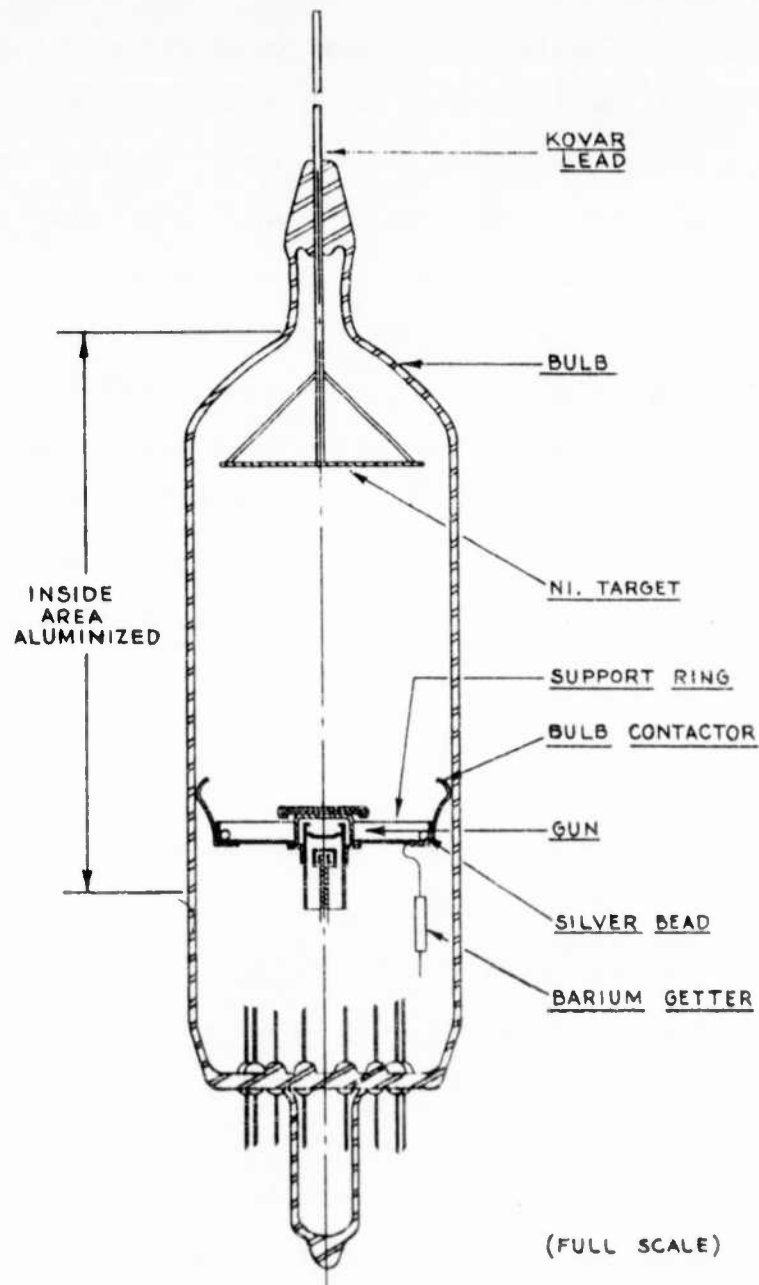
158

KOVAR
LEAD

BULB

INSIDE
AREA
ALUMINIZED

NI. TARGET

SUPPORT RING

BULB CONTACTOR

GUN

SILVER BEAD

BARIUM GETTER

(FULL SCALE)

Figure 51. Design of Retarding Field Tube.

159

Another approach to the problem of narrowing the axial velocity spread in the electron scanning beam is the use of a velocity selector subsequent to the electron gun. The designs considered were similar to those used for determining the energies of particles emitted in nuclear reactions. Most promising was the crossed field selector in which the beam of electrons was subjected to a magnetic field tending to bend the beam up, and an electrostatic field acting to bend it down. Since the action of the magnetic field depended on the particle speed, fast moving electrons would be bent up, while slower moving electrons would be bent down. Electrons moving at the desired speed would be undeviated, and by placing a disk with a small central aperture at the exit end of the system, electrons of one small velocity range would be selected. Other schemes considered required that the electron beam be deflected in a magnetic field and since the radium of curvature of the electrons would depend on the speed of the electron, an appropriately located apertured disc or slit would pass only those in the desired velocity range.

2.   METHODS OF MEASURING ELECTRON VELOCITY DISTRIBUTION

a. Planar Electrode Retarding Field

Concomitant with the problem of developing an electron velocity selector, to narrow the axial velocity spread of the electron beam approaching the target, is the determination of a valid and reproducible method for measuring the electron velocity distribution of the beam. The classical method of determining velocity spread of an electron beam consists of measuring current as a function of retarding potentials applied to a planar collecting electrode. This measurement yields a current versus retarding voltage plot which when differentiated results in a velocity distribution curve. Figure 51 is a cross-sectional view of a typical retarding field tube. The tube was designed to simulate the image orthicon scanning section, employing the normal electron gun structure. The target was replaced by a metal plate to act as an electron collector and retarding field electrode. Silver beads were provided to

160

permit the vacuum evaporation of a clean silvered surface on the collector electrode in order to maintain low secondary electron emission. An axial magnetic focusing field was adjusted for maximum collector efficiency. Cathode current was held constant at 3.1 microamperes by readjusting the modulator grid potential for each value of accelerator potential (G_2 voltage). By maintaining constant cathode emission, the value of the 100% current collection point of each curve (representing total electron beam transmission through an aperture of fixed area) could be made to serve as a measure of the relative current density for each set of operating conditons. Figure 52 clearly shows that the applied collector potential required to collect 100% of the beam electrons decreases with decreasing anode voltage (E_{G2}), indicating that the reduction in current density was at the expense of the slower electrons. It will be noted that the measured collector potentials are all in the positive range. These cannot be interpreted as absolute values, however, as they are substantially elevated by a cathode coating potential drop and by a contact potential difference between the target and the cathode of the tube. These effects result in a displacement of collector current curves along the retarding potential axis. For this reason, data should be interpreted from the standpoint of relative curve slopes rather than absolute positioning of curves. Examination of the curve in Figure 52 corresponding to a G_2 voltage of 300 volts, typical in normal image orthicon operation, shows an energy spread of 0.6 volts for a beam current spread from 10% to 100% of the total collected current. It should be pointed out that the shift in collector potential caused by the variation in applied anode voltage, can also be interpreted as resulting from changes in the cathode surface to base metal potential difference. Reduction in the cathode potential drop with decreasing anode voltage could cause similar shaped but reduced amplitude curves to telescope and seemingly retrace identical high velocity tails.

To demonstrate the electrostatic field pattern of the triode section of the
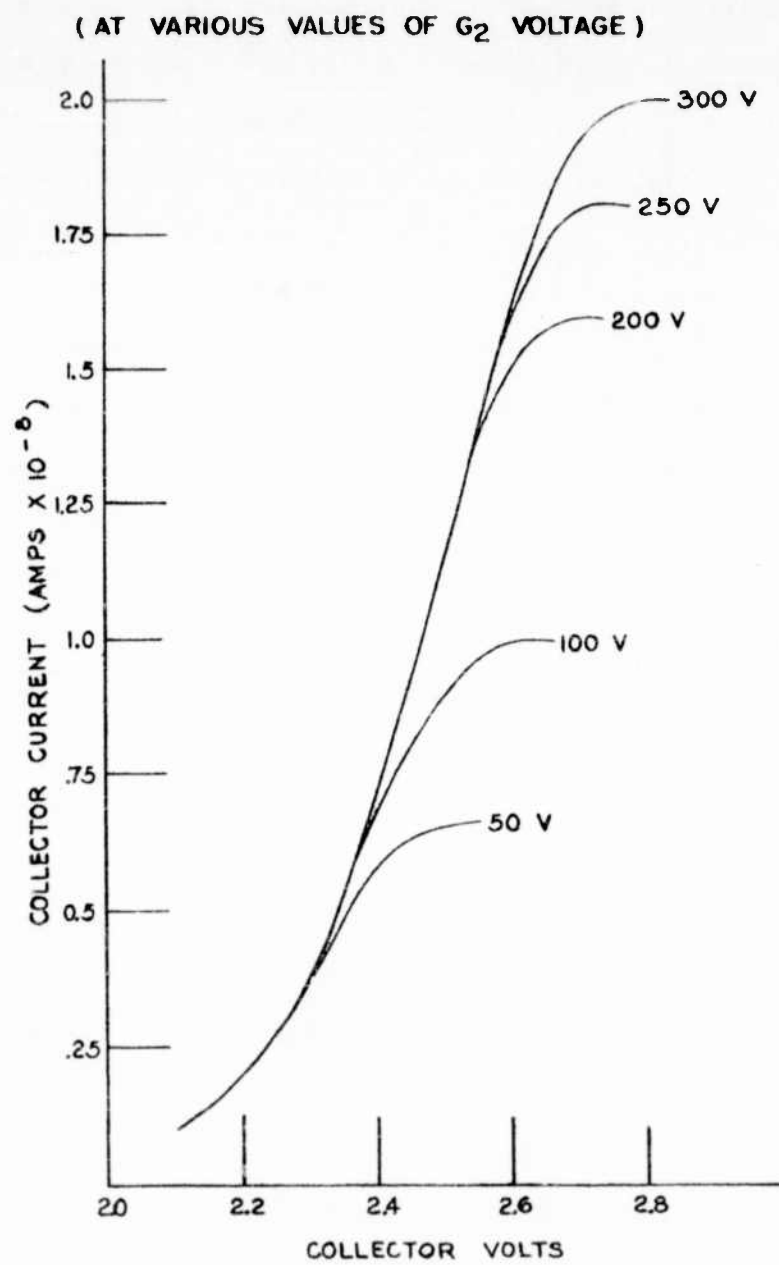
161

Figure 52.   Constant Cathode Current Collector Curves.

162

$E_{G2} = 300$ V

150 V

75 V

50 V

25 V

GRID #1
-54 VOLTS

0 V

-25 V

-10 V

-3 V   -5 V

CATHODE   0 VOLTS
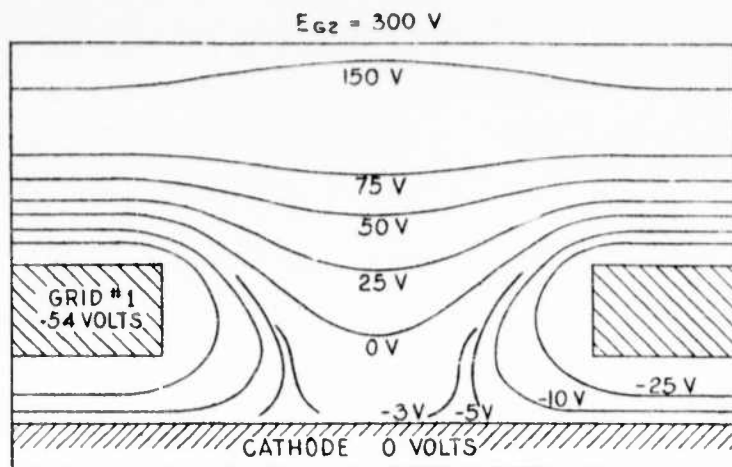
Figure 53.   Accelerating Fields in Image Orthicon Electron Gun.

$E_{G2} = 200$ V

100 V

75 V

50 V

25 V

GRID #1
-35.5 VOLTS

10 V

3V

0V

-3V

-10 V

-5 V

CATHODE   0 VOLTS
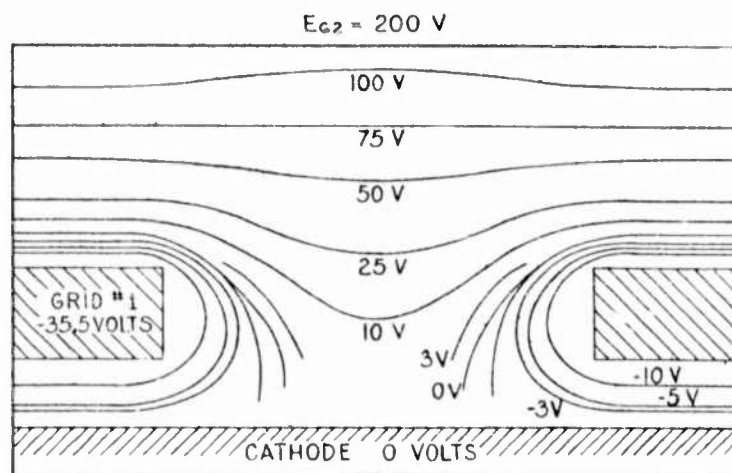
Figure 54.   Accelerating Fields in Image Orthicon Electron Gun.

$E_{G2} = 100$ V

50 V

25 V

GRID #1
-17.5 VOLTS

10 V

5V

-3 V

3V

0 V

CATHODE   0 VOLTS

$I_K = 3.1 \mu A$ $E_{HTR} = 6.3$ V

Figure 55.   Accelerating Fields in Image Orthicon Electron Gun.

163

electron gun, in the immediate vicinity of the cathode, equipotential plots of the structure were made in an electrolytic plotting tank. The results of these plots are shown in Figures 53, 54, and 55 for three conditons of electron voltages chosen to duplicate those which produced a constant cathode current in the experimental retarding field tube described above. The reduction in anode vo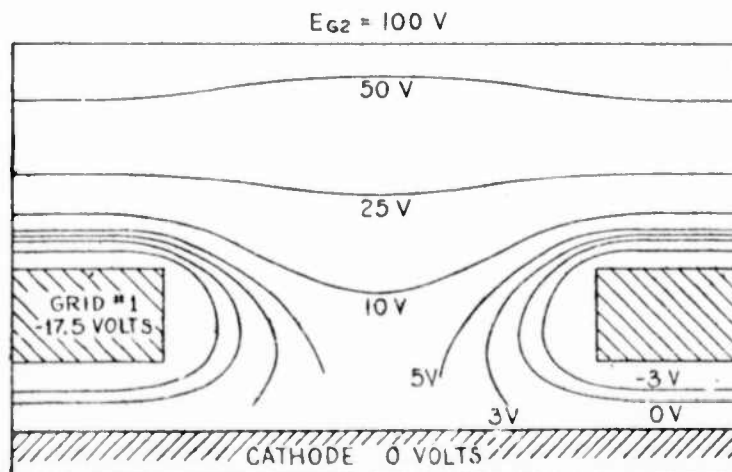ltage (E_{G2}) from 300 to 200 to 100 volts in Figures 53, 54, and 55 respectively was expected to reduce the strong converging action of the triode fields. As pointed out previously, the interaction of this convergent field with the magnetic focusing field is considered partly responsible for the axial velocity spread observed in the electron scanning beam. Examination of the equipotential patterns shows that although the plotting method obviously did not take all the necessary factors into consideration, valid qualitative conclusions could still be drawn. For example, the plot shown in Figure 53 indicates that the current should have been cut off, that is, no electrons should be leaving the cathode. The plot shown in Figure 54 indicates a small emitting area in the center of the cathode, whereas Figure 55 appears to indicate that electrons should be leaving the entire area of the cathode under the control grid G_1 aperture. As stated previously, the electrode voltage conditions were known experimentally to give a constant cathode current of 3.1 microamperes in an actual tube. The factors which were not taken into account in these equipotential plots include the finite initial emission velocity of the electrons, the effect of the space charge directly in front of the cathode, the effect of contact potential differences, and the effect of a potential drop across the cathode coating and in the coating to base metal interface. Because these factors were neglected, a quantitative interpretation of the equipotential plots should not be attempted. In general, however, the expected increase in cathode emitting area and constant reduction in emission current density for lower G_2 voltages appear to be shown along with a reduction in radial field intensities. These are the effects which, according to geometric aberration theory, should yield
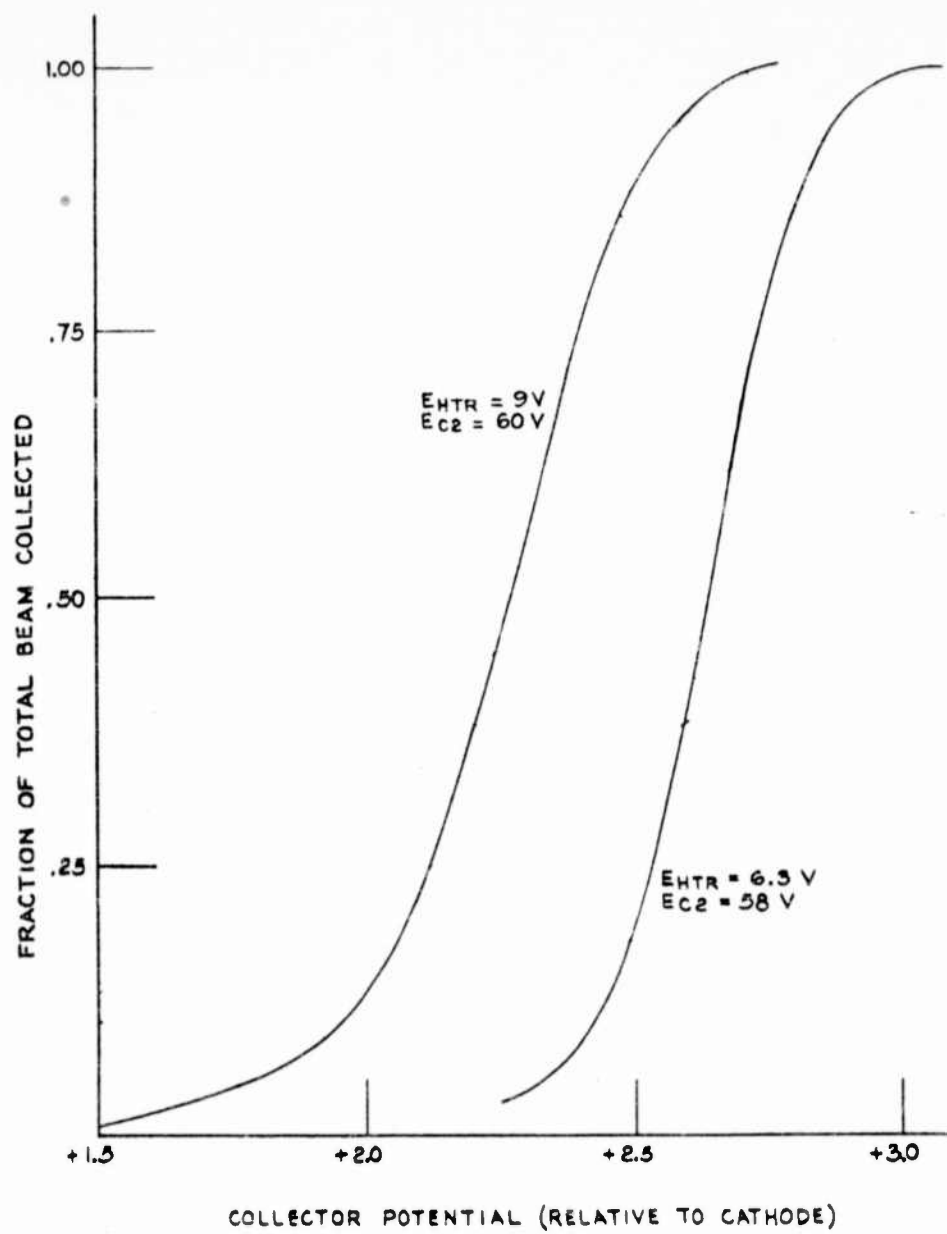
164

Figure 56. Electron Velocity Distribution in Simulated Diode
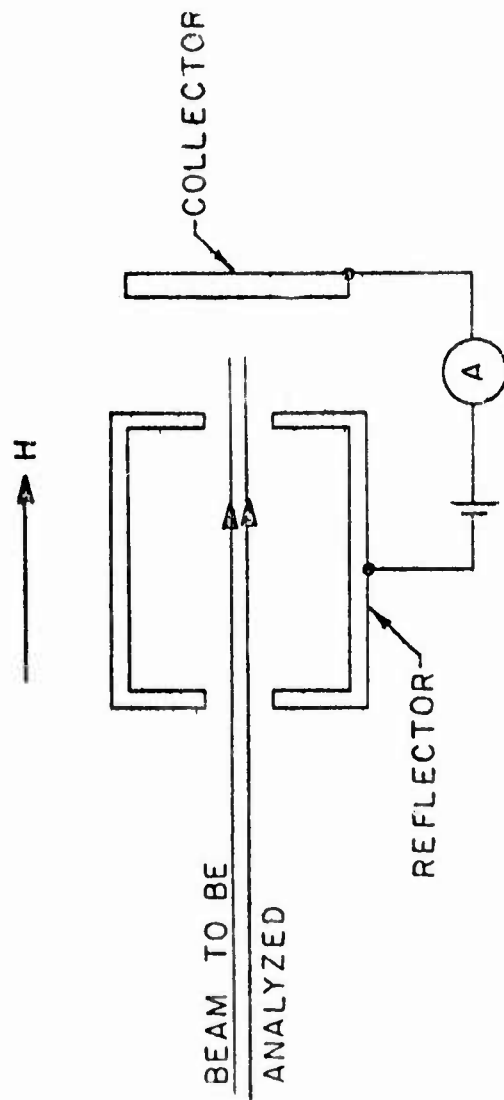
Figure 57. Electron Velocity Analyzer

a decrease in axial velocity spread.

In order to further evaluate the approach of decreasing electron velocity variations by reducing beam convergence, the control grid, (G_1) in an image orthicon triode was adjusted to a positive potential so that the current density over the total area of the cathode was uniform. This uniform cathode emission density was established by adjusting G_1 positive until the current arriving at the anode (G_2) aperture was to cathode current as G_1 aperture area was to cathode emitting area. Under this condition of uniform cathode loading, it was hoped that accelerating equipotentials near the cathode would be approximately parallel to the cathode surface. Except for the finite control grid thickness, this adjustment would thereby produce an emission system of parallel planar equipotentials in which no lateral components of acceleration would exist. In practice, it became necessary to reduce the anode potential substantially in order to generate beam currents of the proper order of magnitude for image orthicon use. Figure 56 shows normalized curves of retarding field data for such a simulated diode at two values of cathode heater voltage.

b. Faraday Cage Analyzer

Based on extensive independent investigations at our Research Laboratories, it had been determined that the planar retarding electrode technique was not definitive below a range of approximately 0.5 volts. This was attributed to the influence of surface conditions at the collecting electrode on the action of electrons at the surface, e.g. the effects of surface charging and secondary emission. On this basis, a system was evolved which demonstrated ability to measure a velocity spread down to 0.2 volts. Essentially, this system of measurement consists of a modified Faraday cage technique which establishes a retarding equipotential surface in free space as the basic analyzer element. As shown in Figure 57, the beam to be analyzed is collimated by an axial magnetic field so as to enter the Faraday cage, to which the retarding potentials are applied. The exit beam is collected by a planar electrode

167

which is maintained at a slightly positive potential. The advantage of such a system appears to be that the intimate surface conditions of the collector do not dictate collector efficiency.

Applying this technique to the measurement of velocity spread in the electron scanning beam of the conventional image orthicon gave a range of 0.6 volts at a beam current of 5×10^{-8} amperes. This measurement reproduced results obtained with the planar retarding electrode technique, thus adding to its validity.

3. EFFECT OF MISALIGNMENTS ON VELOCITY DISTRIBUTION

a. Theory

In the operation of the image orthicon tube, an axial magnetic field is applied to focus scan beam electrons on the target. Both the intensity and direction of this field are important. The intensity is adjusted so that divergent electrons are focused through an integral number of loops onto the target. If the direction of this "axial" field is not perpendicular to the target surface and parallel to the direction of propogation of the electron beam, we may observe a situation in which the entire beam, along with divergent electrons, is being spiraled about the magnetic lines of flux.

In the ideal case, the "axial" magnetic focusing field is, in fact, axial, the electron gun is emitting a beam parallel to the axis, and the target is normal to the axis since the force exerted on the electrons by the axial field can be only in a plane perpendicular to the axis, the magnetic field can not alter axial velocities of the electrons.

In practical I.O. tubes. an alignment coil which is located near the electron gun generates mutually perpendicular transverse (to tube axis) magnetic fields. These fields are adjusted in such a way as to align the electron beam with the focusing field, eliminating spiraling of the beam, as a whole, about the flux lines of the focusing field. It cannot, however, correct for non-perpendicularity of beam
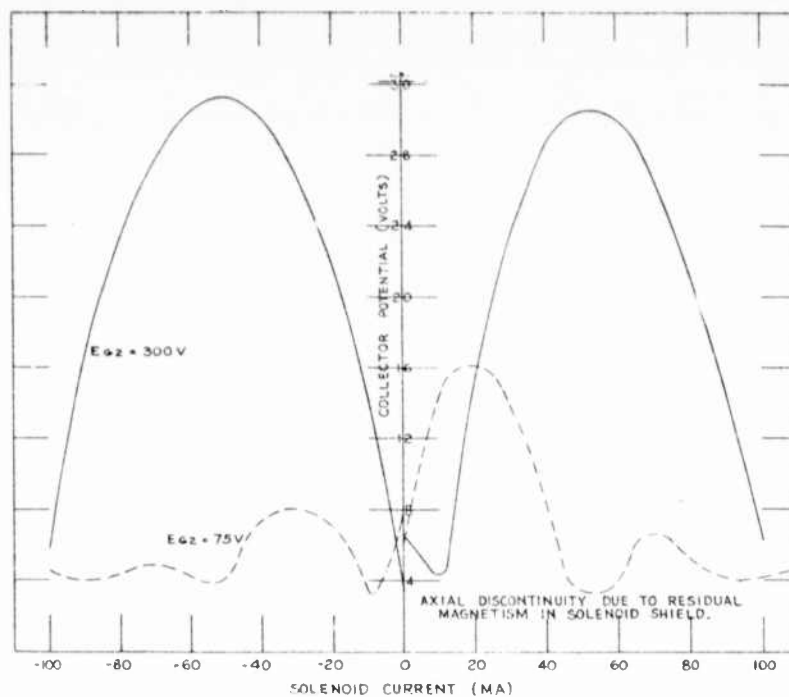
168

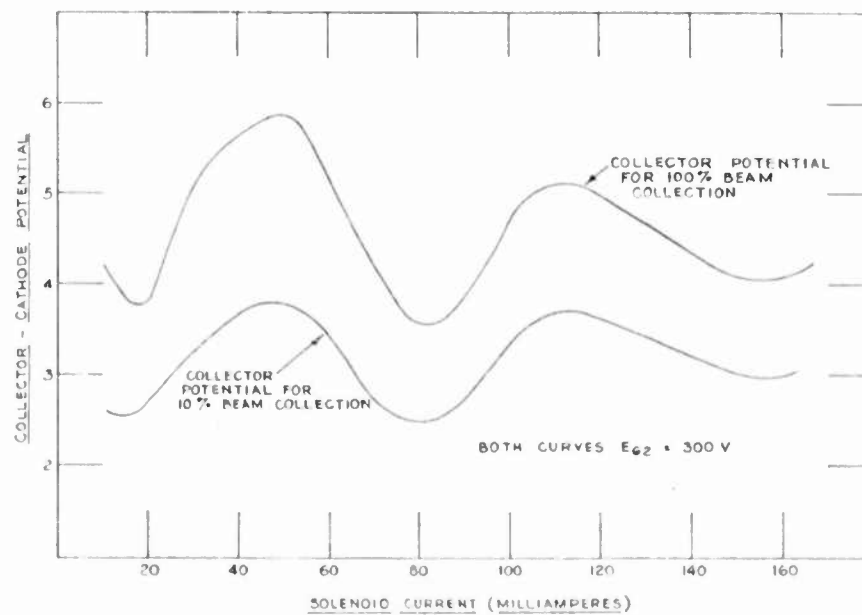Figure 58. Optimum Collector Potential As A Function of Tilted Axial Focusing Field

Figure 59. Collector Potential As A Function of Axial Focusing Field

landing on the target. ^{I}t insures, in fact, that beam landing at the target be as canted as is the intersection of magnetic flux lines with the target.

The consequence of non-orthogonal landing of the beam at the target is a shift of the entire spread toward lower velocities, and a skewing of the distribution toward lower velocities. In addition, increasing the angle of incidence of primary electrons may tend to increase secondary electron yield of the target.

b. Experimental Data

To demonstrate spiraling of the electron beam about magnetic flux lines, a retarding field tube of the type shown in Figure 51 was tilted within a focusing solenoid. Minimum collector voltage at which 100% electron collection took place was plotted as a function of solenoid current. This data is presented in Figure 58. Figure 59 presents the same information except that, in Figure 59, an attempt was made to mechanically align the tube axis with the solenoid axis.

Results presented in Figure 58 are plotted for two values of anode voltage to indicate the dependence of the spiraling upon electron velocity. With the accelerating potential reduced by a factor of 4, the electron speed is cut in half, and the period of the collector efficiency function is halved as well. Collector voltage minima represent points of most nearly normal beam landings at the target.

Figure 59 illustrates that, even with careful alignment of the tube within the focusing solenoid, some beam spiraling persists. As compared with Figure 58, it represents a factor of 5 reduction in the amplitude of spiraling. Moreover, the minima for Figure 59 are of approximately the same amplitude as for Figure 58, indicating the same order of normality of landings. The difference in amplitude between the E_{G2} = 300 V curve in Figure 58 and the corresponding 100% curve in Figure 59 represents the difference in their axial velocity.

In Figure 59, the curve for 10% beam collection potential is also plotted to demonstrate that the entire velocity range shifts as a function of focus field strength.
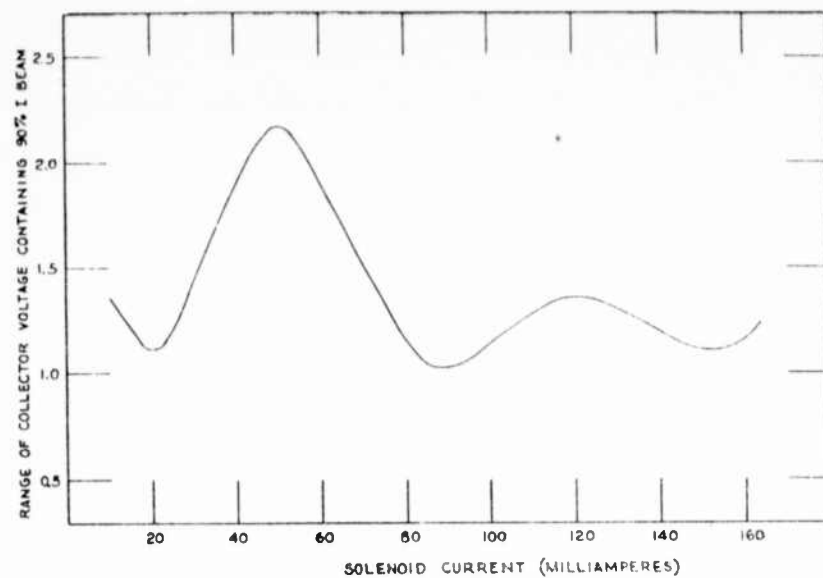
170

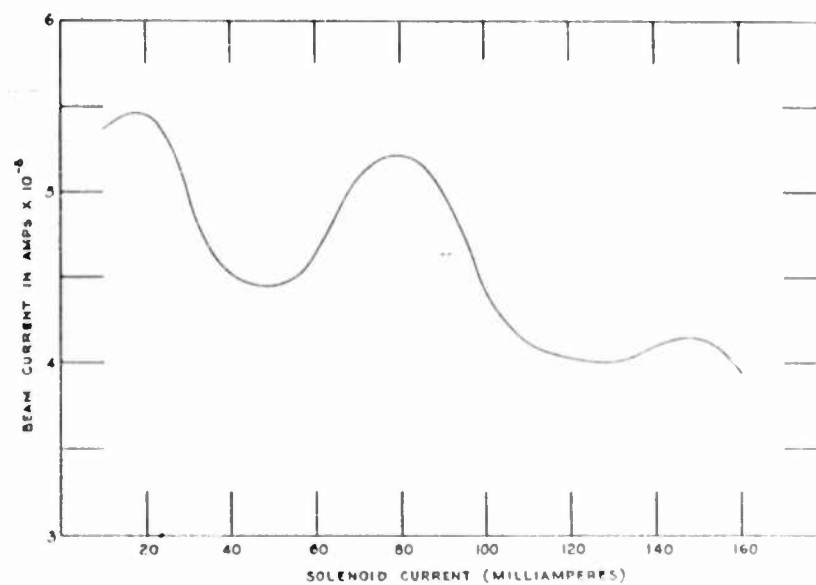Figure 60. Velocity Spread of Slowest 90% of Beam
Electrons

Figure 61. Beam Current Variation as Function of
Axial Magnetic Field.

171

Figure 60 is the result of subtracting the data presented in Figure 59, and shows the "volt-velocity" range of the slowest 90% of beam electrons. It is important to note that the narrowest range of electron velocities coincides with the lowest collector potential, or the most nearly normal beam landing. This indicates that nonorthogonal landings increase velocity spread while reducing absolute velocity normal to the target.

In interpreting the dependence of velocity spread on axial field strength, it was suspected that the periodic minima in spread might be caused by selective filtering of certain portions of the normal velocity distribution by defocusing of the beam at the dynode #1 aperture. This interpretation would predict that velocity spread minima should coincide with beam current transmission minima.

Figure 61 demonstrates that, contrary to this prediction, beam current transmission maxima occur at beam velocity spread minima. Since this fact rules out velocity selection at the dynode #1 aperture, dependence of velocity spread on angle of incidence of the beam upon the target is clearly demonstrated.

By way of summarizing the effect of magnetic fields on velocity spread we can state the following conclusions:

1) Theory predicts that, for an ideal system, magnetic fields would have no effect on velocity spread.

2) In real cases, where misalignments in the electron optical system exist, magnetic fields can be used to reduce velocity spread, by nullifying misalignments.

3) In practical image orthicon tubes, this correction is not completely realized, as there is not a separate magnetic corrector to normalize landings at the target.

4) Magnetic focusing or deflection systems as generally applied, do not contribute to a reduction of intrinsic velocity spread in electron beams.
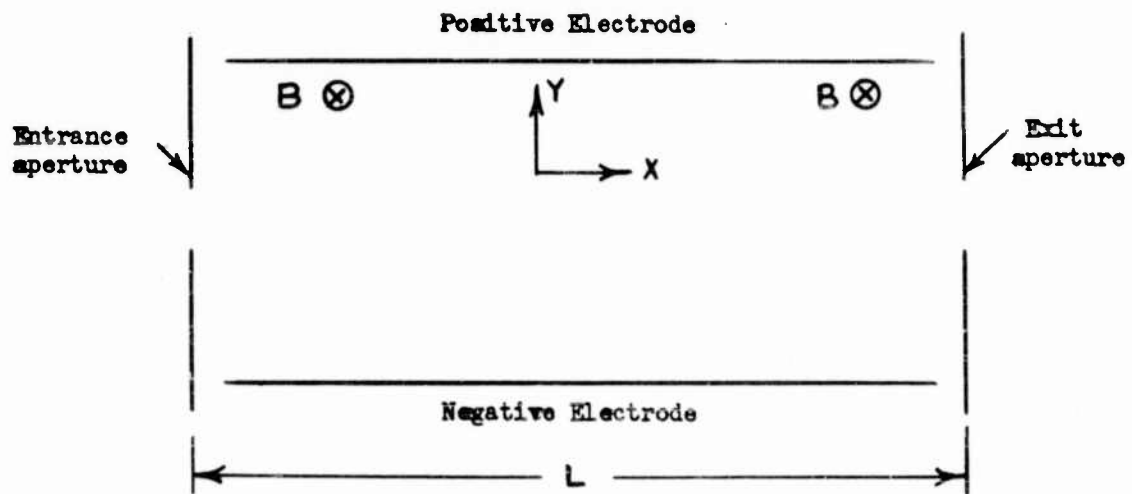
172

Figure 62. Crossed-Fields Velocity Selector.

4. ELECTRON VELOCITY SELECTOR SYSTEMS

a. Crossed-Fields Selector

1.) Analysis of Crossed-Fields Selector

As shown in Figure 62, the crossed-fields velocity selector employs uniform electric and magnetic fields at right angles to each other and to the path of the electron beam. The effects of the two fields cancel each other for electrons of the desired axial velocity. The advantages of such a velocity selection device in an image orthicon structure can be summarized as follows:

1) Can transmit electron scanning beam without selection for complete dis-charge of high light level scenes.

2) Can be varied both in the selected transmission velocity and in the range of velocities transmitted.

3) Lends itself readily to the structure of the scanning section.

The operation and predicted performance limitations of the crossed-fields de-vice shown in the sketch is described in the following mathematical analysis. When an electron is injected with an initial velocity into mutually perpendicular electro-static and magnetic fields, its fundamental equations of motion can be shown to be (Reference 26):

$$X = \frac{a t}{\omega_0} + (1 - \cos\omega_0 t) \frac{V_{oy}}{\omega_0} - \frac{(a - \omega_0 V_{ox})}{\omega_0^2} \sin\omega_0 t \qquad (1)$$

$$Y = \frac{(a - \omega_0 V_{ox})}{\omega_0^2} (1 - \cos\omega_0 t) + \frac{V_{oy}}{\omega_0} \sin\omega_0 t \qquad (2)$$

where:

$$a = -\frac{e\,E_y}{m}$$

$$\omega_0 = \frac{e\,B_z}{m}$$

E_y = electric field intensity

B_z = magnetic field intensity

V_{0x} = axial component of initial electron velocity

V_{0y} = radial component of initial electron velocity

t = time

e = electron charge

m = electron mass

Let: $V_T = \dfrac{a}{\omega_o}$

Equations (1) and (2) then becomes:

$$X = V_T t + (1-\cos\omega_o t)\ \frac{V_{0y}}{V_{0x}} - \left(\frac{V_T - V_{0x}}{\omega_o}\right)\ \sin\omega_o t \tag{3}$$

$$Y = \left(\frac{V_T - V_{0x}}{\omega_o}\right)\ (1-\cos\omega_o t) + \frac{V_{0y}}{\omega_o}\ \sin\omega_o t \tag{4}$$

Case I. Consider the case when $V_{0x} = V_T$ and $V_{0y} = 0$.

Equations (3) and (4) reduce to:

$$X = V_T t$$

$$Y = 0$$

V_T is seen to be the velocity of an electron which passes undeflected through the selector. If we now let x = L, we then have the transit time, T, of an electron with initial velocity V_T travelling through a selector of length L or:

$$T = \frac{L}{V_T} \tag{5}$$

Case II - Consider the case when $V_{0x} \neq V_T$ and $V_{0y} = 0$. Applying these conditions to equations (3) and (4):

$$X = V_T t - \left(\frac{V_T - V_{0x}}{\omega_o}\right)\ \sin\omega_o t \tag{6}$$

$$Y = \left(\frac{V_T - V_{0x}}{\omega_o}\right)\ (1 - \cos\omega_o t) \tag{7}$$

175

It is evident that the maximum Y deflection will occur for some time t_0 such that:

$$\omega_0 t_0 = \pi$$

At the time the Y deflection is maximum, we want $X = L$, so that the electron is located at the end of the selector. For this condition, equation (6) reduces to:

$$L = V_T t_0$$

Setting $t_0 = T$ we obtain:

$$L = V_T \cdot T$$
$$\omega_0 = \frac{\pi}{T}$$

Substituting into equations (6) and (7):

$$X = \frac{Lt}{T} - T \frac{(V_T - V_{ox})}{\pi} \sin \frac{\pi t}{T} \tag{8}$$

$$Y = T \frac{(V_T - V_{ox})}{\pi} \left(1 - \cos \frac{\pi t}{T}\right) \tag{9}$$

These can be expressed as:

$$X = \frac{Lt}{T} - \frac{L}{\pi} \left(1 - \frac{V_{ox}}{V_T}\right) \sin \frac{\pi t}{T} \tag{10}$$

$$Y = \frac{L}{\pi} \left(1 - \frac{V_{ox}}{V_T}\right) \left(1 - \cos \frac{\pi t}{T}\right) \tag{11}$$

Observing that the ratio of electron velocities is directly proportional to the square root of the electron volt energies of the electrons.

$$\frac{V_{ox}}{V_T} = \sqrt{\frac{\phi_{ox}}{\phi_T}}$$

Equation (10) and (11) then become:

$$X = \frac{Lt}{T} - \frac{L}{\pi} \left(1 - \sqrt{\frac{\phi_{ox}}{\phi_T}}\right) \sin \frac{\pi t}{T} \tag{12}$$

$$Y = \frac{L}{\pi} \left(1 - \sqrt{\frac{\phi_{ox}}{\phi_T}}\right) \left(1 - \cos \frac{\pi t}{T}\right) \tag{13}$$

End of the Selector
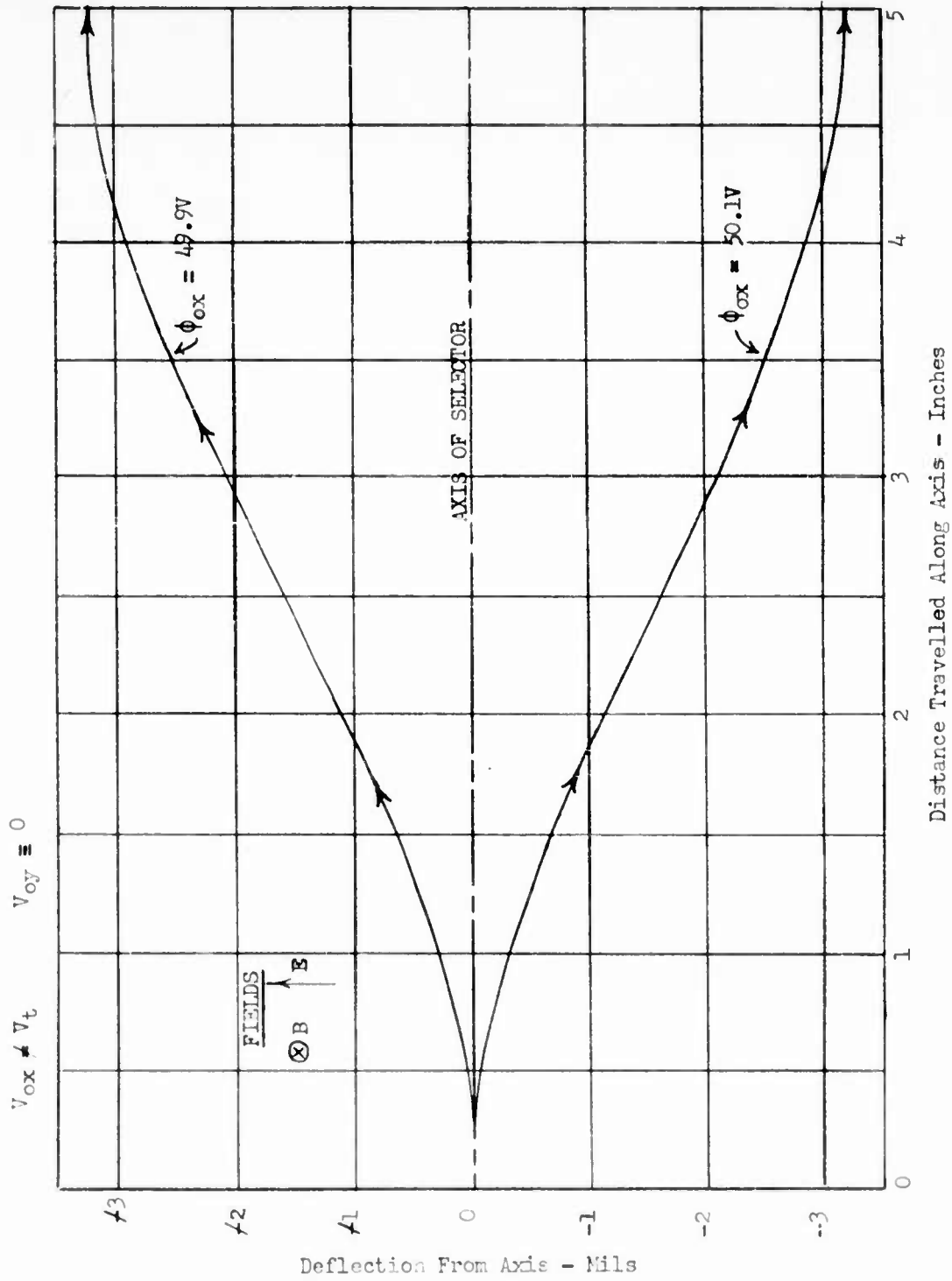
Figure 63. Electron Trajectory in Crossed-Fields Selector

177

Replacing the ratio $\frac{t}{T}$ by R we obtain:

$$X = L \left[R - \frac{1}{\pi} \left(1 - \sqrt{\frac{\phi_{ox}}{\phi_T}} \right) \sin \pi R \right] \qquad (14)$$

$$Y = \frac{L}{\pi} \left(1 - \sqrt{\frac{\phi_{ox}}{\phi_T}} \right) (1 - \cos \pi R) \qquad (15)$$

To determine how these equations predict the performance of the large scale crossed fields selector, let:

$$\phi_{ox} = 50 \pm 0.1 \text{ volts}$$

$$\phi_T = 50 \text{ volts}$$

$$L = 5 \text{ inches}$$

Then:

$$X = 5 \left[R - \frac{1}{\pi} \left(1 - \sqrt{\frac{50 \pm 0.1}{50}} \right) \sin \pi R \right] \qquad (16)$$

$$Y = \frac{5}{\pi} \left(1 - \sqrt{\frac{50 \pm 0.1}{50}} \right) (1 - \cos \pi R) \qquad (17)$$

By selecting values of R from 0 to 1, we compute the corresponding values of X and Y from equations (16) and 17) to obtain an electron trajectory in the crossed field selector as plotted in Figure 63.

Assuming the selector has 0.002 inch entrance and exit aperture diameters, the absolute range of selectivity is determined by setting Y = ± 0.002 inches at t = T (R = 1). Thus from equation (15):

$$\pm .002 = \frac{5}{\pi} \left(1 - \sqrt{\frac{\phi_{ox}}{\phi_T}} \right) \qquad (2)$$

Solving:

$$\sqrt{\frac{\phi_{ox}}{\phi_T}} = 1 \pm 0.000628 \qquad (18)$$

For $\phi_T = 50$ volts

$$\phi_{ox} \text{ (max)} = 50.063 \text{ volts}$$

$$\phi_{ox} \text{ (min)} = 49.937 \text{ volts}$$

Therefore, the absolute range of electron volt energies passing through the selector under the assumed conditions is:

$$\phi_{ox} = 50 \pm 0.063 \text{ volts}$$

Recapitulating the original assumed conditons:

$$V_{ox} \neq V_T$$

$$V_{oy} = 0$$

$$L = 5 \text{ in.} = \text{length of selector}$$

Entrance and exit aperture diameters = 0.002 in.

To determine the range of electron volt energies passed by the selector when $\phi_T = 300$ volts, typical of image orthicon operation, we compute from equation (18):

$$\phi_{ox} = 300 \pm 0.38 \text{ volts}$$

It should be pointed out that B_z and E_y must be adjusted to permit 300 volt electrons to pass through the selector undeflected, but the calculations with the exception of equation (16) and (17) remain the same.

Case III - Consider the case when $V_{oy} \neq C$ and $V_{ox} = V_T$. Applying these conditions to equations (3) and (4) :

$$X = V_T t + (1 - \cos\omega_0 t) \frac{V_{oy}}{\omega_0} \tag{19}$$

$$Y = \frac{V_{oy}}{\omega_0} \sin\omega_0 t \tag{20}$$

Using the previous relations, $V_T = \frac{L}{T}$ and $\omega_0 = \frac{\pi}{T}$ we obtain:

$$X = \frac{Lt}{T} + (1 - \cos \frac{\pi t}{T}) \frac{V_{oy}}{V_T} \frac{L}{\pi} \tag{21}$$

$$Y = \frac{V_{oy}}{V_T} \frac{L}{\pi} \sin \frac{\pi t}{T} \tag{22}$$

Replacing the ratio $\frac{t}{T}$ by R we obtain:

$$X = L \left[R + (1 - \cos \pi R) \frac{V_{oy}}{V_T \pi} \right] \tag{23}$$

$$Y = L \left(\frac{V_{oy}}{V_T \pi} \quad \text{Sin } \pi R \right) \tag{24}$$

Now: $\quad \dfrac{V_{oy}}{V_T} = \sqrt{\dfrac{\phi_{oy}}{\phi_T}}$

Equation (23) and (24) then became:

$$X = L \left[R + \frac{(1 - \cos R \pi)}{\pi} \sqrt{\frac{\phi_{oy}}{\phi_T}} \right] \tag{25}$$

$$Y = \frac{L}{\pi} \sqrt{\frac{\phi_{oy}}{\phi_T}} \quad \text{Sin } R \pi \tag{26}$$

To determine a maximum value for V_{oy}, we assume that all electrons originate at a crossover point located outside the selector 0.250 inches from the 0.002 inch diameter entrance aperture of the selector.
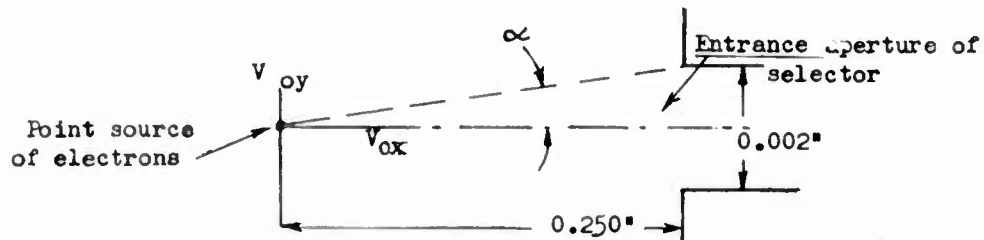
As defined by the entrance angle therefore:

$$\tan \alpha = \frac{.001}{0.250} = \frac{V_{oy}}{V_{ox}}$$

$$\frac{V_{oy}}{V_{ox}} = 0.004$$

180
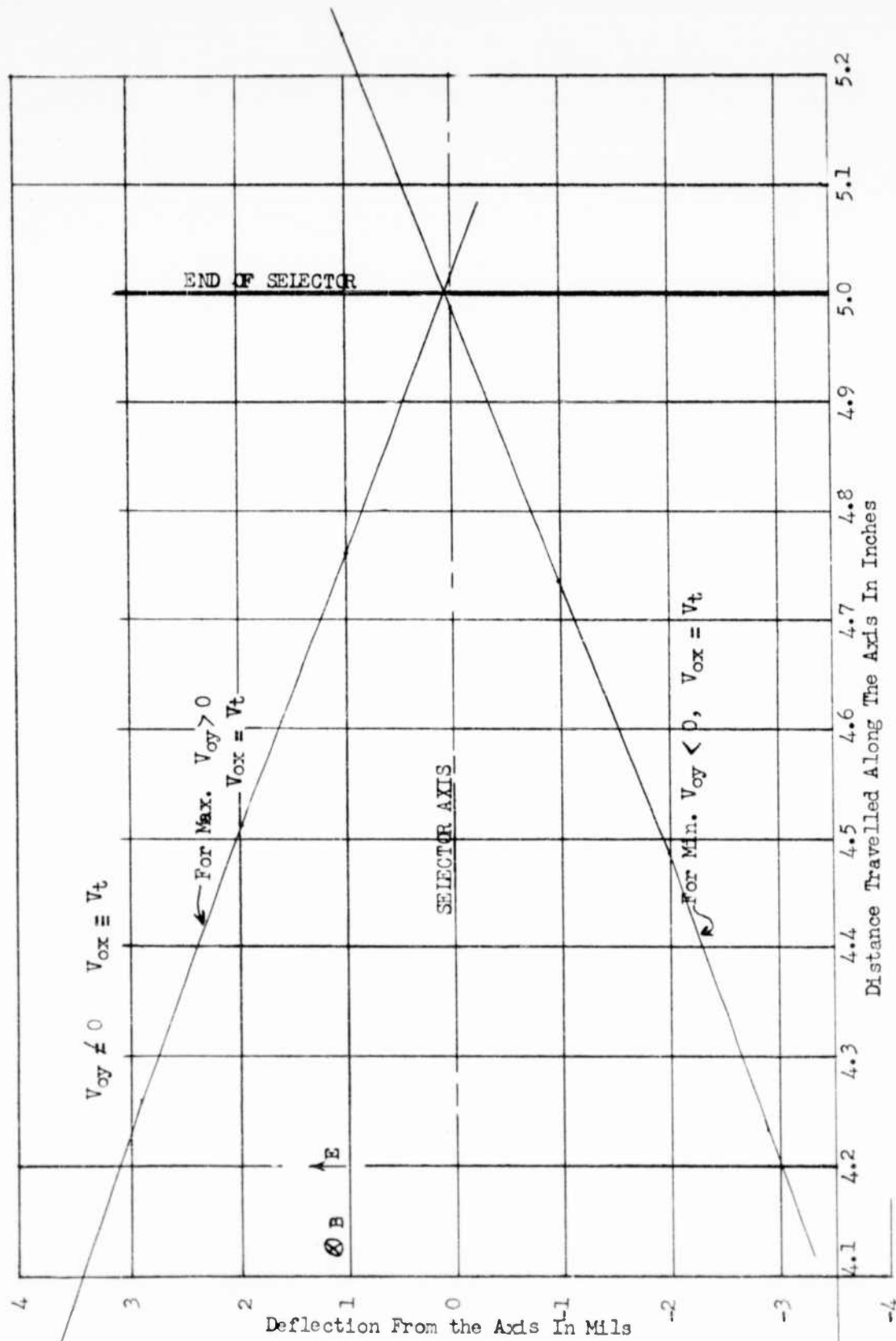
Figure 64. Electron Trajectory in Crossed Fields
Velocity Selector

181

Substituting this value in equations (25) and (26) and letting $L = 5'$ as in our experimental selector:

$$X = 5 \left[R + \frac{0.004}{\pi} \ (1 - \cos R\pi) \right] \qquad (27)$$

$$Y = \frac{5}{\pi} \ (0.004) \ \sin R\pi \qquad (28)$$

By selecting values of R from 0.8 to 1.0, we compute the corresponding values of X and Y from equation (27) and (28) to obtain the electron trajectory plotted in Figure 64.

Case IV. Consider the case when $V_{ox} \neq V_T$ and $V_{oy} \neq 0$. Restating the fundamental equations of motion:

$$X = V_T t + (1 - \cos\omega_o t) \ \frac{V_{oy}}{\omega_o} \ - \ \frac{(V_T - V_{ox})}{\omega_o} \ \sin\omega_o t$$

$$Y = \left(\frac{V_T - V_{ox}}{\omega_o} \right) (1 - \cos\omega_o t) \ + \ \frac{V_{oy}}{\omega_o} \ \sin\omega_o t$$

Applying the relations:

$$V_T = \frac{L}{T}$$

$$\omega_o = \frac{\pi}{T}$$

$$\frac{V_{ox}}{V_T} \qquad \sqrt{\frac{\phi_{ox}}{\phi_T}}$$

$$\frac{V_{oy}}{V_T} = \sqrt{\frac{\phi_{oy}}{\phi_T}}$$

$$R = \frac{t}{T}$$

We obtain:

$$X = L \left[R + \frac{(1 - \cos R\pi)}{\pi} \sqrt{\frac{\phi_{oy}}{\phi_T}} \ - (1 - \sqrt{\frac{\phi_{ox}}{\phi_T}}) \ \sin \frac{R\pi}{\pi} \right] \quad (29)$$

$$Y = \frac{L}{\pi} \left[(1 - \sqrt{\frac{\phi_{ox}}{\phi_T}}) \ (1 - \cos R\pi) \ + \sqrt{\frac{\phi_{oy}}{\phi_T}} \ \sin R\pi \right] \quad (30)$$

182
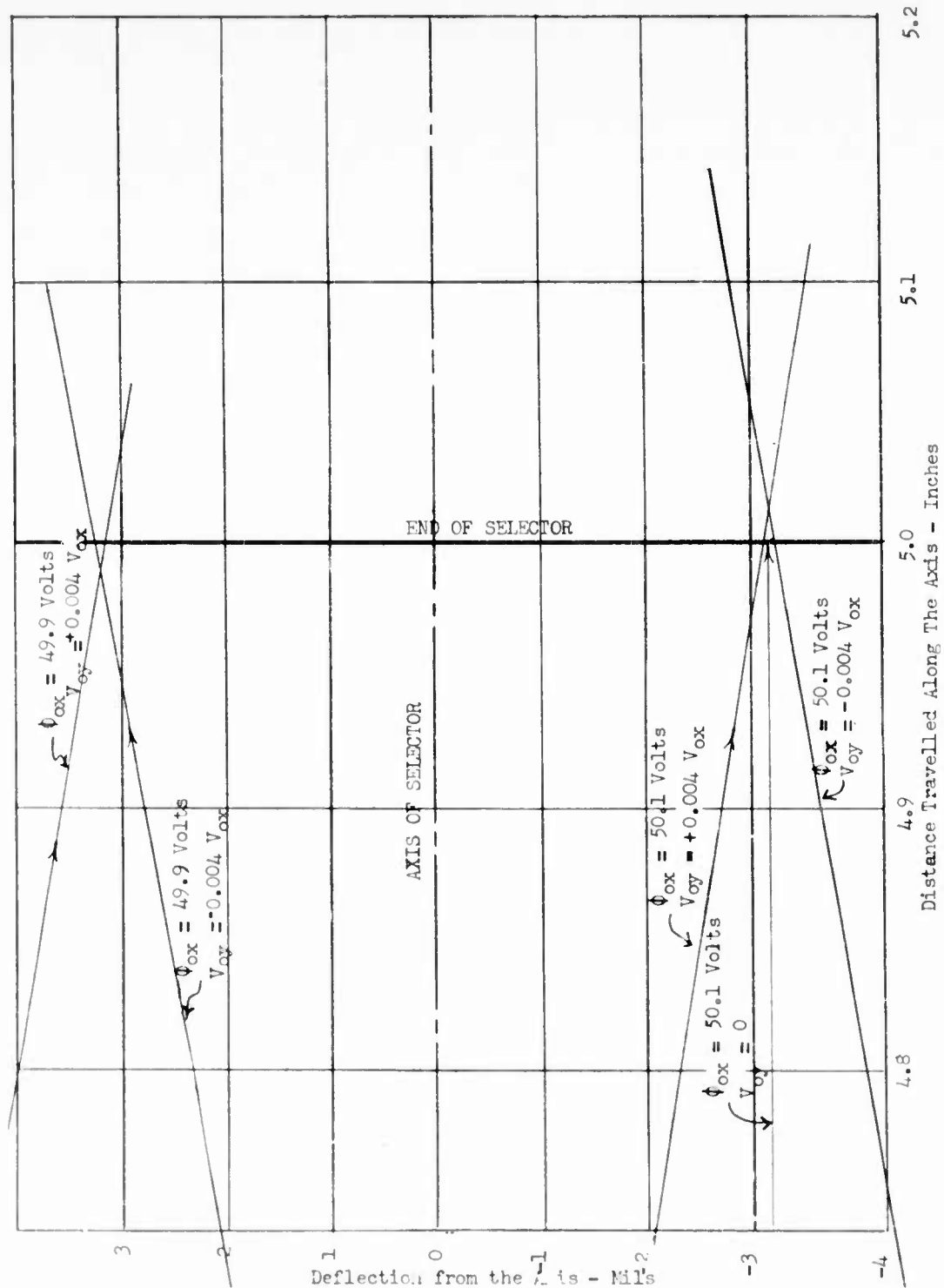
Figure 65. Electron Trajectory in Crossed-Fields Velocity Selector.

Let:

L = 5 inches

ϕ_T = 50 volts

ϕ_{ox} = 50 ± 0.1 volts

$\dfrac{V_{oy}}{V_{ox}}$ = 0.004

By selecting values of R from 0.9 to 1.04, we compute the corresponding values of X and Y from equations (29) and (30) to obtain the electron trajectory plotted in Figure 65.

Comparing Figures 63 and 65, we conclude that the radial components of initial electron velocity have a negligible effect on the range of electron energies passing through the selector.

There remains the problem of determining the maximum current transmitted by the crossed fields selector. Qualitatively one would expect this current to depend on the following factors:

1) Current density of the electron beam at the entrance aperture of the selector.

2) Range of velocities of electron beam entering the selector.

3) Entrance and exit aperture diameters.

4) Length of selector.

5) Range of energies transmitted by the selector.

With certain simplifying assumptions, we can readily evaluate, in a quantitative sense, the current limitations imposed by some of these factors.

184
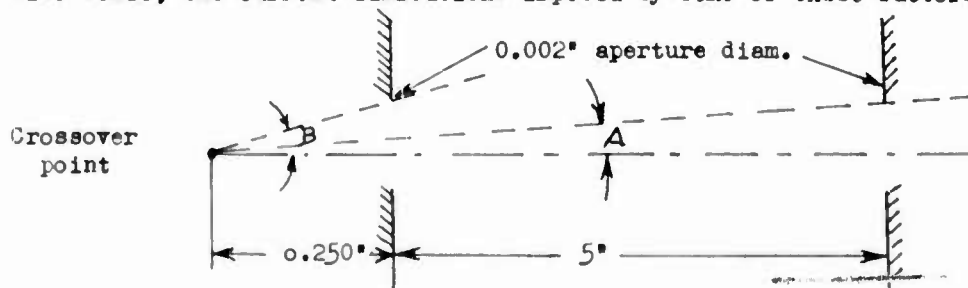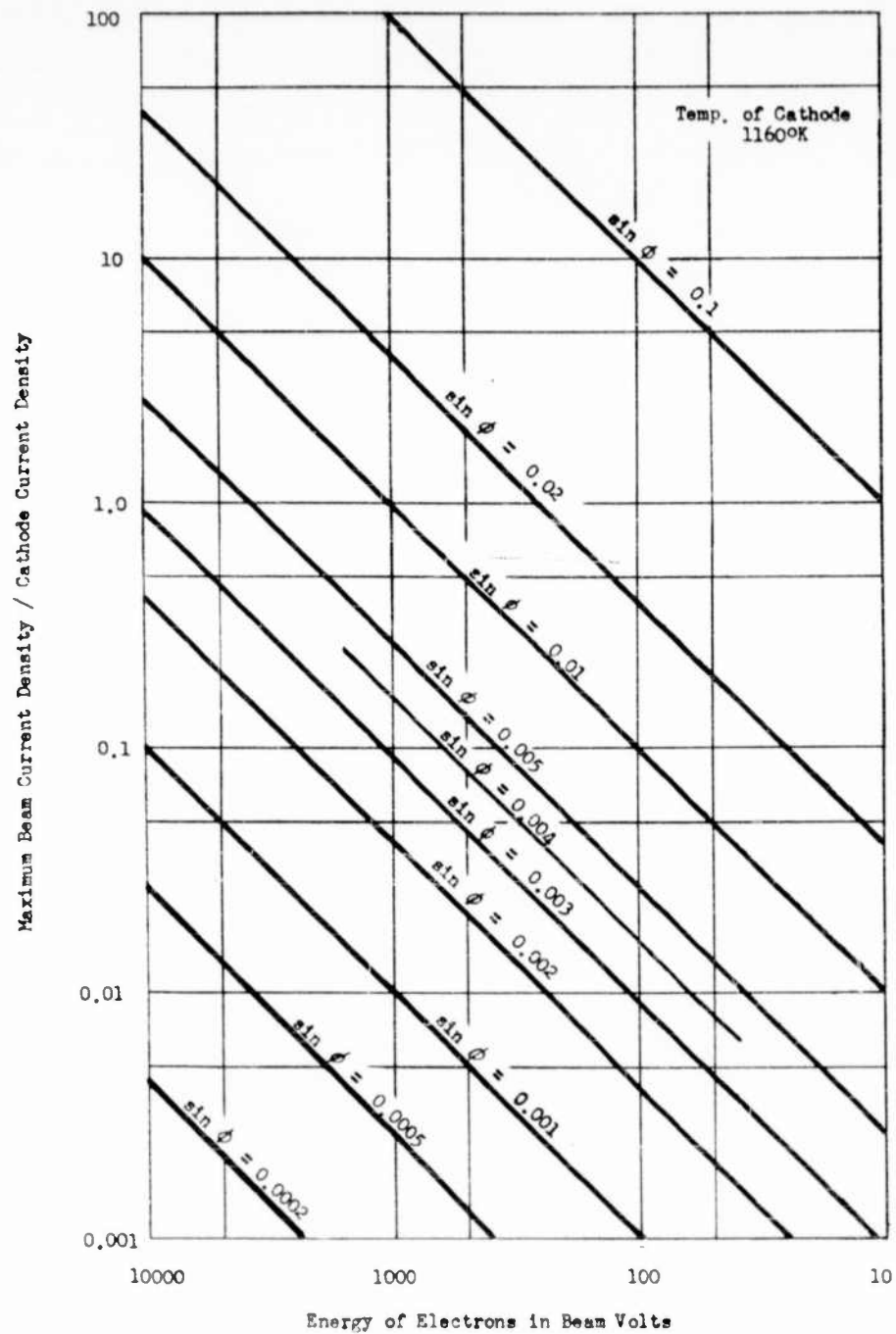
Figure 66. Maximum Current Density Obtainable in a Focused
Spot of Electrons as Function of Final Voltage and
Half Angle of Beam

Referring to the sketch and again using the assumption of a joint crossover located .250" outside the entrance aperture, we observe that the beam divergence half angle , B, is defined as:

$$B = \tan^{-1} \frac{0.001}{0.250} = \tan^{-1} 0.004$$

For this small angle, we can make the following approximation:

$$\tan^{-1} 0.004 = \sin^{-1} 0.004$$

Referring to Figure 66, we obtain an extrapolated theoretical value for the ratio of the maximum beam current density to the cathode current density for this computed value of half angle of beam at a beam voltage of 50 volts. Thus:

$$\frac{J_B}{J_K} = 0.008$$

The maximum beam current density arriving at the entrance aperture is then:

$$J_B = 0.008 \ J_K$$

Assuming a cathode current density, J_K, of 2.6 amperes per square inch, we obtain:

$$J_B = 0.008 \ (2.6) = 0.0208 \ \text{amps/in.}^2$$

The maximum current entering the aperture becomes:

$$I_B = J_B \ A$$

Where A = area of entrance aperture = $\pi \times 10^{-6}$ in.^{2}

$$I_B = 2.08 \times 10^{-2} \times \pi \times 10^{-6} = 6.5 \times 10^{-8} \ \text{amperes}$$

Assuming no selection in the crossed fields device, i.e. no applied fields, the maximum current which can leave the selector is then:

$$I_{exit} = I_B \left(\frac{\tan^2 A}{\tan^2 B} \right)$$

$$I_{exit} = 6.5 \times 10^{-8} \left(\frac{0.250}{5.25} \right)^2$$

$$\boxed{I_{exit} = 1.5 \times 10^{-10} \ \text{amperes}}$$

186

If we assume that the beam current required to discharge the target of an image orthicon at highlight level is approximately 10^{-8} amperes, then the maximum computed current of 10^{-10} amperes, leaving the velocity selector, may be sufficient for operation of the tube at low light or signal levels. In fact, it is at low signal levels that a monoenergetic scanning beam is most desirable. It will be recalled, however, that the calculation of maximum current leaving the selector was only approximate, being based on certain simplifying assumptions. One of these assumptions was the absence of applied fields in the velocity selector which acted as a field free region, limiting the electron beam only by virtue of its entrance and exit apertures. Upon application of a magnetic and electric field, however, the selector will obviously tend to further decrease the outgoing beam by virtue of its energy selection. Furthermore, as pointed out previously, the ratio of the maximum beam current density to the cathode current density at the assumed beam voltage of 50 volts was obtained by extrapolation of the Langmuir theoretical maximum current densities obtainable in a focused spot of electrons.

From these electron beam current considerations, it can be seen that the velocity selector is at best marginal in its ability to transmit both a narrow range of selected energies as well as provide sufficient beam current to discharge the target even at low signal levels.

Conclusions Drawn from Analysis

(1) For a perfectly collimated electron beam with no radial components of initial velocity entering the velocity selector, the range of electron energies passing through the selector is a direct function of the selected velocity ($V_T = \frac{E_Y}{B_Z}$) and the diameter of the exit aperture and an inverse function of the selector length.

187

(2) For a selector length of 5 inches, with entrance and exit aperture diameters of 0.002 inches, and a selected energy of 50 electron volts, the selector has an absolute range of transmitted energies of 50 ± 0.063 electron volts. After selection, such a beam would require acceleration to match the existing image orthicon structure.

(3) For a 300 volt electron beam and other conditions as in (2), the range of transmitted energies is 300 ± 0.4 electron volts. This selected range compares poorly with the 0.22 volt spread predicted fron the emission velocity distribution.

(4) Assuming the crossover point of the electron gun as a point source of electrons, located 0.250 inches from the 0.002 inch diameter entrance aperture of the selector, then the radial components of initial electron velocity have a negligible effect on the selectivity.

(5) From electron beam current considerations, the velocity selector is at best marginal in its ability to transmit both a narrow range of selected energies as well as provide sufficient beam current to discharge the target even at low signal levels.

5. EXPERIMENTAL WORK WITH CROSSED-FIELDS VELOCITY SELECTOR

The early crossed-fields velocity selector consisted of a 0.002 inch entrance aperture, two parallel electrodes with flat faces spaced 0.020 inches apart, an electromagnet core and windings with the pole-piece faces spaced 0.070 inches apart and at right angles to the electrode faces, and a 0.002 inch exit aperture. The entrance aperture was also the beam-forming aperture of a modified image orthicon gun, and reasonable collimation of the entrance beam was assumed.

In the early experimental work, difficulty was encountered in obtaining a useable electron beam from the velocity selectors. Part of this problem was attributable to poor cathode emission which was alleviated somewhat by careful cleaning and heat

treating of the selector structure parts prior to mounting.

Another recognized factor was the need for precise alignment between the electron gun and the selector as well as in the selector device itself. It was further found that exposure of the transmitted beam to electrostatic fields from charged insulators could result in deflection of that beam therefore preventing its passing through the exit aperture. This was solved by careful shielding within the selector. One of the techniques devised to compensate for mechanical misalignments in the electron gun and selector system was the use of horizontal and vertical electrostatic deflecting electrodes to permit bending of the beam as required. Two sets of deflecting electrodes were located between the accelerating anode of the gun and the entrance aperture of the selector and one set of deflecting electrodes was located just behind the entrance aperture of the selector. Mechanical difficulties, however, imposed by the very small space available caused us to discard this technique in favor of newly developed improved means of mechanical alignment.

The finally developed design of the velocity selector is shown pictorially in Figures 67 and 68.

The velocity selector and electron gun system is shown in Figure 69. A large scale crossed-fields selector of this design was constructed and operated in a vacuum bell jar for evaluation. Some work was also performed in a sealed off tube. The results of the experimental tests closely approximated the current transmission calculation of 10^{-10} amperes with no applied deflecting field.

At this time the results of more complete theoretical analyses with improved techniques indicated the very low current transmission and the rather gross selectivity available from such a selector, and work was stopped in favor of other forms of the device.

ELECTRODES
2 REQ'D.

MAGNET CORE
2 HALVES

OTHER END
IDENTICAL
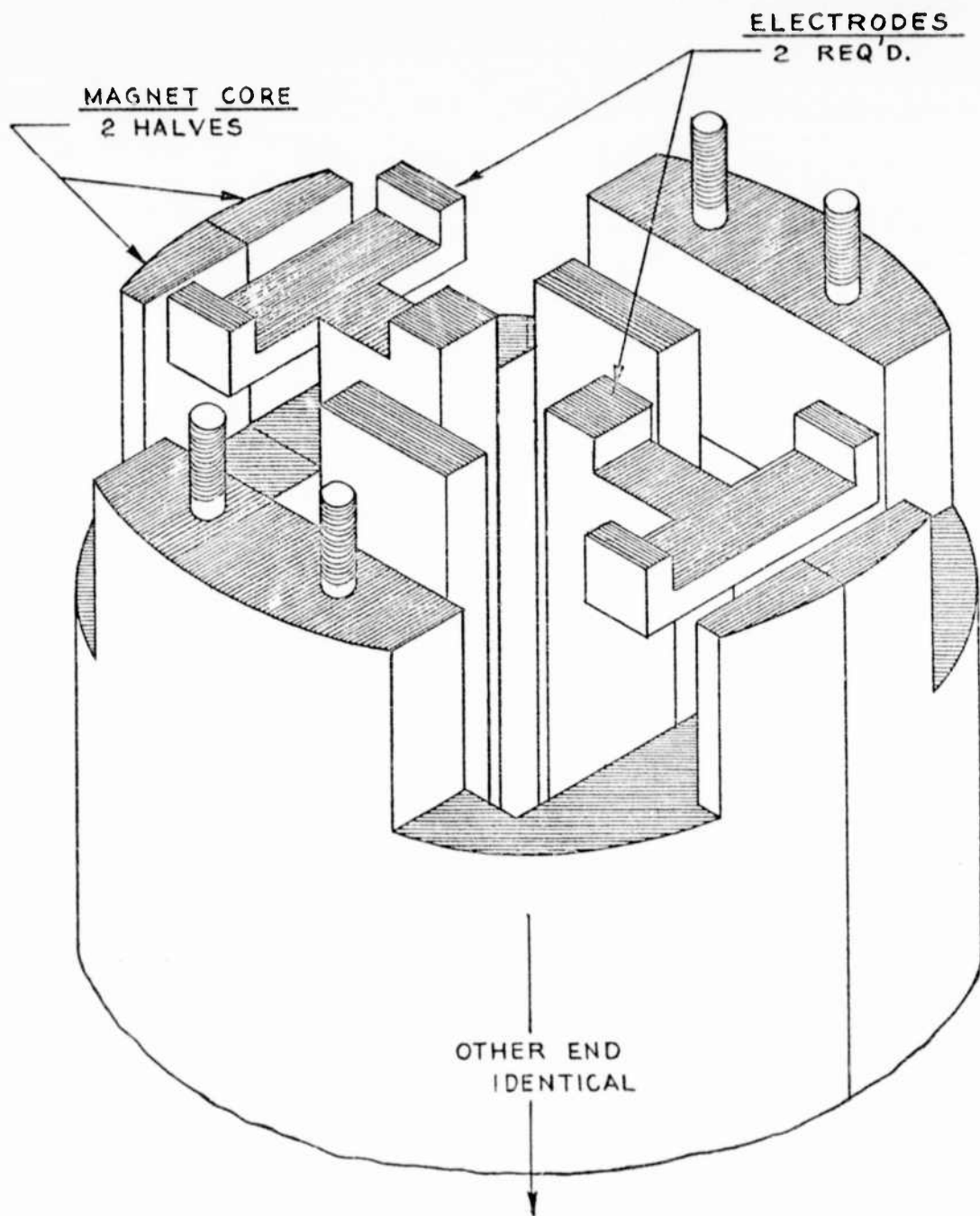
Figure 67. Crossed-Field Velocity Selector (Assembly View)

A — MICA SPACERS
B — INSULATING WASHERS
C — INSULATING SLEEVE
D — SELECTOR MOUNTING NUT

APERTURE & SUPPORT PLATE

SELECTOR MAGNETIC POLE PIECE

CONVENTIONAL IMAGE
ORTHICON ELECTRON GUN

E

SPOT WELD

ELECTRODES
(OMITTED FOR
CLARITY)
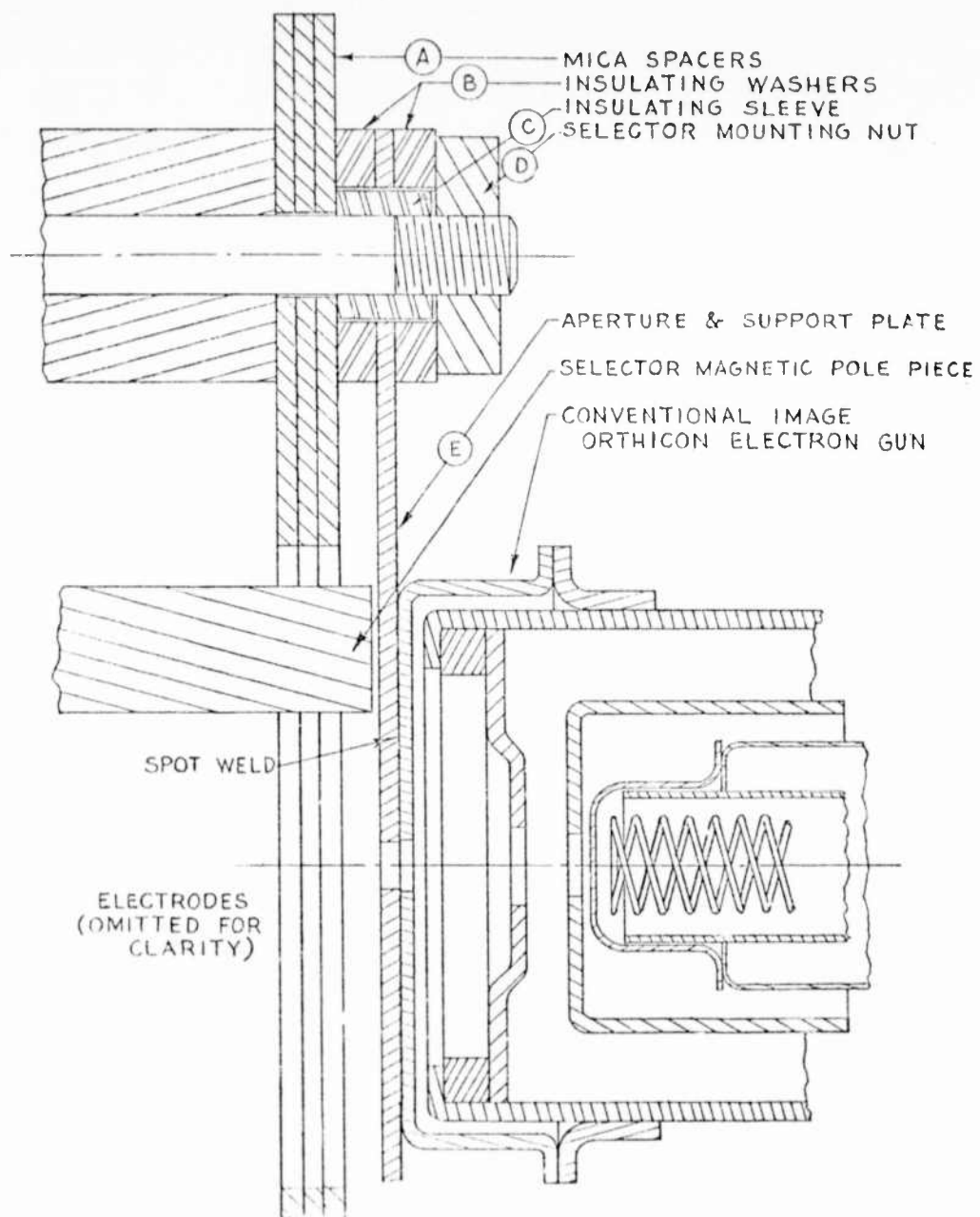
(SCALE - 8 : 1)

Figure 68. Assembly Detail Velocity Selector to Electron Gun

191

COLLECTOR
PLATE

EXIT APERTURE

ELECTROSTATIC
DEFLECTION
PLATES

MAGNETIC
POLE
PIECES (2)

ENTRANCE
APERTURE &
G_2 ASSY.

GRID #1

CATHODE
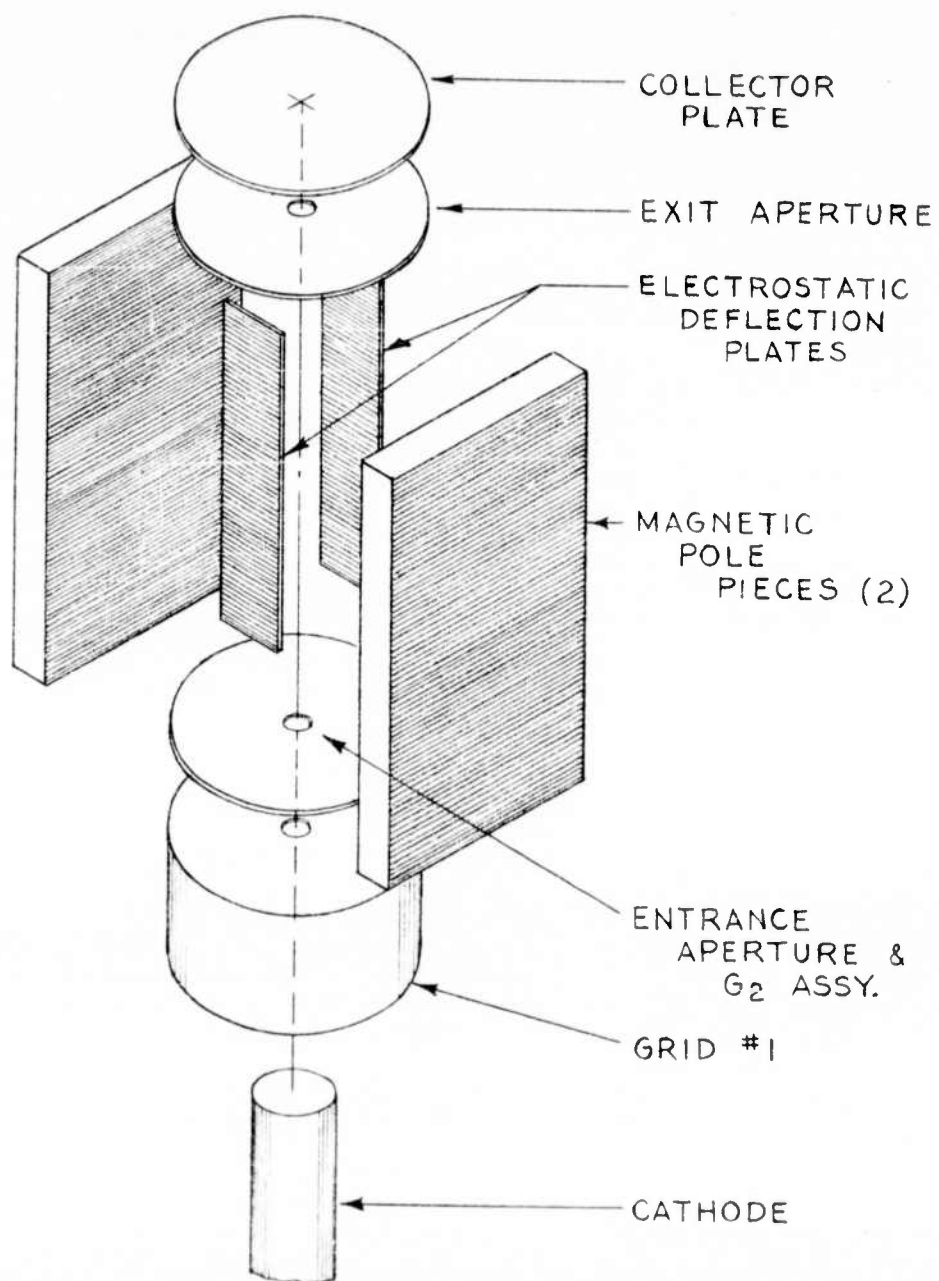
Figure 69. Velocity Selector and Electron Gun.

192

b. Spiral Path Selector

The original design of this type of velocity selector, suggested by R.K.H. Gebel (Reference 27), had a region of uniform magnetic field which the electrons entered at an angle to the field so that they traveled in a helical path. The diameter of this helix varied with the velocity and an aperture was arranged so that the electron passed through it after one half turn of the helix. A modification of this idea was to make use of the variation in the length of turn of the helix with velocity. Figure 70 illustrates the principle of this type of velocity selector.
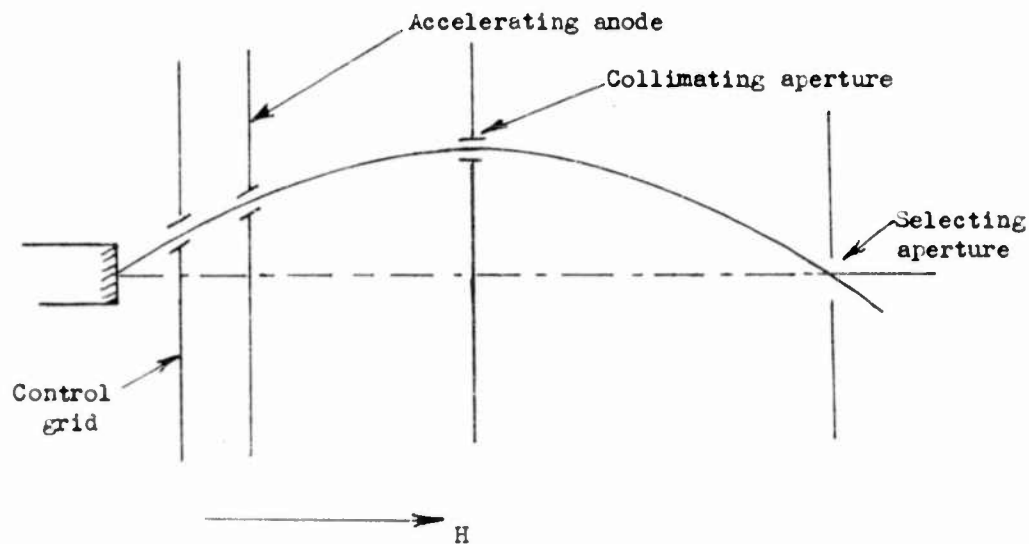
SPIRAL PATH VELOCITY SELECTOR

Figure 70

The electron beam is admitted into the selector through the entrance apertures at an angle of 10° to the axis of the selector. A uniform axial magnetic field causes the beam to travel in a spiral path and pass through the collimating aperture. The trajectories of electrons having axial velocity components greater than a certain selected value would intersect the axis beyond the selecting aperture. However, due to the presence of the aperture, they are not permitted to leave the selector. Correspondingly, trajectories of electrons having velocity components parallel to the axis

193

smaller than the selected value intersect the axis beyond the selecting aperture. These continue on and are stopped by the aperture. It can be seen that only those electrons having the selected axial velocities will pass through the selecting aperture.

The limitation of this type of velocity selector is that the electrons travel in a helix and the ratio $\underline{dV}$, where V is the average energy of the electrons in the beam, $\overline{V}$ depends on the relative diameter of the helical path and the selecting aperture. To obtain high performance, as defined by low dV, it is necessary to make V small. However, since V is numerically equal with the present gun design, to Eg2, the accelerating voltage of the electron gun anode, this smaller value of V results in reduced cathode emission with consequent lower beam current. It is also possible to make the spiral larger, necessitating a larger selector structure, involving a change in many gun and multiplier components and possibly the tube envelope when incorporated in an image orthicon. Reducing the selecting aperture of the selector would decrease the range of electron energies transmitted by the selector but would also decrease the available electron beam current.

Work was initiated on this type of selector during the early part of the contract period but was discontinued in favor of the crossed-fields velocity selector for these reasons.

c. Electron Mirror Selector

The electron mirror selector is an emission system devised by our Research Laboratries for molecular excitation and dissociation energy experiments in which an Einzel lens immersed in a solenoidal magnetic field reflects electrons whose axial velocity component is insufficient to overcome the barrier of the "saddle field".
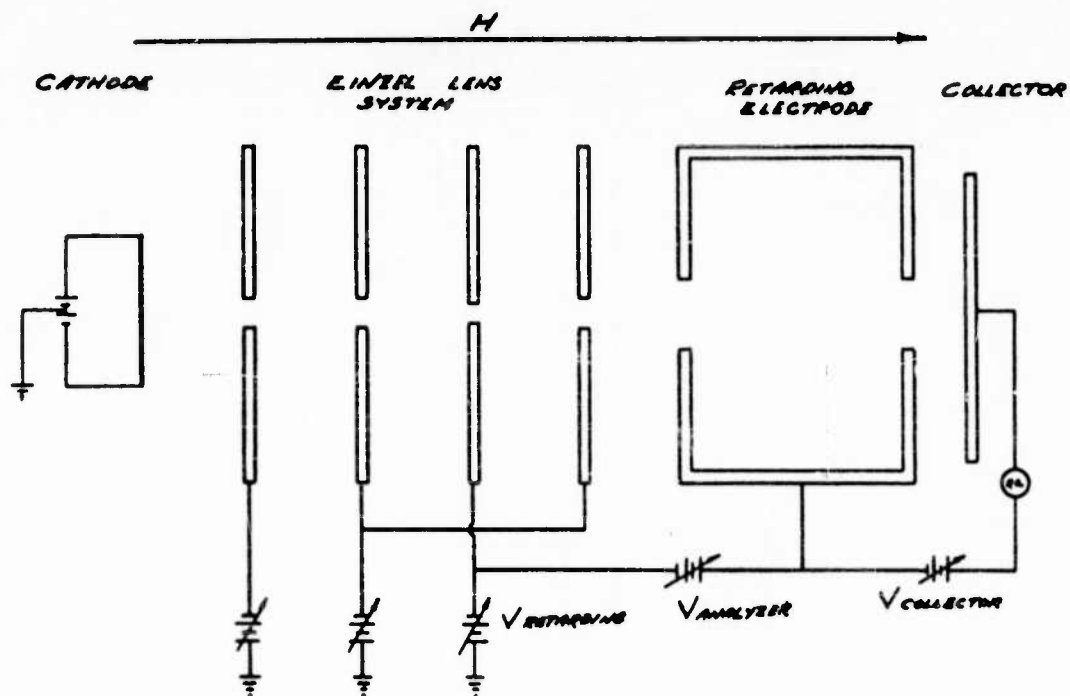
Figure 71.   Velocity Selector - Analyzer

Figure 72. Velocity Selector - Analyzer

Such a system, combined with a Faraday cage analyzer, is shown in Figures 71 and 72. Normally, the selector is operated at the low accelerating voltages, up to 10 volts, appropriate to these molecular experiments. Use of higher voltages in the selector is undesirable since the focusing action of the "saddle field" formed in the retarding electrode might contribute radial components of motion to the electron beam. Since we are concerned with higher accelerating voltages in the image orthicon, some means of post selector acceleration would have to be employed. This could consist of a series of increasingly positive electrodes so that no stray voltage gradients would exist in apertures to contribute a lateral force to the off axis electrons.

In the operation of an image orthicon, it is believed that at low signal levels only the high velocity electrons are effective in discharging the target. Since the low velocity electrons are a constant addition to the return beam noise, their removal from the beam by use of the electron mirror selector, should reduce the noise level in the return beam.

In view of the relative simplicity of this system, as compared to other velocity spread reduction techniques, it is felt that potential barrier velocity filtering may well demonstrate the feasibility of further work on velocity selectors. Although some experimental work was performed on this device in a demountable tube, it was realized that this device also performs best at very low beam voltages, and that one then faces the problem of accelerating the velocity selected beam without causing a further interchange between axial and transverse velocity components. Therefore, although this approach is considered promising, it was shelved to concentrate on a preamplifier approach.

d. Planar Diode Gun

As indicated above, another approach to the problem of minimizing the axial velocity spread is a basic redesign of the electron gun structure to approach the 0.22 volt thermal energy distribution by elimination of transverse velocity components.

197

Of possible methods we have considered, a planar emission system using planar accelerating equipotential surfaces seems most promising. If sufficient, current density is not available from such a structure, a magnetically shielded Pierce gun or similar structure should be useful to obtain more current in a beam free of transverse velocity components.

6. CONCLUSION

The work indicates the velocity selectors we tried or considered are theoretically marginal and actually the mechanical difficulties make them all but impossible. Based on this result, we would not recommend further work in this field. Although insufficient work was completed on the electron-mirror velocity rejecting device to evaluate it thoroughly, this approach seems to be the most promising, and further work might be profitable. It must be stated here that none of the laboratory devices tested here reduce the axial velocity spread of an electron beam and none of the devices seemed sufficiently promising to warrant an operational test in a tube.

Based on this work, we believe that a more fruitful approach to the objective of minimizing the axial velocity spread is a basic redesign of the electron gun structure to approach the 0.22 volt thermal distribution through elimination of transverse-velocity components. Of possible approaches, we have considered, a planar emission system using planar accelerating equipotential surfaces seems most promising. If sufficient current density is not available from such a structure, a magnetically shielded Pierce gun or similar structure should be useful to obtain more current in a beam free of transverse velocity components.

To fully utilize the benefits of a reduced axial velocity spread, additional work must also be done on reducing beam radial velocities and aberrations that occur in the deflection of the scanning beam. In the present 5820 operating at light levels near the knee of the signal vs illumination characteristics, there is

a difference in beam landing energy of 1-1/2 to 3 volts between the center and edge of the target. Fortunately, however, the local target voltage operating point shifts to compensate for these landing errors at very low light level conditions.

HALATION

A standard image orthicon adjusted for near threshold imaging on a dimly lighted scene may be partly or completely disabled by a single bright light source in the field of view, such as a searchlight. Our measurements at various scene light levels show that a light source up to 10^4 times the scene brightness may be tolerated, producing only a localized disturbed area around the light source. Image brightness up to 10^7 times scene illumination levels were studied. Counter measure light sources at these levels seem feasible, and completely disable the tube.

The effect consists of a dark halo surrounded in turn by a white halo which may extend over the whole reproduced scene, blocking out all desired information. It is caused primarily by redistributed electrons from the writing side of the target. The electron image of the light source on the target causes that small area to be charged positively to or slightly above collector mesh potential. A large number of low velocity secondary electrons leave this small area of the target, travel through the collector mesh, are turned back by the field between the collector mesh and photocathode, pass through the collector mesh again and strike the target in a small area around the original image. Since these electrons have energies below the first secondary emission crossover of the target, they charge this area negatively, and since the density of this redistribution current far exceeds that of the primary signal current caused by the dimly lighted scene, this area appears black on the monitor and apparently contains no picture information. Back-scattered electrons with energies ranging up to that of the 300 to 400 volt primaries also leave the image area, pass through the collector mesh and return to the target as a flooding current. Since their energy is above the first secondary emission crossover for the target, the target is charged positively and a white hazy halo, which may cover the entire scene, appears on the monitor. Because the

200

current density of this redistributed current is also far larger than that of the primary information bearing current from the photocathode, the desired scene information is partially or completely lost due to lack of contrast and to noise in the redistributed electron signal.

Because both of these halo effects are essentially unwanted information written on the target, they must be remedied by tube redesign on the writing or photocathode side of the target. Experiments show that increased scanning current, such as would be available if isocon scanning were used, does not significantly improve the tube performance. The effect will basically be found whenever the brightness of one object in the scene greatly exceeds the average scene brightness. The wide extent of the halo appears to be due to the wide energy spread in the secondary and back-scattered electrons and their wide angular distribution as they leave the target. Therefore, we concentrated on measures to improve the collection of secondary and recoil electrons from the target. Theoretical investigations including field plots and trajectory calculations showed that up to 25% of the secondaries leaving the target passed through the collector mesh, are deflected toward the target by the field in the image section, passed through the mesh again and strike the target. For the higher energy back-scattered electrons which caused the white halo effect, these electrons cannot be collected simply by making the mesh more positive with respect to the instantaneous target potential. We therefore have attempted to reduce or eliminate the white halo by greatly increasing the thickness of the collector mesh without decreasing its transmission. A mesh which is thick compared to the hole diameters will pass only those electrons which approach with an angle of incidence close to the normal. The incident electrons from the photocathode will therefore be transmitted, whereas the high energy secondaries which leave the target at angles far from normal and cause the white halo should be eliminated by interception. Note that while this thick mesh will

eliminate the white halo, caused by high energy electrons which pass through the normal collector mesh, the smaller black halo may not be entirely eliminated, since it may be caused in part by low energy electrons which do not pass through the mesh. Experimental verification of the effectiveness of thick collector mesh to eliminate the halo effect was obtained in an image orthicon in which the usual .0002" thick electroformed collector mesh was replaced with a piece of Corning fotoform glass .007" thick having 350 rows per inch of square holes which were .0015" on a side giving 25% optical transmission. The glass mesh was made conductive by aluminizing from both sides using several evaporation sources to coat the inner walls of the holes. A test of this tube with a bright concentrated source in the middle of a dimly lighted test pattern showed no white halo effect under conditions which would have given a completely washed-out picture on a standard image orthicon. The principle, therefore, appears to have been proven, and the remedy should be equally applicable to image orthicons and image isocons. Imaging quality on this tube was poor due to non-uniformities in the fotoform and low optical transmission. As a next step, we, therefore, attempted to make or obtain a high quality, thick, fine textured, high transmission metal collector mesh to fabricate a tube of greater utility for the Air Force.

Efforts to obtain thick electro-formed mesh include work in our own laboratories and work performed on a subcontract with Buckbee-Mears. As noted elsewhere in this report, electro-formed mesh of the type normally used in the image orthicon are formed by plating copper into shallow grooves in a flat glass plate. The thickness of this mesh cannot be built up by further plating after the grooves are once full because the plate tends to mushroom out over the flat glass surface and to close the holes in the resulting mesh. To obtain preferential plating to increase the thickness of the mesh without decreasing the optical transmission, we attempted to produce a physical barrier in or through the holes in an existing piece of mesh.

202

In one experiment, we coated existing pieces of standard mesh with photoresist, exposed from one side with a point source placed at some distance from the mesh so that the resist on one side and in the holes was hardened, and then washed the unexposed resist from the areas shadowed by the mesh bars. We then attempted to plate additional copper onto the rear side of these mesh bars using the hardened photoresist as a form to restrict the shape of the additional copper plate. This experiment was only moderately successful since it proved extremely difficult to remove the hardened photoresist from the mesh without completely destroying it.

A second experiment conducted by Buckbee-Mears involved flowing a viscous fluid through the mesh holes from one side while plating on the other. It was hoped to obtain a balance between the rate of build up of the copper and the rate of flow of the fluid which was to provide a barrier to keep the holes open. This experiment was also not successful in yielding any substantial increase in the thickness of the mesh.

A third experiment mentioned elsewhere in this report involved the use of a moving electrolyte which was forced through the holes in the mesh during the plating process so that an existing mesh could be built up preferentially. Shown elsewhere, an increase in mesh thickness of 2 to 3 times was obtained by this method. However, this .0005" or .0006" thickness was far from the .005" which we considered the minimum necessary to obtain satisfactory interception of obliquely back-scattered electrons.

A fourth experiment also mentioned elsewhere involved experimental production of a plating master from Corning fotoform glass. While deep grooves could be produced in the surface of this glass, they were so irregular that the experimental masters were unuseable. Details of this experiment are given in Section V. The work with Corning occurred at a time when they were moving their fotoform facilities approximately 100 miles from Corning, New York to Bradford, Pennsylvania and was

shelved not so much for lack of promise but because Corning could not work on the development at that time.

After several months, we decided to shelve temporarily the entire thick mesh program, hoping that advances in the state of the mesh making art might contribute the "know how" needed for profitable resumption later in the period of the contract. The approach still seems valid, and we have retained it as a desired goal to be sought on corporate funds whenever a technical advance makes it seem feasible. The military value of a halation free image orthicon, with its ability to accomodate the wider dynamic range needed in televising outdoor scenes, has been reemphasized by customer requests made since this investigation was conducted.

SECTION VIII

IMAGE SECTION DEMAGNIFICATION

As indicated in the theoretical section dealing with the fundamental limitations to forming television images at low light levels, most of our effort has been devoted to increasing the signal current developed at the image orthicon target. One possible way of increasing signal current is through use of a larger photocathode with an appropriately larger lens of the same optical transmission and f number. That this is so may be seen from the following equations.

a) $\quad E_{pc} = \dfrac{E_s RT}{4f^2}(M + 1)$

where:

E_{pc} = photocathode illumination in foot candles

E_S = scene illumination in foot candles

R = reflectivity of scene (diffuse reflection is assumed)

T = optical transmission of lens

M = linear magnification from scene to photocathode

In most cases, M is very much smaller than 1 and is neglected.

b) $\quad I_{pc} = SE_{pc}A$

where:

I_{pc} = signal current from photocathode in microamperes

S = sensitivity of photocathode in microamperes per lumen

E_{pc} = photocathode illumination in foot candles

A = area of photocathode in sq. ft.

Thus, the signal current can be increased directly by use of a larger photocathode provided only that light optics are available to maintain the same f number.

Use of a larger photocathode is also desirable since it permits use of a larger field of view with a given lens. Therefore, we devoted some time to

205

consideration of preamplifier image orthicons with large input photosurfaces, in which electronic demagnification was used to concentrate the photoelectron current on a smaller target area. Two principal approaches were followed. The first, a 5:1 demagnification high voltage electrostatically focused image intensifier, was designed as an integral preamplifier in a single large bulb with an image orthicon using a thin phosphor photo surface member as the transfer means. The high voltage structure was that which has been manufactured at the Westinghouse Tube Division for ten years as the WL5997, and which is normally used for intensification of faint x-ray images. For the second approach, we designed a magnetically focused demagnification image section to permit use of 3" diameter photocathode and to directly focus the resulting photoelectrons on a standard image orthicon target.

The principal problem to be overcome in the high voltage demagnification pre-amplifier was that of reducing dark emission from parts within the tube, which would otherwise result in spurious light being generated at the intensifier output and in turn fed to the image orthicon. While parts were ordered for this approach in the first months of the research program in 1956, only one unsuccessful attempt was made to assemble a tube. The work was then shelved to permit taking advantage of an intensive program instituted at that time under corporate funds to improve the design and processing of the high voltage intensifier structure in the x-ray sensitive version. Although since that time, the manufacturing control achieved for the x-ray sensitive version has been so improved that we had occasionally achieved a yield of 75% on these tubes, and although we have recently placed a visible light sensitive version of this intensifier in production for use as a light amplifier as part of the instrumentation of nuclear physics, we decided not to revive this particular approach. This decision was made jointly with the Air Force task scientist, primarily to avoid any work which could be construed as a duplication of work being performed in another laboratory.

206

While the high voltage demagnification preamplifier offered both the advantages of the larger photocathode and a substantial gain obtained from the high accelerating voltage, the low voltage, magnetically focused, demagnification image section offers only a gain equivalent to the reduction in area. As a reasonable compromise between the gain desired, the benefit of being able to operate the tube in an image orthicon camera with only modest modifications, and our estimate of how sharply the required magnetic focusing field could be altered without disturbing the electron paths in the scanning section, we worked out a tube design in which the electrons from a 3" diameter photocathode would be focused onto the 1.4" diameter target. Other things being equal, this tube should have displayed an increase in sensitivity of four times over standard image orthicons. The image section electrodes and photocathode curvature were laid out in an electrolytic plotting tank, the needed magnetic focusing coils designed in a scaled-up version, and the design checked by magnetic field plots. Although an experimental tube was attempted, this approach was dropped on the basis of a theoretical analysis which indicated that the resolution obtainable with such a sharply flaring magnetic field would be sharply degraded. For the tube we had designed, our theory indicated a resolution of only 100 to 200 T.V. lines. When we considered the rather limited gain we expected to obtain and the requirement for larger light optical lenses with special elements for proper focus on a curved photocathode, the benefits to be gained from this approach did not seem worthwhile.

APPENDIX I

MODULATION PHENOMENA IN THE IMAGE ORTHICON

Technical Memo by R.W. Floyd

For a given operating condition of an Image Orthicon, it is possible to define a time constant $\bar{t}o$ and a maximum output signal I_m. If the output from a target element is measured by the ratio R of the actual output I_{out} to the potential maximum output I_m, and the input by a similar ratio ρ of the actual input signal I_{in} to the maximum output (and therefore maximum input) I_m, analysis shows that R lags behind ρ at low light levels, and that the equations for these lag effects are quite general, depending only on R, ρ, and $\bar{t}o$. The time constant increases at low light levels, and may be as high as 5 seconds at threshold, while the lag effects are visible for durations on the order of several times $\bar{t}o$. These lag effects cause great deterioration of moving scenes at low light levels, and are likely to prove quite undesirable in many military applications. Lag may be reduced, however, by varying several tube parameters, including the target mesh capacitance.

This memorandum examines some of the problems of low light level imaging upon a moving or transient scene, as related to sensitivity, by means of a similar theoretical approach.

In the Image Orthicon, the signal input to the target, I_{in}, is approximately equal to .64 (δ -1) Ipc, where δ is the secondary emission coefficient of the target for 400 volt electrons, and I_{pc} is the photocathode current. The signal output for positive or zero target potential is M . I_{beam}, where I_{beam} is the beam current and M is a modulation ratio imposed by the secondary emission of the scanning side of the target. For negative target potentials, the signal output I_{out} is M . I_{beam} $\exp - \dfrac{Ve}{kT}$ since the fraction of beam electrons which can overcome a retarding potential V is $\exp - \dfrac{Ve}{kT}$. If I_m is defined as M . I_{beam}, $I_{out} = I_m \exp - \dfrac{Ve}{kT}$

208

The ratio R of the actual output signal to the maximum output signal is then

$$\frac{I_{out}}{I_m} = \exp{-\frac{Ve}{kT}}.$$

In the preceding formula V is the retarding potential on the target (positive if the target is negative with respect to the cathode), e is the electronic charge, k is Boltzmann's constant, and T is the temperature of the cathode in ^oK. The net current to the target is $I_{in} - I_{out} = I_{in} - I_m \exp{-\frac{Ve}{kT}}$. Then if the target raster capacitance is C,

$$\frac{dV}{dt} = -\frac{I}{C} = -\left(\frac{I_{in} - I_m \exp{-\frac{Ve}{kT}}}{C}\right) \qquad (1)$$

We will consider periods during which the light level is constant, so that I_{in} is constant. In the interests of mathematical solubility we will use an average value for I_{beam} and I_m as though every target element were continuously read, although in actual operation reading occurs in pulses at 1/30 second intervals. This approximation is permissible because time lags at low light levels are much greater than 1/30 second. Let ρ be defined by $\rho = \frac{I_{in}}{I_m}$, the ratio of actual input to the maximum potential input. Then:

$$\frac{dV}{dt} = -\frac{I_m\left(\rho - \exp{-\frac{Ve}{kT}}\right)}{C}$$

$$\frac{dV}{\rho - \exp{-\frac{Ve}{kT}}} = -\frac{I_m}{C}\, dt$$

Integrating:

$$\frac{V}{\rho} + \frac{kT}{\rho e}\, \log\left(\rho - \exp{-\frac{Ve}{kT}}\right) = -\frac{I_m}{C}\, t + K \qquad (2)$$

where K is an arbitrary constant.

If V_o is the target voltage at t = 0;

$$K = \frac{V_o}{\rho} + \frac{kT}{\rho e}\, \log\left(\rho - \exp{-\frac{V_o e}{kT}}\right)$$

209

Then the general solution of equation (1) is:

$$-\frac{\rho}{C} I_m t = (V - V_0) + \frac{kT}{e} \log \left(\frac{\rho - \exp\left(-\frac{Ve}{kT}\right)}{\rho - \exp\left(-\frac{V_0 e}{kT}\right)} \right) \tag{3}$$

In the particular case where $V_0 = 0$,

$$-\frac{\rho}{C} I_m t = V + \frac{kT}{e} \log \frac{\rho - \exp\left(-\frac{Ve}{kT}\right)}{\rho - 1} \tag{4}$$

If $\rho = 1$ in equation (4), $\log \frac{\rho - \exp\left(-\frac{Ve}{kT}\right)}{\rho - 1}$ may be considered finite only if

$\exp\left(-\frac{Ve}{kT}\right) \equiv 1$, or $V \equiv 0$.

If $\rho = 0$, equation (4) is an identity. However, if $\rho = \Delta \approx 0$, we find:

$$-\frac{\Delta\rho}{C} I_m t = V + \frac{kT}{e} \log \frac{\exp\left(-\frac{Ve}{kt}\right) - \Delta\rho}{1 - \Delta\rho}$$

$$\approx V + \frac{kT}{e} \left\{ -\frac{Ve}{kT} + \Delta\rho \left(1 - \exp\frac{Ve}{kT} \right) \right\}$$

Then $-\frac{I_m}{C} t = \frac{kT}{e} \left(1 - \exp\frac{Ve}{kT} \right)$; $\exp\frac{Ve}{kT} = 1 + \frac{I_m t}{C} \frac{e}{kT}$

$$V = \frac{kT}{e} \log \left(1 + \frac{I_m t}{C} \frac{e}{kT} \right) \tag{5}$$

$$Q = CV = \frac{kTC}{e} \log \left(1 + \frac{I_m t}{C} \frac{e}{kT} \right) \tag{6}$$

The output signal at a given time is a function of the retarding potential seen by the beam; $I_{out} = I_m \exp\left(-\frac{Ve}{kT}\right)$. We recall that $R = \frac{I_{out}}{I_m}$; then

$$R = \exp\left(-\frac{Ve}{kT}\right), \text{ or } V = -\frac{kT}{e} \log R \tag{7}$$

For the case $V_0 = 0$, solving equations (4) and (7).

210

$$-\frac{\rho}{C} I_m t = -\frac{kT}{e} \log R + \frac{kT}{e} \log \left(\frac{\rho - R}{\rho - 1}\right)$$

$$\frac{e}{kT} \frac{\rho I_m t}{C} = \log \frac{(\rho - 1) R}{\rho - R}$$

$$\frac{R (\rho - 1)}{\rho - R} = \exp \left\{\frac{e}{kT} \frac{\rho I_m t}{C}\right\} \quad ; \text{ solving for R,}$$

$$R = \frac{\rho \exp \left\{\frac{e}{kT} \frac{\rho I_m t}{C}\right\}}{\rho - 1 + \exp \left\{\frac{e}{kT} \frac{\rho I_m t}{C}\right\}} \tag{8}$$

If $V_o = 0$, $\rho = 1$, (8) becomes $R \equiv 1$.

If $V_o = 0$, $\rho = 0$ equations (5) and (7) become

$$-\log R = \log \left(1 + \frac{I_m t}{C} \frac{e}{kT}\right) \quad ; R = \frac{1}{1 + \frac{I_m t}{C} \frac{e}{kT}}$$

$$R = \frac{C \frac{kT}{e}}{C \frac{kT}{e} + I_m t} \tag{9}$$

Let a time $\bar{t}$ be defined by $\frac{R}{dR/dt} = \ddot{t}$ in equation (9).

$$\frac{dR}{dt} = \frac{I_m C \frac{kT}{e}}{\left(C \frac{kT}{e} + I_m t\right)^2}$$

$$\bar{t} = \frac{R}{\dot{R}} = \frac{C \frac{kT}{e} + I_m t}{I_m} = \frac{C}{I_m} \frac{kT}{e} + t$$

$$\bar{t}_o = \frac{C}{I_m} \frac{kT}{e} ; \quad \text{then } \bar{t} = \bar{t}_o + t \tag{10}$$

211

$\bar{t}_o$, as defined above, will be called the time constant, and will prove quite useful in describing transient effects.

If $V_o \neq 0$, $\rho = 1$, let $V_o = -\dfrac{kT}{e} \log R_o$

Then equation (3) becomes

$$R = \cfrac{1}{1 + \left(\dfrac{1-R_o}{R_o}\right) \exp\left(-\dfrac{e}{kT} \ \dfrac{I_m t}{C}\right)} \tag{11}$$

It may be seen, however, that a number of variables may be eliminated from the equations by substitution of $\bar{t}$o. Equations (8), (9), and (11) become

$$R = \frac{\rho \exp\left[\rho t / \bar{t}_o\right]}{\rho - 1 + \exp\left[\rho t/\bar{t}o\right]} \qquad (R_o = 1, \ \rho \neq 0) \tag{8'}$$

$$R = \frac{1}{1 + t/\bar{t}o} \qquad\qquad (R_o = 1, \ \rho = 0) \tag{9'}$$

$$R = \cfrac{1}{1 + \left(\dfrac{1-R_o}{R_o}\right) \exp - t \ /\bar{t}o} \quad (R_o \neq 0, \quad \rho = 1) \tag{11'}$$

Finally, the general equation (3) becomes

$$\frac{R}{\rho - R} = \frac{R_o}{\rho - R_o} \qquad \exp \rho t/\bar{t}o \quad (0 \neq R_o \neq \rho \ , \rho \neq 0) \tag{3'}$$

giving R as an implicit function of the parameters R_o, $\bar{t}$o, and ρ , and of the variable t.

This representation shows the lag of signal output ratio R behind the signal input ratio ρ . An R of 1 indicates that the area of the raster under consideration shows white on the kinescope; an R of 0, that the corresponding raster shows black. Similarly, a ρ of 1 corresponds to a fully illuminated area of the photocathode, a ρ of 0 to a dark area of the photocathode.

Graph I — handwritten annotations:

Output Signal Ratio
R

R. Floyd
6-8-56

Graph I

$V_0 = 0 \quad R_0 = 1 \quad \rho = 1$

Transient signals in the
Image Orthicon at low light levels

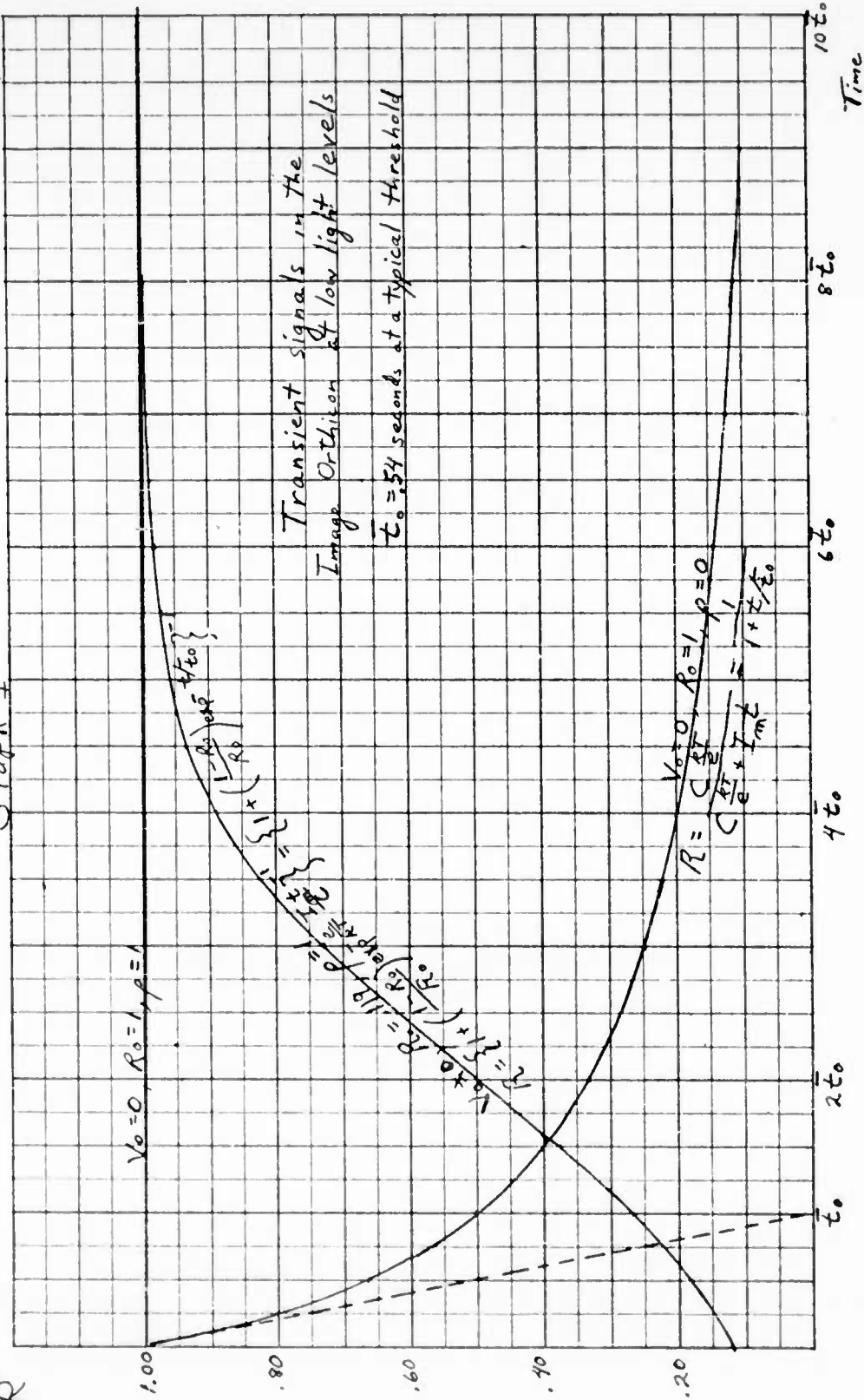$\overline{t_0} = .54$ seconds at a typical threshold

$V_0 = 0 \quad R_0 = 1 \quad \rho = 0$

Time

213

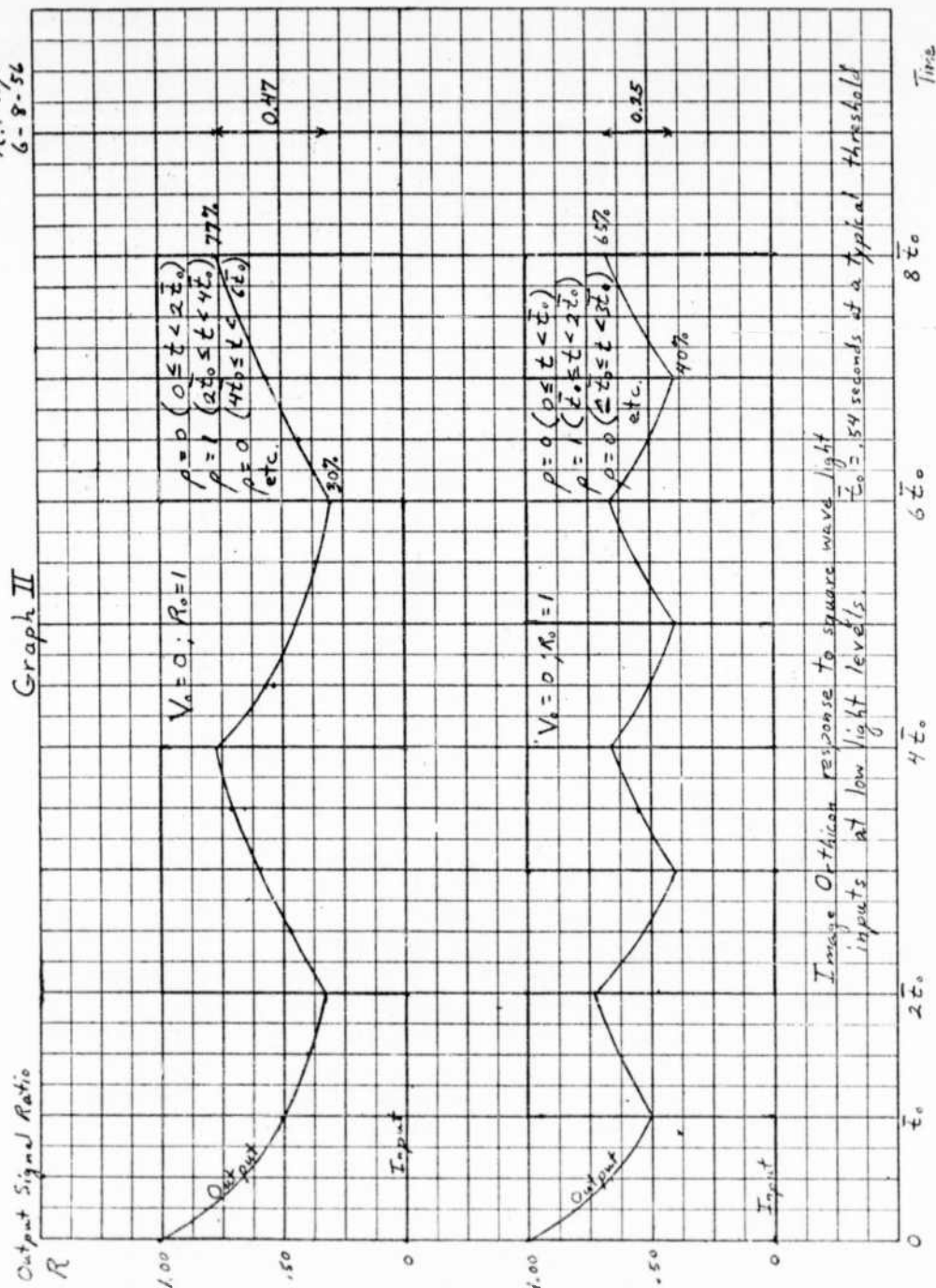Figure 73. Transient Signals in the Image Orthicon at Low Light Levels

Figure 74. Image Orthicon REsponse to Square Wave Light Inputs
at Low Light Levels.

214

The theoretical derivations are completed. It now seems relevant to substitute practical values into the above formulae. It is assumed that $\frac{e}{kT}$ is approximately 11.5; target-mesh capacitance of a standard 2-mil tube is 100 uuf. If photocathode sensitivity is 40 ua/lumen, threshold is 1.5×10^{-5} foot candles, and δ target is 5, then I_{in} at threshold is 16 uua. The proper setting of the beam current is defined by $I_{in} = I_m$, so $I_m = 16$ uua. At the knee of the curve of the tube's transfer characteristic, the light level is 5×10^3 times as great as at threshold. Then $I_m = .08$ ua.

At threshold, $\bar{t}o = \dfrac{10^{-10}}{16 \times 10^{-12} \times 11.5} = 0.54$ seconds, or 16 frame times. At the knee, the time constant is .000108 seconds; this is negligible compared to a frame time. The time constant is equal to one frame time at a light level 16 times threshold. If threshold for a very sensitive tube is 1.5×10^{-6} foot-candles, $\bar{t}o$ is 5.4 seconds at threshold.

The graphs of signal response on the following pages show that, after an object has disappeared from the scene or moved to a different location, a time of several times $\bar{t}o$ is required to register an altered signal on the kinescope (Figure 73). At threshold, for example, a time on the order of 4 $\bar{t}o$ may be required to reproduce a sharp increase in light intensity. A decrease in light intensity will probably be registered on the kinescope in a time 2 $\bar{t}o$. These times are typically two seconds and one second respectively for standard tubes at threshold. These are the lag times which have been observed for standard tubes.

It is noteworthy that, while the equilibrium signal from a stationary scene at low light level is independent of $\bar{t}o$, for a scene which varies at frequencies comparable to $\bar{t}o$ the signal is greatly reduced. For example, if a light is switched on and off so that $\rho = 0$ and $\rho = 1$ for alternate periods of length $\bar{t}o$, the output signal, as shown in the accompanying graph (Figure 74), has a maximum

amplitude R of only 0.25, and an average amplitude of only 0.12. For comparison, the ideal response, for $\bar{t}o$ very small in comparison with the light switching frequency, has a maximum and an average amplitude of 1.00

If the light switches on and off for periods of length τ , where $\tau \gtrsim \bar{t}o$, the signal has a maximum amplitude of .25 τ /$\bar{t}o$, and an average amplitude of .125 τ /$\bar{t}o$. Not only is the greater part of the signal lost, for moving scenes at low light levels, but a 90° phase lag of output behind the input causes distortion of the form of the object. Finally, the output has a different wave form than the input, presenting an "integrated" appearance.

To use even half the available signal from a moving image (say, an n-line bar pattern) the bars must take at least 4 $\bar{t}o$ seconds to pass a particular point on the target. At threshold, this means that a motion of camera or object must be slow enough that 2n seconds are required for the image to cross the raster, in order for half the available signal to be used. Then a 100-line image would be noticeably degraded (i.e., at threshold, would disappear) by an image motion such that it would cross the raster horizontally in 200 seconds. At a factor of 64 above threshold, the point at which 4 $\bar{t}o$ is equal to one frame time, a 100-line image could be seen moving at a speed of 3 seconds per raster width. No significant further improvement would be expected beyond this point, because of the limitation of the 1/30 second scanning rate.

The conclusion to be drawn from the above for low light level operation is the desirability of reduction of the time constant to the smallest possible value. Since $\bar{t}o$ is proportional to the target-mesh raster capacitance, it may be reduced by use of a large target-mesh spacing or by minification of the electron image onto a small target area. The use of a monochromatic beam, filtering out all but a small segment of the wide range of electron velocities produced by the cathode, would also reduce $\bar{t}o$. This might be accomplished by a device comparable to the mass

216

spectrometer, using electric or crossed electric and magnetic fields.

If the choice must be made between large target mesh spacing, and minification onto a small target raster area, the former seems preferable. Minification involves sacrifices in resolution, as well as formidable electron optical problems. On the other hand, wide spacing may be accomplished with only minor changes in tube structure.

Some comments on the validity of this analysis seem relevant here. The assumption of continuous rather than periodic scanning is a necessary one for differential analysis. The error introduced should be small; the time required to reach a certain signal ratio will be in error by less than one frame time. Perhaps the most doubtful assumption is that of Maxwellian velocity distribution in the beam. The beam is formed in a region of high space charge, which may alter the velocity distribution. It may be safe to assume that the beam is emitted from the virtual cathode caused by the space charge, with a Maxwellian distribution. Experimental data are not available to confirm this hypothesis. The effects of target and cathode work functions and contact potentials is to add a constant term to the target retarding potential. The validity of the analysis, however, remains unaffected, provided that the zero of potential is defined as the lowest voltage at which all electrons in the beam reach the target. Lateral leakage along the target surface, and the fact that charge transfer through the target is not instantaneous, are ignored. The writer feels, however, that the above are second order effects, and that the analysis has considerable validity at low light levels.
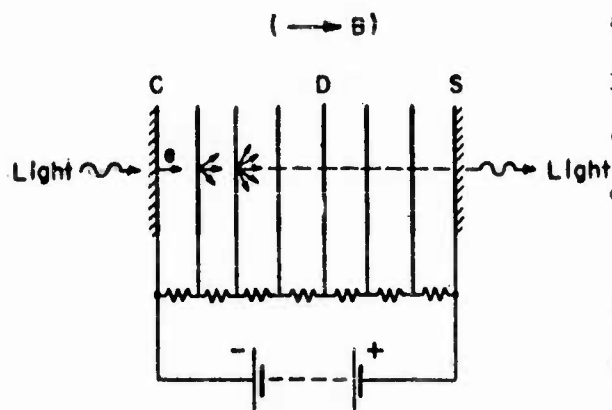
217

RESOLUTION LIMITATIONS IN THE

SECONDARY - ELECTRON IMAGE AMPLIFIER

INTRODUCTION

It is the purpose of this report to describe the physical interrelationships, which are important in the design of the transmission secondary emission intensifier[1,2]. These relationships are used to determine the parameters, which have greatest effect on resolution, and to calculate the theoretical maximum resolution.

1. RESOLUTION

Figure 75 shows a sketch of the image tube. The electron current, which is released from the photocathode G is amplified in the following stages by the transmission secondary electron multiplication of the dynodes D. Due to the parallel arrangement of all of the dynodes it is possible to form an image from the photocathode onto the phosphor screen S at the end of the tube.

The resolving power of this system, both with and without the assistance of a magnetic focusing field is obtained from a knowledge of image forming properties of one stage. In determining the gross properties of electron resolution, no account is taken of spherical aberrations

Figure 75

[1]E.J. Sternglass and M. M. Wachtel - IRE Transactions of the Professional Group on Nuclear Science, V. NS3, pp. 29-32, 1956.

[2].M.M. Wachtel and A. E. Anderson - "The Transmission Secondary Emission Image Multiplier" - Research Report 8-1043-R12 December 16, 1957.

or other defects of higher order. Furthermore it is assumed that all the primaries are absorbed in the foils (the "cathode" of a stage) and that only the low-energy secondaries are emitted from the opposite face with no spreading or modulation of the input image due to film structure or thickness.

1.1 IMAGE FORMATION WITHOUT MAGNETIC FIELD

With no magnetic field electrons are only accelerated by the electric field between the parallel plates. Due to a tangential component in the initial velocity, the electrons, released from any one point on the cathode, will produce a circle of confusion on the front surface of the following dynode. See Figure 76. To estimate the shortest distance between two points on the "cathode", whose images on the "dynode" may just be detected as distinct circles, one must calculate the current distribution across the diameter of one such circle of confusion. The following pair of equations describe the path of an electron in the assumed field:

$$Y = v_{oy} \cdot t \tag{1}$$

$$x = v_{ox} \cdot t + \frac{a}{2} t^2 \tag{2}$$

where the symbols have these meanings in terms of the initial velocity v_o:

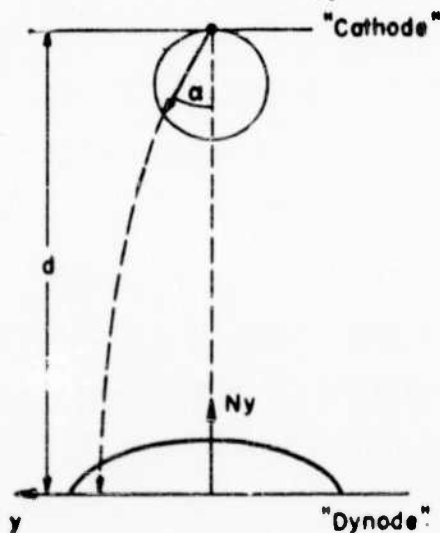$$v_{oy} = v_o \sin \alpha , \ v_{ox} = v_o \cos \alpha \tag{3}$$

Here α is the initial angle and $a = \frac{e}{m} \frac{\varphi}{d}$, where $\frac{e}{m}$ is the specific electron charge, φ the acceleration voltage and d the distance between the foils.

With x = d the time of flight is represented by:

$$t_d = \sqrt{\frac{2d}{a}} = d \sqrt{\frac{2m}{e\varphi}} \tag{4}$$

Figure 76   219

Here v_{ox} is neglected against the average speed of the electrons. Symbolically $\frac{a}{2}\frac{t_d}{v_{ox}} \gg 1$. (With an acceleration voltage of $\varphi = 3.2$ KV and an initial energy of 2 ev one finds $\frac{a\ t_d}{2\ v_{ox}} \approx 20$. Hence the result is exact within 5%). The y-coordinate of the path in the plane of the anode is therefore:

$$Y_d = v_{oy} \quad \sqrt{\frac{2d}{a}} = v_o \quad \sqrt{\frac{2d}{a}} \quad \sin \alpha \qquad (5)$$

It is assumed that the number of electrons N_α leaving the foil with a certain angle α is given by

$$N_\alpha = N_o \cos \alpha \qquad (6)$$

where N_o is the number of electrons starting perpendicular to the plane of the cathode. Therefore, the number of electrons N_y reaching the anode with the coordinate Y is given by

$$N_y = N_o \quad \sqrt{1 - \frac{Y^2\ a}{v_o^2\ 2d}} \qquad (7)$$

Hence, the electrons are elliptically distributed over the spot diameter. See Figure 2. The radius (p) of the focal spot is obtained by setting $\alpha = 90°$ in (5). Then

$$Y_{max} = p = v_o \sqrt{\frac{2d}{a}} = 2\ d\ \frac{v_o}{v_{end}} = 2d \sqrt{\frac{\varphi_o}{\varphi_e}} \qquad (8)$$

where φ_o and φ_e are the initial and end voltages respectively.

Thus we have the diameter 2_p of an image, created from a point source. However, we are interested in the image of an extended slit. The tedious calculation, which is omitted here, shows that the current distribution in the image of a line differs only slightly from the distribution in the image of a point. The distribution of a line is, in the first approximation, parabolic instead of elliptic. The half width of the point distribution is larger than that of the line distribution by about the factor 1.3. For the uniformly illuminated, extended slit one finds a current distribution which is represented by a bellshaped curve.

220

The limit in resolving the images of two parallel slits should be reached with a separation of 0.75 p. For slit width equal to slit spacing, the curves, representing the electron distribution, cross at half the maximum amplitude with this spacing.

From the above calculation it turns out that the quantity p, the radius of the circle of confusion of a point source seems to be a reasonable limiting distance between two extended sources. Then the resolution is given by

$$R_e = \frac{1}{p} = \frac{1}{2d}\sqrt{\frac{\varphi_e}{\varphi_o}}$$

(9)
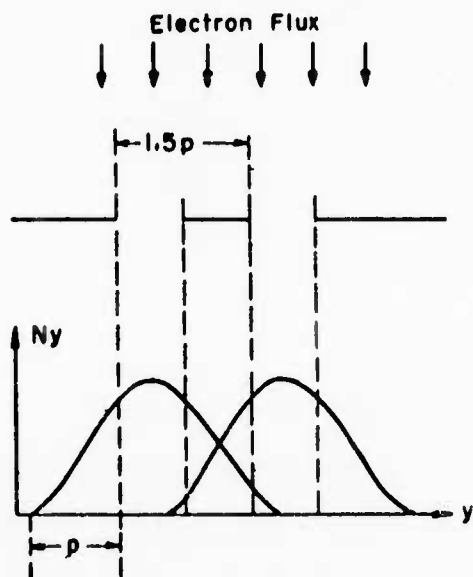
For a stage with d = 5 mm, φ_{end} = 3.2 KV and φ_o = 2 ev, the calculated resolution is R_e = 4 line pairs per mm. This is in agreement with experimental results.

1.2 FOCUSING WITH MAGNETIC FIELD

The use of an axial magnetic field in focusing the electrons which are released from each foil leads to a very much better image at the following electrode. The period of the spiral path of the electrons in the magnetic field, which determines the time of flight between the foils, does not depend on the initial velocity. One sees from

$$\frac{mv_{oy}^2}{r} = Be\,v_{oy}; \text{ and } v_{oy} = \frac{2\pi r}{T} \quad (10)$$

221

that the period

$$T = \frac{2\pi m}{eB}$$ (11)

In these equations e is the electron charge, m the electron mass, r the radius of the spiral path in the plane perpendicular to the magnetic field and B the magnetic flux density.

The distance travelled in the direction of the field is

$$x = \frac{at_f^2}{2} + v_{ox} t_f$$ (12)

The condition for focusing requires that the time of flight, t_f, be equal to an integral multiple, n, of the period.

$$t_f = nT$$ (13)

Substituting (11) and (12) in (13); letting $x = d$, $v_{ox} = o$, and solving for B, we have:

$$B = \frac{n\pi m}{e} \sqrt{\frac{2a}{d}} \quad \text{and since} \quad a = \frac{e\varphi_e}{dm}$$

$$B = \frac{n\pi}{d} \sqrt{\frac{2m}{e}} \sqrt{\varphi_e}$$ (14)

From (12) one sees that the condition of focusing is satisfied only for an initial velocity with one specific x-component which, in this case, we assume to be zero. A finite initial velocity , v_{ox}, will therefore cause the point of focus to be displaced by the amount, Δx. This displacement must, of course, be small compared with the interdynode distance d.

$$\Delta x = v_{ox} t_f = v_{ox} \sqrt{\frac{2d}{a}}$$ (15)

These faster electrons produce at the focal plane $v_{ox} = 0$, a circle of confusion, whose size one easily finds by help of the aperture angle β at the anode (Figure 4). We have

222

$$\frac{v_{end\ y}}{v_{end\ x}} = \tan\beta \tag{16}$$

where $\quad v_{end\ y} = v_{oy}; \ v_{end\ x} \approx v_{end}$ \hfill (17)

The aperture angle of the beam at the cathode is

$$\frac{v_{oy}}{v_{ox}} = \tan\alpha \tag{18}$$

The radius of the circle of confusion becomes

$$p = \Delta x, \ \tan\beta = \Delta x \cdot \frac{v_{end\ y}}{v_{end\ x}} = \Delta x \ \frac{v_{oy}}{v_{end}} \tag{19}$$

Since the secondaries start with cosine distribution, which means an average deflection angle of $45°$, we can write for the average components of the initial velocities:

$$\overline{v}_{ox} = \overline{v}_{oy} = \frac{\overline{v}_o}{\sqrt{2}} \tag{20}$$

So with (15) follows:
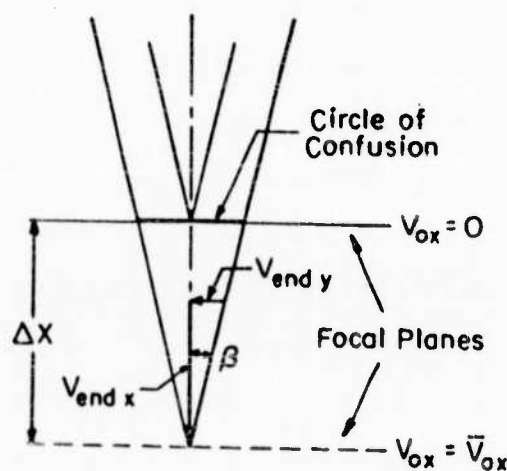
$$2p = 2\,\overline{v}_{ox} \ \sqrt{\frac{2d}{a}} \ \frac{\overline{v}_{oy}}{v_{end}}$$

and using (20)

$$2p = \frac{\overline{v}_o^{\,2}}{v_{end}} \ \sqrt{\frac{2d}{a}} = \frac{\overline{v}_o^{\,2}}{v_{end}} \ t_f \tag{21}$$

or

$$2p = \frac{2\overline{v}^2}{v^2_{end}} \ d = 2d \ \frac{\varphi_o}{\varphi_e}$$

where φ_o is the voltage corresponding to the average initial velocity $\overline{v}_o$.

Circle of Confusion

$V_{ox} = 0$

$V_{end\ y}$

Focal Planes

ΔX

β

$V_{end\ x}$

$V_{ox} = \overline{V}_{ox}$

Because p is the radius of the circle of confusion due to an average initial velocity, the resolution is defined as $R = \frac{1}{2p}$, leading to:

$$R_{\Delta v_o} = \frac{1}{2p} = \frac{1}{2d} \frac{\varphi_e}{\varphi_o} \tag{22}$$

where Δv_o in the subscript indicates the limit in resolution due to spread in initial energy of the electrons. This resolution compared with that obtained without magnetic field turns out to be (Eq. 22/Eq. 9)

$$R_{\Delta v_o} = R_e \sqrt{\frac{\varphi_e}{\varphi_o}} \tag{23}$$

With $\varphi_e = 3.2$ KV, $\varphi_o = 2$V, $d = 5$ mm, we find $R_{\Delta vo} = 160$ line pairs per mm, 40 times better than without employing a magnetic field (see page 221.)

In addition to the limitation of resolution due to the finite initial velocity of the electrons we also have to account for focal deviations due to inaccuracy in the quantities involved in the focal conditions; such as magnetic flux density, accelerating electric field and dynode distances.

1.3 Limitations in the Resolving Power due to Variations in Magnetic Field Strength

Variations in the amount of the magnetic flux density reduce resolution. In the first approximation changes in direction only cause image distortion. A variation in magnetic flux density changes the period of the electron movement in this field and displaces the focus before or behind the plane of the anode. Using the period, calculated in equation (11), the change in period can be expressed as:

$$\Delta T = -2\pi \frac{m}{e} \cdot \frac{1}{B^2} \cdot \Delta B \tag{24}$$

For the displacement we have:

$$\Delta x = v_{end} \cdot n \cdot \Delta T = \frac{-2\pi nm}{B^2 e} \, v_{end} \, \Delta B \tag{25}$$

224

where n indicates the number of revolutions in the path. With the end velocity
of the electrons fixed by the electric field strength, we find:

$$\Delta x = -\frac{2\pi n}{B^2} \sqrt{2m \frac{\varphi_e}{e}} \ \Delta B \tag{26}$$

To find out the diameter of the circle of confusion, we have to consider, as
pointed out before, the ratio of the increased x-component of velocity to the
y-component at the anode:

$$2p = 2\Delta x \ (1/2) \sqrt{\frac{\varphi_o}{\varphi_e}} = \frac{2\pi n}{B^2} \sqrt{\frac{2m}{e} \varphi_o} \Delta B \tag{27}$$

So we find for the resolving power

$$R_{\Delta B} = \frac{1}{2p} = \frac{B}{2\pi n} \sqrt{\frac{e}{2m \varphi_o}} \ \frac{B}{\Delta B} \tag{28}$$

1.4 Deviations in the Electric Field Strength

Variations in the electric field strength change the acceleration and by that
the time of flight of the electrons between the foils. One finds the dislocation
of the focus from:

$$t_f = \sqrt{\frac{2dm}{eE}} \text{ and therefore } \Delta t_f = \sqrt{\frac{2dm}{eE}} \ (1/2) \ \frac{\Delta E}{E} \tag{29}$$

leading to

$$\Delta x = v_{end} \ . \ \Delta t_f = -d \frac{\Delta E}{E} \tag{30}$$

The diameter of the circle of confusion is therefore:

$$2p = 2d \ (1/2) \sqrt{\frac{\varphi_o}{\varphi_e}} \ \frac{\Delta E}{E} \tag{31}$$

So the limit in resolution due to variations in electric field strength turns
out to be:

$$R_E = \frac{1}{d} \sqrt{\frac{\varphi_e}{\varphi_o}} \ \frac{E}{\Delta E} \tag{32}$$

225

1.5 Mechanical Deviations

Of further interest is the influence of uncertainties in the mechanical dimensions of the tube, particularly uncertainties in foil separations. We now have to consider not only that the displacement of the foil dislocates the focal plane relative to the path of the electrons, but also that there is a deviation in the path of the electrons themselves due to the change in electrical field strength. The latter condition arises because the voltages on the stages are fixed. One finds for the deviation in time of flight from this equation

$$t_f = d \cdot \sqrt{\frac{2m}{e\varphi_e}} \tag{33}$$

$$t_f = \sqrt{\frac{2m}{e\varphi_e}} \cdot \Delta d \tag{34}$$

and from

$$2p = 2\Delta x \cdot (1/2)\sqrt{\frac{\varphi_c}{\varphi_e}} \; ; \; \Delta x = v_{end} \cdot \Delta t = \Delta t \sqrt{\frac{2e \; \varphi_e}{m}}$$

$$2p = 2 \, d \sqrt{\frac{\varphi_c}{\varphi_e}} \tag{35}$$

or

$$R_{\Delta d} = \frac{1}{2 \, \Delta d} \sqrt{\frac{\varphi_e}{\varphi_c}} \tag{36}$$

In this connection it is of interest to know the mechanical deformation of the foils due to the electric field forces. Earlier measurements by E. J. Sternglass on unsupported Al_2O_3 films showed a maximum deformation (displacement at the center of the film) of about 0.6 mm at $E = 800$ V/mm. The thickness was several hundred angstroms. In the image tube the foils are pulled by the electrical field from both sides. Therefore, only the difference in field strength at the foil causes deformation. For an average foil separation of 5 mm and an initial deformation of

226

TABLE 6

Theoretical Overall Resolution

of a Four-Stage Tube

B Gauss	Cathode Stage	Multiplier Stage	Phosphor Stage	R overall line pairs/mm
418	52	52	53	23

It must be mentioned once more that these results give only an estimation of what one can expect at the best. Besides ignoring higher order errors in the image formation, we did not pay attention to image distortion due to non-uniformity of the electric field between the electrodes. This factor becomes considerable if the separations are large. An arrangement must be provided to avoid serious distortion by this effect. To first order the non-uniformity of the electric field does not affect the resolution but gives rise only to image distortion. For the application in nuclear photography this cannot be allowed because it changes the relative curvature of the image to the original path. This could lead to wrong conclusions concerning the energy and momentum transfer of the particle in the stopping material. Nevertheless the above consideration will give a rough estimation of the limits in resolution which could approximately be achieved with the resolution limitations in the secondary-electron image amplifier.

APPENDIX III

CONTRAST IN THE TRANSMISSION SECONDARY EMISSION

IMAGE INTENSIFIER

The following work makes certain assumptions and considers only certain factors while ignoring others which are believed to be of second order.

If all electrons at each of the stages of the TSEM were converted to low energy secondaries, there would be no question that the contrast would be very good. It is known, however, that there is a fraction of primary electrons which penetrate the dynodes emerging on the exit side with relatively high energies. (These electrons have been defined as having more than 50 volts energy in all measurements.) Such electrons cause a decrease in contrast due to the diffiuclty of focusing them. Unfocused electrons cause a "halo" around every signal element.

To estimate the influence of penetrating primaries on the contrast of an output image of the TSEM we consider only those electrons which have penetrated one dynode stage (Figure 77). The number of electrons in the halo produced by the penetrating electrons relative to the number of electrons in the signal spot is

$$\frac{N_{halo}}{N_s} = (n-1) \ \frac{\eta_1 \delta_2}{\delta_1^2} + \frac{\eta_1}{\delta_1} \tag{1}$$

where: n = number of dynode stages

η_1 = number of penetrating electrons per incoming electron

δ_1 = secondary emission ratio for signal electrons

δ_2 = secondary emission ratic for electrons which have penetrated the preceding dynode film and arrive with an energy larger than that of the signal electrons.

The relative number of electrons at the output produced by electrons which have penetrated two succeeding stages is

232

Figure 77 — Schematic of electron trajectories in TSEM.

DWG. 1924588

Dia. of Signal Spot (ϕ)

Dia. of Halo (D)
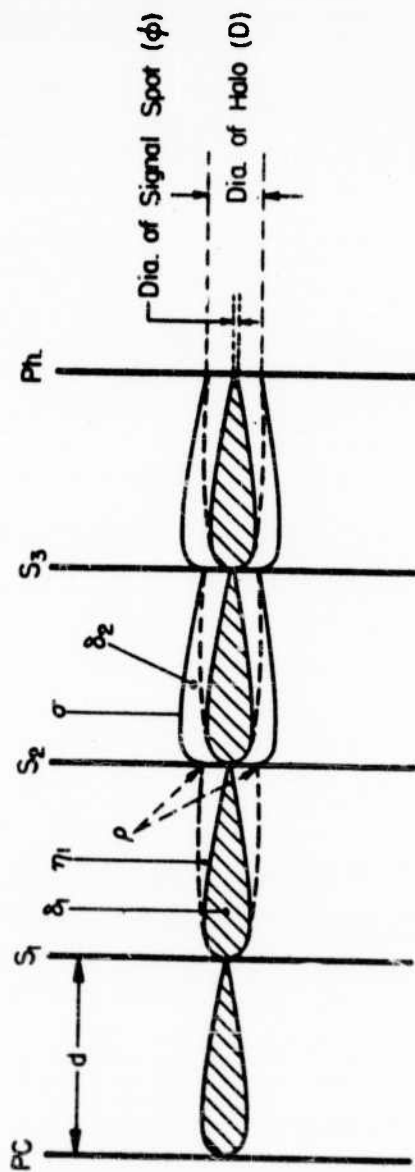
ρ = Diameter of circle of confusion formed by primaries penetrating S_1 and incident on S_2.

σ = Envelope of paths of secondaries formed in S_2 by penetrating primaries incident on S_2.

δ_1 = Secondary emission ratio of signal electrons.

δ_2 = Average secondary emission ratio of penetrating primaries

η_1 = Fraction penetrating primaries

PC = Photocathode

S_1, S_2, S_3 = Dynodes

Ph = Phosphor

d = Interdynode distance

$$\frac{N_{halo(2)}}{N_s} = (n - 2) \quad \frac{\eta_1 \eta_2 \delta_3}{\delta_1^3} + \frac{\eta_1 \eta_2}{\delta_1^2} \tag{2}$$

η_2 = penetration ratio of electrons which already have penetrated one dynode.

δ_3 = secondary emission yield of the above electrons at the third dynode.

Since η_1 η_2, ... are numbers smaller than one and δ_1, δ_2, ... are decreasing numbers with increasing subscripts, the expressions for "higher order" penetration processes are usually small compared to the first order expression (1) and may be neglected in this estimate.

To calculate the contrast of the signal spot to the immediate surround, the area of the spot and the halo must be considered. The area of the signal spot is roughly $\frac{1}{R^2}$ where R is the resolution of the image tube in line pairs per unit length.

The radius of the halo depends on the ratio of flight time of the penetrating electrons to the flight time of the "signal" electrons. This ratio gives the fractional part of the circumference of the circle in the plane perpendicular to the tube axis the fast electrons have completed. The angle these fast electrons have completed is:

$$\frac{t_f}{t_{se}} = \frac{(d\ B)(V_{ox})}{V} \left(\sqrt{\frac{2e\ V}{m\ V_{ox}^2} + 1} - 1 \right) \tag{3}$$

234

1/2 mm the difference turns out to be about 1/5 of the absolute field strength. With an absolute field strength of 600 V/mm (3 KV on a distance of 5 mm) the largest additional deformation is less than 1 mm. The direction of this additional deformation of the thin foils leads to a small intensification of errors caused by deviations in the foil separations.

To review all of the preceding influences on the resolution, we rewrite the final expressions of each effect:

Resolution per stage due to

(a) spread in initial velocity: $R_{\Delta v_c} = \dfrac{1}{2\,d}\,\dfrac{\varphi_e}{\varphi_e}$

$$(22)$$

(b) variation in magnetic flux density:

$$R_{\Delta B} = \frac{B}{2\pi n}\ \sqrt{\frac{e}{2m\,\varphi_o}}\ \frac{B}{\Delta B}$$

$$(28)$$

(c) variation in electric field strength:

$$R_{\Delta E} = \frac{1}{d}\sqrt{\frac{\varphi_e}{\varphi_o}}\ \frac{E}{\Delta E}$$

$$(32)$$

(d) variation in distances between parallel electrodes:

$$R_{\Delta d} = \frac{1}{2\,\Delta d}\ \sqrt{\frac{\varphi_e}{\varphi_o}}$$

$$(36)$$

Assuming a gaussian distribution in electron current density across the circle of confusion and using the independance of all of the above factors, one can calculate the total resolving power of one stage in the following equation:

$$\frac{1}{R_{stage}} = \sqrt{\frac{1}{R_{\Delta v_c}^2} + \frac{1}{R_{\Delta B}^2} + \frac{1}{R_{\Delta E}^2} + \frac{1}{R_{\Delta d}^2}}$$

$$(22)$$

227

In the following tables we give some examples of quantitative values of the different contributions due to spread in initial velocity, variation in electrical field strength, magnetic flux density and electrode distances.

TABLE 1
($\varphi_e = 3600$ volts; $\varphi_o = 2$ volts)

d(mm)	5	10	15	30	
$R_{\Delta v_o} = \dfrac{900}{d}$	180	90	60	30	line pairs/mm
$R_{\Delta E} = \dfrac{4250}{d}$ for $\Delta E/E = 0.01$	850	425	283	142	line pairs/mm
$R_{\Delta d} = \dfrac{21.25}{\Delta d}$ $\Delta d = 0.1$ mm	213	213	213	213	line pairs/mm

TABLE 2
($\varphi_e = 10{,}000$ volts; $\varphi_o = 2$ volts)

d(mm)	5	10	15	30	
$R_{\Delta v_c} = \dfrac{2500}{d}$	500	250	167	84	Line pairs/mm
$R_{\Delta E} = \dfrac{7000}{d}$ for $\Delta E/E = 0.01$	1400	700	467	234	line pairs/mm
$R_{\Delta d} = \dfrac{35}{\Delta d}$ $d = 0.1$ mm	350	350	350	350	line pairs/mm

TABLE 3

B	1255	628	419	209	Gauss

$$\Delta B = \frac{3.34 \times 10^{-3} B}{n} \cdot \frac{B}{\Delta B}$$

$n = 1$ $\quad \frac{\Delta B}{B} = 0.02$	210	105	70	35	
$\frac{\Delta B}{B} = 0.01$	420	210	140	70	
$\frac{\Delta B}{B} = 0.005$	840	420	280	140	
$n = 2$	105	52	35	17	line pairs/mm
$n = 3$	70	35	23	11	
$\frac{\Delta B}{B} = 0.02 \quad n = 4$	53	26	17	8	
$n = 6$	35	18	11	6	

Table 4 shows the magnetic flux density as a function of electrode separation and number of nodes in the electron path for a stage voltage of 3.6 KV (Eq. 14).

TABLE 4

d(mm)	5	10	15	30	
$n = 1$ B	1255	628	419	209	gauss
$n = 2$	2510	1255	838	418	gauss

It turns out that the contribution due to uncertainty in electric field strength is usually negligible. The contribution by the uncertainty in electrode distance can be kept fairly low. The main influence comes in case of large electrode distance from the inaccuracy in magnetic field strength and from the spread in initial velocity. It is possible to compensate changes in magnetic field strength along the tube axis by adjusting the stage voltage.

(This voltage can be changed by 10% without effecting the yield considerably). Also
by this means one may compensate for differences in the electrode distances from
stage to stage. However, radial variation in field strength as well as non-paral-
lel placement of the dynodes give rise to distortions for which there is no com-
pensation. The maximum value of radial variation in magnetic field and electrode
separation, therefore, must be less than the tabulated values of both quantities.

Table 5 gives the total resolution, calculated with equation (22), for one
stage under different conditions as they occur in different parts of the tube; a
typical multiplier stage, the first multiplier stage after the photocathode, and
the last stage forming the image on the phosphor. From these figures the overall
resolution of a four-stage tube is calculated by a formula of type (22) and the
results are given in Table 6.

TABLE 5

Total Resolution Per Stage

	d	Δd	v_{end}	φ_0	$\frac{\Delta E}{E}$	B	$\frac{\Delta B}{B}$	n	Resolution Line pairs/mm
	mm	mm	KV	Volts		Gauss			
Typical	5	0.1	3.6	2	0.01	1255	0.005	1	133
Multiplier	10	.1	3.6	2	.01	628	0.01	1	76
stage or	15	.1	3.6	2	.01	418	0.01	1	52
Cathode	30	.1	3.6	2	.01	209	0.02	1	22
Stage									
	17.5	.2	10	2	0.01	1255	0.02	2	75
Phosphor						628		1	75
Stage	26.5					418		1	53
	53					209		1	28

230

1. The penetration ratio η , should be as small as possible.

2. The yield for penetrating electrons δ_2 should be as small as possible compared with the yield δ_1.

3. The resolution of the system should be as high as possible.

4. The ($\propto \sin \varphi$) of the penetrating electrons should be maximized.

APPENDIX IV

RESOLUTION LIMITATIONS IN THE FRONT SURFACE
SECONDARY EMISSION SCREEN AMPLIFIER

Shown in Fig 78 is a sketch of the image section structure under consideration. Electrons emitted by the photocathode PC are accelerated toward the first multiplier screen D and focused by the axial magnetic field. Secondary electrons generated at the front surface of the mesh bars are emitted toward the photocathode into a retarding electric field region, reverse direction and are accelerated through the open areas of the screen to the succeeding dynode. The spacings between dynode stages and between the final dynode and target T are relatively small. Because of the compactness of the multiplier structure, the presence of the axial magnetic field should have little effect on the secondary electron trajectories between dynode stages and is therefore neglected. The secondary electron trajectories are parabolic during the time that the electrons leave the plane of the dynode and return to the same dynode plane. After they have returned to the originating plane, they are accelerated to the succeeding dynode in a parabolic path. In this analysis, uniform plane parallel electric fields are assumed to exist in all stages and the effects of field penetration in open areas of the screen are neglected. Mesh bars are also assumed to have rectangular cross-sections with mesh bar widths equal to the widths of open areas.

The maximum height to which the secondary electrons will rise in the retarding field is:

$$Y_{m} = \frac{V_{o} \cos^2 \theta}{E} \quad (mm) \tag{1}$$

Where θ is the angle that the initial velocity makes with respect to the retarding potential field gradient E in volts per mm and Vo is the initial emission
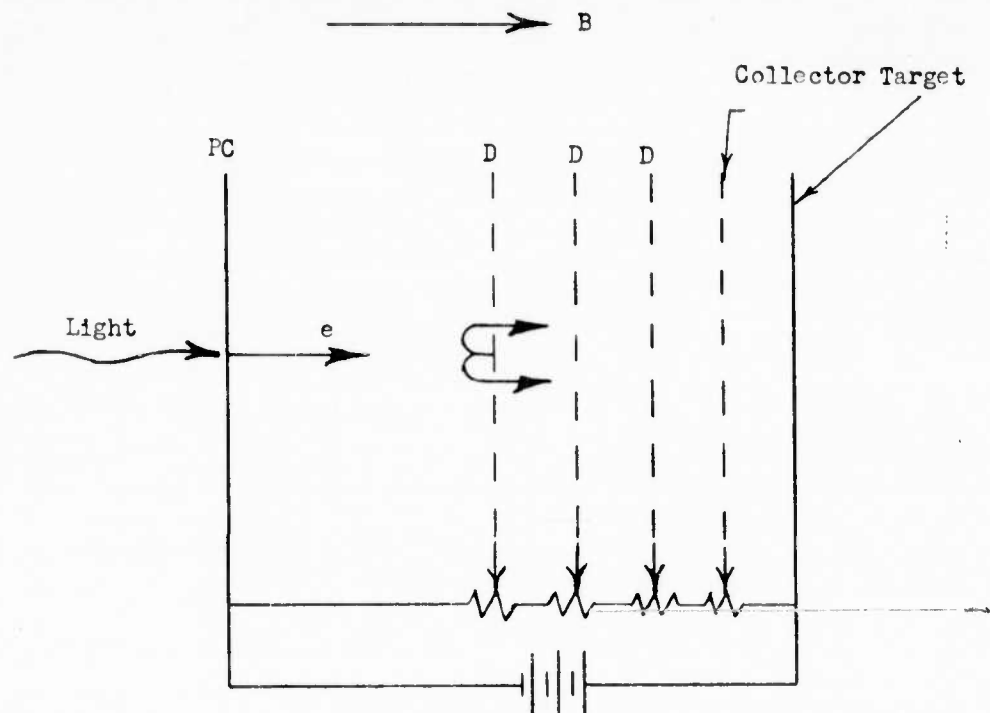
Figure 78.   Front Surface Secondary Emission Amplifier

241

velocity in volts. In the calculations, an average initial velocity of 2 volts is used.

The horizontal displacement corresponding to this height is:

$$X_m = \frac{2 \text{ Vo Sin } \theta \text{ Cos} \theta}{E} \quad (mm) \tag{2}$$

The radius of the circle of confusion corresponding to this displacement is 2 X m = p. We now define limiting resolution as:

$$R_1 = \frac{1}{2p} \quad \left(\frac{\text{line pairs}}{mm}\right) \tag{3}$$

After the secondary electrons have returned to the plane from which they originated, additional radial spread occurs between dynode stages and in the final dynode to target stage. This inter-dynode stage spread is approximately defined by:

$$X = 2d \sqrt{\frac{V_0}{V}} \quad \text{Sin } \propto \quad (mm) \tag{4}$$

Where V is the inter-stage potential difference in volts, d is the stage spacing in mm and $\propto$ is the angle which the initial velocity makes with respect to the normal to the plane of the dynode. In deriving Eq (4), the assumption was made that the initial emission velocity of secondary electrons is negligibly small compared to their average velocity between stages.

The resulting limiting resolution of the secondary electron image is obtained by combining the lateral spreads and is expressed by:

$$R_2 = \frac{1}{2 (p + X)} \quad \left(\frac{\text{line pairs}}{mm}\right) \tag{5}$$

Fig 79 shows a sketch of the parameters involved.

242

where

t_f and t_{se} = flight times of penetrating and secondary electrons respectively

B = magnetic flux density

V = stage voltage

$\mathbf{v}_{ox}$ = velocity component of the electrons in the direction of the axis of penetrating electrons at the penetrated film

d = inter-stage distance

e and m are the electronic charge and mass

It is seen that this ratio depends on v_{ox}; that is, the mean energy and the scattering angle of the penetrating electrons. For a scattering angle in the order of 20-30° and an average energy of 0.6 Ep after penetration (Ep is primary energy) the completed angle is such that the radius of the resulting circle of confusion, produced by the primaries, is in the same order of magnitude as the radius (r) of the circle that the fast electrons travel in the plane perpendicular to the tube axis. The area of the circle of confusion is approximated by

$$\pi r^2 = \pi \left(V_{oy} \; \frac{m}{eB} \right)^2 \tag{4}$$

or with $v_{oy} = v_o \sin \varphi$ and $v_o^2 = \propto \frac{2e}{m} V_{st}$, where V_{st} is the stage voltage and $\propto$ the average energy of the penetrating electrons relative to the primary energy:

$$\pi r^2 = \pi \propto \frac{2m}{e} \; \sin^2 \varphi \; \frac{V_{st}}{B^2} \tag{5}$$

Introducing the focal condition which establishes the relation between stage voltage and magnetic field

$$B^2 = \frac{k^2 \pi^2}{d^2} \left(\frac{2m}{e}\right) V_{st} \qquad (6)$$

where k is the number of revolutions per stage, one finds

$$F = \pi r^2 = \frac{\propto d^2 \sin^2 \varphi}{k^2 \pi} \qquad (7)$$

Since we assumed for the signal spot size $f = \frac{1}{R^2}$, where R is the resolution in line pairs per mm , we might replace π by 4 and find for the ratio of the signal spot area to area of the halo.

$$\frac{f}{F} = \frac{4 k^2}{R^2 d^2 \propto \sin^2 \varphi} = \frac{\text{area of signal}}{\text{area of halo}} \qquad (8)$$

Because the stage distance d and the number of revolutions k is a constant for a given tube we write

$$\frac{f}{F} = \frac{S}{R^2 \propto \sin^2 \varphi} \qquad \text{where} \quad S = \frac{4k^2}{d^2} \qquad (9)$$

The ratio of the brightness in the signal spot to the brightness in the surrounding halo for a single point is

$$\left(\frac{B_H}{B_S}\right)_{\text{point}} = \frac{N_{halo}}{N_S} \cdot \frac{f}{F} = \left[(n-1)\frac{\eta_1 \delta_2}{\delta_1^2} + \frac{\eta_1}{\delta_1}\right] \frac{S}{R^2 \propto \sin^2 \varphi} \qquad (10)$$

236

With the help of Eq (10) the contrast c of the signal spot to surrounding neighborhood can be found

$$c = \frac{B_S - B_H}{B_S} = 1 - \frac{B_H}{B_S} \tag{11}$$

Substituting in Eq (10) the values for a 4 stage tube:

$$n = 4; \quad \eta_1 = 0.2; \quad \delta_2 = \delta_1 = 5 \quad S \approx 0.08 \frac{1}{mm^2};$$

$$\alpha = 0.6; \quad \sin^2 \varphi = 0.2; \quad R = 10 \quad lp/mm$$

we find

$$\frac{B_H}{B_S} \approx 10^{-3} \qquad \text{or the contrast is practically one for a reproduced}$$

single spot.

Estimating the contrast in the neighborhood of a single line, one must consider the fact that the brightness of the overlapping halos of neighboring points adds up and thus the contrast decreases. The number of "halo disks", P, which add up in the immediate neighborhood of a single line is given by the ratio of halo diameter, 2r, to signal spot diameter, $\frac{1}{R}$.

$$P = \frac{2r}{1/R} , \quad \text{or with Eq (7)}$$

$$P = \frac{R \, d \, 2 \, \sin \varphi}{\pi} \sqrt{\frac{\alpha}{K^2}} \tag{12}$$

To find the brightness ratio for a line, Eq (10) must be multiplied by P:

$$\left(\frac{B_H}{B_S}\right)_{\text{line}} = \left[n-1 \quad \frac{\eta_1 \delta_2}{\delta_1^2} + \frac{\eta_1}{\delta_1} \right] \quad \frac{4}{\pi R \sin \varphi} \sqrt{\frac{S}{\propto}} \quad (13)$$

Using the above stated values for a four stage tube, the ratio is

$$\left(\frac{B_H}{B_S}\right)_{\text{line}} \approx 2 \times 10^{-2}$$

The ratio for two parallel lines which can just be resolved will be about twice as much as that given in Eq (13). The brightness of halo will continue to increase at a rate less proportionally with the increase in the number of lines added in the immediate vicinity of a given line. The assumption that the brightness ratio will not be more than about 10^{-1} for a set of just resolvable parallel lines should not be too far from the actual situation. The contrast for two crossed sets of just resolvable lines then is not much less than 0.8.

It should be mentioned once more, however, that these results are only estimates, since we considered only the most important group of penetrating electrons, namely, those which have penetrated a film once. Those electrons which penetrated more dynodes will give rise to a decrease in the above contrast figures. Also, electrons back scattered from a film will introduce additional background brightness. Because of this complexity it is difficult to account for the effects of all these "background" electrons in a reliable way. An experiment must give the answer.

Nevertheless the equations developed here show the important factors involved in the contrast of an image. Particularly Eq (13) shows that for good contrast:
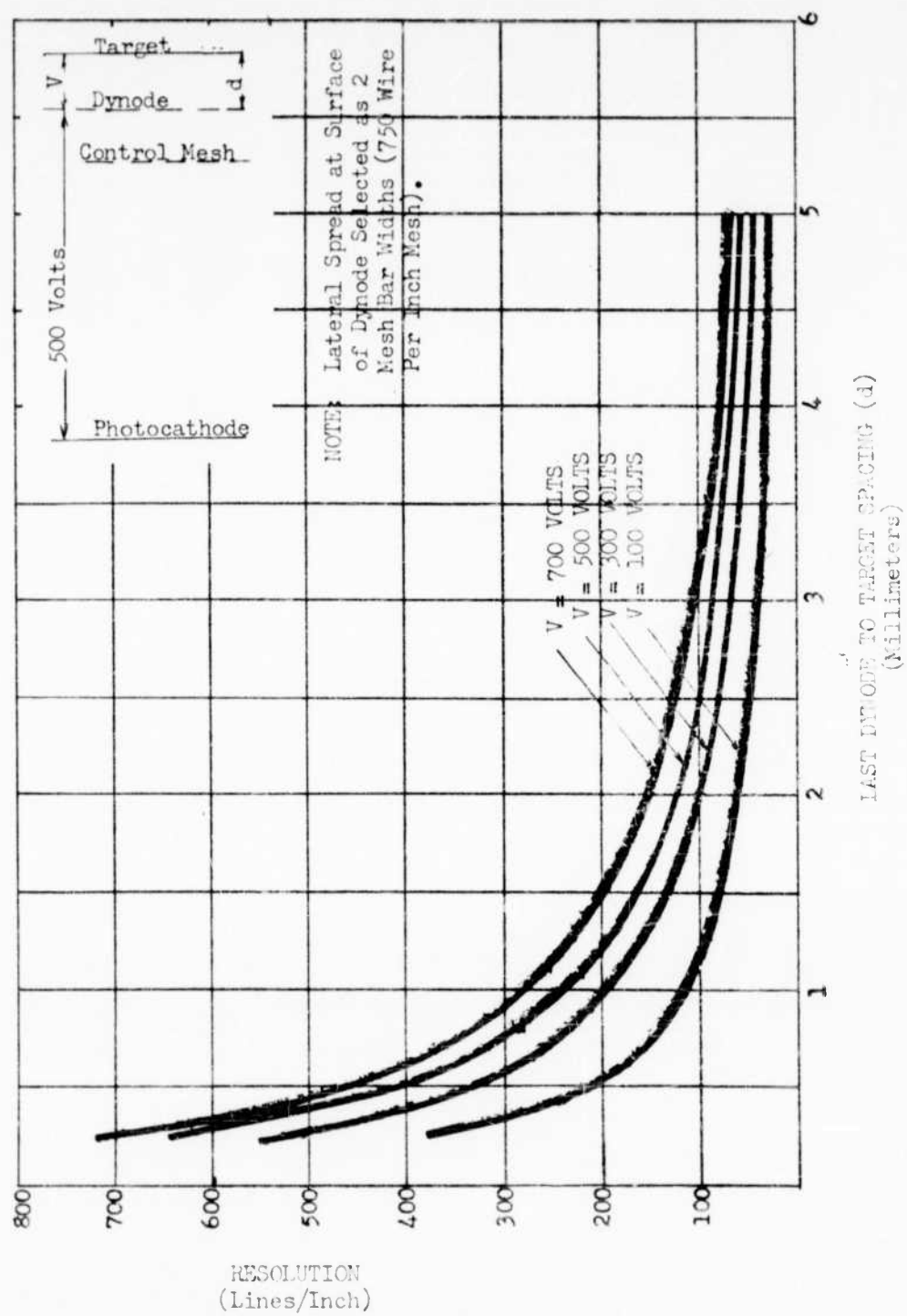
238

Figure 82. Single Stage Resolution (With Field Control Mesh)
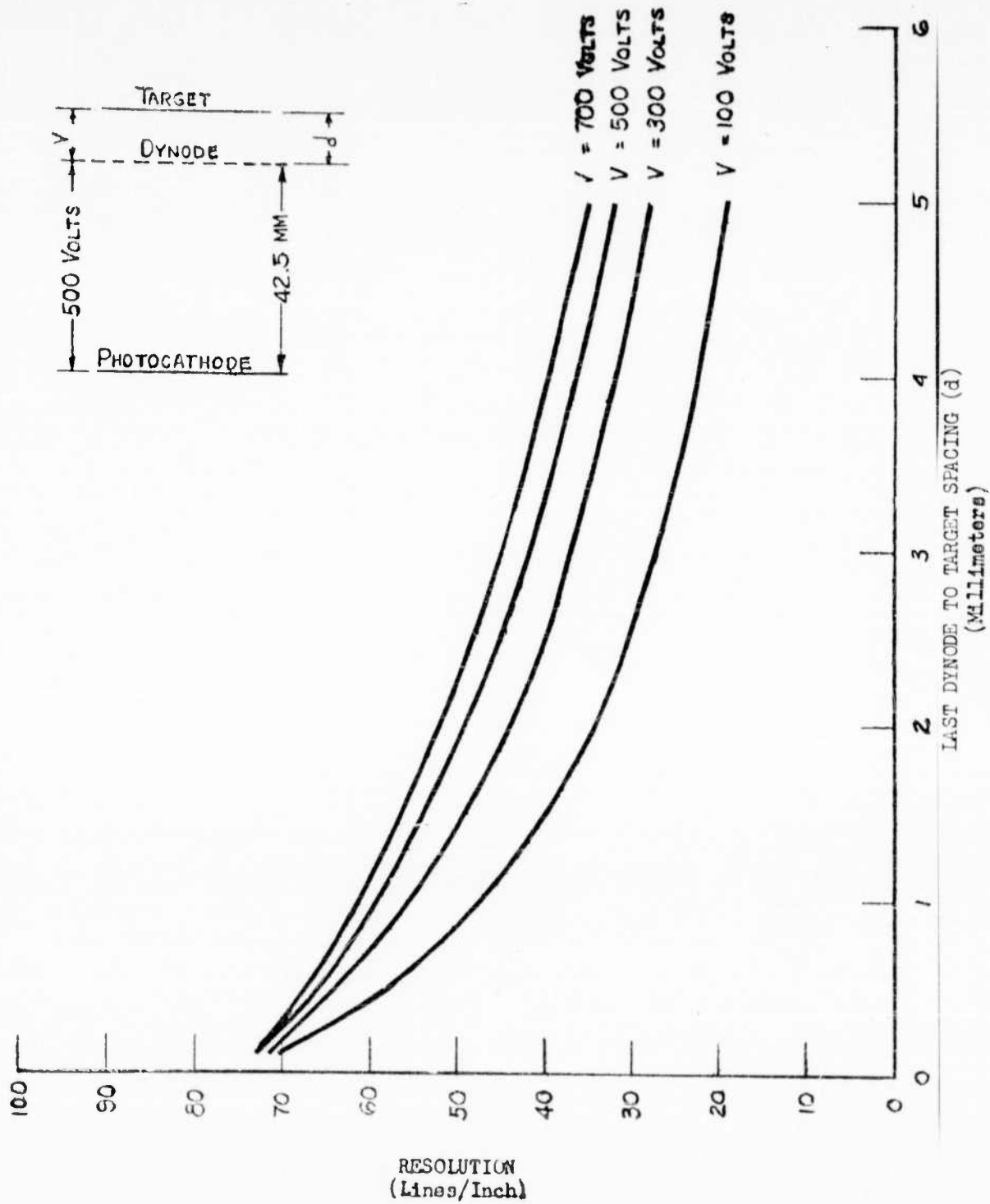
247

Figure 83. Single Stage Resolution (Without Field Control Mesh)

263

Let us assume a fine-mesh screen dynode with a 750 wire per inch structure. Referring to Fig 3, we can adjust the retarding field in front of the first dynode to limit the lateral excursions of the secondaries so that electrons emitted at any mesh bar at an angle θ equal to 45° will return through the immediate adjacent open areas of the screen. For the 750 wire per inch structure selected, this lateral spread is approximately .034 mm with a corresponding retarding field of 240 volts per mm. Combining the assumed lateral spread of two mesh bars widths in the retarding field region with the inter-dynode stage spreads shown in Fig 81, the resulting resolution of the image formed at the target of a single stage tube is shown in Fig 82, as computed with Eq (5). Fig 83 shows the calculated resulting resolution of a single stage tube when no field control mesh is used. Comparing these two curves, the need for a field control mesh preceding the first dynode becomes evident. Also apparent is the necessity for very close inter-dynode stage spacing for electrostatic focusing of the secondary electrons.

Thus far it has been shown that a retarding field control mesh in front of the first dynode serves the purpose of providing a means of reducing lateral spread. Let us now consider secondary electron trajectories at subsequent dynode stages. As was shown from Eq (3), to limit the lateral excursion of secondary electrons emitted at the mesh bars of a 750 wire per inch screen to the immediate adjacent open areas requires an electric field intensity of approximately 240 volts per mm. If the inter-dynode stage spacing was increased to the extent where this field condition existed while maintaining a reasonable dynode primary voltage, the lateral spread of secondaries would impose a serious limitation in resolution. It has also been demonstrated that very close dynode spacings result in low electron gain, due to the high retarding field gradients in front of the dynodes preventing the escape of secondary electrons from the dynode surfaces through the open areas of the screen. To maintain the close inter-dynode stage spacings required for good

249

resolution and yet establish the low field gradient in front of the emitting dynode in order to obtain high electron gain, a field free region is established in the near vicinity of the dynode surface. This is accomplished by locating a high transmission screen in front of and very close to the dynode surfaces subsequent to the first dynode and operating each screen at the corresponding dynode potential. This results in an increase in lateral spread at the surface of the dynodes beyond the width of the mesh bar, permitting the transmission of secondary electrons through adjacent open areas of the screen, thereby producing an increase in gain. Using this technique, electron gains as high as 6 were obtained. It is clear that the spacing between this field control mesh and the surface of the dynode becomes an important factor in the determination of the resolution capability of the dynode stage.

Shown in Table I are the overall system resolutions computed from Eq (5). The dynode in this theoretical design consists of a fine-mesh screen with a structure of 750 wires per inch. Where a field control mesh is employed, the initial lateral spread of the secondary electrons in the retarding field region is assumed to extend only two mesh bar widths, where the angle of emission is 45° with respect to the normal to the mesh bar. As described previously, this lateral spread is determined by the field control mesh located in front of each dynode. The lateral spreads occurring in the inter-dynode stages and in the final dynode to target stage are computed for various assumed spacings.

Table II shows the computed overall system resolutions with stage spacings approximating those used in constructed tubes. With the exception of the increased stage spacings, the assumed conditions are as described for Table I. It will be observed that this design gives a marked reduction in overall resolution compared to the close-spaced tube in Table I.
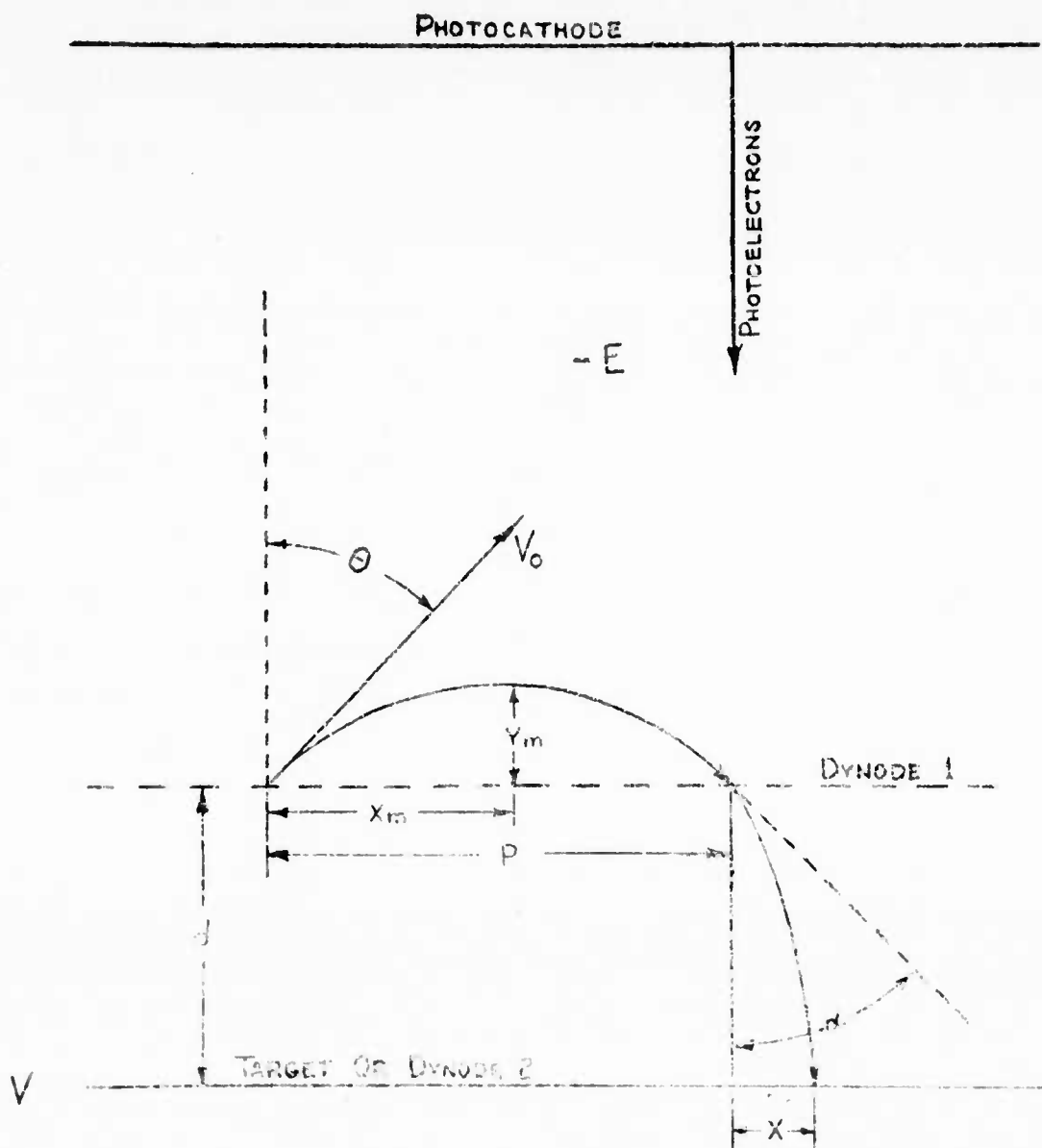
Figure 79. Secondary Electron Trajectory

243

Referring to Eq (2), it is seen that the initial lateral spread of secondary electrons emitted from the front surface of the first dynode is inversely proportional to the retarding electric field in front of the dynode. Using a typical operating voltage of 500 volts between the photocathode and first dynode, with a stage spacing of 42.5 mm, the resulting diameter of the circle of confusion is 0.68 mm. This value is computed for an emission angle θ of 45° corresponding to a condition of maximum lateral spread at the originating surface. From Eq.(3) we then obtain a limiting resolution of 1.5 line pairs per mm. Two methods could be used to reduce this lateral spread of secondary electrons. One method would be to increase the retarding field in front of the first dynode by increasing the photocathode to dynode voltage. However, the required large increase in voltage would result in a decrease in the secondary emission yield for the materials investigated. The second method, which we have tried experimentally, involves the insertion of a field control mesh located in front of and close to the first dynode. A high retarding field can be established with the application of a relatively low potential on the control mesh, resulting in a reduction in lateral spread at the surface of the dynode. Fig 80 shows graphically the lateral spread at the surface of the first dynode as a function of retarding field intensities computed with Eq (2).

The inter-dynode stage lateral spread, however, cannot be ignored. In fact, the lateral spread between dynodes can be the limiting factor in determining resolution. The lateral spread between dynodes as a function of stage spacing and accelerating voltage is plotted in Fig 81 as computed with Eq (4). The angle $\propto$ with which the secondaries enter the accelerating field, is taken as 45°. This angle does not necessarily give the maximum lateral excursion, but is selected so as to correspond with the angle of emission of the secondaries into the retarding field which was chosen to give maximum spread at the plane of the dynode.
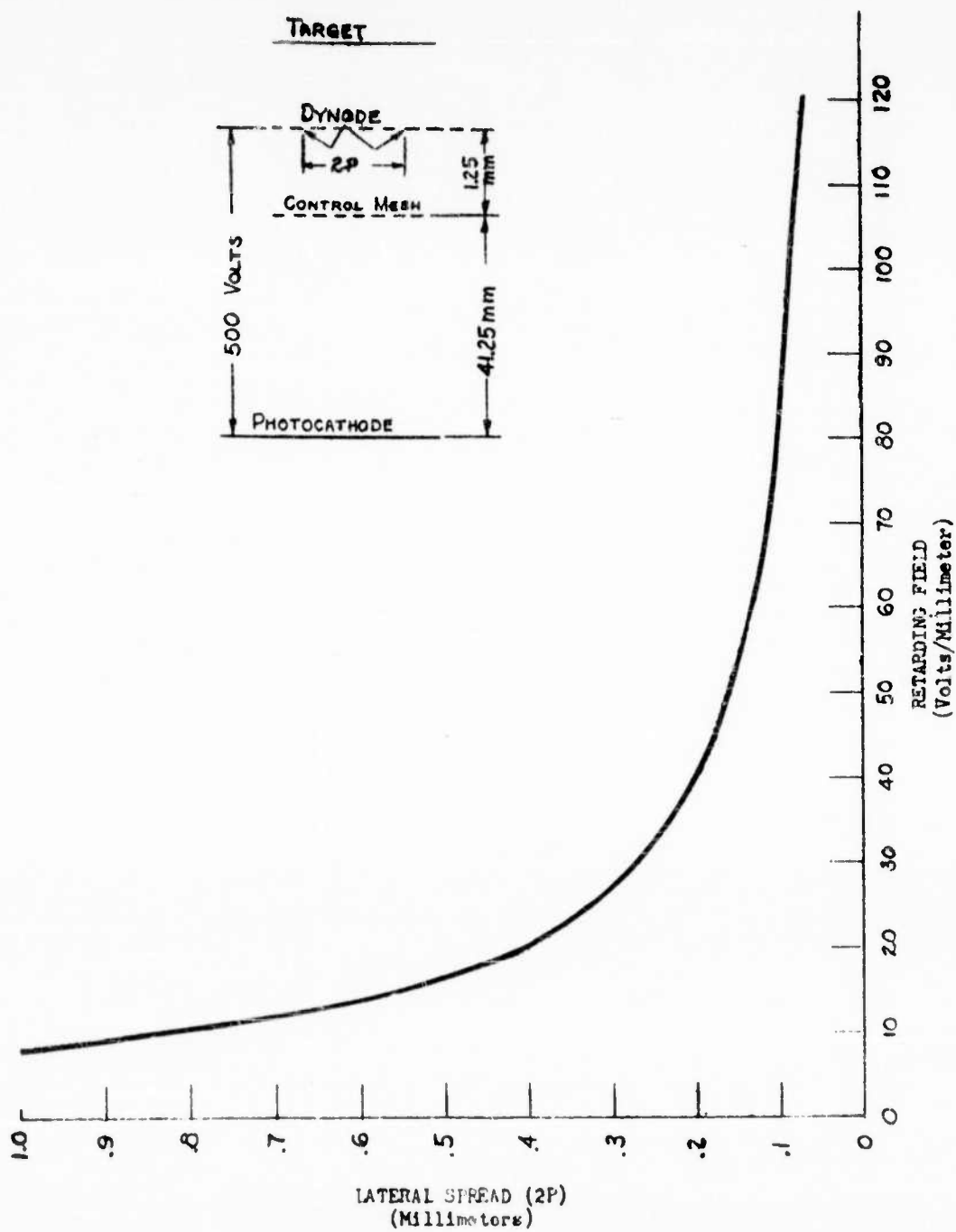
244

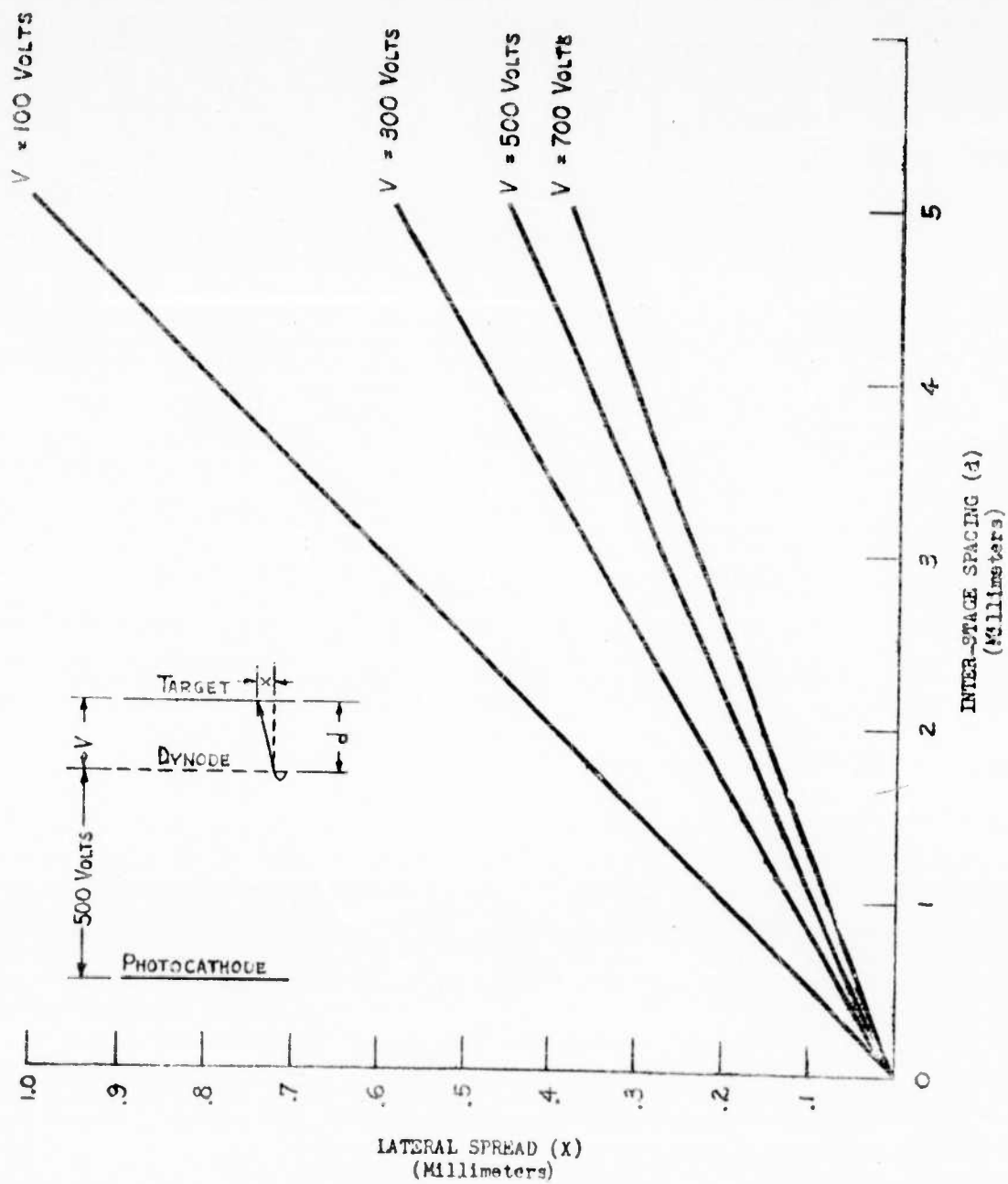Figure 80. Lateral Spread of Secondary Electrons at First Dynode as a Function of Retarding Field

Figure 81. Lateral Spread of Secondary Electrons Between
Dynode Stages

REFERENCES

1. "Noise Limitation to Resolving Power in Signal Generating Image Pickup Tubes"- Coltman & Anderson, Westinghouse Research Report 8-1501-R1.

2. "Interpretation of Secondary Electron Emission from Homogeneous Solids," E. J. Sternglass, Phys. Rev. 76, 189 (A) (1949).

3. "Secondary Electron Emission and Atomic Shell Structure," E. J. Sternglass, Phys. Rev. 80, 925 (L) (1950).

4. "Theory of Secondary Electron Emission under Electron Bombardment," E. J. Sternglass, Phys. Rev. (In Publication); See Also summary in Handbuch d. Physik, Vol. 21, 323 (1956) and Proc. 13th Ann. Electronics Conf., M.I.T. (March 1953) p. 55.

5. "Energy Expenditure per Ion Pair in Solids," E. J. Sternglass, Phys. Rev. 95, 609 (A) (1954), Bull. Am. Phys. Soc. 29, No. 4, 21, (1953).

6. "Theory of Secondary Electron Emission by High Speed Ions," E. J. Sternglass, Report of 15th Ann. Electronics Conf., M.I.T., P. 88-94 (1955), Phys. Rev. 108, 1, (1957).

7. "Measurement of Low-Energy Electron Absorption in Metals and Insulators," M. M. Wachtel and E. J. Sternglass, Phys. Rev. 99, 646 (A) (1955).

8. "Back-Scattering of Kilo-Volt Electrons," E. J. Sternglass, Phys. Rev. 95, 345-358 (1954).

9. "Back-Scattering of 5 to 20 kev Electrons from Metals and Insulators," J. E. Holiday and E. J. Sternglass; Report of 15th Ann. Electronics Conf., M.I.T., P. 81-88 (1955), J. Appl. Phys. 28, 1189 (1957).

10. "Scattering of Electrons on Thin Films with Energies below 10 keV," H. Kanter, Westinghouse Scientific Paper 6-41003-2-P4, Bull. Am. Phys. Soc. II, 4, 420 (1959).

11. "Relation Between Electron Energy Distribution and Secondary Emission," H. Kanter, Bull. Am. Phys. Soc. II, 5, 69 (1960).

12. "High Speed Electron Multiplication by Transmission Secondary Electron Emission," Rev. Sc. Instr. 26, 1202 (1955).

13. "Transmission Secondary Electron Multiplication for High Resolution Counting and Imaging," M. M. Wachtel and E. J. Sternglass, Phys. Rev. 100, 1238 (A) (1955).

14. "Transmission Secondary Electron Multiplication for High Speed Pulse Counting," E. J. Sternglass and M. M. Wachtel, Trans. I.R.E., Prof. Group. Nucl. Studies, Vol. NS-3, No. 4, 29, (1956).

15. "High Speed Electron Multiplication by Transmission Secondary Electron Emission," E. J. Sternglass, Rev. Sc. Instr. 26, 1202, (1955).

16. "Feasibility of Transmission Secondary Emission for Image Intensification," M. M. Wachtel and E. J. Sternglass, Bull. Am. Phys. Soc. 1, 38, (1956).

17. "Proceedings of the Second Symposium on Advances in Fast-Pulse Techniques for Nuclear Counting," A. E. Anderson, held at the Ernest O. Lawrence Radiation Laboratory, Berkeley, California, February 12 and 13, 1959, pp. 8-12.

18. "Recent Developments in Multistage Image Intensifiers Using Transmission Secondary Emission," by M. M. Wachtel, D. Doughty, and A. E. Anderson, in book Advances in Electronics, Vol. 12, New York, Academic Press (To be published).

19. "Image Intensification by Transmission Secondary Electron Emission," M. M. Wachtel, D. D. Doughty, G. Goetze, A. E. Anderson and E. J. Sternglass, Rev. of Sc. Instr. (In publication).

20. "Self Supported Transmission Secondary Emission Film Studies," M. M. Wachtel and A. E. Anderson, Westinghouse Research Report 6-94715-1-R1, Oct. 1957 to July 1958. (Final report, Dept. of Terestrial Magnetism, Carnegie Institution of Washington).

21. "Image Intensifier System", M. M. Wachtel, Westinghouse Research Report 415FD288-R1, May 21, 1959. (Final Report for Engineer Research and Development

Laboratory, Fort Belvoir, Virginia, Contract No. DA-44-009 Eng 3492).

22. "The Transmission Secondary Emission Image Intensifier," Proc. of the Image Intensifier Symposium, sponsored by U. S. Army Engineer Research and Development Laboratories, Warfare Vision Branch, Electrical Eng., Fort Belvoir, Va. Oct. 6-7, 1958; to appear as a Chapter in Advances in Electronics and Electron Physics, Photoelectronic Image Devices, Vol. XII, Academic Press, New York, A. E. Anderson.

23. "The Transmission Secondary Emission Image Intensifier and Its Application To Low Light Level Imaging," to be published in June issue of Transactions of the Professional Group on Nuclear Science of the I.R.E., 1960.

24. "Magnetically Focused Secondary Emission Screen-Type Image Intensifier," Chicago Midway Laboratories CML-56-TN-P108-4, August 1956.

25. "On Image Defects Arising From the Electron Velocity Distribution In The Reading Beam of Image Orthicons," Hans Heil, Image Intensifier Symposium, Oct. 6-7, 1958, pp 201-214.

26. "Vacuum Tubes," Spangenberg, McGraw-Hill, 1948, Eq. 18.18, 18.19, p. 634.

27. "An Image Orthicon With A Narrow Range of Electron Energy In The Scanning Beam," R.K.H. Gebel, WADC Tech. Note 58-118, April 1958.

TABLE I

OVERALL SYSTEM RESOLUTION
OF CLOSE SPACED MESH DYNODE TUBES

Stage	Design		Dynode Spacing (Inches)	V (Volts)	Vo (Volts)	Estimated Current Gain	Resolution (Lines/Inch)
Photocathode to First Dynode Stage			1.67	500	0.5		2000 (Estim
Dynode 1 to 2	1. Without Field Control Mesh in Front of Dynode 1	Case 1 Case 2 Case 3	.002 .005 .010	700	2.0	4	74 73 71
	2. With Field Control Mesh in Front of Dynode 1	Case 1 Case 2 Case 3	.002 .005 .010	700	2.0	4	1220 960 700
Dynode 2 to 3	1. Without Field Control Mesh in Front of Dynode 2	Case 1 Case 2 Case 3	.002 .005 .010	700	2.0	Low	---
	2. With Field Control Mesh in Front of Dynode 2	Case 1 Case 2 Case 3	.002 .005 .010	700	2.0	4	1220 960 700

251

TABLE I (Continued)

Stage	Design	Dynode Spacing (Inches)	V (Volts)	Vo Volts	Estimated Current Gain	Resolution (Lines/Inch)
Dynode 3 to Target	1. Without Field Control Mesh in Front of Dynode 3	Case 1 .002 Case 2 .005 Case 3 .010	700	2.0	Low	---
	2. With Field Control Mesh in Front of Dynode 3	Case 1 .002 Case 2 .005 Case 3 .010	700	2.0	4	1220 960 700

To determine overall system resolution R_T:

$$\frac{1}{R_T} = \sqrt{\left(\frac{1}{R_{pc}-D_{y1}}\right)^2 \quad \left(\frac{1}{R_{D_{y1}-D_{y2}}}\right)^2 \quad \left(\frac{1}{R_{D_{y2}-D_{y3}}}\right)^2 \quad \left(\frac{1}{R_{D_{y3}-T}}\right)^2}$$

Case 1: $\quad \frac{1}{R_T} = \sqrt{\frac{1}{(2000)^2} \quad \frac{3}{(1220)^2}}$; $\quad R_T = 660$ lines/inch

Case 2: $\quad \frac{1}{R_T} = \sqrt{\frac{1}{(2000)^2} \quad \frac{3}{(960)^2}}$; $\quad R_T = 535$ lines/inch

Case 3: $\quad \frac{1}{R_T} = \sqrt{\frac{1}{(2000)^2} \quad \frac{3}{(700)^2}}$; $\quad R_T = 375$ lines/inch

252

TABLE II

OVERALL SYSTEM RESOLUTION
OF WIDE SPACED MESH DYNODE TUBE

Stage	Design		Dynode Spacing (Inches)	V (Volts)	Vo (Volts)	Estimated Current Gain	Resolution (Lines/Inch)
Photocathode to First Dynode Stage			1.67	500	0.5		2000 (Estima
Dynode 1 to 2	1. Without Field Control Mesh in Front of Dynode 1		.040	700	2.0	4	61
	2. With Field Control Mesh in Front of Dynode 1	Case 1	.040	700	2.0	4	270
		Case 2	.080		2.0		137
Dynode 2 to 3	1. Without Field Control Mesh in Front of Dynode 2		.040	700	2.0	Low	---
	2. With Field Control Mesh in Front of Dynode 2	Case 1	.040	700	2.0	4	270
		Case 2	.080				137

253